University of Nevada, Reno

Developing a Systems and Community-based Approach for Removing Excess Fluoride from Drinking Water in Rural Northern Ghana

A dissertation submitted in partial fulfillment of the
requirements for the degree of Doctor of Philosophy in
Hydrogeology

by

Laura Craig

James M. Thomas/Dissertation Advisor

August, 2015

THE GRADUATE SCHOOL

We recommend that the dissertation
prepared under our supervision by

LAURA CRAIG

Entitled

Developing a Systems and Community-based Approach for Removing Excess Fluoride from Drinking Water in Rural Northern Ghana

be accepted in partial fulfillment of the
requirements for the degree of

DOCTOR OF PHILOSOPHY

James M. Thomas, Advisor

Alexandra Lutz, Committee Member

David L. Decker, Committee Member

Lisa L. Stillings, Committee Member

Wei Yang, Committee Member

Kate A. Berry, Graduate School Representative

David W. Zeh, Ph. D., Dean, Graduate School

August, 2015

ABSTRACT

Excess fluoride in drinking water is a serious health risk in many parts of the world – particularly in developing countries. Unfortunately, removing excess fluoride from drinking water can be costly and, as a result, beyond the capacity of many poor communities. The health impacts of those who consume high fluoride water over several years range from mild dental fluorosis, which is cosmetic, to crippling skeletal fluorosis, which is disabling. This research addresses the problem of dental fluorosis in an area of northern Ghana with pockets of high fluoride groundwater, which is the primary source of drinking water. It investigates the viability of using laterite collected in the study area and Ghanaian bauxite, for use in low-cost, small-scale fluoride adsorption filters. It also considers whether activated alumina would be a more appropriate sorbent, though the cost would be notably higher since it must be purchased and imported. The possibility of delivering alternative, untreated low fluoride water to fluoridic areas is evaluated as well. In addition to addressing the ongoing challenge of providing clean and reliable sources of drinking water in rural northern Ghana, this research documents the distribution of dental fluorosis in the study area and estimates daily fluoride intake from drinking water and food, in order to determine whether the World Health Organization (WHO) recommended limit of 1.5 mg L^{-1} for fluoride in drinking water is appropriate for Ghana, which is hot year-round and where water consumption is expected to be high.

The laboratory results indicate that, at the pH of the local groundwater (~7) and equal sorbent-to-solution ratios of 6.67 g L^{-1}, activated alumina is notably better at adsorbing fluoride than bauxite or laterite, and bauxite is slightly better than laterite. Activated alumina has the advantage of a high surface area and high fluoride adsorption

at pH 6-7. Bauxite is a very good sorbent per unit area but is limited by a low surface area and adsorbs fluoride best at pH <6. Laterite has higher surface area than bauxite but, due to its mineralogy, adsorbs best at pH <4.5. The field data collected in the study area identified communities with high fluoride (3.1-4.5 mg L^{-1}) and low fluoride (<0.5 mg L^{-1}) groundwater. Bongo granite is the source of groundwater fluoride, and concentrations decrease with distance from granitic areas. The low fluoride areas may be good locations for collecting groundwater and piping to communities with high fluoride groundwater.

Survey data indicate that the WHO recommended fluoride limit of 1.5 mg L^{-1} is too high for Ghana, due to high water intake. But when considering that providing low fluoride water is not cost-free, the WHO recommended limit is currently acceptable for older children and adults. However children under 6-8 years need a limit <1.0 mg L^{-1} (ideally 0.6 mg L^{-1}), and even lower in the first two years of life, since they are the most vulnerable to dental fluorosis. The survey results also show that only 24% of participants understand the cause of damaged teeth. Therefore, an aggressive long-term educational program is needed along with providing low fluoride water, in order to help affected communities understand the importance of drinking treated or alternative sources of low fluoride water.

ACKNOWLEDGEMENTS

I first want to thank Jim Thomas for accepting me as a graduate student and supporting my interest in doing a project in Ghana. I also want to thank the rest of my committee members: Alexandra Lutz, Dave Decker, Kate Berry, Wei Yang, and Lisa Stillings. Each of my six committee members provided invaluable knowledge and support for this research. This project would not have been possible without generous funding from the University of Nevada-Reno, the Desert Research Institute, a U.S. Environmental Protection Agency Science to Achieve Results Graduate Research Fellowship, as well as a Geological Society of America Student Research Grant and a Sigma Delta Epsilon-Graduate Women in Science Nell Mondy Fellowship. The field work would not have been possible without the help of the Bongo District Assembly – in particular Faustina Atipoka Awaane and Richard Mda; and the community of Namoo – most notably Tony Atanga and Philomina Atanga. I want to honor Richard, who died too soon on April 30, 2015. We will continue this work in his name. I also thank my parents for letting me be. My father the engineer died on February 7, 2015, always convinced that I was also an engineer. Hopefully being a hydrologist is close enough.

CONTENTS

LIST OF TABLES

LIST OF FIGURES

CHAPTER 1

Introduction

Overview

The World Health Organization (2011) considers access to safe drinking water both a public health issue and a basic human right. Microbial contamination of drinking water is a primary health concern worldwide, with chemicals such as arsenic, fluoride, nitrate, selenium, and uranium also responsible for adverse health effects due to exposure from drinking water (WHO, 2011). Poor drinking water quality is most pronounced in the developing world; and it is a particular challenge in countries where infrastructure is weak, funding is inadequate, and technically trained professionals are scarce.

In rural northern Ghana (Fig. 1.1 study area), where incomes are among the lowest in the country, groundwater is generally considered the most economically feasible source of safe drinking water. However in some areas the groundwater contains naturally occurring fluoride at concentrations up to three times higher than the World Health Organization (WHO) recommended limit of 1.5 mg L^{-1} for drinking water (Apambire et al., 1997; Apambire, 2000). Because of the health risk, many drilled boreholes delivering water with elevated fluoride concentrations remain closed. But finding other sources of safe water in this water-stressed region is often difficult for reasons including poor hydrogeology, lack of resources, and logistical access. In situations such as this, attaching a low-cost, simple water treatment system to a drilled borehole hand-pump well with high fluoride water may be a solution. Additional extenuating factors such as cost, effectiveness, and acceptance by the affected

communities must also be considered in designing and implementing a water treatment system to ensure that it will be effectively used and maintained.

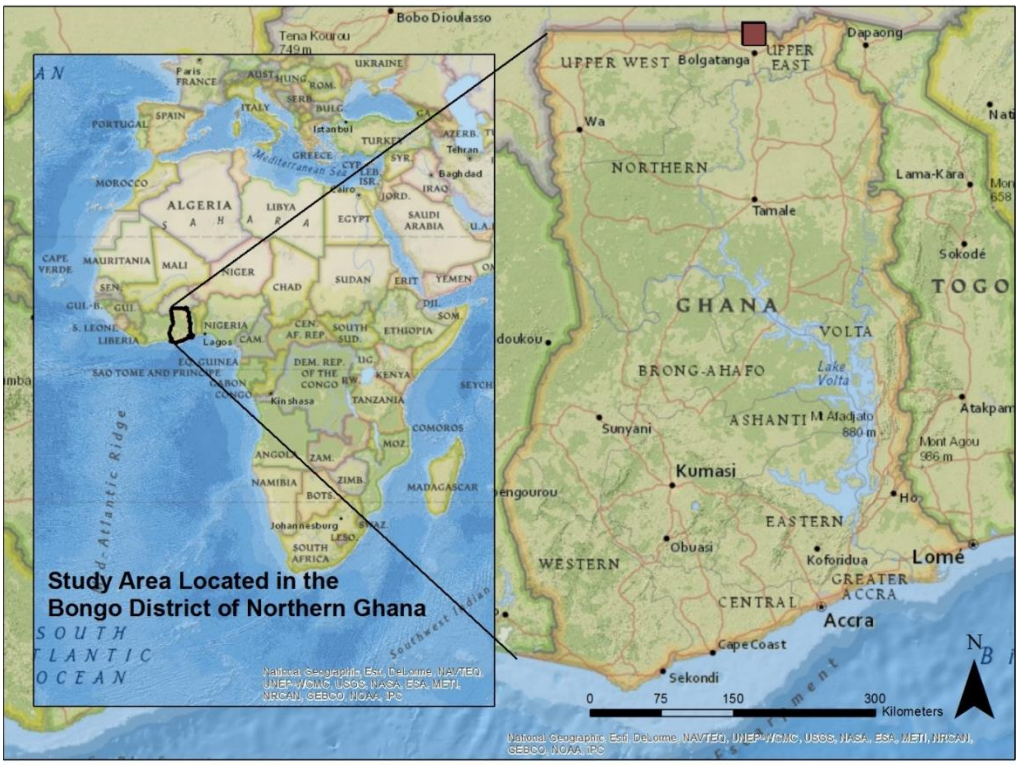

Fig. 1.1. Map of Ghana with the location of the study area in northern Ghana, marked by the brown square.

Background

Fluoride sources

Fluorine is the most reactive and electronegative of all elements and is not found in its elemental form in the environment (Hem, 1985; Weinstein and Davison, 2004). In solution it tends to form the ion fluoride (F^-), and because fluoride carries the same charge as hydroxide (OH^-) and is close in size, the two ions frequently exchange on mineral structures (Hem, 1985). As a result, fluoride forms mineral complexes with several cations and is present in several common minerals (Fawell et al., 2006) such as fluorspar, apatite, mica, hornblende, and cryolite (Murray, 1986). As a general rule,

fluoride-rich water (mostly as groundwater) is located in (1) sediments of marine origin (e.g. parts of the United States), (2) volcanic rocks (e.g. Rift Valley in East Africa), and (3) granite and gneissic rocks (e.g. West Africa including Ghana, and parts of Asia) (Fawell et al., 2006). Fluorite and fluorapatite, two fluoride-rich minerals that frequently occur in igneous and sedimentary rocks (Fawell et al., 2006), are present in the Bongo and Sekoti granitic rocks of northern Ghana (Apambire et al., 1997; Apambire, 2000). Because of its solubility, fluorite likely contributes the majority of aqueous fluoride in groundwater in northern Ghana (Apambire, 2000).

Health effects from fluoride exposure

Drinking water is considered the main source of fluoride intake, and people living in hot climates with high water consumption are potentially at increased risk of exposure (Murray, 1986). It is widely agreed that fluoride is considered beneficial to teeth and bones and – like other essential nutrients – it is healthful in small amounts but damaging at high concentrations (Fawell et al., 2006). When consumed, 70 to 90% of fluoride is absorbed in the body and, due to its geochemical behavior, 99% is retained in calcium-rich areas, such as the bones and teeth (dentine and enamel) (Fawell et al., 2006). In temperate climates, a fluoride concentration of 1 mg L^{-1} in drinking water has been associated with decreased dental caries (Fawell et al., 2006), but higher concentrations in or near developing tooth enamel can result in dental fluorosis in children (Whitford, 1997). Dental fluorosis is an irreversible condition that causes discoloration of the teeth, erosion of enamel, and pitting (Whitford, 1997), and has been identified in northern Ghana (Apambire et al., 1997; Apambire, 2000). Concentrations above 1.5 mg L^{-1} are associated with dental fluorosis, concentrations between 3 and 6 mg L^{-1} are associated

with skeletal fluorosis, and concentrations above 10 mg L^{-1} are associated with crippling skeletal fluorosis (WHO, 1984; WHO, 2008). Skeletal fluorosis, which affects all ages, has been documented in several countries including India, China, and parts of Africa (Fawell et al., 2006). Skeletal fluorosis can result in osteosclerosis, ligamentous and tendinous calcification, and bone deformity (Fawell et al., 2006).

To protect human health, the WHO developed guidelines recommending a daily fluoride intake of 1.5 mg L^{-1} or less (WHO, 2011). The WHO findings and recommended values should not be considered fixed, however, but rather should be adapted to local conditions such as water consumption and diet (Fawell et al., 2006). It is particularly important to consider climate and water consumption when developing national standards (WHO, 1996). Although water is considered the major source of fluoride exposure, water consumption data are generally only available for countries in temperate regions such as Canada (CMNHW, 1981), the United States (Ershow and Cantor, 1989), and the United Kingdom (Hopkin and Ellis, 1980). In hot climates of the developing world, collecting representative water consumption data with which to set national standards is a challenge, because so many communities are rural and depend on communal hand-pump and open wells rather than piped water distribution systems that are more common to urban areas. The absence of a central water distribution system, therefore, makes data more difficult to collect.

The effects of high fluoride intake are evident from results of dental surveys conducted in portions of northern Ghana that showed, of 2,111 children examined, 78.7% had some form of dental fluorosis (Fig. 1.2), with about 8% suffering from severe dental fluorosis (Apambire, 2000). Apambire et al. (1997) did not measure daily water intake

but estimated it at about 3-4 L day^{-1}, due to year-round hot conditions. Based on this estimate, Apambire (2000) recommended a maximum fluoride concentration in drinking water of 0.4-0.6 mg L^{-1} for the communities within the study area, which is less than half of the WHO guideline.

Fig. 1.2. Children with dental fluorosis Bongo District, Upper East Region, Ghana (Atipoka, 2009).

Fluoride removal from drinking water

Controlling excess fluoride in drinking water is difficult where advanced de-fluoridation techniques are unavailable (Fawell et al., 2006). Under these conditions, if another source of drinking water exists, then the recommendation usually is to close the contaminated hand-pump well and find another source. In cases where a safe alternative source is not available, which is frequently true in northern Ghana (CWSA-CIDA, 2005), a simple de-fluoridation system coupled with a maintenance program may be needed. In communities with limited resources, the most promising de-fluoridation methods are adsorption, co-precipitation, or contact precipitation (Fawell et al., 2006). Adsorption media include bone charcoal, clay, synthetic activated alumina, and other laboratory

synthesized sorbents such as iron oxide (Streat et al., 2008a and 2008b) and hydroxyapatite (Verwilghen et al., 2006; MacDonald et al., 2011). Co-precipitation techniques, such as Nalgonda which was developed in India, utilize aluminum sulfate and lime to remove fluoride; and calcium and phosphate compounds are common filter media for contact precipitation (Fawell et al., 2006).

Several fluoride removal techniques have been tested in parts of rural Africa, but the preferred method under most conditions has been adsorption using indigenous materials (Zevenbergen et al., 1996; Mjengera and Mkongo, 2003). The most promising local adsorption material to date in northern Ghana appears to be laterite (Cumberbatch et al., 2008) or, specifically, its most aluminum rich ore, bauxite (Ayamsegna et al., 2008). Activated alumina has also proven a very effective sorbent for fluoride removal (Hao and Huang, 1986; Farrah et al., 1987; Fletcher et al., 2006), but it must be purchased and imported to Ghana. An example of a fluoride adsorption filter attached to a hand-pump well is presented in Fig. 1.3.

Fig. 1.3. Fluoride adsorption filter attached to a hand-pump well in rural northern Ghana (World Vision, 2014)

Research objectives

The objectives of this research are to address the problem of dental fluorosis in the Bongo District of the Upper East Region of Ghana, which is caused by the intake of high fluoride groundwater. The specific objectives are to:

- Assess local hydrogeology, hydrogeochemistry, and distribution of groundwater fluoride in Namoo, Bongo District, Upper East Region, Ghana.
- Quantify daily water consumption, and identify the distribution of dental fluorosis and its correlation to groundwater fluoride concentrations in drinking water.
- Evaluate the effectiveness of indigenous laterite and bauxite as fluoride adsorption media, and compare them to activated alumina as a fluoride sorbent.
- Evaluate the effectiveness of activated alumina as a fluoride adsorbent under varied initial conditions.

Research approach

Assess hydrogeology and hydrogeochemistry in northern Ghana study area of Namoo

Field data were collected to get baseline information on the hydrogeology and hydrogeochemistry of the study area, and to document the range and distribution of groundwater fluoride concentrations. The locations of wells and their elevations were marked using a global positioning system (GPS). Seasonal water levels were measured manually using water level tape to determine the direction of groundwater flow; and a water level-logger was installed in two closed boreholes to document seasonal changes in water level. Water samples were collected in the wet and dry seasons to measure fluoride

concentrations, major ions, pH, conductivity, and dissolved oxygen. The location of outcrops of Bongo granite was also documented with samples collected for x-ray diffraction and x-ray fluorescence analysis to identify its mineralogy and confirm that it is the source of groundwater fluoride.

Quantify daily water consumption, and identify the distribution of dental fluorosis and correlated groundwater fluoride concentrations in drinking water

The second component of the field research in the study area was to estimate the level of exposure to fluoride from drinking water, and correlate fluoride concentrations in drinking water to the distribution and severity of dental fluorosis. Three sets of house-to-house surveys were conducted to estimate household size, identify household water sources, document the daily diet, identify cases of dental fluorosis, and assess the level of understanding of the cause of discolored and damaged teeth (dental fluorosis). To estimate the level of fluoride exposure from drinking water, the daily water consumption of 27 individuals from ages 5 to about 70 years was monitored over several days. The data were used to recommend limits of fluoride in drinking water, and to better understand the correlation between fluoride concentration in drinking water and the distribution of dental fluorosis in children and adults.

Evaluate the effectiveness of indigenous laterite and bauxite as fluoride adsorption media, and compare to activated alumina as a fluoride sorbent

The third component of this research focused on evaluating the simple, low-cost method of adsorption for removing excess fluoride from drinking water. In this chapter two indigenous sorbents were evaluated as potential low-cost sorbents for use in de-fluoridation filters. One was laterite which was collected in the study area, and the other bauxite, which was provided by an aluminum mine in western Ghana. Their adsorption

capacity was also compared to that of activated alumina which is well established as an effective sorbent for fluoride removal from water (Hao and Huang, 1986; Farrah et al., 1987; Fletcher et al., 2006).

The physical and chemical properties of the three sorbents were determined using several methods. The pH dependent surface charge was determined by conducting fast acid-base titrations (5-10 minute stabilization time between titrant additions). The surface area was determined by the Brunauer, Emmett, Teller (BET) method (Brunauer, et al., 1938; Lowell and Shields, 1991), and pore area and volume by the Barrett, Joyner, Halenda (BJH) method (Barrett et al., 1951; Lowell and Shields, 1991). Microporosity (< 2 nm) of each sorbent was determined by creating *t*-plots (Gregg and Sing, 1982; Hay et al., 2011), and the mineralogy was identified using both x-ray diffraction and x-ray fluorescence.

To evaluate the fluoride adsorption capacity, batch adsorption experiments were conducted on each sorbent. One set of experiments evaluated fluoride adsorption at an initial fluoride concentration of 10 mg L^{-1} and varied pH at three ionic strengths. The other set of experiments evaluated fluoride adsorption at neutral pH, one ionic strength and varied fluoride concentrations. Freundlich and Langmuir isotherms were used to estimate the macroscopic distribution of fluoride between solution and sorbent under assumed equilibrium conditions. To identify the adsorption reactions occurring on each sorbent, the generalized two-layer surface complexation model (Dzombak and Morel, 1990) in the PHREEQC program was used (Parkhurst and Appelo, 1999).

Evaluate the effectiveness of activated alumina as a fluoride adsorbent under varied initial conditions

The goal of the fourth component of this research was to evaluate the adsorption capacity of activated alumina under varied initial conditions to help determine whether it changes with extended hydration and at varied grain sizes. This work included laboratory experiments to assess pH dependent surface charge and fluoride adsorption capacity of activated alumina at a range of prior hydration periods (24 hours up to 16 or 30 weeks in deionized water). The physical and chemical properties were determined as described in the previous section, except that the acid-base titrations were much slower, allowing the titrant to equilibrate overnight before taking a pH reading.

To evaluate fluoride adsorption capacity, batch adsorption experiments were conducted at near neutral pH, constant ionic strength and varied fluoride concentrations. To identify the adsorption reactions occurring on each sorbent, the generalized two-layer surface complexation model (Dzombak and Morel, 1990) in the PHREEC program was used (Parkhurst and Appelo, 1999). Batch adsorption experiments were also conducted at near neutral pH, one ionic strength, and initial fluoride concentration of 10 mg L^{-1} to evaluate fluoride adsorption versus time at two grain sizes.

References

Apambire, W.B., Boyle, D.R., Michel, F.A. 1997. Geochemistry, genesis, and health implications of fluoriferous groundwaters in the upper regions of Ghana. Environmental Geology 33(1) 13-23.

Apambire, W.B. 2000. Geochemical Modeling and Geomedical Implications of Fluoriferous Groundwaters in the Upper East Region of Ghana. Unpublished Ph.D. dissertation, University of Nevada-Reno, Reno, NV.

Atipoka, F.A. 2009. Water supply challenges in rural Ghana. Desalination 248, pp. 212-217.

Ayamsegna, J.A., Apambire, W.B., Bakobie, N., Minyila, S.A., 2008. Removal of fluoride from rural drinking water sources using geomaterials from Ghana. Access to Sanitation and Safe Water: Global Partnerships and Local Actions 33rd Int. Conf., Accra, Ghana.

Barrett, E.P., Joyner, L. G., Halenda P.P., 1951. The determination of pore volume and area distributions in porous substances. I. Computations from nitrogen isotherms. J. Am. Chem. Soc. 73, 373-380.

Brunauer, S., Emmett, P.H., Teller, E., 1938. Adsorption of gases in multimolecular layers. J. Am. Chem. Soc. 60, 309-319.

CMNHW (Canadian Ministry of National Health and Welfare). 1981. Tap water consumption in Canada. (Document number 82-EDH-80). Public Health Affairs Directorate, Department of National Health and Welfare, Ottawa, Ontario.

Cumberbatch, T., Atipoka, F., Ayamgah, G., Batir, B., Berger, D., Freed, L., Momada, F., Nyarku, M., Pervez, N., Ponce, B., Rana, S., Venugopal, V., and Volk, L. 2008. The Development of an Indigenous Filter. EPA P3 Award: A National Student Competition for Sustainability Focusing on People, Prosperity, and Planet (2007). Cooper Union for the Advancement of Science and Art, New York.

CWSA-CIDA (Community Water and Sanitation Agency and Canadian International Development Agency). 2005. Briefing Paper for District Assemblies on Fluoride in NORWASP Districts. Field Paper #28.

Dzombak, D.A., Morel, F.M.M., 1990. Surface Complexation Modeling: Hydrous Ferric Oxide. John Wiley & Sons Inc., New York.

Ershow, A.G., Cantor, K.P. 1989. Total Water and Tapwater Intake in the United States: Population-Based Estimates of Quantities and Sources. No. 263-MD-810264, National Cancer Institute.

Farrah, H., Slavek, J., Pickering, W.F., 1987. Fluoride interactions with hydrous aluminum oxides and alumina, Aust. J. Soil Res., 55-69.

Fawell, J., Bailey, K., Chilton, J., Dahi, E., Fewtrell, L., and Magara, Y. 2006. Fluoride in Drinking-water. WHO Drinking-water Quality Series, World Health Organization, Geneva.

Fletcher, H.R., Smith, D.W., Pivonka, P., 2006. Modeling the sorption of fluoride onto alumina. J. Environ. Eng. 132, 229-246.

Gregg, S.J., Sing, K.S., 1982. Adsorption, Surface Area, and Porosity. Academic Press, London.

Hao, O.J., Huang, C.P., 1986. Adsorption characteristics of fluoride onto hydrous alumina. J.

Hay, M.B., Stoliker, D.L., Davis, J.A., Zachara, J.M., 2011. Characterization of the intragranular water regime within subsurface sediments: Pore volume, surface area, and mass transfer limitations. Water Resour. Res. 47, 1-19.

Hem, J.D. 1985. Study and Interpretation of the Chemical Characteristics of Natural Water. Water Supply Paper 2254, 3rd edition. US Geological Survey, Washington D.C., 263 pp.

Hopkin, S.M., Ellis, J.C. 1980. Drinking Water Consumption in Great Britain. Technical Report TR 137, Water Research Centre, Medmenham, UK.

Lowell, S., Shields, J.E., 1991. Powder Surface Area and Porosity. Chapman and Hall Ltd., New York.

MacDonald, L.H., Pathak, G., Singer, B., Jaffé, P.R., 2011. An integrated approach to address endemic fluorosis in Jharkhand, India. J. Water Res. Prot. 3, 457-472.

Mjengera, H., Mkongo, G. 2003. Appropriate defluoridation technology for use in fluoridic areas in Tanzania. Phys. Chem. Earth 28, 1097-1104.

Murray, J.J. [Ed.]. 1986. Appropriate Use of Fluorides for Human Health. World Health Organization, Geneva.

Parkhurst, D.L., Appelo, C.A.J., 1999. User's guide to PHREEQC (version 2) – A computer program for speciation, batch-reaction, one-dimensional transport, and inverse geochemical calculations. U.S. Geological Survey, Denver CO.

Streat, M., Hellgardt, K.L., Newton, N.L.R., 2008a. Hydrous ferric oxide as an adsorbent in water treatment Part 1. Preparation and physical characterization. Process. Safety Environ. Prot. 86, 1-9.

Streat, M., Hellgardt, K.L., Newton, N.L.R., 2008b. Hydrous ferric oxide as an adsorbent in water treatment Part 3. Batch and mini-column adsorption of arsenic, phosphorous, fluorine, and cadmium ions. Process. Safety Environ. Prot. 86, 21-30.

Verwilghen, C., Rio, S., Nzihou, A., Gauthier, D., Flamant, G., Sharrock, P.J., 2006. Preparation of high specific surface area hydroxyapatite for environmental applications. J. Mater. Sci. 42, 6062-6066.

Weinstein, L. H., Davison, A.W. 2004. Fluorides in the Environment. CABI Publishers, Massachusetts.

Whitford, G.M. 1997. Determinants and mechanisms of enamel fluorosis. Ciba Foundation Symposium 205, 226-241.

WHO (World Health Organization). 1984. Fluorine and Fluorides. Environmental health Criteria 36. World Health Organization, Geneva.

WHO (World Health Organization). 1996. Guidelines for Drinking-water Quality. Volume 2. Health Criteria and Other Supporting Information, 2nd edition. World Health Organization, Geneva.

WHO (World Health Organization). 2008. Guidelines for Drinking Water Quality. Volume 1, 3rd edition. World Health Organization, Geneva.

WHO (World Health Organization). 2011. Guidelines for Drinking Water Quality. Volume 1, 4th edition. World Health Organization, Geneva.

Zevenbergen, C., van Reeuwijk, L.P., Frapporti, G., Louws, R.J., and Schuiling R.D. 1996. A simple method for defluoridation of drinking water at village level by adsorption on Ando soil in Kenya. Sci. Total Environ. 188, 225-232.

CHAPTER 2

THE HYDROGEOLOGY AND HYDROGEOCHEMISTRY OF A FLUORIDIC AREA IN THE UPPER EAST REGION OF GHANA

Craig, Laura, Thomas, James, M., Lutz, Alexandra

Abstract

Groundwater in the Upper East Region of Ghana contains naturally occurring fluoride due to the dissolution of minerals in the local granite. Groundwater is the primary source of drinking water in the region and in many communities the fluoride concentrations are high enough to cause dental fluorosis. This study evaluates the hydrogeology and hydrogeochemistry in an area with groundwater fluoride concentrations ranging from 0.2 to 4.6 mg L^{-1}. The results show that the higher elevation recharge areas, with outcrops of Bongo granite, have elevated concentrations of fluoride in the groundwater, posing the highest risk of fluorosis in the nearby communities. The lower elevation areas, which are the farthest from the granitic area, have the lowest groundwater fluoride (<0.5 mg L^{-1}) and the lowest risk of fluorosis. The lower elevation communities are also the optimum locations to install boreholes, or use existing boreholes for piping low fluoride groundwater to the higher fluoride areas. Although the initial costs of developing a water system would be high, this is a potentially viable option for providing low fluoride water to communities suffering from fluorosis.

1. Introduction

The Upper East Region of Ghana is semi-arid, poor, and primarily rural with most residents working as subsistence farmers. The majority of households rely on groundwater collected from drilled boreholes with hand-pumps or hand-dug open wells for their domestic water. Groundwater is generally considered a safe and economical source of drinking water, but there are pockets in the Upper East Region where the groundwater contains concentrations of naturally occurring fluoride well above the World Health Organization recommended limit of 1.5 mg L^{-1} (WHO, 2011). The source of groundwater fluoride is Bongo granite (Apambire, 1996; Apambire et al., 1997; Apambire, 2000); and the result of consuming high fluoride groundwater is an increase in cases of dental fluorosis (Apambire, 1996; Apambire et al., 1997; Apambire, 2000), as well as an increased risk of skeletal fluorosis. Due to the health risks of drinking high fluoride water, many drilled boreholes remain closed because the fluoride in these wells exceeds 1.5 mg L^{-1}.

This study focuses on the Namoo electoral area in the Bongo District of the Upper East Region of Ghana, which borders Burkina Faso. The objective of this study is to characterize the hydrogeology, geochemistry, and groundwater chemistry of Namoo to better understand the distribution of groundwater fluoride, and to identify conditions that may influence its concentration. The results of this study will also help identify areas with low fluoride groundwater to target for well drilling, which would save money on drilling costs and provide additional sources of low fluoride drinking water in a very poor, water stressed region.

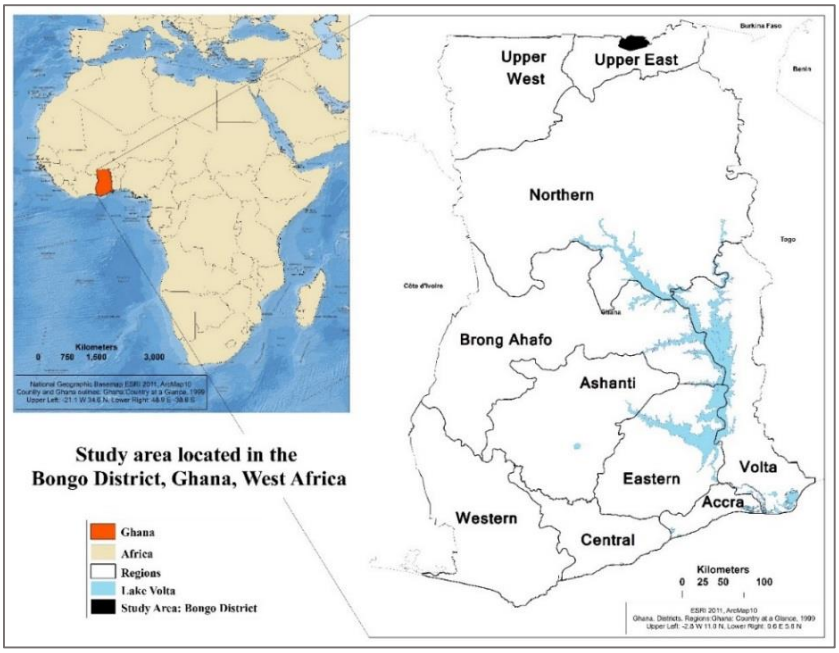

Fig. 2.1. The location of the Bongo District in the Upper East Region of Ghana. The community of Namoo is an electoral area within the Bongo District.

2. Materials and Methods

2.1. Study area characterization: hydrogeology and climate

The study area of Namoo is in the Bongo District, Upper East Region of Ghana (Fig. 2.1), and was chosen because of the ongoing problem of dental fluorosis from consuming fluoride-rich groundwater (Apambire et al., 1997; Apambire, 2000, Atipoka, 2009). To map the location and elevation of wells in the study area, hand-dug open wells (Fig. 2.2a-c) and drilled borehole hand-pump wells (Fig. 2.2d) were identified and marked with a Garmin eTrex Vista® global positioning system (GPS). Obtaining accurate elevation measurements from hand-held GPS devices is difficult, so to minimize the relative error, all of the elevation readings were recorded in a single day with a clear sky and maximum satellite strength. All elevations are shown as meters above sea level. Water level in the wells was measured once manually during the wet season (September 2012) and dry season (April 2013) with a Solinst® water level meter. Additional

measurements were taken in the closed boreholes (not in use = no hand-pumps) in November 2011. Depth to the bottom of hand-dug open wells (open wells) was determined by lowering a weighted rope to the bottom of each well. To continuously monitor changes in groundwater levels, Schlumberger Diver® water level-loggers were installed in two closed boreholes with a barometric pressure logger also located in the study area. Each Schlumberger Diver® recorded pressure every 30 minutes: one from April-October and the other from April-December 2013. Beginning in late July 2012, seasonal variation in the climate was monitored by installing a Decagon® weather station to record air temperature, relative humidity, wind speed, solar radiation, and precipitation every 30 minutes. Pumping rates were also collected for 13 drilled boreholes with hand-pumps (hand-pump wells) in the Bongo District.

Fig. 2.2. Photographs of (a) mostly covered hand-dug open well, (a) completely uncovered hand-dug open well, (c) completely covered hand-dug open well, and (d) drilled borehole with hand-pumps. A closed drilled borehole has no hand-pump or spout as seen in (d) – just the pipe with a small cover.

2.2. Groundwater chemistry

Water samples were collected from 40 open wells and 17 hand-pump wells (including closed wells) in the study area during the late wet (September), late dry (April), and shoulder (October-November) seasons and analyzed for fluoride concentrations. Hand-pump wells were pumped for several minutes before collecting samples and were usually in use by community members which further purges the well. As a result, the samples collected from these wells provide a consistently accurate representation of the groundwater chemistry. Open wells were used regularly and their samples provide an accurate representation of the chemistry of the water being consumed.

2.2.1. Field analyses: fluoride, conductivity, temperature, pH, alkalinity, dissolved oxygen

The water samples were collected in Nalgene© polypropylene copolymer centrifuge tubes. They were analyzed the same day for fluoride using an Orion 4-star meter and fluoride ion selective electrode, with TISAB III added to the sample just before analysis (APHA, 1998). The fluoride ion selective electrode was calibrated by creating calibration curves using 1 and 10 mg $F^- L^{-1}$ standards or 0.1 and 1 mg $F^- L^{-1}$ standards, depending upon the concentration of the sample, with the electrode calibrated every eight to ten samples to maintain an accuracy within 5%. The accuracy of the calibration curve was also checked with 5 mg $F^- L^{-1}$ standard for the higher range calibration curve, and 0.5 mg $F^- L^{-1}$ for the lower range calibration curve. The majority of samples, including those from all hand-pump wells and open wells with fluoride concentrations above 2.5 mg L^{-1}, were analyzed again at the Desert Research Institute in Reno, Nevada using a new

fluoride ion selective electrode. The repeat analysis was done to confirm accuracy within 5%. The pH was measured immediately upon collection using a gel-filled Ag/AgCl pH electrode attached to an Orion 4-star meter. The conductivity and temperature were also measured immediately upon collection using an Oakton® conductivity meter, as was dissolved oxygen using a YSI 55 dissolved oxygen meter. Alkalinity was measured the day of collection using a Hach© field alkalinity kit.

2.2.2. Laboratory analyses: major ions

Seventeen hand-pump and 34 open well samples collected during the wet and dry seasons were also analyzed for major ions. These samples were filtered in the field with a 0.45 µm filter and collected in two 30 ml Nalgene© bottles. One bottle was for major anion analysis and the other for major cation analysis. The anion samples were kept frozen, or refrigerated, and were analyzed within 28 days of collection. The cation samples were acidified to pH <2 with concentrated HNO_3 after filtration. All major ion analyses were conducted in a USEPA Certified laboratory. Analysis of chloride (Cl^-), nitrate (NO_3^-), and sulfate (SO_4^{2-}) were conducted using a Dionex© Model ICS 2000 ion chromatograph, and analysis of sodium (Na^+), calcium (Ca^{2+}), potassium (K^+), and magnesium (Mg^{2+}) were conducted using a Thermo Elemental SOLAAR M5 atomic adsorption spectrometer.

2.3. X-ray diffraction and x-ray fluorescence analyses of Bongo granite

Samples of Bongo granite were collected at the ground surface from three locations in the study area with high fluoride groundwater. These samples were analyzed using x-ray diffraction (XRD) and x-ray fluorescence (XRF). Each bulk sample was prepared by hand grinding an oven dried fraction (<2mm) to a grain size under 500 µm

and then grinding to a powder in a McCrone mill for 8 minutes in 10 ml of methanol. The samples were then air dried overnight, gently re-crushed in a pestle and mortar to break up aggregates formed during drying and side-loaded into a sample holder. The resulting XRD scans were viewed and interpreted using Bruker XRD data evaluation software called EVA, with background corrections performed before interpretation. Minerals were identified by matching reference mineral patterns stored in the ICDD (International Centre for Diffraction Data) database to the observed peaks.

X-ray fluorescence analyses were conducted with a Rigaku Primus II wavelength dispersive spectrometer (WDXRF) that is capable of detecting elements from atomic number (Z) 4 (beryllium) through atomic number 92 (uranium) at concentrations from the low parts per million (ppm) range up to 100% by weight. Quantification was performed using the Fundamental Parameters (FP) standard-less quantification software associated with the system. The relative accuracy usually ranges from better than 5% up to ~20% for major elements.

3. Results

3.1. Study area characterization: hydrogeology and climate

The average maximum and minimum air temperatures for the study area were recorded from August 2012 to September 2013, and the total monthly precipitation from August 2012 through December 2013 (Fig. 2.3).The total precipitation for 2013 was about 84 cm, from early March through October; and August 2012 through July 2013 had 100 cm of precipitation. The highest monthly rainfall occurred in September 2012 (32 cm) and August 2013 (25 cm). The average, standard deviation, minimum, maximum, and median values for relative humidity, wind speed, air temperature, and solar radiation

are presented in Table 2.1. The solar radiation values presented in Table 2.1 include only the non-zero readings within the 12 hours of daylight from 6:30-7:00 am to 6:30-7:00 pm, with data collected for just three months due to equipment malfunction. The data collected indicate that the highest daily solar radiation was usually about 1:00-2:00 pm, and the highest daily air temperatures were around 3:00-4:00 pm. March usually had the highest air temperatures. The lowest air temperatures were December-January, the lowest relative humidity was December-February, and the strongest winds were January-February. This period is the Harmattan season, which is characterized by low-humidity and northeasterly trade winds.

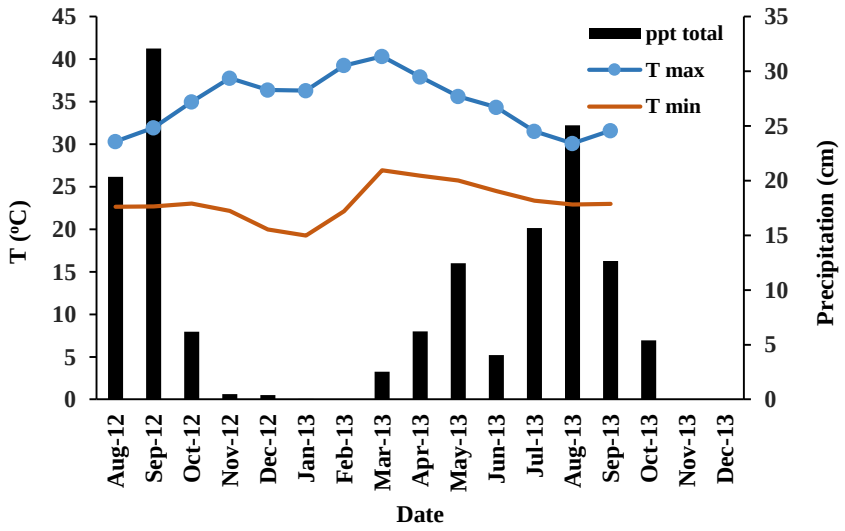

Fig. 2.3. The average monthly maximum and minimum air temperatures and total monthly precipitation in Namoo from mid-2012 to late 2013. Total precipitation for 2013 was about 84 cm.

Table 2.1. Climate parameters relative humidity (RH), air temperature (T), wind speed, solar energy measured in Namoo. Values presented are the daily maximum (max), minimum (min), average (avg), standard deviation (std dev), and median (med) values.

Parameter	Dates	Avg	Std Dev	Min	Max	Med
RH	7/27/12-9/25/13	0.59	0.30	0.01	1.0	0.62
T (ºC)	7/27/12-9/25/13	29.0	6.8	16.0	43.1	27.9
Wind (m s^{-1})	7/27/12-1/29/14	0.6	0.9	0.0	9.6	1.0
Solar (W m^{-2})[a]	7/27/12-10/24/12	397.3	280.7	1.8	1076.7	376.3

[a]Daylight only - 12 h day^{-1}.

The elevation contours, location of granitic areas, and location of high, moderate, and low fluoride wells are presented in Fig. 2.4. The wet and dry season water level contours are presented in Fig. 2.5 using water levels measured from the same wells during each season. The groundwater flow lines mirror elevation for the most part, which is consistent with Martin (2006) interpretations, and the groundwater flow direction is nearly identical in dry and wet seasons. Groundwater flow is radially away from the highest elevation recharge area in the northwest part of the study area. Most of the groundwater flows to the east toward an ephemeral stream located just outside of Namoo.

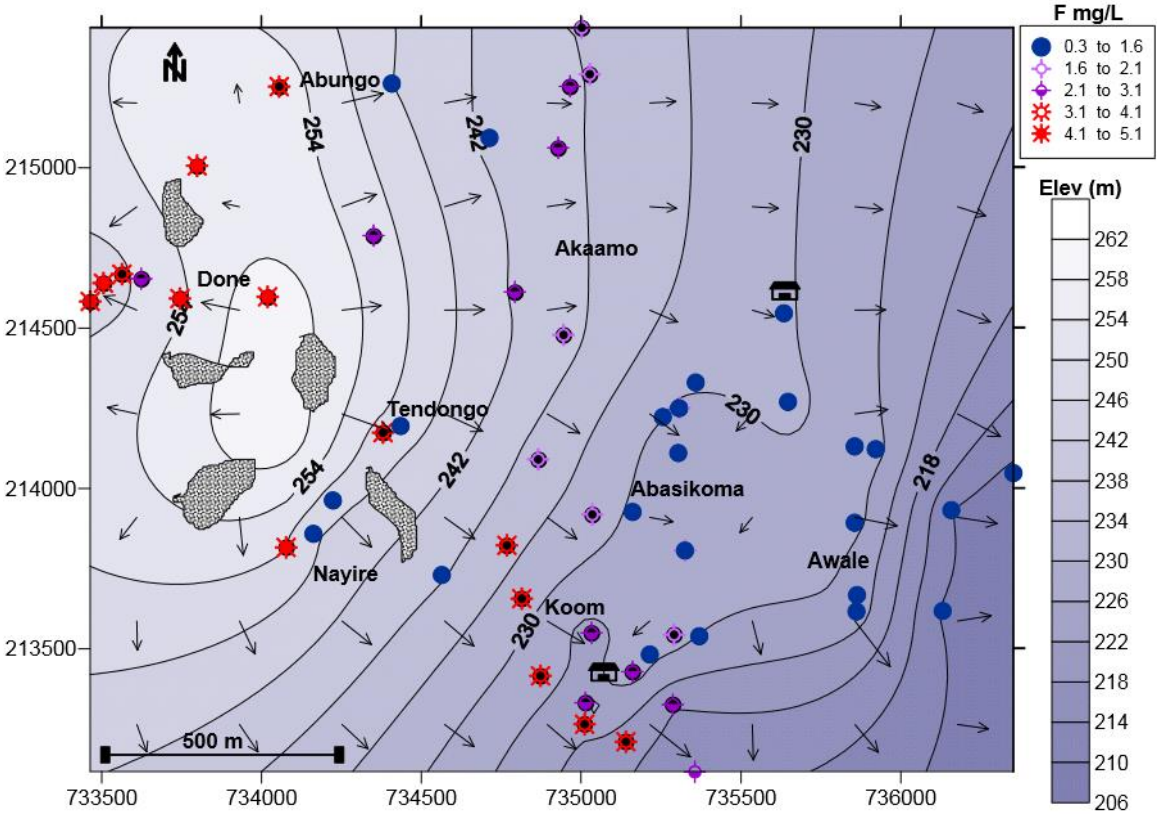

Fig. 2.4. A contour elevation map of Namoo and assumed groundwater flow direction (arrows) based on elevation, the location of high, moderate, and low fluoride wells (colored circles), Bongo granite (mesh filled polygons), primary schools (buildings), and the eight communities of Done, Tendongo, Nayire, Koom, Abungo, Abasikoma, Akaamo, and Awale. The Bongo granite is in the areas of Done, Tendongo, and Nayire. The map was created using Surfer®.

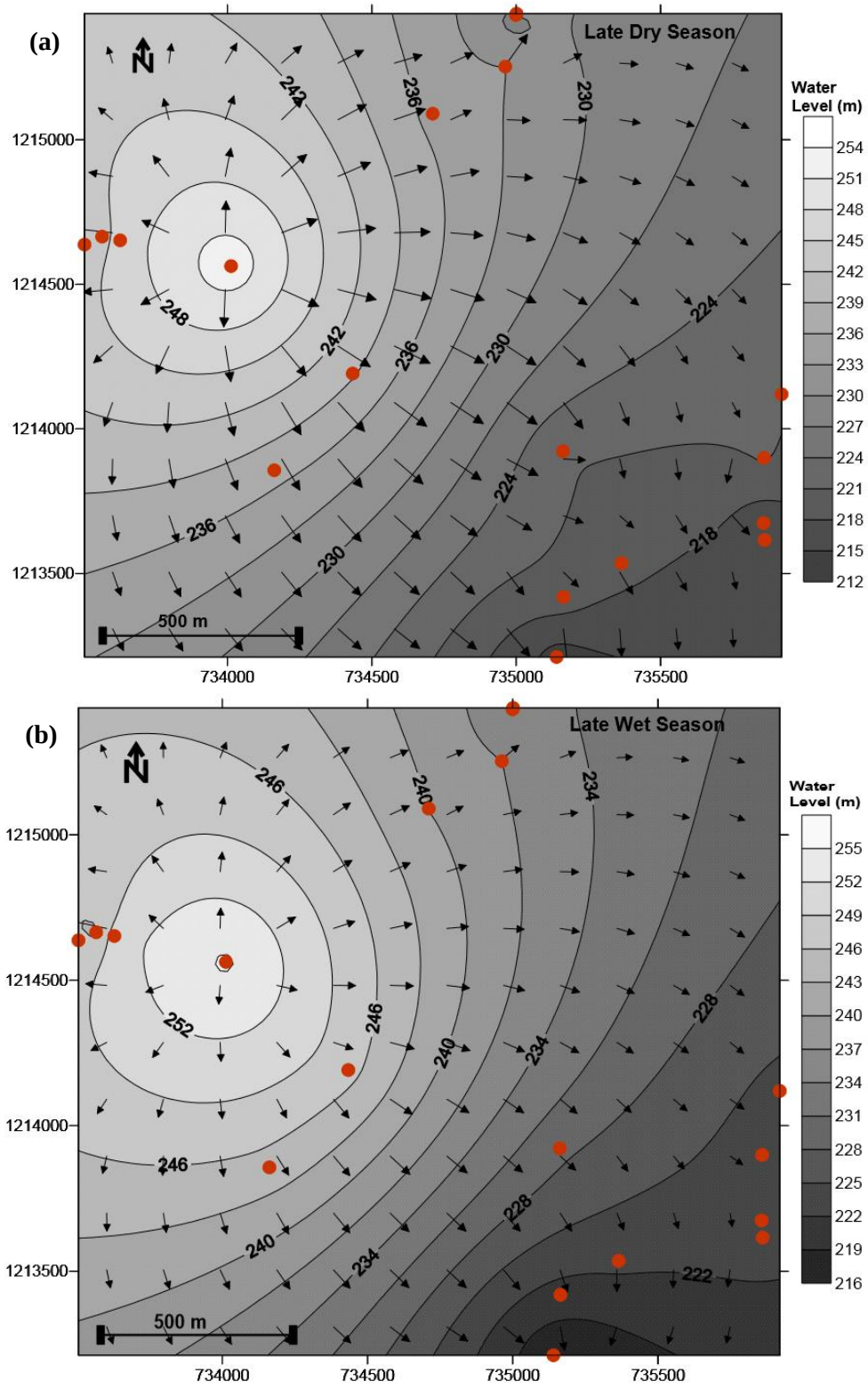

Fig. 2.5. Contours based on measured groundwater levels in (a) dry and (b) wet season with direction of groundwater flow (arrows) generally from high to low elevation. The brown circles are the location of water level measurements in wet and dry season (same wells both seasons). Maps were created using Surfer®.

The study area contains eight communities: Done, Abungo, Tendongo, Nayire, Akaamo, Abasikoma, Koom, and Awale (Fig. 2.4). Two primary schools are shown in Fig 2.4, with two junior high schools located within 100 m of the primary schools. Done in the northwest part of the study is the highest elevation community and is the location of most of the Bongo granite. This area is also where elevated groundwater fluoride is most concentrated, with groundwater fluoride concentrations decreasing in the direction of groundwater flow and with distance from the granitic area. Groundwater fluoride concentrations and water chemistry will be discussed further in section 3.2.

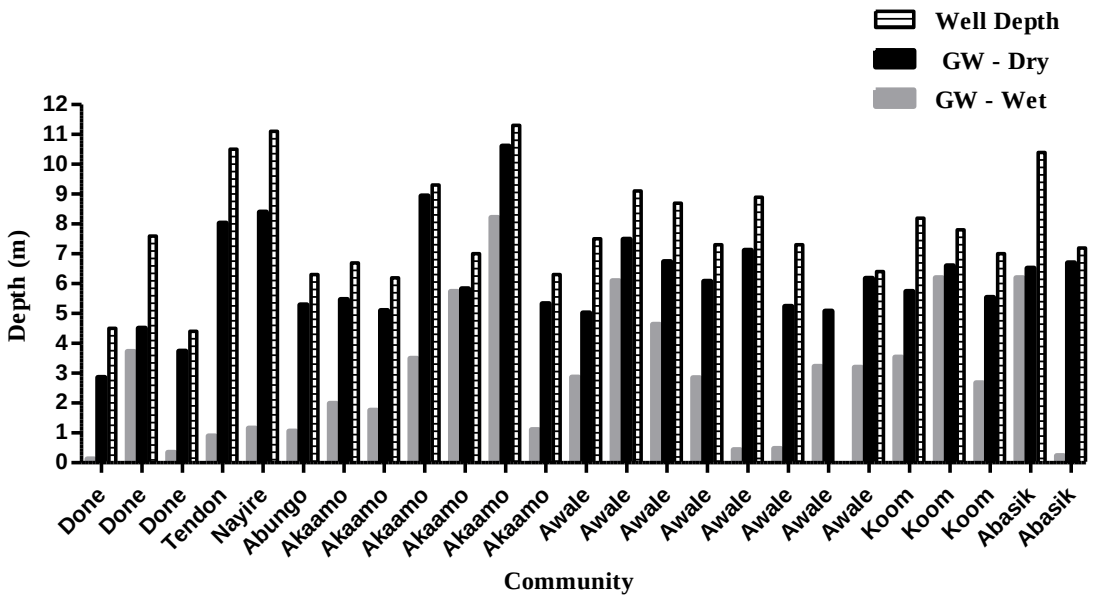

Fig. 2.6. The depth to groundwater and well depth from ground surface in the late wet (September 2012) and dry (April 2013) seasons in 25 open wells, separated by community.

In Fig. 2.6, the seasonal changes in groundwater levels and depth to the bottom of 25 open wells is presented. The late dry season measurements were taken in April of 2013 and the late wet season measurements were taken in September 2012. The wells with very high wet season water levels fluctuate the most, while those with deeper wet season water levels show less seasonal fluctuation. Some very high use open wells may

also have measurable decreases of water levels. During this study, the water level in the open wells never dropped below the well depth. Table 2.2 presents the average, maximum, minimum, and median water levels and well depth for most of the hand-dug wells in the eight communities.

Table 2.2. Open well measurements for well depth and depth to groundwater (GW) for late wet (September 2012) and late dry (April 2013) seasons.

Depth (m)	Avg	Std Dvn	N[a]	Min	Max	Med
To GW September	2.9	2.3	31	0.1	8.2	2.9
To GW April	6.2	1.7	31	2.8	10.6	5.8
Well Depth	7.8	1.8	30	4.4	11.3	7.4

[a]Number of wells used in the calculations.

Table 2.3. The manually measured depth to groundwater for six closed boreholes and approximate elevation. The water level measurements were taken before the hand-pumps were installed in each borehole, after which point no more measurements were taken (X = no measurement).

Community	Elev (m)	November 2011 (m)	September 2012 (m)	April 2013 (m)	September 2013[a] (m)
Done upper	261	5.3	5.6	8.0	5.1 (28th)[a]
Done lower	253	2.2	X	X	X
Done lower	249	1.6	0.6	3.2	0.5 (1st)[a]
Tendongo	248	7.6	X	X	X
Nayire	250	10.8	11.4	X	X
Koom	232	5.1	X	X	X

[a]The highest measured water level for 2013, presented in Fig. 7, with the peak one month apart for two Done wells, showing the approximate day in parentheses.

Measuring groundwater levels in the hand-pump wells was not possible because they were in use. However, Table 2.3 presents manual measurements taken from closed wells (before hand-pumps installed). The closed wells with water levels closest to the surface are in the Done community (249 and 253 m), and with the lowest water level relative to the surface is in Nayire (250 m). Fig. 2.7 shows water level measurements recorded every two hours in 2013 for two of the closed wells in Done. The closed well at elevation 249 m (lower Done) with a water level close to the land surface has its lowest level in April, its highest in late August, and responds quickly to precipitation. The higher elevation closed well in upper Done (261 m) is more delayed in its response to precipitation with its lowest water level in July and highest in late September. The

seasonal fluctuation in groundwater of 3.2 m measured from the Done 261 m elevation closed well is also greater than the seasonal fluctuation of 2.7 m at 249 m elevation measured in lower Done.

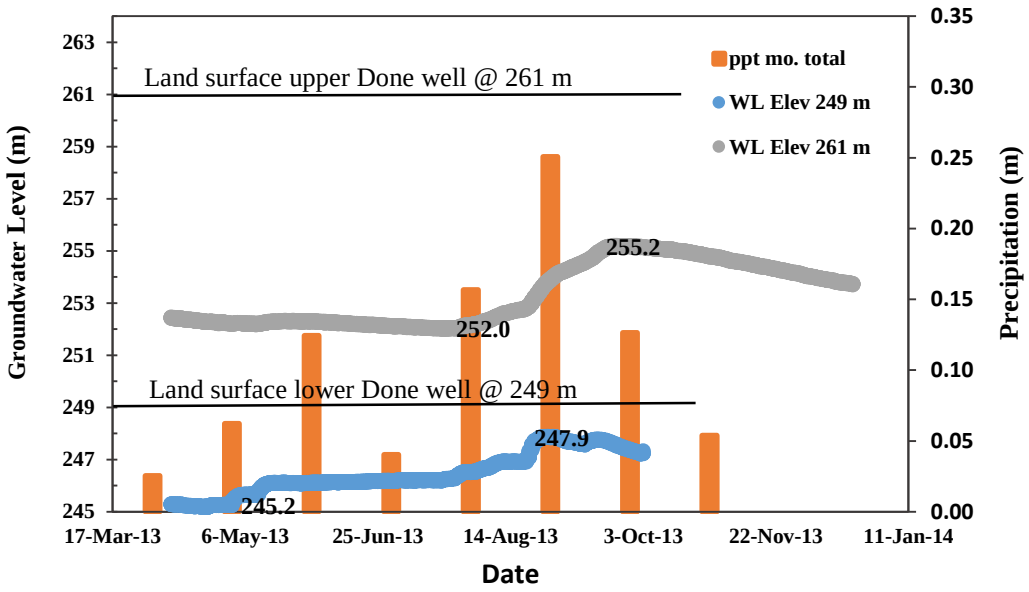

Fig. 2.7. Monthly total precipitation for 2013 and groundwater level measured and recorded every two hours between April and October or December 2013 in two drilled boreholes before installing hand-pumps. Both are located in the community of Done, with one at high elevation (261 m) and the other in the lower elevation part of Done (249 m). The lower Done well with groundwater level closer to land surface has its lowest water level in April and highest in late August. The higher elevation upper Done well with a groundwater level measured at ~ 6-9 m lower than land surface has its lowest water level in July and highest in late September. The latter well responds more slowly to precipitation input and has greater seasonal groundwater fluctuation.

3.2. Groundwater chemistry

3.2.1. Field analyses: fluoride, conductivity, temperature, pH, alkalinity, dissolved oxygen

Groundwater samples were collected and analyzed for 17 hand-pump and 40 open wells. Samples were collected in the late shoulder (October-November 2011), Wet (September 2012), and dry (April 2013) seasons. The results of fluoride (F^-) concentrations in hand-pump wells (including closed wells) are presented in Table 2.4, and open wells in Table 2.5, with the installation year in the right-hand column.

Table 2.4. The fluoride (F^-) concentrations of drilled wells in the Namoo study area, including the approximate year the well (and hand-pump) was installed. The first drilled wells were installed in the 1970s but the year is not certain. Samples were collected for the wet, dry, and shoulder seasons. Highlighted values have average fluoride concentrations above the WHO (2011) recommended limit of 1.5 mg L^{-1}.

No.	Shoulder F^- mg L^{-1}	Wet F^- mg L^{-1}	Dry F^- mg L^{-1}	Avg F^- mg L^{-1}	Year Installed
1	0.7	0.6	0.6	0.6	1970s
2	3.0	2.9	2.8	2.9	1970s
3	1.5	1.6	1.6	1.6	1970s
4	2.6	2.6	2.5	2.6	1970s
5	1.5	1.6	1.6	1.6	1999
6	0.7	0.9	0.5	0.7	2005
7	2.2	2.1	2.1	2.1	2005
8	1.5	1.7	1.5	1.6	2005
9	4.6	3.7	4.5	4.3	2008
10	1.0	0.7	1.0	0.9	2010
11	no sample	1.9	2.0	2.0	2011
12	closed [2.3]	2.8	2.9	2.9	2011
13	closed [0.7]	2.4	2.5	2.4	2011
14	closed [3.6]	3.3	3.5	3.4	2012
15	closed [5.6]	closed [5.0]	4.5	4.5	2012
16	closed [3.7]	closed [3.5]	closed [3.4]	3.5[b]	2013
17	closed [3.7]	closed [3.0]	closed [3.8]	3.4[b]	2013

[b]These wells were closed during the scheduled sampling periods so the samples collected may have incorrect fluoride concentration because the sample water was not from a flushed/regularly used well. They were opened in late 2013.

All wells are listed chronologically by the year installed. The fluoride concentrations measured in the closed wells are less reliable because the water was stagnant; therefore, those concentrations are not considered representative and are only used in determining the average concentration if there is no measurement from a borehole with the hand-pump installed (these are wells 16 and 17 in Table 2.4). However, they are both within 50 m of well 14 which was opened in 2012 and has similar fluoride concentrations. The highest groundwater fluoride concentrations are usually in the deeper hand-pump wells. Four of the five drilled boreholes with fluoride above 3.0 mg L^{-1} had hand-pumps installed in 2012 and 2013, and were subsequently open for public use. Hand-pump wells with the highest fluoride concentrations are in or adjacent to the granitic area (Fig 2.4). The only well that showed much seasonal change in fluoride, ranging from 3.7-4.6 mg L^{-1}, is number 9 in Table 2.4 which is at the edge of lower Done. No drilling logs are

available for this well to determine the well depth, the depth to water, and the lithology. Of the 17 hand-pump wells, only three have average fluoride concentrations at or below the WHO recommended limit of 1.5 mg L^{-1} (WHO, 2011).

Table 2.5. The fluoride (F^-) concentrations of open wells installed in the study area, with the year installed if known. Samples were collected for the wet, dry, and shoulder seasons. Highlighted values have average fluoride concentrations above the WHO (2011) recommended limit of 1.5 mg L^{-1}.

No.	Shoulder F^- mg L^{-1}	Wet F^- mg L^{-1}	Dry F^- mg L^{-1}	Average F^- mg L^{-1}	Year Installed
1	2.7	2.7	3.8	3.1	no date
2	0.5	0.3	3.5	1.4	no date
3	no sample	0.4	1.0	0.7	no date
4	1.8	1.7	1.6	1.7	no date
5	no sample	1.3	1.1	1.2	no date
6	no sample	no sample	1.2	1.2	no date
7	0.5	0.4	0.6	0.5	no date
8	no sample	no sample	0.8	0.8	no date
9	no sample	0.4	no sample	0.8	no date
10	0.4	0.5	0.3	0.4	1993
11	1.8	1.7	1.6	1.7	1994
12	1.5	2.7	1.8	2.0	1994
13	0.5	0.4	0.8	0.6	1994
14	0.6	0.7	no sample	0.7	1995
15	0.4	0.3	0.5	0.4	1996
16	0.4	0.2	0.6	0.4	1997
17	0.9	0.6	0.8	0.8	1998
18	0.5	0.5	0.5	0.5	2003
19	0.6	0.6	3.8	1.7	2004
20	0.4	0.3	0.4	0.4	2004
21	1.6	0.5	1.4	1.2	2004
22	0.7	0.2	0.5	0.5	2004
23	0.6	0.2	0.7	0.5	2004
24	1.0	0.6	1.0	0.9	2004
25	1.7	1.7	1.8	1.7	2004
26	0.5	0.5	1.5	0.8	2004
27	no sample	no sample	0.8	0.8	2004
28	no sample	no sample	1.2	1.2	2004
29	1.1	0.7	1.0	0.9	2004
30	0.4	0.4	no sample	0.4	2004
31	0.6	0.5	0.6	0.5	2006
32	2.4	2.5	2.4	2.4	2006
33	0.7	0.8	0.8	0.8	2006
34	0.4	0.4	0.6	0.5	2007
35	1.5	1.3	1.5	1.4	2007
36	no sample	no sample	1.2	1.2	2007
37	2.4	2.5	2.3	2.4	2007
38	0.3	0.2	0.3	0.3	2008
39	2.7	2.6	2.5	2.6	2008
40	0.4	no sample	0.5	0.5	2010

Table 2.5 presents the seasonal fluoride concentrations for 40 open wells in Namoo. The open wells, which are shallower than the hand-pump wells, generally have lower fluoride concentrations and more seasonal fluctuation. Just one open well has an average value above 3.0 mg L^{-1}, although most of the year it is 2.7 mg L^{-1}, and 9 of the 40 open wells have fluoride concentrations above the WHO recommended limit (WHO, 2011). Most of the highest fluoride open wells are in Done and Koom, with a few moderately high fluoride wells in the Akaamo (Fig. 2.4).

The pH, alkalinity as bicarbonate (HCO_3^-), and conductivity are presented in Table 2.6 for the hand-pump wells and in Table 2.7 for open wells, using wet and dry season data only. The average, minimum, maximum, and median values are presented at the bottom of each table. The temperature and dissolved oxygen are not included in the table, but the values did not vary dramatically. The groundwater temperature for all wells averaged 30.1 ^oC (std dvn = 0.9), and the dissolved oxygen averaged 4.3 mg L^{-1} (std dvn = 0.9). Silica concentrations collected in 2010 from 10 hand-pump wells in the Bongo district (including Namoo) ranged from 60-86 mg L^{-1} with an average of 76 mg L^{-1}.

3.2.2. Laboratory analyses: major ions

Major anions and cations were analyzed for groundwater samples collected in the late wet (September) and dry (April) seasons for hand-pump wells (Table 2.6) and open wells (Table 2.7). The average, minimum, maximum, and median values are listed in the bottom rows of each table. The fluoride concentrations presented in Tables 2.6 and 2.7 include wet and dry season data only (no shoulder season as included in Tables 2.4 and 2.5).

Table 2.6. Average wet and dry season water chemistry data for hand-pump wells (standard deviation in brackets). Overall, average, minimum, maximum, and median values are at the bottom of the table. Shaded values are above WHO (2011) recommended safe limit: 1.5 mg F^- L^{-1} and 50 mg NO_3^- L^{-1}.

No.	pH [stdv]	Cond µS cm^{-1} [stdv]	HCO_3^- mg L^{-1} [stdv]	F^- mg L^{-1} [stdv]	SO_4^{2-} mg L^{-1} [stdv]	NO_3^- mg L^{-1} [stdv]	Cl^- mg L^{-1} [stdv]	Na^+ mg L^{-1} [stdv]	K^+ mg L^{-1} [stdv]	Ca^{2+} mg L^{-1} [stdv]	Mg^{2+} mg L^{-1} [stdv]
1	7.0[0.1]	399[27]	167[--]	2.6[0.0]	5.7[0.4]	32.8[3.8]	17.2[1.9]	24.2[0.6]	3.7[0.9]	34.9[0.5]	16.6[0.4]
2	7.0[0.1]	352[50]	159[--]	2.1[0.1]	4.3[0.1]	23.7[0.9]	12.4[0.2]	26.5[0.3]	2.8[0.3]	26.6[0.3]	13.2[0.3]
3	7.1[0.1]	316[42]	114[72]	1.6[0.0]	2.7[1.1]	15.1[3.8]	30.1[31.4]	23.0[0.2]	2.5[0.5]	24.6[0.1]	12.4[0.4]
4	7.3[0.1]	416[49]	244[--]	2.0[0.1]	7.1[3.0]	8.6[0.3]	6.8[1.4]	35.0[5.3]	5.1[0.9]	36.4[8.1]	14.1[0.7]
5	7.1[0.1]	416[40]	137[56]	2.9[0.1]	7.1[0.3]	46.0[2.5]	26.7[0.2]	23.4[0.1]	2.9[0.0]	37.2[0.6]	16.6[0.1]
6	6.3[0.2]	289[35]	74[28]	0.6[0.0]	5.8[2.0]	47.8[13.8]	19.9[5.7]	29.4[0.1]	3.5[0.4]	19.1[3.0]	6.8[0.4]
7[a]	6.9[0.2]	207[24]	95[--]	4.5[----]	2.2[0.0]	24.6[2.8]	3.0[0.8]	18.0[1.7]	1.9[0.6]	16.2[0.8]	6.8[0.7]
8	7.2[0.0]	392[37]	212[2]	0.7[0.3]	5.9[0.71	16.4[1.9]	12.6[4.7]	28.2[0.7]	5.4[3.2]	34.3[0.7]	15.7[0.2]
9	7.2[0.0]	379[42]	277[47]	0.9[0.2]	3.3[3.1]	0.3[0.2]	2.4[0.9]	31.3[0.4]	4.6[0.5]	31.6[1.3]	14.7[0.1]
10	7.1[0.1]	340[16]	221[28]	1.6[0.1]	2.2[0.8]	7.8[4.7]	4.5[1.1]	21.4[0.8]	2.8[0.3]	29.4[1.4]	16.2[0.8]
11	7.1[0.0]	297[30]	179[23]	1.6[0.0]	1.9[0.1]	17.3[0.6]	6.7[0.4]	23.6[0.1]	2.6[0.8]	31.8[0.2]	12.2[0.1]
12	6.9[0.0]	389[40]	123[14]	2.5[0.1]	6.1[0.2]	61.8[0.3]	23.2[2.1]	22.3[0.1]	2.4[0.1]	32.9[0.2]	15.3[0.2]
13	7.2[0.1]	322[18]	174[29]	4.1[0.6]	2.8[0.1]	31.9[1.3]	9.9[1.6]	17.1[0.5]	3.0[1.6]	32.3[2.9]	13.6[0.6]
14	7.4[0.3]	437[52]	206[47]	3.4[0.2]	4.1[3.5]	32.1[29.7]	13.5[14.2]	21.4[0.1]	4.7[3.6]	43.5[0.4]	18.5[0.3]
15	7.1[0.4]	384[66]	142[--]	3.4[0.5]	7.8[0.6]	43.4[20.0]	18.6[0.4]	25.9[1.8]	4.1[0.6]	35.0[2.5]	12.6[0.6]
16[b]	7.0[0.6]	292[13]	81[9]	3.5[0.1]	3.6[0.1]	61.8[6.0]	10.0[1.3]	27.0[1.6]	3.0[0.8]	21.2[3.5]	8.4[0.1]
17[b]	7.0[0.2]	296[37]	156[16]	2.9[0.1]	2.4[---]	22.4[0.3]	8.2[0.1]	17.2[0.2]	2.2[0.8]	22.9[0.1]	14.4[0.3]
Avg	**7.0**	**348**	**162**	**2.4**	**4.4**	**29.0**	**13.3**	**24.4**	**3.3**	**30.0**	**13.4**
Stdv	**0.2**	**61**	**57**	**1.2**	**2.0**	**18.2**	**8.2**	**4.9**	**1.1**	**7.3**	**3.4**
Min	**6.3**	**207**	**74**	**0.6**	**1.9**	**0.3**	**2.4**	**17.1**	**1.9**	**16.2**	**6.7**
Max	**7.4**	**437**	**277**	**4.5**	**7.8**	**61.8**	**30.1**	**35.0**	**5.4**	**43.5**	**18.5**
Med	**7.1**	**352**	**159**	**2.5**	**4.1**	**24.6**	**12.4**	**23.6**	**2.9**	**31.8**	**14.1**

[a]Well was closed/not flushed prior to wet season sampling; [b]well closed for both wet and dry season/not flushed prior to sampling.

Table 2.7. Average wet and dry season water chemistry data for open wells. Overall average, minimum, maximum, and median values are at the bottom of the table. Shaded values are above WHO (2011) recommended limit: 1.5 mg F^- L^{-1} and 50 mg NO_3^- L^{-1}.

No.	pH [stdv]	Cond µS cm^{-1} [stdv]	HCO_3^- mg L^{-1} [stdv]	F^- mg L^{-1} [stdv]	SO_4^{2-} mg L^{-1} [stdv]	NO_3^- mg L^{-1} [stdv]	Cl^- mg L^{-1} [stdv]	Na^+ mg L^{-1} [stdv]	K^+ mg L^{-1} [stdv]	Ca^{2+} mg L^{-1} [stdv]	Mg^{2+} mg L^{-1} [stdv]
1	7.4[0.1]	316[33]	161[14]	1.7[0.0]	3.1[0.1]	14.2[1.3]	6.3[0.1]	25.5[0.1]	2.0[0.1]	26.7[1.6]	11.0[0.0]
2	7.3[0.0]	327[29]	176[12]	1.0[0.7]	7.9[4.8]	4.4[1.3]	12.9[11.5]	25.5[2.9]	3.4[1.6]	30.8[1.0]	9.4[1.9]
3	7.4[0.0]	367[59]	187[27]	2.4[0.1]	3.9[0.2]	19.5[2.5]	10.1[1.2]	27.4[4.7]	2.3[0.2]	37.5[0.7]	12.0[0.4]
4	7.2[0.1]	410[71]	193[---]	2.5[0.0]	6.5[2.1]	32.1[1.6]	16.9[0.2]	27.2[1.9]	3.3[0.1]	40.0[3.2]	12.7[0.4]
5	7.3[0.0]	425[100]	236[42]	1.2[0.2]	3.9[4.4]	5.7[4.4]	10.2[11.9]	39.7[15.6]	3.1[0.8]	39.3[3.2]	13.6[0.0]
6	6.8[---]	363[---]	148[---]	0.7[---]	14.1[---]	6.6[0.0]	19.8[---]	24.3[---]	9.4[---]	27.9[---]	8.5[---]
7	7.4[0.2]	453[64]	214[---]	2.4[0.1]	4.9[6.2]	13.8[18.0]	8.8[11.3]	46.4[2.0]	2.1[0.5]	36.9[0.2]	12.4[0.1]
8	7.1[0.4]	317[11]	136[28]	0.5[0.1]	11.5[1.3]	26.6[0.0]	18.2[4.7]	17.8[1.5]	13.1[0.6]	37.6[6.6]	5.0[0.0]
9	7.3[---]	417[---]	205[---]	1.0[---]	18.4[---]	42.1[---]	19.3[---]	22.2[---]	5.6[---]	56.6[---]	10.2[---]
10	7.2[0.0]	411[223]	129[20]	0.3[0.1]	12.8[14.6]	36.3[30.1]	32.8[34.9]	37.2[19.2]	2.9[2.7]	36.4[19.0]	7.2[1.5]
11	7.3[0.1]	268[35]	130[54]	0.3[0.2]	3.7[1.7]	19.0[1.9]	5.7[1.9]	10.3[6.3]	10.7[9.0]	29.0[5.4]	7.7[5.4]
12	7.2[0.0]	411[223]	193[77]	0.5[0.1]	8.2[7.7]	20.4[3.8]	19.0[17.3]	35.4[21.2]	1.4[0.2]	38.0[14.8]	12.0[3.4]
13	7.4[0.1]	261[33]	110[52]	0.4[0.1]	5.8[4.9]	21.9[6.0]	11.0[7.3]	19.4[0.1]	2.2[0.9]	23.7[4.2]	8.7[6.2]
14	7.4[0.2]	210[1]	85[20]	0.5[0.4]	2.6[1.3]	26.8[6.6]	10.6[10.3]	13.3[0.7]	4.6[3.0]	18.2[0.7]	5.8[4.1]
15	7.1[NA]	1091[---]	300[---]	0.4[---]	38.6[---]	97.4[---]	93.8[---]	41.2[---]	149[---]	64.2[---]	17.0[---]
16	7.3[0.0]	212[83]	120[38]	0.4[0.3]	2.0[0.6]	10.4[13.5]	7.5[4.5]	18.3[6.6]	4.2[3.4]	19.4[7.9]	5.9[6.2]
17	7.2[0.0]	472[272]	170[84]	0.4[0.1]	11.3[12.3]	42.3[21.6]	29.4[25.6]	44.3[33.6]	2.2[1.4]	42.7[18.5]	8.4[1.4]
18	7.4[0.1]	418[119]	323[12]	0.5[0.0]	9.8[5.3]	2.2[1.9]	13.1[13.2]	43.6[16.3]	7.1[5.4]	50.8[2.5]	24.2[2.0]
19	7.2[0.1]	667[99]	254[21]	0.7[0.1]	11.0[1.6]	72.8[2.8]	43.7[5.4]	44.5[6.0]	5.0[1.7	53.1[1.3]	30.2[0.4]
20	7.4[NA]	489[---]	232[---]	0.4[---]	20.7[---]	4.9[---]	18.8[---]	46.0[---]	3.6[---]	46.8[---]	7.4[---]
21	7.3[0.1]	213[13]	109[---]	0.6[0.3]	2.9[0.4]	9.7[8.1]	6.9[1.1]	16.7[3.0]	2.4[1.3]	22.0[3.5]	5.1[1.3]
22	7.2[---]	244[---]	------	1.2[---]	2.5[---]	13.7[---]	6.7[---]	25.3[---]	2.3[---]	21.4[---]	7.3[---]
23	7.4[0.0]	374[49]	207[35]	0.8[0.0]	4.0[0.4]	30.3[0.9]	8.5[3.6]	25.8[0.4]	4.2[3.6]	33.7[1.1]	15.0[1.6]
24	7.4[0.2]	491[214]	253[35]	1.7[0.1]	2.9[2.7]	5.8[4.4]	28.0[21.6]	37.9[17.3]	2.0[0.5]	47.4[18.5]	15.3[1.6]
25	7.5[0.1]	417[204]	262[50]	1.4[0.1]	6.3[5.2]	3.9[0.2]	11.1[11.1]	45.1[32.1]	1.9[0.6]	31.4[9.1]	12.8[0.0]
26	7.5[0.2]	288[74]	185[6]	2.2[0.6]	1.2[1.2]	5.5[4.8]	4.6[4.2]	36.1[12.1]	1.6[0.1]	18.0[1.3]	8.1[0.9]
27	7.9[---]	620[---]	315[---]	1.4[---]	13.5[---]	6.6[---]	15.5[---]	103.0[---]	4.0[---]	11.6[---]	12.6[---]
28	7.4[0.2]	436[177]	238[64]	1.7[0.2]	4.1[2.6]	3.7[0.4]	11.9[11.4]	34.8[17.4]	2.0[0.1]	35.0[8.8]	18.2[3.8]
29	7.0[0.3]	157[86]	-------	0.4[0.1]	1.4[0.1]	15.5[13.2]	6.0[2.1]	7.5[1.7]	4.2[2.0]	20.5[14.4]	3.0[1.5]
30	7.1[0.1]	325[68]	167[57]	3.3[0.8]	6.4[3.3]	31.0[25.0]	14.6[8.3]	19.7[5.7]	3.4[0.0]	34.0[7.5]	10.4[3.9]
31	7.2[0.2]	237[117]	126[122]	2.2[2.4]	3.3[0.9]	18.8[4.7]	8.8[1.1]	14.3[8.6]	1.9[0.1]	25.5[14.9]	7.7[6.0]
32	7.0[0.2]	223[193]	109[102]	1.9[2.2]	4.8[5.0]	22.4[12.8]	12.1[0.4]	16.4[11.3]	5.4[3.7]	21.7[22.2]	7.9[8.8]
33	7.2[0.0]	209[5]	95[1]	0.5[0.1]	3.4[1.4]	23.5[8.1]	3.6[0.5]	11.7[4.8]	2.3[0.3]	22.6[3.3]	5.9[2.4]
34	7.3[---]	349[---]	239[---]	0.5[---]	3.8[2.8]	5.3[1.9]	8.9[6.0]	27.9[5.4]	2.1[0.1]	37.8[1.7]	8.7[5.4]
Avg	**7.3**	**379**	**185**	**1.1**	**7.7**	**21.0**	**16.3**	**30.3**	**8.1**	**33.5**	**10.8**
Stdv	**0.2**	**172**	**66**	**0.8**	**7.3**	**20.1**	**16.2**	**17.3**	**25.0**	**12.2**	**5.5**
Min	**6.8**	**157**	**85**	**0.3**	**1.2**	**2.2**	**3.6**	**7.5**	**1.4**	**11.6**	**3.0**
Max	**7.9**	**1091**	**323**	**3.3**	**38.6**	**97.4**	**93.8**	**103**	**149**	**64.2**	**30.2**
Med	**7.3**	**365**	**185**	**0.7**	**4.8**	**17.2**	**11.5**	**26.5**	**3.2**	**33.8**	**9.0**

3.2.3. Comparing water chemistry parameters using Spearman correlation coefficients

The correlation between the concentration of various water chemistry parameters and fluoride concentrations presented in Table 2.8 were calculated in GraphPad Prism using the Spearman correlation coefficient (r) from -1 to +1, and the corresponding p value. A negative r value indicates an inverse correlation while a positive r value indicates a direct correlation. The closer the r value is to -1 or +1, the stronger the correlation. The size of the p value strengthens or weakens the statistical significance of the correlation. Using a 95% confidence interval, a maximum p value of 0.05 indicates statistical significance (as opposed to random sampling), and a value greater than 0.05 indicates no statistical significance. The results presented in Table 2.8 show no correlation between each water chemistry parameter and the fluoride concentration with the exception of magnesium which has a direct correlation. There are also statistically significant direct correlations between nitrate and chloride, and between bicarbonate and calcium (Table 2.8). See Helsel and Hirsch (2002) for description of Spearman method of statistical analyses.

Table 2.8. Spearman correlation coefficients (r) from -1 to 1, and p value to determine statistical strength of the correlation (95%) between the concentrations of two ions in groundwater. A negative r value indicates an inverse correlation and a positive r value a direct correlation. A p value >0.05 indicates that the correlation is not real.

Ions Compared	r	p	Correlation
SO_4^{2-} vs. F^-	-0.248	0.079	none
pH vs. F^-	-0.175	0.219	none
NO_3^{2-} vs. F^-	0.176	0.218	none
Ca^{2+} vs. F^-	-0.145	0.311	none
HCO_3^- vs. F^-	-0.052	0.723	none
Cl^- vs. F^-	-0.104	0.470	none
K^+ vs. F^-	-0.231	0.104	none
Na^+ vs. F^-	-0.107	0.455	none
Mg^{2+} vs. F^-	0.371	0.007	direct
NO_3^{2-} vs. Cl^-	0.421	0.002	direct
HCO_3^- vs. Ca^{2+}	0.614	<0.0001	direct

3.3. X-ray diffraction and x-ray fluorescence analyses of Bongo granite

The XRF results are presented in Table 2.9 and XRD results in Table 2.10. The XRD results show that all samples are mostly quartz and feldspar: plagioclase (albite) and alkali (microcline), with minor amphibole and calcite. Sample 3 also has minor biotite. Similarly, the XRF results presented show that the three granite samples are mostly alumino-silicate by weight, followed by potassium (in microcline and mica) and sodium (in albite). All three samples contain a small amount of fluorine. Granite sample 1 has 800 mg kg^{-1} fluorine and the other two granite samples have 1400 mg kg^{-1} fluorine. The fluorine levels in the three granite samples collected in this study are consistent with the fluorine in Bongo granite presented in Apambire et al. (1997), which averaged 792 mg kg^{-1} fluorine and ranged from 200-2000 mg kg^{-1} (n = 12).

Table 2.9. XRF analyses of Bongo granite collected in three locations in the study area, where groundwater fluoride concentrations are high.

Element[a]	**Weight % Granite 1**	**Weight % Granite 2**	**Weight % Granite 3**	**mg kg^{-1} Granite 1**	**mg kg^{-1} Granite 2**	**mg kg^{-1} Granite 3**
O	51.8	50.9	50.7	518000	509000	507000
Si	31.1	28.9	27.9	311000	289000	279000
Al	7.29	8.27	8.09	72900	82700	80900
K	3.26	4.36	4.65	32600	43600	46500
Na	3.74	3.4	3.12	37400	34000	31200
Fe	0.95	1.7	2.31	9500	17000	23100
Ca	1.09	1.09	1.46	10900	10900	14600
Mg	0.24	0.35	0.5	2400	3500	5000
Ti	0.11	0.3	0.39	1100	3000	3900
Sr	0.96	0.15	0.17	960	1500	1700
Ba	0.12	0.17	0.2	1200	1700	2000
F	0.08	0.14	0.14	800	1400	1400
P	0.054	0.093	0.176	540	930	1760
Mn	0.024	0.033	0.047	240	330	470
Rb	0.02	0.027	0.022	200	270	220
Zr	0.017	0.023	0.031	170	230	310
Ce	0.016	0.01	0.012	160	100	120
S	0.019	0.005	0.004	190	50	40
La	0.01	0.005	0.007	100	50	70
Total %	***100.0***	***99.9***	***99.9***	--	--	--

[a]Minor elements not listed (all under 0.01 wght %) include: Pb, Cl, Ga, Ni, Cu, Zn, Cr.

Table 2.10. XRD analyses of Bongo granite collected in three locations in the study area, where groundwater fluoride concentrations are high.

No.	Quartz [α-SiO_2]	Plagioclase[a] (Albite) [$NaAlSi_3O_8$]	Alkali[a] (Microcline) [$KAlSi_3O_8$]	Amphibole[b,c] [$(Mg,Fe,Al)_5(Si,Al)_8O_{22}(OH)_2$][b]	Calcite [$CaCO_3$]	Mica[c] (Biotite) [$K(Mg,Fe)_3(Al,Si3O10)(OH)_2$]
1	19.9%	52.2%	21.7%	5%	1.2%	-
2	33.7%	50.4%	14%	0.9%	1%	-
3	28%	51.7%	16.4%	1.1%	1.2 %	1.6 %

[a]Feldspar; [b]example of an amphibole, which can also contain Ca, K, Na; [c]minerals that may contain fluorine.

4. Discussion

4.1. Geology and hydrogeology

The geology of Namoo has two main types of underlying rock (Fig. 2.8). One is a K-feldspar-rich granitoid, which is mainly Bongo granite and monzonite (2097 +/- 2 Ma). The Bongo granite is represented by the light pink portion on the left side of Fig. 2.8, and is part of the Eburnean Plutonic suite (Geological Map of Ghana (2009), from Murray, 1960, Geological Survey Department of Ghana). In Fig. 2.4 it is the area comprising Done, Tendongo, and Nayire with outcrops of Bongo granite shown in Fig. 2.4 on the left. The other underlying rock type, which is represented by the dark pink on the right side of Fig. 2.8, is hornblende-biotite tonalite, minor granodiorite, minor quartz, and minor diorite (2134 +/- 1 Ma). It is part of the Tamnean Plutonic suite (Geological Map of Ghana (2009), from Murray, 1960, Geological Survey Department of Ghana). In Fig. 2.4 this area comprises Akaamo, Abasikoma, and Awale. The communities of Koom and Abungo, and even parts of Akaamo, likely start at the edge of the transition from Eburnean Plutonic suite (Bongo granite area) into The Tamnean Plutonic suite (Fig. 2.4 and 2.8).

The portion of the study area underlain by, and containing outcrops of, Bongo granite is also the region with the highest fluoride groundwater (Fig. 2.4). The Bongo

granite contains biotite (sample 3 only) and amphibole (see Table 2.10), both of which can contain fluorine (Boyle, 1976). The most important minerals generally affecting aqueous fluoride concentrations are fluorite (CaF_2), apatite ($Ca_{10}(PO_4)_6(F, OH, Cl)_2$), micas (e.g. biotite), amphiboles (see Table 2.10), and villiaumite (NaF) – but especially fluorite due to its higher solubility than the other minerals (Apambire, 1996; Apambire et a., 1997). Bongo granite analyzed by Murray (1960) contained the same minerals as the samples presented in Table 2.10, except calcite, and also included trace accessory fluorine (Table 2.9). In addition, 25 thin sections of Bongo granite collected by Apambire (2000) summarized the mineralogy as follows: quartz 4-30%, microcline 22-75%, plagioclase 3-40%, with more variable biotite and horneblende. Low concentrations of fluorite at 0.1-0.2% and apatite at 0.1-1% were also identified in the thin sections.

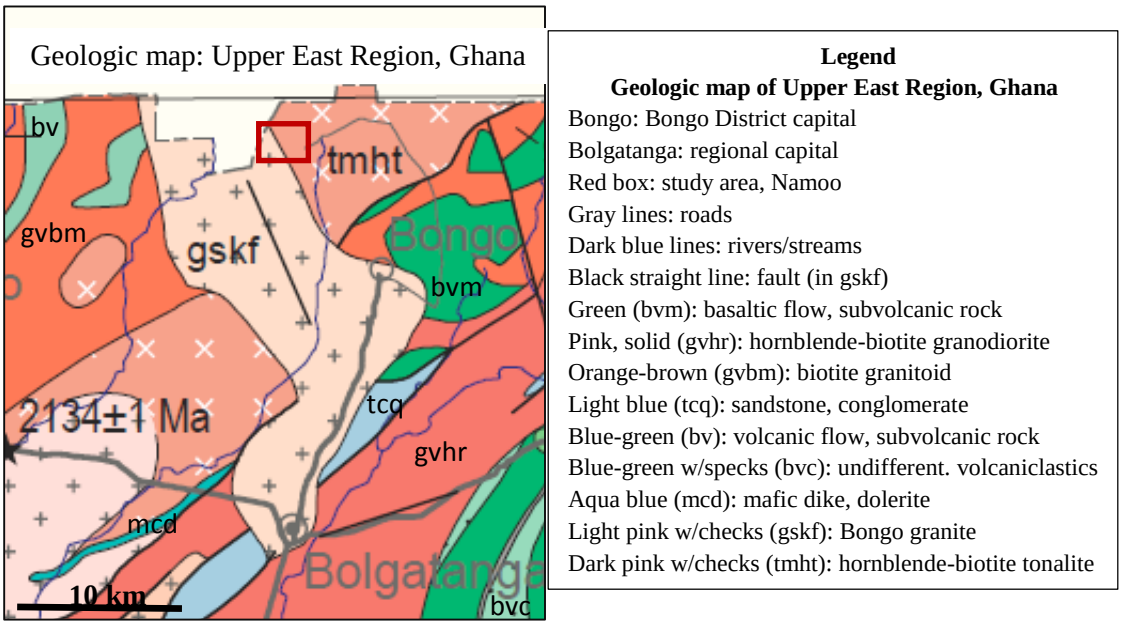

Fig. 2.8. Major geology on the study area of Namoo (red box), Bongo District, Upper East Region, Ghana. Two distinct underlying rock types exist: gskf (2097 +/- 2 Ma) = k-feldspar-rich granitoid mainly Bongo granite and monzonite, and tmht (2134 +/- 1 Ma) = hornblende-biotite tonalite, minor granodiorite, minor quartz diorite. From Geological Map of Ghana (2009), modified from Murray (1960), Geological Survey Department of Ghana.

The fluorite and apatite concentrations were likely too low to be identified in the XRD analyses of Bongo granite presented in this work (Table 2.10), although fluorine is present in the Bongo granite samples (Table 2.9).

The study area is within a basement aquifer, which is described by Wright (1992) as having two hydrologically connected components. One is an overlying cover that is mostly clay or clay-sand mixtures with high porosity but low permeability, and the other is fractured bedrock which is more conductive. The weathered over-layer can be as thick as 100 m, but is generally no more than 30 m, with the vast majority of wells in the region installed within the over-layer (Apambire et al., 1997). Martin (2006) documented that the median borehole depth was 37 m for 32 well logs, with the majority of drilled wells installed through the weathered zone and a few meters into fresh rock. However, only 3 of the 32 boreholes were categorized as tapping the fractured rock, while the others tapped the regolith aquifer. Well yield information was not collected in the study area, but the yields for 13 other boreholes in the Bongo District were provided by the Community Water and Sanitation Agency in the regional capital of Bolgatanga. The range was 13-100 L min^{-1}, with an average value of 34.7 L min^{-1}. Nine of the 13 boreholes had a yield of 30 L min^{-1} or higher. Martin and van de Giesen (2005) determined that groundwater exploitability in the region is good for drilled wells with a yield of 30-80 L min^{-1} and extraction depth up to 50 m, and is moderate for drilled wells with yields between 13-30 L min^{-1} and the same extraction depth.

Groundwater recharge from precipitation was not estimated for this study, but Martin and van de Giesen (2005) estimated approximately 4 cm of recharge for 90 cm rainfall – about 4.4% – for areas in Ghana and Burkina Faso with weathered rock

(sources: Diluca and Müller, 1985; Dieng et al., 1991 and references therein; Millville, 1991). Martin (2006) observed that higher water levels in wells tend to be in the higher elevation granitic areas, which may be due to increased recharge rates coupled with decreased conductivity. Dominico and Schwartz (1998), also state that high elevation areas are generally considered recharge zones. In the current study, the highest elevation area of Done (Fig. 2.4, 2.9) also has relatively high water levels measured from boreholes – especially in lower Done (Table 2.3).

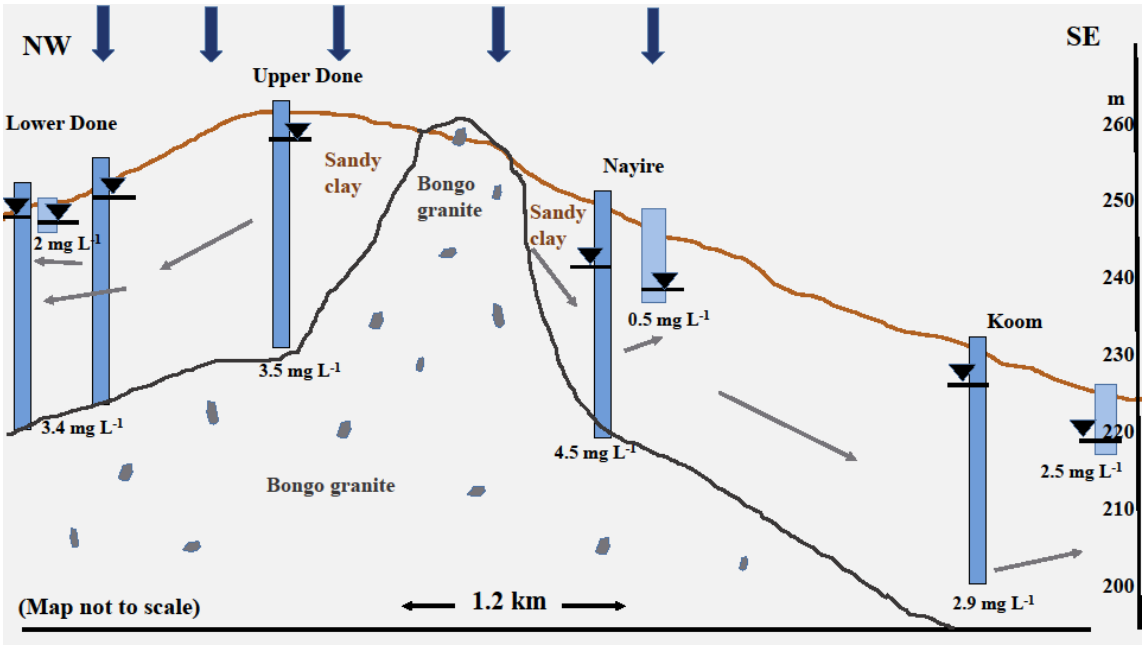

Fig. 2.9. Cross section of the highest groundwater fluoride portions of the study area (Done, Nayire). Done is a recharge zone (wide vertical arrows) and is the main location of Bongo granite. Nayire has both very high and very low fluoride groundwater. Thin arrows show the direction of groundwater flow and average fluoride concentrations are presented (in mg L^{-1}) by each well. Deeper wells are drilled and were closed when measurements were taken in November 2011. The shallow wider wells are hand-dug open wells. The inverted black triangles are the water level.

In addition, with one exception in Done, the communities of Done, Tendongo, Nayire, and Abungo have high wet season water levels in shallower hand-dug open wells. The higher elevation areas (e.g. 242-261 m) tend to have the most elevated wet season water levels and greatest seasonal fluctuation, and are likely within the recharge area with

low conductivity. Open wells in the Tendongo and Nayire areas show the greatest fluctuation between wet and dry seasons in the entire study area, and both wells are deeper than most of the open wells in the study area (Fig. 2.6). The continuous water level measurements from Done boreholes in Fig. 2.7 show a drop in the water level by late September to early October. The borehole in lower Done (249 m) has a water level close to the land surface. Because of this, it responds to precipitation sooner and more quickly than the upper Done borehole (elev. 261 m) (see Table 2.3, Fig. 2.7 and 2.9).

4.2. Groundwater fluoride and water chemistry

An anomaly in the distribution of fluoride occurs in the community of Nayire where both the lowest (0.6 mg L^{-1}) and the highest (4.5 mg L^{-1}) average borehole groundwater fluoride concentrations in the study area are within 100 m of each other. In Table 2.6, they are wells 6 and 7 respectively. Well 6 (0.6 mg F^{-} L^{-1}) has lower pH and bicarbonate, and slightly higher conductivity than well 7 (4.5 mg L^{-1}). Only calcium and magnesium are similar in both wells; otherwise, the concentrations of other dissolved ions are higher in well 6 than well 7 (see Table 2.6). It is surprising to find a very low fluoride borehole so close to the Bongo granite. The high fluoride borehole was apparently drilled through a thick layer of rock, presumably Bongo granite. In general, the lowest groundwater fluoride concentrations are in the community of Awale. Most of the wet season water levels in Awale are approximately 3 m below land surface (Fig. 2.6). It is also the lowest elevation area in Namoo and approximately 500 m to the east is a seasonally flowing riverbed. The low elevation, water level measurements, and proximity to an ephemeral river indicate that most groundwater flow in Awale is generally toward the river discharge zone. Increased hydraulic conductivities are

expected in low elevation areas like Awale, which is away from the granitic area and close to a discharge area (Martin, 2006).

The high fluoride communities are, as expected, in or close to the Bongo granite with a decrease in groundwater fluoride at increased distance from the granitic areas. There does not appear to be a statistically significant correlation between major-ion water chemistry and fluoride concentrations (Table 2.8), with one exception - there is a statistically significant direct correlation between magnesium and fluoride (Table 2.8). This may be due to the dissolution of fluorine containing biotite and amphibole since both likely contain magnesium (Table 2.10). Results from Chae et al. (2006) indicate that biotite in granite are correlated to elevated fluoride concentrations in groundwater; and Kanisiwa (1979) identified both biotite and amphibole in granite as high in fluorine.

There is a strong direct correlation between nitrate and chloride (Table 2.8), which is likely due to the abundant agricultural activity and animal waste as fertilizer (Appelo and Postma, 2005). Human waste may also contribute nitrate and chloride, but in most cases it would not be concentrated in one area since latrines are not common. Schools have urinals, and a very small minority of households have latrines or a septic tank, which is even less common. In four wells (two open and two hand-pump) the nitrate is above the recommended limit for preventing methemoglobinemia or blue baby syndrome (see highlighted wells, Table 2.6, 2.7) (WHO, 2011).

There is also a statistically significant correlation between bicarbonate and calcium (Table 2.8). The Piper diagram (Fig. 2.10) indicates that most groundwater in the study area is classified as Ca-Mg-HCO_3 water (60-80% Ca-Mg). Just three samples are under 50% Ca-Mg – one was collected from an open well in Awale (very high potassium,

Table 2.7 #32 – unusually high conductivity) and two from open wells in Akaamo (one with very high sodium and the other with low calcium and magnesium). Apambire et al. (1997) found that groundwater samples collected in locations near Bongo granite are spread between Ca-Mg-HCO_3 and Ca-Na-HCO_3 groundwater, with most in the latter category. Results of this current study, however, identified most groundwater samples as Ca-Mg-HCO_3. In addition, although the Bongo granite is ~50% albite ($(NaAlSi_3O_8)$ in Table 2.10), which is sodium-rich, high Na-HCO_3 groundwater is not present in Namoo. The relevance is that high Na-HCO_3 conditions often contribute to high fluoride groundwater due to ion exchange between calcium in solution and sodium on the solid surface, resulting in a decrease in dissolved calcium as it exchanges with sodium which then causes more dissolution of fluorite (Chae et al. 2007). Apambire et al. (1997) similarly documented that elevated pH and sodium (high Na-HCO_3) groundwater conditions which frequently result in high fluoride water are not occurring in the region.

Feldspar and quartz dissolution likely influence groundwater chemistry in Namoo, with minor contributions from calcite, biotite, fluorite, and amphibole - especially in the recharge areas. Most groundwater in Namoo has moderate to elevated bicarbonate (Fig. 2.11), which is consistent with data presented in Apambire et al. (1997). In general, the bicarbonate concentrations are relatively low in the recharge areas of upper Done and Nayire (most < 100 mg $HCO_3^- L^{-1}$), and are highest in Akaamo and Abasikoma (> 200 mg $HCO_3^- L^{-1}$). The dissolution of silicates and movement along the flowpath tends to result in increased bicarbonate concentrations (Dominico and Schwartz, 1998), as observed in this study. Precipitation contributes CO_2 charged groundwater which dissolves minerals, resulting in increased bicarbonate (alkalinity) and cations in solution.

These weak acid- strong base reactions also tend to result in the formation of kaolinite (Dominico and Schwartz, 1998).

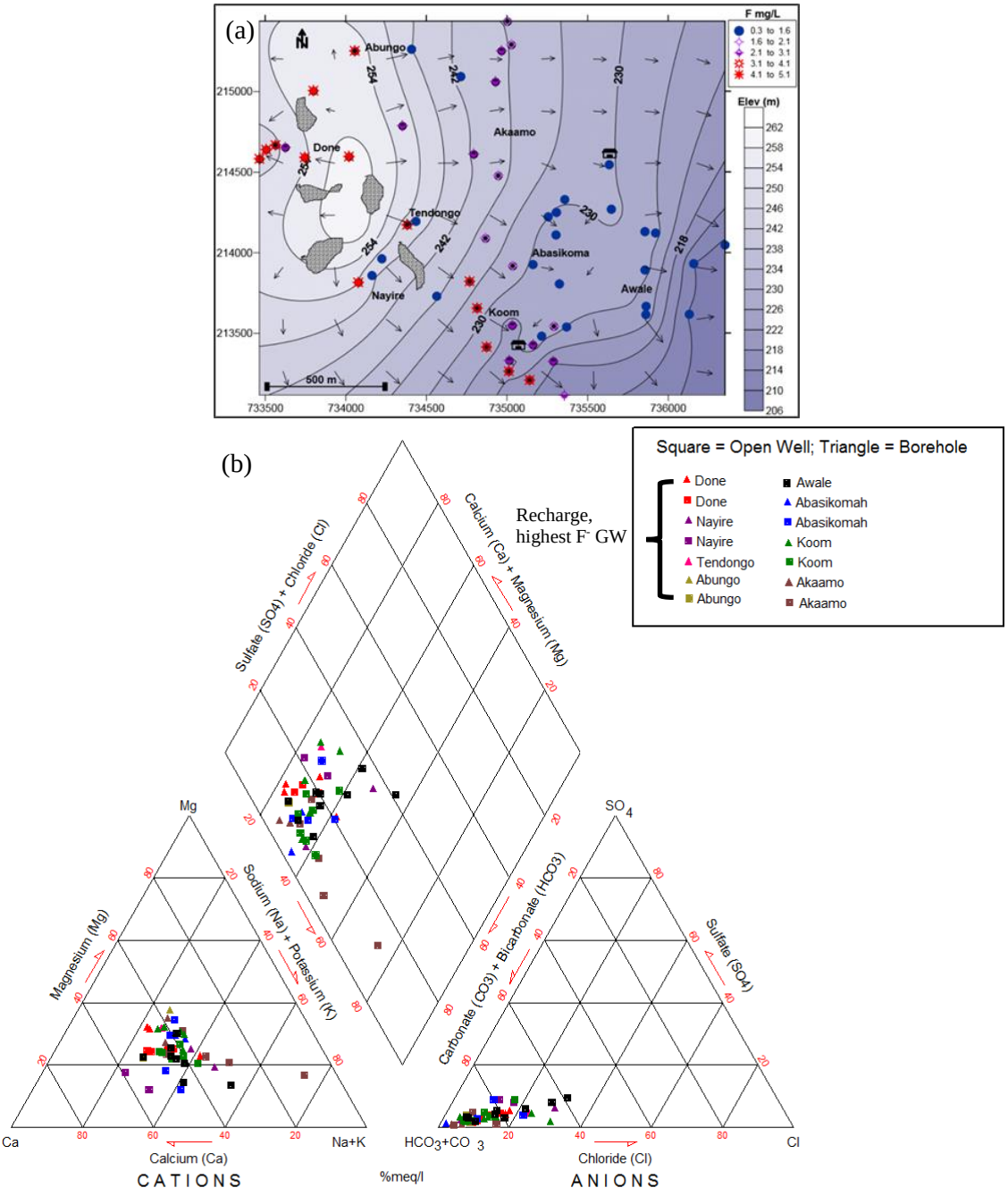

Fig. 2.10. (a) Map of study area with location of communities, wells and fluoride concentrations, and general direction of groundwater flow; (b) Piper diagram of the distribution of major ions in water samples collected from open wells and drilled wells (boreholes). The four communities, Done-Abungo, in the left column of the legend are within or close to Bongo granite and at higher elevation. The four communities in the right column are getting farther from Bongo granite (except part of Koom) and are at lower elevation/down gradient from main recharge area (see (a)).

The stiff diagrams in Fig. 2.11 present the average major ion concentrations for open wells (OW) and deeper drilled boreholes (BH) with hand-pumps in each of the eight communities. The cations are widely and evenly distributed, with calcium usually slightly higher than magnesium, sodium, and potassium (Fig. 2.11). The most notable exception is groundwater in the Akaamo open wells (primarily due to one very high sodium open well – see Fig. 2.10). The anions are dominated by bicarbonate (Fig. 2.10, 2.11), which is important regarding the possible use of fluoride adsorption filters to remove excess fluoride from drinking water. This is because bicarbonate competes with fluoride for adsorption sites (Tang et al., 2009), and may hinder the fluoride adsorption capacity of the filters if the bicarbonate concentration is high enough.

Fig. 2.11 indicates that the shallow open wells (OW) and deeper borehole (BH) hand-pump wells in Koom have similar average water chemistry, and near-by Awale has similar groundwater chemistry to Koom (Awale has OWs only and lower fluoride). In Abasikoma the average groundwater chemistry in the shallow (OW) and deeper (BH) wells is similar, with slightly higher bicarbonate than in Awale and Koom groundwater, which are located just to the east and south (Fig. 2.4). In Done, where the groundwater level is highest, the shallow and deep well water chemistries are clustered close together in the Piper diagram (Fig. 2.10) and the average water chemistries presented in the stiff diagrams in Fig. 2.11 are similar as well. The overall general pattern presented in Fig. 2.11 is that the communities with highest groundwater fluoride, which are in the recharge zone, have lower average dissolved ions and lower bicarbonate. These would be Done, Nayire, Tendongo, and Abungo, which are also within or close to the granitic area. The

lower dissolved ion concentrations are likely due to precipitation recharge, where the other more distant communities are moving closer to discharge zones, which results in groundwater with higher ionic concentrations and bicarbonate due to continued evolution of groundwater chemistry along the flowpath.

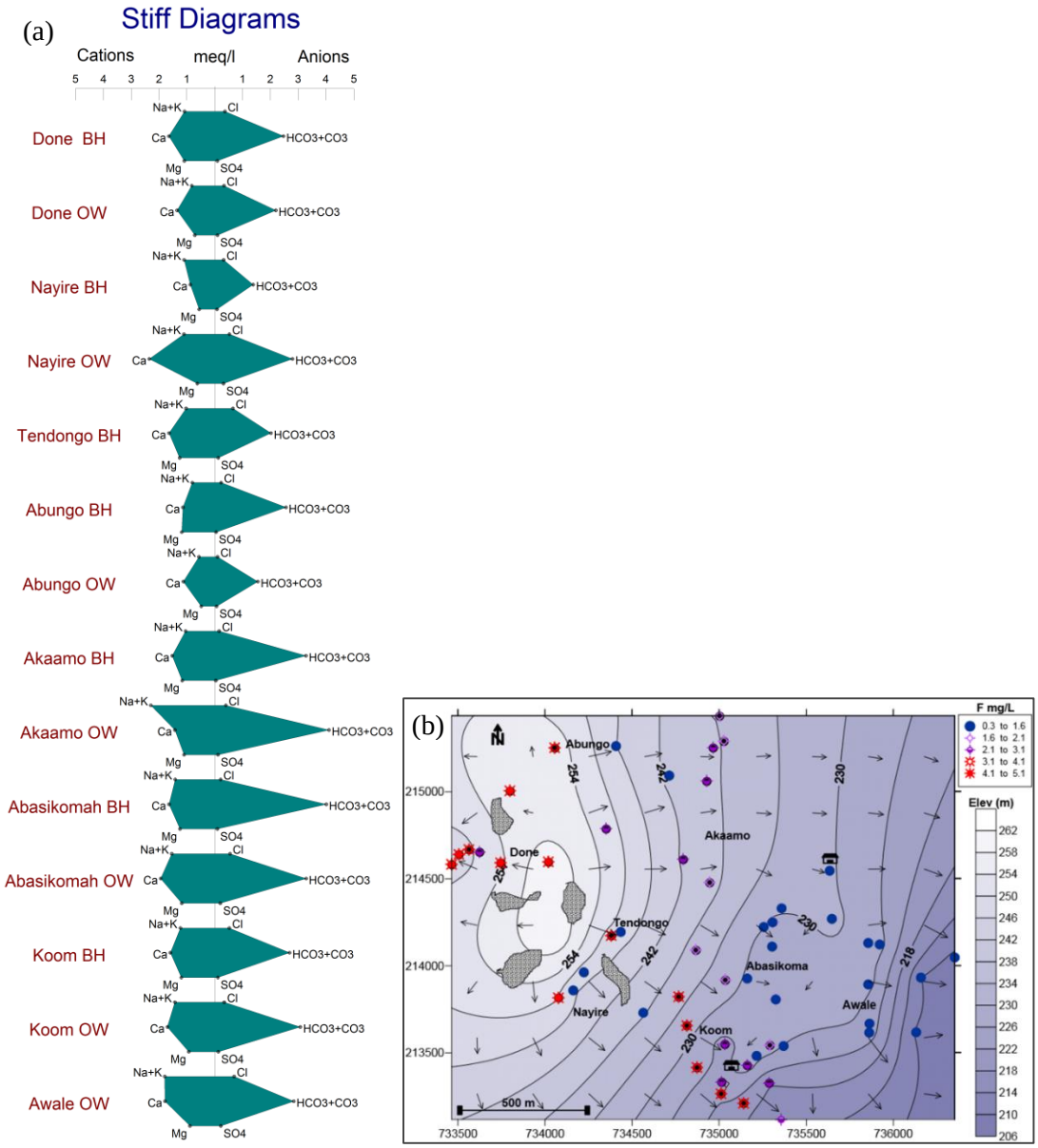

Fig. 2.11. (a) Stiff diagrams of average major ion concentrations for hand-pump boreholes (BH) and hand-dug open wells (OW). Awale has no BHs, and Tendongo has one OW but with incomplete water chemistry data so it was omitted. Done-most of Abungo above are in or near Bongo granite. Other parts of Abungo and part of Koom are close as well. Akaamo, Abasikoma, Awale, and other parts of Koom are the farthest from Bongo granite, and at lower elevation (down gradient); (b) map of study area with location of communities, wells and fluoride concentrations, and general direction of groundwater flow.

4.3. Saturation indices of major minerals in Namoo groundwater

PHREEQC (Parkhurst and Appelo, 1999) was used to determine the saturation indices of fluorite and other major minerals using the average concentrations of major ions in the hand-pump wells at the bottom of Table 2.6, and in open wells at the bottom of Table 2.7. Using the PHREEQC database the results show that, under these conditions, groundwater reaches saturation with respect to fluorite at fluoride concentrations above 4.7 mg L^{-1} for hand-pump wells and above 4.6 mg L^{-1} for open wells. These fluoride concentrations are about the maximum fluoride concentrations found in the study area. Other potential minerals, such as calcite, aragonite, and dolomite, were under-saturated, so if present in the aquifers they would dissolve. This may explain why the highest fluoride concentrations in the area are around 4.6 mg L^{-1}, both for this study and in Apambire et al. (1997). Such conditions may prevent further dissolution of fluorite from rock.

When input parameters of the solution are varied, the most notable change in the dissolved fluoride concentrations is due to calcium because it influences fluorite precipitation. For example, increasing the calcium concentration to its maximum of 64.2 mg L^{-1} (Table 2.7 open wells) results in saturation of fluorite in groundwater at a fluoride concentration of 3.6 mg L^{-1}. Manipulating the other ions had little or no impact on the saturation index of fluorite. Table 2.8 indicates no correlation between calcium concentration and fluoride concentration in water, where PHREEQC shows an inverse correlation. This may be because the calcium concentrations in most groundwater are < 40 mg L^{-1}, which may be too low to influence the fluoride concentration (Table 2.6, 2.7).

The results in Table 2.8 show a strong direct correlation between calcium and bicarbonate (likely calcite dissolution), and chloride and nitrate (from agriculture).

In addition to running PHREEQC to determine the saturation indices of major minerals using the average water chemistry values for open wells and hand-pump wells, the water chemistry data from each well (Table 2.6, 2.7) were also used as input values to determine the saturation indices of major minerals. Silica was consistently super-saturated and talc ($Mg_3Si_4O_{10}(OH)_2$) was often super-saturated, using the concentration of 66 mg SiO_2 L^{-1} in all simulations. Fluorite (CaF_2) was just below saturation at the highest groundwater fluoride concentrations, and was well below saturation at lower groundwater fluoride concentrations. Calcite ($CaCO_3$) and dolomite ($CaMg(CO_3)_2$) were occasionally super-saturated, in particular for open wells – most of the open wells in Akaamo and Abasikoma, and one in Awale, due to higher bicarbonate concentrations (Fig. 2.11). The trend is notable under-saturation (with the exception of fluorite) in the recharge areas in and near Bongo granite, with increasing saturation of major minerals along the flowpath from the primary recharge zones to the discharge zones. Groundwater fluoride concentrations and fluorite saturation decrease as well with distance from the recharge zones. The reason for the decrease in groundwater fluoride is not clear. Dilution and dispersion as groundwater travels radially away from the granitic area and into the larger surrounding areas likely play a role (see Fig. 2.4, 2.5). In addition, fluoride may adsorb to clay (such as kaolinite). Kaolinite ($Al_2Si_2O_5(OH)_4$) is not a strong sorbent for fluoride (Coetzee et al., 2003), but if it is abundant in the aquifer(s) within the study area then even a small percentage of fluoride adsorbing to the aluminols will result in a continuous drop in concentration with distance travelled.

4.4. Potential locations for installing low fluoride wells and for piped water from existing low fluoride hand-pump wells

The optimum location for drilling low-fluoride boreholes to pipe groundwater to higher fluoride areas is Awale which is about 1.5-2 km from the granitic area (Fig. 2.4). The entire community has groundwater fluoride well under 1.0 mg L^{-1}, and it appears to be within a discharge zone so it should have high hydraulic conductivity. In addition to Awale for installing low fluoride boreholes, Abasikoma also has no wells with fluoride above 1.2 mg L^{-1} and is closer to the high fluoride areas. Unfortunately, installing boreholes in any of the other communities may pose a cost risk due to the increased probability of tapping groundwater with fluoride concentrations above the WHO limit of 1.5 mg L^{-1}. The money may be better spent developing a piped system and installing solar panels and wind mills to provide the electrical energy needed to transport the water; and the potential for using solar and wind energy is notable (Table 2.1).

Along with drilling new boreholes, the yield of existing low fluoride hand-pump wells could be obtained to determine their viability for pumping, storing, and then distributing low fluoride water to other communities. This would remove the high cost of drilling a new well. The best choice would be a hand-pump well in Nayire with an average fluoride concentration of 0.6 mg L^{-1}. One concern, however, is that because it is so close to high fluoride groundwater, excessive pumping rates may result in pulling higher fluoride water into the well, which would limit the amount of water that could be pumped and stored. Therefore, the possibility of tapping high fluoride groundwater would first need to be investigated. In addition, there are other existing hand-pump wells that should be considered. One is in Abasikoma with an average fluoride concentration of

0.7 mg L^{-1}, another is at the Abasikoma-Awale border with an average fluoride concentration of 0.9 mg L^{-1}, and a third is at the Abasikoma-Koom border, just west of Awale, with an average fluoride concentration of 1.6 mg L^{-1}. The advantage of the Abasikoma-Awale borehole in particular, is that the groundwater fluoride in the area is very low, but it is also the farthest from the communities with high fluoride groundwater. Of course, the yield of these hand-pump wells would also influence their feasibility as an abundant source of low fluoride drinking water in Namoo.

5. Conclusions

The study area of Namoo in the Bongo District of the Upper East Region of Ghana relies almost entirely on groundwater for household use. In an effort to improve access to water, 12 wells have been drilled and installed with hand-pumps since 2005 and 23 hand-dug open wells have been installed since 2003. Five of these newer open wells and 10 of the newer drilled boreholes with hand-pumps have groundwater fluoride concentrations above the WHO recommended limit of 1.5 mg L^{-1}. Five of the most recently drilled boreholes have an average of 3.4-4.5 mg L^{-1} of fluoride. In addition, four of the newly drilled boreholes remained closed due to high fluoride concentrations, but community members had the hand-pumps installed, thus making them useable. Consuming such high concentrations of fluoride puts users at risk of severe dental fluorosis as well as skeletal fluorosis, which is even more serious (WHO, 1984; WHO, 2011). Therefore, either treated water or other sources of low fluoride water are needed in these communities, and in other similar areas in the region.

Low-cost and low technology water treatment, and small-scale rainwater catchment systems are being considered. Another option that should be considered is to

locate areas with low groundwater fluoride and high enough yield, thus allowing for collection and transport to high fluoride communities. The upfront costs are high, but the long-term access to a reliable water source also increases substantially. If installed properly, the day-to-day maintenance should be low for years to come, unlike water treatment systems which require continual maintenance. However, as with all proposed solutions for improving access to high quality drinking water in very poor communities, the question of who will cover the cost is always present and is rarely resolved. Government subsidized projects would be optimal at least to get them established, but to date this does not appear to be an option.

Acknowledgements

This research was generously supported by the University of Nevada, Reno, the Desert Research Institute, a U.S. Environmental Protection Agency Science to Achieve Results Graduate Research Fellowship, and a Sigma Delta Epsilon-Graduate Women in Science Nell Mondy Fellowship. We thank the Bongo District Assembly for its support, Philomina and Tony Atanga for assisting with the field work, as well as the community of Namoo for its support.

References

Apambire, W.B. 1996. Groundwater Chemistry and the Genesis and Distribution of Groundwater Fluoride in the Bolgatanga and Bongo Districts, Ghana. Unpublished M.S. thesis. Carleton University, Ontario, Canada.

Apambire, W.B., Boyle, D.R., Michel, F.A. 1997. Geochemistry, genesis, and health implications of fluoriferous groundwaters in the upper regions of Ghana. Environmental Geology 33(1) 13-23.

Apambire, W.B. 2000. Geochemical Modeling and Geomedical Implications of Fluoriferous Groundwaters in the Upper East Region of Ghana. Unpublished Ph.D. dissertation, University of Nevada-Reno, Reno, NV, USA.

Atipoka, F.A. 2009. Water supply challenges in rural Ghana. Desalination 248, pp. 212-217.

APHA (American Public Health Association). 1998. Standard Methods for the Examination of Wastewater. American Public Health Association, American Water Works Association, Water Environment Federation publication. APHA, 20th Ed, Washington D.C.

Appelo, C.A.J, Postma, D. 2005.Geochemistry, groundwater, and pollution. CRC Press, second ed., Boca Raton.

Boyle, D.R. 1976. The chemistry of fluoride and its application in mineral exploration 386 p. The University of London, Imperial College of Science and Technology.

Chae, G.T., Yun, S.T., Kim, K., Mayer, B. 2006. Hydrogeochemistry of sodium bicarbonate type bedrock groundwater in the Pocheon spa area, South Korea: rock-water interaction and hydrologic mixing. J. Hydrol. 321, 326-343.

Chae, G.T., Yun, S.T., Mayer, B., Kim, K. H., Kim, S. Y., Kwon, J.S., Kim, K., Koh, Y.K. 2007. Fluorine chemistry in bedrock groundwater of South Korea. Sci. Tot. Environ. 385, 272-283.

Coetzee, P.P., Coetzee, L.L., Puka, R., Mubenda, S., 2003. Characterization of selected South African clays for defluoridation of natural waters. Water SA 29, 331-338.

Dieng, B, Bazie, P., Schmitt, A. 1991. Transfer d'Eau en Milieu Poreux non Saturé. Recharge des Nappes en Climat Soudano-Sahélien. In Utilisation Rationelle de l'Eau des Petits Bassins Versants en Zone Aride. 131-137. Paris: AUPELF-UREF.

Diluca, C., Müller, W. 1985. Evaluation Hydrogeologique des Projets d'Hydraulique en Terrains Cristallins du Bouclier Ouest Africain. Hanover: BGR.

Domenico, P.A., Schwartz, F.W. 1998. Physical and Chemical Hydrogeology. 2nd edition. John Wiley and Sons, Inc. New York.

Helsel, D.R., Hirsch, R.M. 2002. Statistical Methods in Water-Resources, Ch. A3. In: Techniques in Water Resources Investigations of the United States Geological Survey, Book 4 Hydrologic Analysis and Interpretation. U.S. Geological Survey.

Kanisiwa, S. 1979. Content and behavior of fluorine in granitic rocks, Kitakami Mountains, northwest Japan. Chem. Geol. 24, 57-67.

Martin, N. 2006. Development of a water balance for the Atankwidi catchment, West Africa – A case study of groundwater recharge in a semi-arid climate. Ecology and Development Series No. 41, Göttingen, Germany.

Martin, N., van de Giesen, N., 2005. Spatial distribution of groundwater production and development potential in the Volta River basin of Ghana and Burkina Faso. Int. Water Resourc. Assoc. 30, pp. 239-249.

Milville, F. 1991. Étude Hydrodynamique et Quantification de la Recharge des Aquifères en Climat Soudano-Sahélien: Application à un Bassin Expérimental au Burkina Faso. In Soil Water Balance in the Sudano-Sahelian Zone. IAHS Publication no. 199, Proceedings of an International Workshop, Niamey. Niger. Wallingford: IAHS Press.

Murray, R.J. 1960. The geology of the "Zuarungu" 1/2o Field Sheet. Ghana Geological Survey Bulletin 25.

Parkhurst, D.L., Appelo, C.A.J., 1999. User's guide to PHREEQC (version 2) – A computer program for speciation, batch-reaction, one-dimensional transport, and inverse geochemical calculations. U.S. Geological Survey, Denver CO.

Tang, Y., Guan, X., Su, T., Gao, N., Wang, J. 2009. Fluoride adsorption onto activated alumina: Modeling the effects of pH and some competing ions. Colloids Surfaces A: Physicochem. Eng. Aspects 337, 33-38.

WHO (World Health Organization). 1984. Fluorine and Fluorides. Environmental health Criteria 36. World Health Organization, Geneva.

WHO (World Health Organization). 2011. Guidelines for Drinking Water Quality. Volume 1, 4th edition. World Health Organization, Geneva.

Wright, E.P. 1992. The hydrogeology of crystalline basement aquifers in Africa. Geological Society Special Publication no. 66, London.

CHAPTER 3

RECOMMENDATION FOR FLUORIDE LIMITS IN DRINKING WATER BASED ON ESTIMATED DAILY FLUORIDE INTAKE IN THE UPPER EAST REGION, GHANA

Craig, Laura, Lutz, Alexandra, Berry, Kate A., Yang, Wei

Published in: Science of the Total Environment 532 (2015), 127-137.

Abstract

Both dental and skeletal fluorosis caused by high fluoride intake are serious public health concerns around the world. Fluorosis is particularly pronounced in developing countries where elevated concentrations of naturally occurring fluoride are present in the drinking water, which is the primary route of exposure. The World Health Organization recommended limit of fluoride in drinking water is 1.5 mg $F^- L^{-1}$, which is also the upper limit for fluoride in drinking water for several other countries such as Canada, China, India, Australia, and the European Union. In the United States the enforceable limit is much higher at 4 mg $F^- L^{-1}$, which is intended to prevent severe skeletal fluorosis but does not protect against dental fluorosis. Many countries, including the United States, also have notably lower unenforced recommended limits to protect against dental fluorosis. One consideration in determining the optimum fluoride concentration in drinking water is daily water intake, which can be high in hot climates such as in northern Ghana. The results of this study show that average water intake is about two times higher in Ghana than in more temperate climates and, as a result, the fluoride intake is higher. The results also indicate that to protect the Ghanaian population against dental fluorosis, the maximum concentration of fluoride in drinking water for children under 6-8 years should be 0.6 mg $F^- L^{-1}$ (and lower in the first two years of life), and the limit for older children and adults should be 1.0 mg $F^- L^{-1}$. However, when considering that water treatment is not cost-free, the most widely recommended limit of 1.5 mg $F^- L^{-1}$ - which is currently the limit in Ghana - may be appropriate for older children and adults since they are not vulnerable to dental fluorosis once the tooth enamel is formed.

1. Introduction

Fluorine is the most reactive and electronegative of all elements and, as a result, is not found in its elemental form in the environment (Hem, 1985; Weinstein and Davison, 2004). In solution, fluorine tends to ionize to the anion fluoride (F^-). Because fluoride has the same charge and is a similar size as hydroxide (OH^-), it tends to replace hydroxide on mineral structures (Hem, 1985). The outcome of this ion exchange is the presence of fluoride in several common mineral species (Fawell et al., 2006; WHO, 2011) such as fluorspar, apatite, mica, hornblende, and cryolite (Murray, 1986). Fluoride-containing minerals that frequently occur in igneous and sedimentary rocks, are present in the Bongo and Sekoti granitic rocks in the Upper East Region of Ghana (Apambire et al., 1997; Apambire, 2000). Dissolution of these minerals results in notably elevated fluoride concentrations in the near-by groundwater (Apambire et al., 1997; Apambire, 2000; WHO, 2004; WHO, 2011), putting communities that rely on high fluoride groundwater for their drinking water at risk of dental and skeletal fluorosis.

Low concentrations of fluoride in drinking water are considered beneficial by reducing the incidence of dental caries (Fawell et al., 2006; WHO, 2011). However, slightly higher concentrations can cause dental fluorosis in children and adolescents (Whitford, 1997). Dental fluorosis results in permanent discoloration of the teeth, erosion of enamel and pitting (Whitford, 1997), and is prevalent worldwide (Fawell et al., 2006), including the Upper East Region of Ghana (Apambire et al., 1997; Apambire, 2000). Mild dental fluorosis can occur when children consume water with fluoride concentrations from 0.9-1.2 mg F^- L^{-1} (Dean, 1942; WHO, 2011) or even lower (Galagan

and Lampson, 1953; Apambire, 2000), though concentrations above 1.5 mg $F^- L^{-1}$ are more commonly associated with dental fluorosis (WHO, 1984; WHO, 2011).

A more serious adverse health effect caused by long-term exposure to high concentrations of fluoride is skeletal fluorosis, which can result in an increased risk of bone fractures, increased bone density, calcification of the ligaments and tendons, and bone deformity (crippling skeletal fluorosis) (Fawell et al., 2006; NRC, 2006; USEPA, 2010a). Skeletal fluorosis has been documented in regions around the world including parts of India, China, several countries in Africa (Fawell et al., 2006; USEPA, 2010a), and a small number of cases in the United States (USEPA, 2010a and references therein). No cases of skeletal fluorosis have been documented in Ghana to date. Although the dose-response causing skeletal fluorosis is less linear than that for dental fluorosis (NRC, 2006), drinking water concentrations from 3-6 mg $F^- L^{-1}$ are generally associated with skeletal fluorosis, and concentrations above 10 mg $F^- L^{-1}$ are generally associated with crippling skeletal fluorosis (WHO, 1984; WHO, 2011).

To protect human health, the World Health Organization (WHO) developed international guidelines recommending a daily fluoride limit of 1.5 mg $F^- L^{-1}$ (WHO, 2011). However the WHO also qualified this statement by recommending the limit be adapted to local conditions such as climate, water consumption and diet (Fawell et al., 2006; WHO, 2011). In developing national standards and targets, it is particularly important to consider factors like climate, possible fluoride sources, and lifestyle (WHO, 2011). Because water is considered the major contributor of fluoride exposure (Dean, 1942; NRC, 2006), average daily intake of water is used in setting fluoride limits in drinking water (e.g. WHO, 1993; USEPA, 2010b). Unfortunately, regional water

consumption data are generally only available for countries with temperate climates such as Canada (CMNHW, 1981), the United States (Ershow and Cantor, 1989), and the United Kingdom (Hopkin and Ellis, 1980).

In many developing countries, including Ghana, collecting representative water consumption data with which to set national standards is a challenge. This is partly because communities often lack a reliable centralized water distribution system and instead use a variety of communal sources such as wells, rainwater catchment, lakes and streams for household water. Estimating water consumption is also difficult because most households are not accustomed to using exact measurements and taking note of water intake, so asking individuals to estimate how much water is consumed per day may not provide accurate data.

The intent of this study conducted in Ghana's Upper East Region is to (1) monitor daily water intake of selected individuals from young children to elderly adults in order to estimate potential ranges of daily fluoride intake, (2) map the distribution of dental fluorosis in an area with groundwater fluoride concentrations under 1 mg F^- L^{-1} up to 4.6 mg F^- L^{-1}, and (3) correlate patterns of dental fluorosis with fluoride concentrations of the household drinking water. The purpose of collecting these data is to provide recommendations for safe target limits of fluoride in drinking water in order to best protect vulnerable members of the community from dental and skeletal fluorosis. Both the health effects and the challenge of water treatment are considered in making these recommendations.

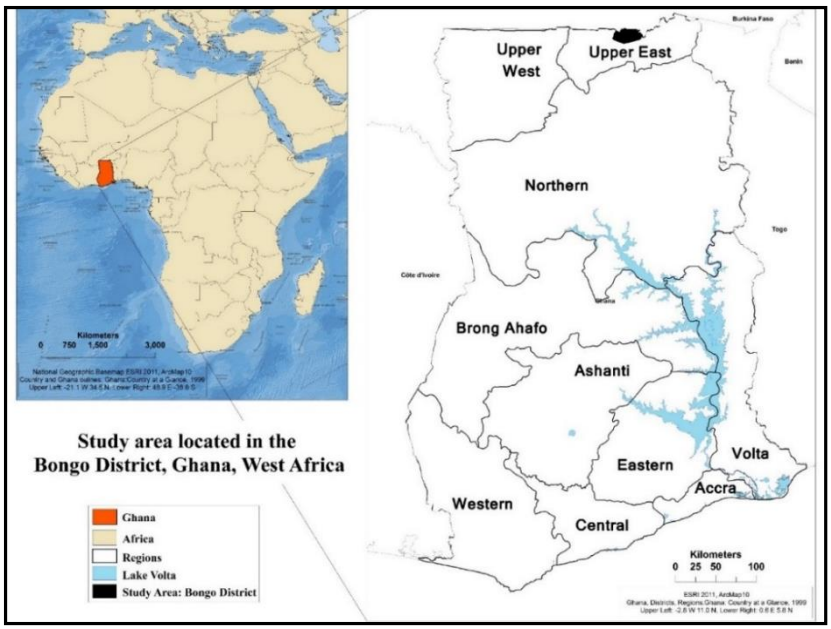

Fig. 3.1. A map of the location of the Bongo District in the Upper East Region, Ghana.

2. Materials and Methods

2.1. Study area

The study area for this research is in the electoral area of Namoo in the Bongo District, Upper East Region of Ghana (Fig. 3.1). This site was chosen because of the ongoing problem of dental fluorosis in the Bongo District due to the abundance of fluoride-rich groundwater (Apambire et al., 1997; Apambire, 2000; Atipoka, 2009). The Namoo electoral area was specifically recommended for a baseline study by the Bongo District Assembly because several borehole drilled wells remained closed due to high fluoride groundwater. To map the location of wells and the distribution of groundwater fluoride in the study area, all hand-dug open wells and borehole drilled hand-pump wells were marked with a Garmin eTrex Vista® global positioning system (GPS), with the installation date documented. GPS was also used to mark the location of houses in the study area. In addition, year-round changes in air temperature and precipitation were

monitored using a Decagon® weather station that was programmed to take and record a reading every thirty minutes.

2.2. Drinking water sampling and analysis

Water samples were collected from 40 hand-dug open wells and 17 borehole drilled hand-pump wells in the study area during the late wet (September), late dry (April), and shoulder (October-November) seasons and analyzed for fluoride concentrations. Eight samples of sachet water from four local water purification companies were also analyzed for fluoride concentrations to verify that they had been treated to remove excess fluoride. All water samples were collected in Nalgene© polypropylene copolymer centrifuge tubes. They were analyzed the same day using an Orion 4-star meter and fluoride ion selective electrode, with 1 ml TISAB III added per 10 ml sample just before analysis (APHA, 1998). The fluoride ion selective electrode was calibrated before use and checked after every eight to ten sample analyses to maintain an accuracy within 5%. The majority of samples, including those from all hand-pump wells and open wells with fluoride concentrations above 2.5 mg F^{-} L^{-1}, were analyzed again at the Desert Research Institute in Reno, Nevada using a new fluoride ion selective electrode. The repeat analysis was done to confirm accuracy within 5%. In addition to testing the fluoride concentration in drinking water, two samples of locally purchased bags of Lipton® tea were prepared with boiled fluoride-free water to determine whether tea could be another source of fluoride for residents who consume it in the morning.

2.3. Data collection using human subjects

All house-to-house survey and water consumption monitoring questions and protocols were submitted to the Institutional Review Board at the University of Nevada,

Reno for prior approval. Informed verbal consent was required from all adult participants, and from the parents of child participants.

2.3.1. House-to-house surveys

Three sets of house-to-house surveys were conducted in the study area of Namoo to estimate the population and household size, identify seasonal water sources for drinking and washing, evaluate the daily diet, determine the level of understanding of the cause of fluorosis, and observe whether any household members showed signs of dental fluorosis. To obtain a baseline understanding of the distribution of dental fluorosis in the study area, the investigators asked consenting adult survey participants whether anyone in the home had discolored teeth.

A photograph was shown to adult household members with pictures of teeth at different phases of dental fluorosis (Fig. 3.2). The best match to a photograph was chosen for each member identified as having dental fluorosis. If a household member was identified as having dental fluorosis, the investigators looked at the teeth to confirm it. In a small minority of cases, the household member with dental fluorosis was not present, so the investigators relied on the survey participants' description of the degree of dental fluorosis (from Fig. 3.2).

Teeth with extensive white opaque markings and or some brown discoloration were identified as affected with dental fluorosis (as presented in Fig. 3.2). However because the mildest stages of dental fluorosis are frequently misdiagnosed (NRC, 1993), slight white markings considered questionable to very mild dental fluorosis were not counted. Residents with dental fluorosis who were born outside of the study area were also not included. The investigators noted whether the affected household member was

an adult or a child (under 18 years), and the estimated level of dental fluorosis was documented using the categories presented with the photographs in Fig. 3.2 (from Viswanathan et al., 2009).

Fig. 3.2. Degrees of dental fluorosis generally following Dean's classification index (Dean, 1942), with 0 = no dental fluorosis and 4 = severe dental fluorosis. These photos were shown to community members in the study area of Namoo in northern Ghana as examples of dental fluorosis to aid in identifying the degree of dental fluorosis of members in the house. Reprinted from Viswanathan et al. (2009) with permission from Elsevier Ltd.

Because the evaluations were not conducted by a dentist, caution was taken in positively identifying cases of dental fluorosis. In addition, to be less intrusive, the investigators only examined the teeth that were visible when spreading the lips. The U.S.

National Research Council noted that teeth most affected by dental fluorosis are posterior teeth so just evaluating anterior (front) teeth may not be sufficient in properly accounting for the prevalence and severity of dental fluorosis (NRC, 2006). As a result, the number of cases of dental fluorosis is underestimated. The intent of this component of the study, however, is to document trends.

2.3.2. Water consumption data

Daily water consumption was monitored in the study area to determine average water intake based on age, gender, and activity level. There were twenty seven participants ranging from age five to approximately 70 years. Adults who were accustomed to drinking sachet water monitored themselves by counting the number of 500 ml water packets consumed in a day, and others were monitored by a project investigator. Children were monitored by a project investigator whose job was to provide, measure, and document the volume of water consumed in one day. The children were monitored for many days with the measurements collected in the first few days excluded. This was done to prevent recording abnormally high water consumption data due to forced water intake. If the participant was monitored for less than three quarters of the day or if there was doubt about the accuracy of measurements, the data were not used. As a result, for some of the participants only one or two days of measured water intake were included in this study.

2.4. Determining optimum daily fluoride intake (mg $kg^{-1}day^{-1}$)

In order to recommend an optimum concentration of fluoride in drinking water, the daily maximum safe dose of fluoride consumed per unit body weight needed to be determined. In this study, several optimum daily doses of fluoride (in mg kg^{-1} day^{-1}) were

examined from a variety of existing sources. A single optimum daily dose was then chosen to calculate safe daily fluoride intake. The safe daily dose was compared to the daily fluoride intake range for participants in this study. The daily fluoride intake was estimated (in mg kg^{-1} day^{-1}) from drinking water and water consumed in food. The volume of water consumed in food was not directly measured, but was achieved by measuring the total volume of food eaten from a bowl (e.g. soup and starch) and estimating the percent water consumed. In many cases the weight of the participant was not recorded, but was estimated based on age, height, size, and gender, with the U.S. Center for Disease Control weight charts used to calculate the body weight of participants ages 5-20 years (Kuczmarski et al., 2002).

3. Results

3.1. Description of study area

The study area, which comprises most of the Namoo electoral area, is divided into eight communities: Done, Tendongo, Nayire, Koom, Abungo, Akaamo, Abasikoma, and Awale (Atanga, T. personal communication, 2011). It covers 5 square kilometers and is rural, with a dispersed population of approximately 2,500 (surveys this study). The region has one rainy season from about March-October and the air temperature is hot year-round (Fig. 3.1S). The air temperature in Namoo which was monitored August 2012 through September 2013 recorded an average temperature of 29 ^{o}C, average monthly minimum of 19.3 ^{o}C (January 2013) and maximum of 40.3 ^{o}C (March 2013) (Fig. 3.1S). The survey responses show that the approximately 200 households tend to be large and include extended family. As a result, average household size is 13 people (std dvn = 12). Namoo is also poor, with the vast majority of residents living and working as subsistence farmers

that rely on rain-fed agriculture. Although power lines were installed in Namoo around the year 2000 (Atanga. T. personal communication, 2011), only ten percent of the homes have electricity (survey results).

The water sources are decentralized and all residents rely on community hand-dug open wells, or borehole drilled hand-pump wells. There are 40 open wells in use and 17 hand-pump wells. In 2011, six of the hand pump wells, which were drilled in 2004 and 2005, remained closed because the fluoride concentrations exceeded the WHO limit of 1.5 mg $F^- L^{-1}$. Between late 2011 and late 2013 all six of the closed hand-pump wells were opened. Two of the hand-pump wells were opened with the approval of the Bongo District Assembly, because the fluoride concentration was under 3.0 mg $F^- L^{-1}$ and the users were in need of a more viable and accessible water source than they had at the time. The other four were opened by community members themselves without prior approval from the local government.

The installation date for nine of the open wells is not known, but it is assumed most are older wells – pre-2000. The four hand-pump wells from the 1970s were the first borehole drilled hand-pump wells installed in Namoo (Atanga, T. personal communication, 2011). Another was installed in 1999, and the other hand-pump wells were installed between 2004 and 2013. The open wells with inscribed installation dates were built between 1993 and 2010. Overall, sixty two percent of the wells were installed after 2002.

3.2. Drinking water fluoride concentrations

The distribution of groundwater fluoride is presented in Fig. 3.3 using shaded contours as determined from the fluoride concentrations measured in each well (black

diamonds, Fig. 3.3). The trend shows the highest groundwater fluoride in the northwest area (adjacent to outcrops of Bongo granite), and decreasing to the east and south (black arrow, Fig. 3.3).

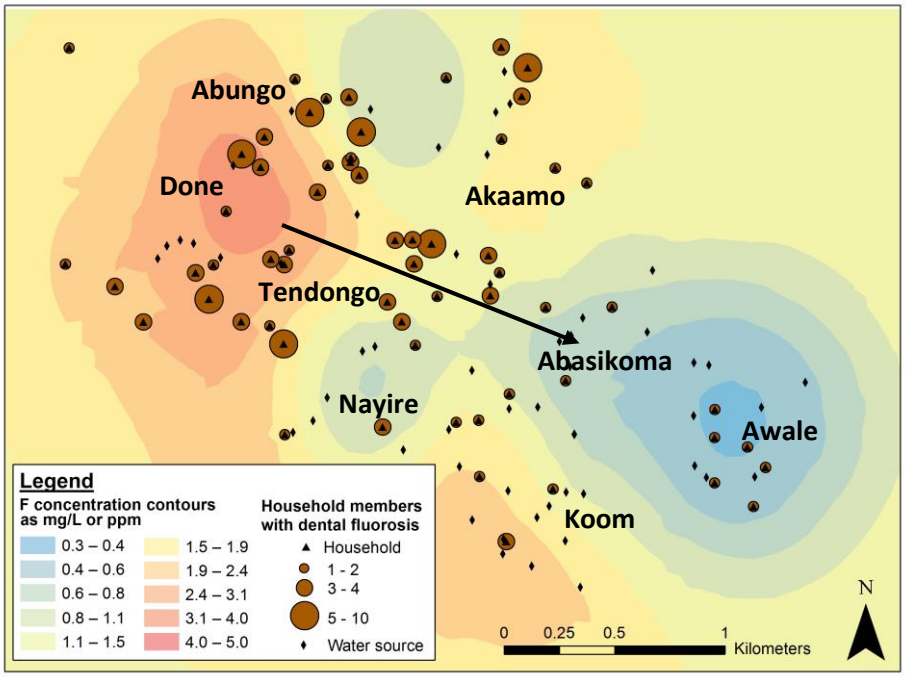

Fig. 3.3. Fluoride concentration contours showing the general distribution of groundwater fluoride in Namoo. The distribution of dental fluorosis in the home is identified by the brown circles surrounding the black triangles. The location of water sources (hand-dug open or borehole drilled hand-pump well) are identified by the black diamonds. The eight communities are also named. The black arrow shows the trend from highest groundwater fluoride and dental fluorosis communities to lowest.

Table 3.1 presents the average annual fluoride concentrations for all borehole drilled hand-pump wells and the year the hand-pumps were installed. The average is taken from samples collected in the late wet (September), late dry (April), and shoulder (October-November) season for most wells. All of the hand-pump wells with average fluoride concentrations above 3.0 mg F^{-} L^{-1} were installed after 2007, and only three of the 17 hand-pump wells have average fluoride concentrations under 1.5 mg F^{-} L^{-1}.

Table 3.1. Fluoride (F^-) concentrations of borehole drilled hand-pump wells in Namoo, and year installed. The first hand-pump wells installed in the 1970s but the year is not certain. Highlighted wells Have average F^- concentration above1.5 mg L^{-1}.

No.	Average F (mg L^{-1})	Std Dev	N[b]	Year Installed
1	0.7	0.0	3	1970s
2	2.9	0.1	3	1970s
3	1.6	0.1	3	1970s
4	2.6	0.1	3	1970s
5	1.6	0.1	3	1999
6	0.7	0.2	3	2005
7	2.1	0.1	3	2005
8	1.6	0.1	3	2005
9	4.3	0.5	3	2008
10	0.9	0.1	3	2010
11	2.0	0.1	2	2011
12	2.9	0.1	2	2011
13	2.4	0.1	2	2011
14	3.4	0.1	2	2012
15	4.5	NA	1	2012
16	3.5[a]	0.1	2	2013
17	3.4[a]	0.5	2	2013

[a]Wells closed during sampling periods: samples may have incorrect fluoride concentration because the sample was not from flushed/regularly used well; [b]number of samples.

Using the seasonal average data for the 17 hand-pump wells, the minimum concentration was 0.7 mg F^- L^{-1}, the maximum 4.5 mg F^- L^{-1}, the median 2.3 mg F^- L^{-1} and the overall average 2.2 mg F^- L^{-1} (std dvn = 1.1). The average annual fluoride concentrations of the shallow hand-dug open wells are presented in Table 3.2. Just nine of the 40 hand-dug open wells have average fluoride concentrations above 1.5 mg F^- L^{-1}. Using the averages for the 40 open wells, the minimum concentration was 0.3 mg F^- L^{-1}, the maximum 3.1 mg F^- L^{-1}, the median 0.8 mg F^- L^{-1} and the overall average 1.1 mg F^- L^{-1} (std dvn = 0.7). Most of these values are notably lower than those for the hand-pump wells presented in Table 3.1.

Table 3.2. Fluoride (F^-) concentrations of hand-dug open wells in Namoo, with the year installed. Wells with no date likely installed pre-2003. Highlighted wells average F^- concentration above 1.5 mg L^{-1}.

No.	Average F (mg L^{-1})	Std Dev	N[a]	Year Installed
1	3.1	0.6	3	no date
2	1.4	1.8	3	no date
3	0.7	0.5	2	no date
4	1.7	0.1	3	no date
5	1.2	0.1	2	no date
6	1.2	NA	1	no date
7	0.5	0.1	3	no date
8	0.8	NA	1	no date
9	0.4	NA	1	no date
10	0.4	0.1	3	1993
11	1.7	0.1	3	1994
12	2.0	0.6	3	1994
13	0.6	0.2	3	1994
14	0.7	0.1	2	1995
15	0.4	0.1	3	1996
16	0.4	0.2	3	1997
17	0.8	0.1	3	1998
18	0.5	0.0	3	2003
19	1.7	1.9	3	2004
20	0.4	0.1	3	2004
21	1.2	0.6	3	2004
22	0.5	0.2	3	2004
23	0.5	0.3	3	2004
24	0.9	0.3	3	2004
25	1.7	0.0	3	2004
26	0.8	0.6	3	2004
27	0.8	NA	1	2004
28	1.2	NA	1	2004
29	0.9	0.2	3	2004
30	0.4	0.0	2	2004
31	0.5	0.1	3	2006
32	2.4	0.0	3	2006
33	0.8	0.0	3	2006
34	0.5	0.1	3	2007
35	1.4	0.1	3	2007
36	1.2	NA	1	2007
37	2.4	0.1	3	2007
38	0.3	0.1	3	2008
39	2.6	0.1	3	2008
40	0.5	0.1	2	2010

[a]Number of samples in average.

3.3. Survey results

3.3.1. Dental fluorosis in the community

Fig. 3.3 also maps the distribution of dental fluorosis in the home. According to the survey, 36% of the households have family members with dental fluorosis. In the northwest end of the study area near a cluster of high fluoride wells, 62% of households have members with dental fluorosis. Slightly to the southeast with mostly low to moderate levels of groundwater fluoride, 35% of households have members with dental fluorosis. The far southeast end of the study area has all low fluoride wells (< 1.0 mg L^{-1}), and 13% of households have members with dental fluorosis. The communities with most of the cases of dental fluorosis are Done, Abungo, and Akaamo. Those with the fewest and mildest cases are Abasikoma, Awale, and parts of Koom.

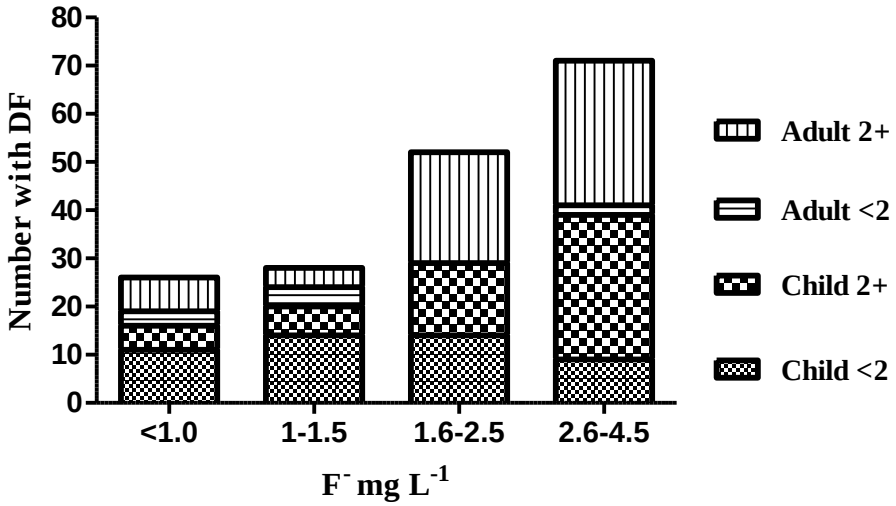

Fig. 3.4. Distribution of dental fluorosis (DF) and average fluoride concentration of household drinking water as identified by house-to-house survey participants. The <2 range of dental fluorosis is milder dental fluorosis and the 2+ is moderate to severe.

Fig. 3.4 presents a bar graph of the distribution of dental fluorosis in children and adults versus the average fluoride concentration of the household water. The cases of dental fluorosis are separated into two categories of less severe (<2 = opaque white

streaks with some slight brown markings) or more severe (2+ = pronounced brown markings on some or all of visible teeth) using the photographs from Viswanathan et al. (2009). Just 177 cases of dental fluorosis (or about 8% of the population) were identified by survey participants. Of those identified with dental fluorosis, 58.7% are children. Nearly 88% of the adults with dental fluorosis fall in the 2+ category while 53.8% of children with dental fluorosis are in the 2+ category. The number of cases of dental fluorosis, as well as the number of cases of 2+ dental fluorosis, increases with an increase in fluoride concentration; but dental fluorosis is also identified in homes with drinking water fluoride below 1.0 mg L^{-1}, including 12 cases of 2+ dental fluorosis (Fig. 3.4).

3.3.2. Household water sources

The preferred source of drinking water is from the hand-pump wells rather than the open wells. This is because groundwater from hand-pump wells contains less sediment, is less prone to microbial contamination, and the water is easier to collect. Sixty percent of households stated that they collect fluoride-free rainwater for household use during the wet season. Forty four percent of households that collect rainwater also drink it and the others only use it for washing. A small minority of households buy bundles of commercially purified low fluoride sachet water for drinking, but generally not daily.

3.3.3. Daily diet

When asked about diet, the response was the same for nearly all households. The staple is a millet (or corn) mush called TZ ("teezed") that is made by mixing flour with water and then cooking the mixture until it is thick. The TZ is eaten with soup, such as green leaf soup that usually contains pulverized groundnuts (peanuts). Most households

eat this at every meal. Rice is also part of the diet, but millet TZ is more common. Beans are part of the diet as well, but not always eaten daily. Meat (goat, sheep, fowl, beef, and dry fish) is eaten rarely in most households because it is expensive, and when it is included in a meal the portion is small.

The minority of households in Namoo with a regular income (e.g. government workers) often consume bread with tea, coffee, or cocoa and milk as part of the breakfast. These households tend to have more protein and calcium in the diet than the majority of residents in Namoo without a steady salary. Canned mackerel, which is consumed occasionally by those able to afford it can have notably elevated concentrations of fluoride (Table 3.1S). In addition, residents who drink tea likely consume more fluoride: two Lipton® tea bags purchased in Ghana and brewed with fluoride-free water each had fluoride concentrations of 2.3 and 2.4 mg F^{-} L^{-1} for 200 ml steeped 3 minutes. The majority of residents in Namoo currently lack the income to buy tea or canned fish regularly, however, so in most cases it will not contribute to overall fluoride exposure.

3.4. Daily drinking water consumption

Daily drinking water intake was monitored for 27 participants of approximate age range from five to 70 years, in order to estimate the daily water consumption and potential fluoride intake from water in a region that is hot year-round, and where the residents live without air conditioning and are outdoors and active much of the day. Table 3.3 presents the age range, gender, estimated weight, time of year the monitoring occurred (see Fig. 3.1S for temperatures), and daily water consumption. The range for all drinking water intake measurements is from 1.0-6.8 L consumed per day, depending primarily upon age, weight, and activity level of the participant (Table 3.3). In evaluating

the average values for each adult, the minimum value is 1.4 L day^{-1}, the maximum is 5.7 L day^{-1}, the median is 3.2 L day^{-1}, the overall average is 3.3 L day^{-1} (std dvn = 1.0). Using the average values for each child, the minimum is 1.0 L day^{-1}, the maximum is 2.4 L day^{-1}, the median is 1.6 L day^{-1}, and the overall average is 1.7 L day^{-1} (std dvn = 0.4).

Table 3.3. Water consumption data for 27 residents of Namoo, approximate age range 5 to 70 years. Highlighted rows indicate individuals with dental fluorosis (<2) from consuming water with 2.6 mg F^- L^{-1} to 2005, and 2.1 mg F^- L^{-1} from 2005-present. Monitoring level: 1 = self-monitored; 3 = monitored by PI or adult family member ¾ of the day; 3+ = monitored by PI or adult family member > ¾ of the day; 4 = monitored by PI or adult family member entire day.

Age (Yrs)	Gender	Approx Wt (Kg)	Monitor Level	2011-2013 Month	Wat Cons Avg (L)	Range (L)	Std Dvn	N[a]
>35	F	51	1	Nov/Aug/Apr	2.9	1.9-4.7	0.6	42
>35	M	72	3+ to 4	Nov/Aug/Apr	4.0	2.5-6.3	1.6	8
>35	M	68	1	Apr-May	3.3	2.9-3.9	0.5	4
>35	M	55	3+	May	1.3	NA	NA	1
>35	F	64	1	May	3.5	NA	NA	1
>35	F	55	1	Aug/May	2.2	1.9-2.7	0.3	4
>35	F	66	3+	May	3.1	NA	NA	1
18-35	F	57	3+ to 4	Nov/Aug/Apr	2.6	1.9-3.8	0.7	10
18-35	F	75	3+ to 4	April-May	5.7	5.0-6.8	1.0	3
18-35	F	57	4	May	4.1	3.9-4.5	0.3	4
18-35	F	68	4	Nov	2.9	NA	NA	1
18-35	F	66	1	May	3.3	2.9-3.4	0.3	4
18-35	M	68	1	May	3.0	2.5-3.5	0.7	2
18-35	F	55	1	May	3.2	2.9-3.4	0.4	2
18-35	F	90	3+ to 4	May	3.9	3.5-4.3	0.6	2
18-35	**F**	**64**	**4**	**May**	**3.1**	**NA**	**NA**	**1**
11-17	M	50	4	Nov	2.3	1.2-3.2	0.8	4
11-17	**F**	**28**	**3**	**Aug**	**1.0**	**NA**	**NA**	**1**
11-17	F	55	1	Aug	1.6	NA	NA	1
11-17	**M**	**40**	**3+ to 4**	**Aug**	**2.4**	**2.0-2.8**	**0.4**	**3**
5-10	**F**	**19**	**3+ to 4**	**Nov/May**	**1.9**	**1.7-2.1**	**0.2**	**3**
5-10	M	28	3	Aug	1.9	NA	NA	1
5-10	M	16	3	Aug	1.5	NA	NA	1
5-10	M	31	4	Aug	1.7	1.5-1.9	0.2	3
5-10	M	19	3+	Aug	1.4	1.4	0.0	2
5-10	F	26	3	Aug	1.2	NA	NA	1
5-10	**M**	**22**	**3+**	**Aug**	**1.3**	**NA**	**NA**	**1**

[a]N is the number of measurements used to determine daily water consumption for each participant.

3.5. Safe daily dose of fluoride per kg body weight

The estimated safe daily dose of 0.06 mg F^- per kg body weight used in this study is based on conclusions from selected studies cited below. The optimal daily intake to both minimize dental fluorosis and maximize protection from dental caries is in the range

of 0.05-0.07 mg F^- per kg body weight, according to Levy (1994) and Heller et al. (1999, 2000). The Institute of Medicine (1997) determined that 0.05 mg F^- per kg body weight per day from drinking water provides optimum anti-caries protection. The safe dose determined by both Dean (1942) and Hong et al. (2006a) to prevent severe dental fluorosis is 0.06 mg F^- per kg body weight. This current study has chosen a safe dose of 0.06 mg F^- per kg body weight per day as optimum for preventing severe dental fluorosis and maximizing dental caries protection by combining 0.05 mg F^- per kg body weight per day from water (Institute of Medicine, 1997), and 0.01 mg F^- per kg body weight per day from food (McClure, 1943).

3.6. Estimated daily fluoride intake, and safe daily dose for Namoo, Bongo District

Table 3.4 presents a set of values for each of the 27 participants in the water consumption study showing (1) the daily fluoride intake from water when consuming 1, 2, and 4 mg F^- L^{-1} water, (2) in brackets the daily fluoride intake from water per kg body weight when consuming 1 mg F^- L^{-1} water, (3) the safe total daily mg fluoride consumed per day, and (4) the optimum maximum concentration of fluoride in water. To calculate the safe total mg F^- per day for each participant, the value of 0.06 mg F^- per kilogram body weight per day is used (includes fluoride in water and in food). The calculated contribution from water intake (1, 2, 4 mg F^- L^{-1}) is presented and compared to the overall safe daily F^- limit from water and food. The contribution from food adds an average of 0.5 mg F^- day^{-1} (range 0.2-0.9 mg F^- day^{-1}) to the calculated values from water intake. For the majority of participants, when consuming water with fluoride at the low value of 1 mg F^- L^{-1} (and excluding the contribution from food), the recommended safe daily fluoride intake is still exceeded. The safe concentration (mg F^- L^{-1}) in drinking and

cooking water for each participant is based on 0.05 mg F^- per kg body weight per day as the contribution from water.

Table 3.4. Estimated fluoride (F^-) intake from water at 1, 2, 4 mg F^- L^{-1} in drinking/cooking and safe maximum daily F^- intake for 27 residents of Namoo. The calculated safe daily F^- intake in (consumed) water is based on the estimated weight of each individual and acceptable level of 0.05 mg F^- per kg per day; and the total acceptable level per day of 0.06 mg F^- per kg. The volume of water consumed is both from drink and food (e.g. rice, soup, porridge). Highlighted rows indicate individuals with dental fluorosis (<2) from consuming water with 2.6 mg F^- L^{-1} to 2005, and 2.1 mg F L^{-1}, 2005-present.

Age (Yrs)	Gender	Approx Wt (Kg)	Wat Con[a] Avg (L)	(1 mg L^{-1})[b] mg day^{-1}	(2 mg L^{-1}) mg day^{-1}	(4 mg L^{-1}) mg day^{-1}	Safe F^- mg day^{-1}	Safe Wat mg F^- L^{-1}
>35	F	51	3.4	3.4 (0.07)	6.8	13.6	3.06	0.8
>35	M	72	4.7	4.7 (0.07)	9.4	18.8	4.32	0.8
>35	M	68	4.0	4.0 (0.06)	8.0	16.0	4.08	0.9
>35	M	55	1.5	1.5 (0.03)	3.0	6.0	3.30	1.8
>35	F	64	4.1	4.1 (0.06)	8.2	16.4	3.84	0.8
>35	F	55	2.8	2.8 (0.05)	5.6	11.2	3.30	1.0
>35	F	66	3.7	3.7 (0.06)	7.4	14.8	3.96	0.9
18-35	F	57	3.1	3.1 (0.05)	6.2	12.4	3.42	0.9
18-35	F	75	6.4	6.4 (0.09)	12.8	25.6	4.50	0.6
18-35	F	57	4.7	4.7 (0.08)	9.4	18.8	3.42	0.6
18-35	F	68	3.3	3.3 (0.05)	6.6	13.2	4.08	1.0
18-35	F	66	3.9	3.9 (0.06)	7.8	15.6	3.96	0.8
18-35	M	68	3.7	3.7 (0.05)	7.4	14.8	4.08	0.9
18-35	F	55	3.8	3.8 (0.07)	7.6	15.2	3.30	0.7
18-35	F	90	4.6	4.6 (0.05)	9.2	18.4	5.40	1.0
18-35	**F**	**64**	**3.7**	**3.7 (0.06)**	**7.4**	**14.8**	**3.84**	**0.9**
11-17	M	50	2.7	2.7 (0.05)	5.4	10.8	3.00	0.9
11-17	**F**	**28**	**1.3**	**1.3 (0.05)**	**2.6**	**5.2**	**1.68**	**1.1**
11-17	F	55	2.3	2.0 (0.04)	4.0	8.0	3.06	1.4
11-17	**M**	**40**	**2.8**	**2.8 (0.07)**	**5.6**	**11.2**	**2.46**	**0.7**
5-10	**F**	**19**	**2.1**	**2.1 (0.11)**	**4.2**	**8.4**	**1.14**	**0.5**
5-10	M	28	2.2	2.2 (0.08)	4.4	8.8	1.56	0.6
5-10	M	16	1.7	1.7 (0.09)	3.4	6.8	1.14	0.6
5-10	M	31	2.1	2.1 (0.07)	4.2	8.4	1.62	0.7
5-10	M	19	1.7	1.7 (0.09)	3.4	6.8	1.14	0.6
5-10	F	26	1.6	1.6 (0.06)	3.2	6.4	1.56	0.8
5-10	**M**	**22**	**1.6**	**1.6 (0.07)**	**3.2**	**6.4**	**1.20**	**0.7**

[a]Drinking water Table 3.3, plus water in food; [b]Numbers in parentheses are the calculated fluoride intake from water in mg per kg body weight per day when consuming water with 1 mg F^- L^{-1}.

The safe limit in drinking and cooking water of the 27 participants in the study is as follows: for children between 5 and 10 years old it is 0.5-0.8 mg F^- L^{-1}; 11 to 17 years it is 0.7-1.3 mg F^- L^{-1}; and over 17 years it is 0.7-1.8 mg F^- L^{-1}. The values in parentheses in the 1 mg F^- L^{-1} column of Table 3.4, which estimate the daily fluoride from water per kg body weight, range from 0.03-0.11 mg F^- per kg per day with an average value of

0.065 mg F^- per kg per day. These values, using a fairly low fluoride concentration of 1 mg L^{-1}, are closest to the 0.05 mg F^- per kg body weight per day considered optimal for fluoride intake from water.

4. Discussion

4.1. Fluoride exposure in the Upper East Region, Ghana

The major sources of fluoride are drinking water, food, dental products (mostly tooth paste), pesticides (NRC, 2006; USEPA, 2010b), and tea (Shu et al., 2003; Wong et al., 2003; Yi and Cao, 2008). Additional fluoride exposure from air occurs in some areas around the world due to industrial emissions (ATDSR, 2003; Jagtap et al., 2012), electrical utilities, coal, and volcanoes (ATDSR, 2003). Food contains at least trace levels of dietary fluoride (WHO, 2011), with higher concentrations determined by the food source and environmental conditions. Once ingested, the amount of bioavailable fluoride absorbed from food is also variable, and depends on other dietary factors (Ericsson, 1968; Whitford, 1994a; Cremer and Buttner, 1970; Cerklewski, 1997). However, fluoride in drinking water is generally considered the largest dietary contributor (NRC, 2006; USEPA, 2010b; Jagtap et al., 2012).Water also contributes significantly because nearly 100% of fluoride consumed in water is absorbed in the gastrointestinal tract (Whitford, 1994b; 1996).

There is no industry in the region so fluoride exposure from air due to industrial emissions is not a factor. Also, the vast majority of residents in the study area lack the financial means to buy dental products, fertilizer, pesticides, or tea so exposure to fluoride from these sources is minimal in most households. There is some fluoride intake from the food since at least trace concentrations of fluoride are found in all food (WHO,

2011), but it is expected that the bulk of fluoride exposure is from water consumed through drinking and cooking. An additional seasonal factor is that water consumed with food often increases if the food supply is low, such as during late dry season and early planting season. When food is limited, one solution is to dramatically increase the water to millet flour ratio during preparation in order to increase the volume consumed and fill the stomach. Also vegetables preserved by drying are added to soup in larger quantities during the dry season, thus requiring more water in the soup.

There are possible sources of fluoride from the diet such as leafy greens and millet, which are staples, as well as black eyed beans and groundnuts. Amalraj and Pius (2013) observed that, in parts of South India, leafy greens have fluoride concentrations ranging from 0.58-6.98 mg kg^{-1}, millet from 1.29-4.94 mg kg^{-1}, and black eyed beans from 1.16-4.21 mg kg^{-1} (Amalraj and Pius, 2013) with the variation dependent upon location, and sometimes the species. In Tanzania, Malde et al. (1997) found that two samples of groundnuts contained 2.2 and 4.3 mg fluoride kg^{-1}. Table 3.1S provides a range of fluoride concentrations in various foods consumed in the United States that may also be consumed in northern Ghana. Because no analyses were conducted for fluoride levels in food products from Namoo, this study used the value by McClure (1943) of 0.01 mg F^- per kg body weight per day – or an estimated 0.5 mg F^- kg^{-1} food consumed daily for an adult. This value is more consistent with the range presented in Table 3.1S than with the above results from Amalraj and Pius (2013) and Malde et al. (1997) and may be low, but is a safe conservative estimate.

4.2. Daily water intake in the Upper East Region, Ghana

The effects of climate and activity level on water consumption have not been studied extensively (USEPA, 2011). However, there are a few studies from the United States that estimate water intake in hot climates and for active members of the population. Data from a Galagan and Vermillion (1957) study conducted in California indicate that water intake can more than double under very hot conditions. Similarly, a U.S. Army study conducted to prepare for water needs in field combat ranging from light to heavy activity, estimated that twice as much water would be needed in a hot climate compared to a temperate climate (US Army, 1983). The measured daily water intake collected in this study in northern Ghana (Table 3.3) was also notably higher for every age group than the estimates provided for temperate climates. This is due to both high year-round air temperatures, and the lifestyle in rural Ghana.

For children ages 5-17 years the range of water intake from drinking using all measurements was 1.0-3.2 L per day with an average of 1.7 L (std dvn = 0.4); and for adults 1.3-6.8 L per day with an average of 3.3 L (std dvn = 1.0). The daily water consumption mirrored the activity level and the person's size. The more active and heavier the person, the more water consumed, as expected. The average water consumption measured in this study is about double the average for temperate climates, which is consistent with the findings for hot climates in the United States discussed earlier in this section.

4.3. Dental fluorosis and fluoride intake under varied climatic conditions

Increased water intake in hot climates has been correlated to increased fluoride intake and higher rates of dental fluorosis in the United States. Galagan and Lampson

(1953) conducted a fluorosis study in Arizona where the mean annual average temperature was 70 ^{o}F (21 ^{o}C), and drinking water fluoride concentrations ranged from 0.4-1.2 mg F^{-} L^{-1}, which are considered low. The results indicate that there was a higher percentage of children with dental fluorosis in this study than those from Dean (1942) with similar drinking water fluoride concentrations but with annual average temperatures of 50 ^{o}F (10 ^{o}C). Galagan and Lampson (1953) documented that locations with drinking water fluoride concentrations of 0.8 and 1.2 mg F^{-} L^{-1} had cases of severe dental fluorosis. Dean (1942) identified a higher drinking water fluoride concentration of 2.0 mg F^{-} L^{-1} as the threshold for severe dental fluorosis in the more temperate climates. Galagan and Lampson (1953) concluded that the difference in incidents of dental fluorosis was due to higher water consumption.

4.4. Dental fluorosis and fluoride intake in Upper East Region, Ghana

The presence of elevated groundwater fluoride concentrations in parts of the Upper East Region in Ghana have been known since 1978 (Apambire et al., 1997). But the impact of consuming high fluoride water was not understood until 1993 when health professionals were asked to investigate the cause of stained teeth in children and identified it as dental fluorosis (Apambire et al., 1997). In a subsequent study in the Bolgatanga and Bongo Districts of the Upper East Region, Apambire (2000) used data from dental exams on 2,100 children ages 5-20 years to document the dental effects on consuming drinking water with fluoride concentrations up to 4.6 mg F^{-} L^{-1}. The Dean's index (Dean, 1942) was used to classify the degree of dental fluorosis from none (normal) to severe. The results of statistical analyses determined that 0.8 mg F^{-} L^{-1} was the average drinking water fluoride concentration for children with normal teeth. For

questionable, very mild to mild dental fluorosis the average was 1.33 mg $F^- L^{-1}$; for moderate fluorosis it was 2.76 mg $F^- L^{-1}$; and for severe dental fluorosis it was 3.04 mg $F^- L^{-1}$.

This current study was conducted in a smaller section of the same area as the Apambire (2000) study, and the method used here for identifying dental fluorosis was less rigorous. The high fluoride area has average groundwater fluoride concentrations from 1.7-4.5 mg $F^- L^{-1}$, and the low fluoride area has groundwater concentrations well below 1.0 mg $F^- L^{-1}$ in all of its wells year-round. The most severe fluorosis and the highest number were in the high fluoride area - but 13% of households in the very low fluoride areas also had cases of dental fluorosis, which was unexpected. In other studies, a small fraction of the population has shown to be vulnerable to dental fluorosis, even at fluoride concentrations under 1.0 mg L^{-1} (e.g. Galagan and Lampson, 1953; Apambire, 2000). This suggests that additional unidentified sources of fluoride and or individual sensitivity also affect the exposure risk (NRC, 2006).

Another concern is that five of the borehole drilled hand-pump wells with fluoride concentrations above 3.1 mg L^{-1} (four in the "high fluorosis community", Done) were opened between 2008 and 2013. As a result the incidence of dental fluorosis - especially severe dental fluorosis - is expected to increase if the water is left untreated or another low fluoride water source is not provided.

4.5. Skeletal fluorosis in the Upper East Region, Ghana

Skeletal fluorosis is a bone and joint condition with a range of symptoms including joint stiffness, bone fractures, and bone deformity. In northern Ghana, there have been no documented cases of skeletal fluorosis. The maximum groundwater fluoride

concentrations in the Upper East Region are 4.6 mg F^- L^{-1} (Apambire et al., 1997; Apambire, 2000), which is consistent with the maximum fluoride concentrations found in the groundwater in this study. Because the highest fluoride wells were installed in the study area between 2008 and 2013, with average fluoride concentrations 3.4-4.5 mg F^- L^{-1}, the elevated risk of skeletal fluorosis is recent with symptoms possibly not occurring for several years or even decades. The WHO (1984, 2011) has recommended 3 mg F^- L^{-1} as the limit for minimizing the risk of skeletal fluorosis. High water intake is likely to increase susceptibility to more severe forms of skeletal fluorosis in fluoride ranges at and above 3 mg F^- L^{-1}.

Table 3.5. Selected guidelines for fluoride (F^-) in drinking water around the world. The lowest limits are intended to minimize dental fluorosis (DF).

Source	Year	F^- Standard/Guideline (mg L^{-1})	Notes
WHO[a]	2011	1.5	Adapt guideline to local climate
Australia[b]	2011	1.5	
Canada[c]	2010	1.5 (recommends 0.7)	0.7 optimal for dental health
China[d]	2002	1.0 drinking/1.5 other uses	Surface water guidelines
European Union[e]	2014	0.8 F^- added /1.5 F^- natural	1.5 for naturally occurring F^-
India[f]	2012	1.5 (recommends 1.0)	Lower std to minimize DF
Tanzania[g]	2007	8.0 effluent/1.5-4.0 drinking	Lower-upper limit drinking water
U.S. EPA[h]	2010	4.0 (recommends 2.0)	4.0 enforceable/ 2.0 secondary std
U.S. HHS[i]	2011	recommends 0.7	0.7 optimal for dental health

[a]WHO (2011); [b]NHMRC, NRMMC (2011); [c]Health Canada (2010); [d]MEPPRC (2002); [e]DECLG (2014); [f]BIS (2012); [g]TBS (2007); [h]USEPA (2010b); [i]USDHHS (2011).

4.6. Range of limits for fluoride in drinking water

The recommended or required limit for fluoride in drinking water varies from country to country. The fluoride limits recommended by the WHO, U.S. Environmental Protection Agency, other U.S. public health agencies, European Union, Canada, Australia, Tanzania, India, and China are listed in Table 3.5. In the United States, some government agencies have proposed lower recommendations for the safe limit of fluoride in drinking water, however only the U.S. Environmental Protection Agency can set an

enforceable standard which considers the cost of treatment versus adverse effects to the consumer (USEPA, 2010b). The U.S. Environmental Protection Agency recommended limit of 2 mg $F^- L^{-1}$ is intended to protect against severe dental fluorosis in children and is not enforced (dental fluorosis is not identified as an adverse health effect). The enforceable limit of 4 mg $F^- L^{-1}$ is to protect the consumers from crippling skeletal fluorosis which is considered an adverse health effect (USEPA, 2010b). The U.S. National Research Council (2006) review of the Environmental Protection Agency's drinking water standards agreed that mild to moderate dental fluorosis are cosmetic effects, but felt that severe dental fluorosis has adverse health impacts because it damages tooth enamel and reduces the ability to protect against tooth decay (NRC, 2006 - supporting studies include: Fejerskov et al., 1990; Burt and Eklund, 1999; Aoba and Fejerskov, 2002). As a result it recommended the enforceable limit be lowered in order to protect the population against severe dental fluorosis.

4.7. Recommended limits of fluoride in drinking water for Ghana

When installing new boreholes, Ghana currently follows the WHO recommended limit of 1.5 mg $F^- L^{-1}$. As a result, many boreholes in the Upper East Region remain closed because the groundwater fluoride concentration exceeds this limit. What is being evaluated in this study is whether the WHO limit is appropriate for Ghana, when considering climate and water intake, as well as the cost of treatment. The daily fluoride intake can be very high in areas where water consumption is high (Table 3.3) and much of the drinking water, especially from borehole drilled wells, has notably elevated concentrations of fluoride (Table 3.1). Apambire et al. (1997) speculated that daily water intake in northern Ghana may be as high as 3-4 L per day, due to year-round high

temperatures. To minimize the number of cases of dental fluorosis and prevent severe dental fluorosis, Apambire (2000) recommended a limit for fluoride in drinking water of 0.4-0.6 mg L^{-1}.

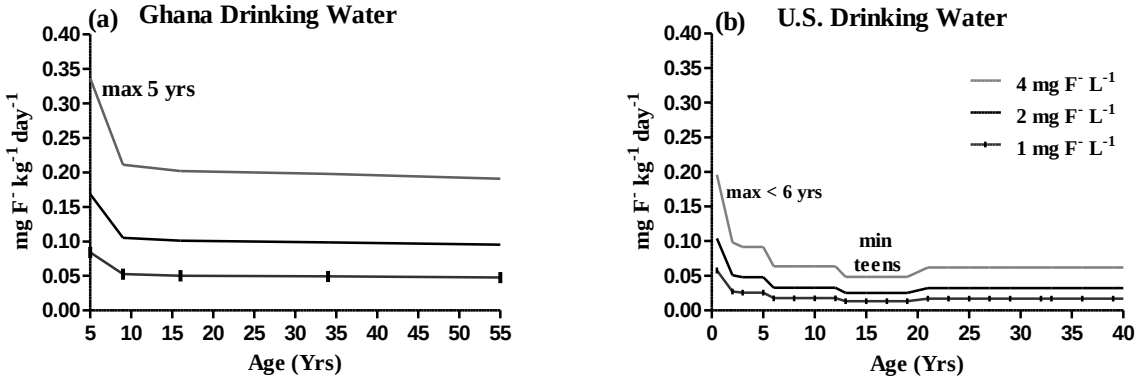

Fig. 3.5. Estimates of daily fluoride intake per unit weight from drinking water only at 1, 2, and 4 mg F^- L^{-1} in (a) Ghana and (b) United States. Modeled data from the United States is from the National Research Council (NRC, 2006). There are no data for Ghana under 5 years old. According to these data, the fluoride intake in Ghana from drinking water is ~3 times higher than in the U.S.

In addition, age is an important factor when evaluating fluoride intake and recommending limits in drinking water. For example, the first 6-8 years of life are the most critical risk period for dental fluorosis (NRC, 2006), with the first two years of life considered the most susceptible to developing fluorosis in permanent maxillary incisors (Hong et al., 2006b). Fluoride intake per unit weight is also highest during the first five years (Fig. 3.5). Therefore, to minimize the risk of dental fluorosis, children under 6-8 years should drink water with a maximum fluoride concentration of 0.6 mg F^- L^{-1}, and even lower for the first year or two, because the highest consumption of fluoride per kg body weight occurs during this period (NRC, 2006) (Fig. 3.5b). Setting a lower limit for children would be difficult. However, when possible, providing commercially treated very low-fluoride drinking water, or even rainwater, are recommended for young children as a preventive measure against dental fluorosis.

Because older children, and adults in particular, are less vulnerable to dental fluorosis than young children they can also safely consume higher concentrations of fluoride in drinking water than young children, so the WHO recommended limit of 1.5 mg $F^- L^{-1}$ should not put them at serious risk of dental fluorosis. When considering the cost of treatment in northern Ghana, the WHO limit for older children and adults may be adequate, even though the results presented in Table 3.4 indicate the limit should be 1.0 mg $F^- L^{-1}$ or lower in most cases. The maximum safe limit to protect against skeletal fluorosis for life-long residents who consume water with elevated fluoride concentrations for years or even decades may be slightly higher than 1.5 mg $F^- L^{-1}$. Other health impacts of consuming excess fluoride, including reproductive and developmental changes, neurological effects, and impacts on the immune, gastrointestinal, renal, hepatic and endocrine systems, and carcinogenicity (NRC, 2006; Ozsvath, 2009 and references therein) are not addressed here because data are limited and adverse health effects are still not clear.

Because the hand-pump wells with the highest average fluoride concentrations (3.4-4.5 mg $F^- L^{-1}$) were installed between 2008 and 2013, the more extreme effects from consuming high fluoride water, such as severe dental fluorosis and skeletal fluorosis may not appear for many years. As a protective measure against skeletal fluorosis, an interim upper limit of fluoride in drinking water may be <3.0 mg $F^- L^{-1}$ with the goal of an upper limit at the WHO guideline of 1.5 mg L^{-1} (older children/adults). The initial recommendation for children under 6-8 years old should be 1.0 mg $F^- L^{-1}$ with the goal of 0.6 mg $F^- L^{-1}$ and even lower for the first 2 years of life.

5. Conclusions

The challenges of setting drinking water standards in the developing world that protect the majority of the population can be tremendous due to the expense of treatment and difficulty in monitoring and enforcing established regulations. With these constraints in mind, a range of goals may be the most appropriate. The WHO (2011) recommends setting initial guidelines that are realistic, with target guidelines as a future goal that may be achieved when the cost of treatment is lowered or the government and or community has greater capacity to subsidize an alternative water source or a treatment facility. In northern Ghana, the greatest drinking water challenge, apart from improved access, is high concentrations of fluoride in groundwater. The Bongo District, where this problem is quite pronounced, is the poorest part of Ghana (Atipoka, 2009). It is also rural with water sources decentralized, so providing a safe, low-cost, low fluoride source of drinking water to those pockets of affected communities is difficult. In addition, this area is water-stressed, so keeping hand-pump wells (which tend to have higher fluoride than hand-dug open wells) closed due to fluoride concentrations above 1.5 mg F^{-} L^{-1} makes community members angry.

There is no effective way to prevent fluorosis that is also cost-free. Recommending a limit for young children that is lower than the limit for older children and adults is cost effective while still minimizing adverse health effects to all. The challenge here is implementation and management, both of which will require extensive education on fluoride intake and fluorosis. Steps forward in addressing the problem of fluorosis will need to include ongoing educational programs, beginning with the schools and health clinics, to help the residents understand fluorosis; for currently only 24% of

the population in the study area understands that high fluoride drinking water is the cause of discolored and damaged teeth (data from this study). An educational program in the schools could possibly be coupled with a thorough dental evaluation of the school children, conducted by a dentist, in order to get a more accurate estimate of the incidence of dental fluorosis in the study area while raising awareness. Also, providing a source of low fluoride water to the schools (especially primary and pre-school) for the children to drink during the day will help decrease exposure. However, without a widespread understanding of the cause of fluorosis, and an interest in addressing it, any proposed solutions and management programs will likely fail. In addition, if the extreme poverty in these communities is not addressed in parallel, the described public health issues will continue to be neglected. Under such conditions, access to sufficient and reliable sources of food and water will, understandably, always be the priority.

Acknowledgements

This research was generously supported by the University of Nevada, Reno, the Desert Research Institute, and a U.S. Environmental Protection Agency Science to Achieve Results Graduate Research Fellowship. We thank the Bongo District Assembly for approving this study, and Philomina and Tony Atanga for assisting with the field work, as well as the community of Namoo for its participation and support. We also thank two anonymous reviewers and the editor for providing helpful comments.

Chapter 3: Supplementary data

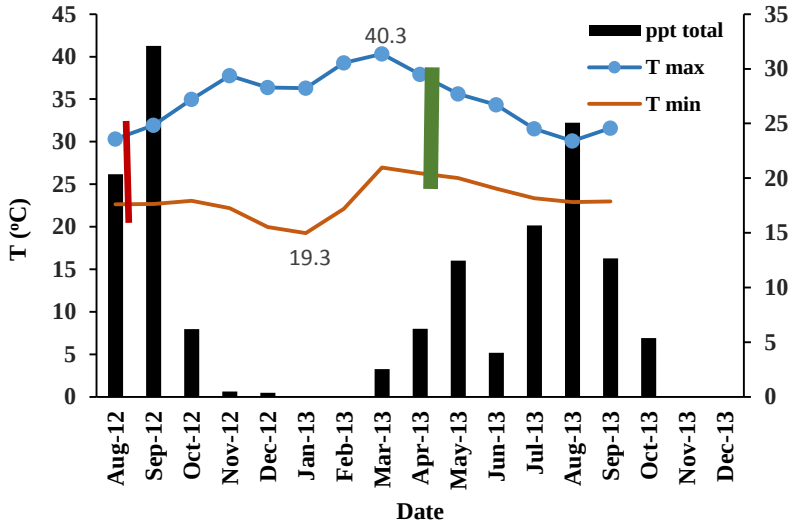

Fig. 3.1S. Average monthly minimum and maximum air temperature in Namoo, Bongo District, Upper East Region, Ghana from August 2012 to September 2013. Red and green vertical bars identify approximate temperatures for the bulk of the water consumption monitoring periods, with the majority in April-May (green thicker vertical bar). The average monthly maximum temperature is 40.3 ºC and minimum is 19.3 ºC for this period.

Table 3.1S. The estimated fluoride content in foods from McClure (1943, 1949), and selected foods from Cholak (1960) and USDA (2005). Taken from tables presented in USEPA 2010b. The items chosen from McClure (1943, 1949) are occasionally or frequently consumed in northern Ghana, except spinach; and the milk is usually powdered or concentrated liquid.

	McClure (1943, 1949)	Cholak (1960)	USDA (2005)
Food Item	**Range mg F^- kg^{-1}**	**Range mg F^- kg^{-1}**	**Range mg F^- kg^{-1}**
Orange	0.22	--	--
Banana	0.23	--	0.01
Tomato	0.24 to 0.9	--	0.02
Spinach[a]	0.21 to 1.8	--	0.38
Black eyed beans (peas)	0.23	--	--
Peanuts (groundnuts)	0.20	--	--
Wheat flour	0.27 to 0.45	--	--
Spaghetti, dry	0.80	--	0.18
Rice cooked[b]	<0.1 to 0.67	--	0.41
Bread[b]	1.0	--	0.49
Milk, fresh	0.07 to 0.55	0.07 to 0.55	0.03
Eggs	0.12 to 1.18	0.0 to 1.48	0.05
Beef	<0.2 to 0.67	0.2 to 0.33	0.22
Mutton (sheep)	<0.20	--	--
Chicken	1.40	1.40	0.15
Fish, fresh	1.49 to 1.63	0.1 to 84.47	0.18
Mackerel, canned	12.10	--	--
Coffee[b]	0.2 to 1.6	--	--
Chocolate milk	0.5 to 2.0	--	--
Tea[b]	4.1 to 398	--	--

[a]Included as an example of a green leafy vegetable, but spinach is not part of the diet in northern Ghana;
[b]the fluoride concentration will also depend on the fluoride concentration of water used for preparation.

References

Amalraj, A., Pius, A. 2013. Health risk from fluoride exposure for a population in selected areas of Tamil Nadu South India. Food Sci. and Human Wellness 2, 75-86.

Aoba, T., Fejerskov, O. 2002. Dental fluorosis: Chemistry and biology. Crit. Rev. Oral. Biol. Med. 13, 155-170.

Apambire, W.B., Boyle, D.R., Michel, F.A. 1997. Geochemistry, genesis, and health implications of fluoriferous groundwaters in the upper regions of Ghana. Environmental Geology 33, 13-23.

Apambire, W.B. 2000. Geochemical Modeling and Geomedical Implications of Fluoriferous Groundwaters in the Upper East Region of Ghana. Unpublished Ph.D. dissertation, University of Nevada-Reno, Reno, NV.

APHA (American Public Health Association). 1998. Standard Methods for the Examination of Wastewater. American Public Health Association, American Water Works Association, Water Environment Federation publication. APHA, 20th Ed, Washington D.C.

Atipoka, F.A. 2009. Water supply challenges in rural Ghana. Desalination 248, 212-217.

ATSDR (Agency for Toxic Substances and Disease Registry). 2003. Toxicological Profile for Fluorides, Hydrogen Fluoride, and Fluorine. U.S. Department of Health and Human Services, Division of Toxicology/Toxicology Information Branch, Atlanta, GA.

BIS (Bureau of Indian Standards). 2012. Indian Standard Drinking Water – Specification, Second Revision. IS 10500. Bureau of Indian Standards, New Delhi.

Burt, B.A., Eklund, S.A. 1999. Dentistry, Dental Practice, and the Community. 5th ed. W.B. Saunders Co., Philadelphia, PA.

Cholak, J. 1960. Current information on the quantities of fluoride found in air, food, and water. Arch. Indust. Health 21, 312-315.

CMNHW (Canadian Ministry of National Health and Welfare). 1981. Tap water consumption in Canada. (Document number 82-EDH-80). Public Health Affairs Directorate, Department of National Health and Welfare, Ottawa, Ontario.

Cerklewski, F.L. 1997. Fluoride bioavailability-nutritional and clinical aspects. Nutr. Res. 17, 907-929. DOI: 10.1016/S0271-5317(97)00057-2.

Cremer, H.D., Buttner, W. 1970. Absorption of fluorides. In: Fluorides and human health. WHO monograph No. 59, World Health Organization Geneva, p. 75-91.

Dean, H.T. 1942. The investigation of physiological effects by the epidemiology method. In: Fluoride and Dental Health. Pub. Am. Assoc. Advance. Sci. no. 19, 23-31.

DECLG (Department of the Environment, Community and Local Government). 2014. European Union (Drinking Water) Regulations. S.I. 122. Stationary Office, Dublin.

Ericsson, Y. 1968. Influence of sodium chloride and certain other food components on fluoride absorption in the rat. J. Nutr. 96, pp 60-68.

Ershow, A.G., Cantor, K.P. 1989. Total Water and Tapwater Intake in the United States: Population-Based Estimates of Quantities and Sources. No. 263-MD-810264, National Cancer Institute.

Fawell, J., Bailey, K., Chilton, J., Dahi, E., Fewtrell, L., and Magara, Y. 2006. Fluoride in Drinking-water. WHO Drinking-water Quality Series, World Health Organization, Geneva.

Fejerskov, O., Manji, F., Baelum, V. 1990. The nature and mechanisms of dental fluorosis in man. J. Dent. Res. 69 (Special Issue), 692-700.

Galagan, D.J., Lamson, G.G. 1953. Climate and endemic dental fluorosis. Public Health Reports. Vol. 68, 497-508.

Galagan, D.J., Vermillion. 1957. Climate and Fluid Intake. Public Health Reports. Vol. 72 (6), 484-490.

Health Canada. 2010. Guidelines for Canadian Drinking Water Quality: Guideline Technical Document – Fluoride. Water, Air and Climate Change Bureau, Healthy Environments and Consumer Safety Branch, Health Canada, Ottawa, Ontario.

Heller, K.E., Sohn, W., Burt, B.A., Eklund, S.A. 1999. Water consumption in the United States in 1994-96 and implications for water fluoridation policy. J. Public Health Dent. 59, 3-11.

Heller, K.E., Sohn, W., Burt, B.A., Feigal, R.J 2000. Water consumption and nursing characteristics of infants by race and ethnicity. J. Public Health Dent. 60, 140-146.

Hem, J.D. 1985. Study and Interpretation of the Chemical Characteristics of Natural Water. Water Supply Paper 2254, 3rd edition. US Geological Survey, Washington D.C., 263 pp.

Hong, L, Levy, S., Warren, J., Broffitt, B., Cavanaugh, J. 2006a. Fluoride intake levels in relation to fluorosis development in permanent maxillary central incisors and first molars. Caries Res. 40, pp 494-500.

Hong, L, Levy, S.M, Broffitt, B., Warren, J.J, Kanellis, M.J., Wefel, J.S., Dawson, D.V. 2006b. Timing of Fluoride intake in relation of development of fluorosis on maxillary central incisors. Commun. Dent. Oral Epidemiol. 34, 299-309.

Hopkin, S.M., and Ellis, J.C. 1980. Drinking Water Consumption in Great Britain. Technical Report TR 137, Water Research Centre, Medmenham, UK.

Institute of Medicine. 1997. Dietary Reference Intakes for Calcium, Phosphorous, Magnesium, Vitamin D, and Fluoride. National Academies Press, Washington D.C.

Jagtab, S., Yenkie, M.K., Labhsetwar, N., Rayalu, S. 2012. Fluoride in drinking water and defluoridation of water. Chemical Reviews 112, 2454-2466.

Kuczmarski, R.J., Ogden, C.L., Guo, S.S. et al. 2002. 2000 CDC growth charts for the United States: Methods and development. National Center for Health Statistics. Series 11, Data from the National Health Survey no. 246, Washington D.C.

Levy, S.M. 1994. Review of fluoride exposures and ingestion. Community Dent. Oral Epidemiol. 22, 173-180.

Malde, M.K., Maage, A., Macha, E., Julshamn, K., Bjorvatn, K. 1997. Fluoride content in selected food items from five areas in East Africa. J. Food Comp. Anal. 10, 233-245.

McClure, F.J. 1943. Ingestion of fluoride and dental caries. Quantitative relations based on food and water requirements of children 1-13 years old. Am. J. Dis. Child. 66, pp 362-369. [Republished 1962, 85, pp 283-286. U.S. Public Health Service].

McClure, F.J. 1949. Fluoride in foods. Public Health Reports vol. 64 (34), 1061-1074.

Murray, J.J. [Ed.]. 1986. Appropriate Use of Fluorides for Human Health. World Health Organization, Geneva.

MEPPRC (Ministry of Environmental Protection of People's Republic of China). 2002. Environmental Quality Standards for Surface Water. GB-3838-2002, Ministry of Environmental Protection of People's Republic of China, Beijing.

NHMRC, NRMMC. 2011. Australian Drinking Water Guidelines Paper 6. National Water Quality Management Strategy. National Health and Medical Research Council, National, Resource Management Ministerial Council, Commonwealth of Australia, Canberra.

NRC (National Research Council). 1993. Health Effects of Ingested Fluoride. National Academies Press, Washington D.C.

NRC (National Research Council). 2006. Fluoride in Drinking Water: A Scientific Review of EPA's Standards. National Academies Press, Washington D.C.

Ozsvath, D.L. 2009. Fluoride and environmental health: a review. Rev. Environ. Sci. Biotechnol. 8, 59-79.

Shu, W.S., Zhang, Z.Q., Lan, C.Y., Wong, M.H. 2003. Fluoride and aluminum concentrations of tea plants and tea products from Sichuan Province, PR China. Chemosphere 52, 1475-1482.

TBS (Tanzania Bureau of Standards). 2007. Environmental Management (Water Quality Standards) Regulations. Tanzania Bureau of Standards, Dar es Salaam.

US Army. 1983. Water consumption: Planning factors study. Fort Lee VA: Directorate of Combat Developments, U.S. Army Quartermaster School.

USDA (U.S. Department of Agriculture). 2005. USDA National Fluoride Database of Selected Foods and Beverages, Release 2. Nutrient Data Laboratory, Agricultural Research Services, U.S. Department of Agriculture. Beltsville, MD.

USDHHS (U.S. Department of Health and Human Services). 2011. Proposed HHS Recommendation for Fluoride Concentration in Drinking Water for Prevention of Dental Caries, 76 Federal Register 2383, Washington D.C.

USEPA (U.S. Environmental Protection Agency). 2010a. Fluoride: Dose-Response Analysis for Non-Cancer Effects. Health and Ecological Criteria Division, Office of Water, U.S. Environmental Protection Agency, Washington D.C. EPA 820-R-10-019.

USEPA (U.S. Environmental Protection Agency). 2010b. Fluoride: Exposure and Relative Source Contribution Analysis. Health and Ecological Criteria Division, Office of Water, U.S. Environmental Protection Agency, Washington D.C. EPA 820-R-10-015.

USEPA (U.S. Environmental Protection Agency). 2011. Exposure Factors Handbook. National Center for Environmental Assessment, Office of Research and Development, EPA/600/R-090/052F, U.S. Environmental Protection Agency, Washington D.C.

Viswanathan, G., Jaswanth, A., Gopalakrishnan, S., Siva ilango, A., Aditya, G. 2009. Determining the optimal fluoride concentration in drinking water for fluoride endemic regions in South India. Sci. Total Environ.407, 5298-5307.

Weinstein, L. H., Davison, A.W. 2004. Fluorides in the Environment. CABI Publishers, Massachusetts.

Whitford, G.M. 1994a. Effects of plasma fluoride and dietary calcium concentrations on GI absorption and secretion of fluoride in the rat. Calcif. Tissue Int. 54, pp 421-425.

Whitford, G.M. 1994b. Intake and metabolism and metabolism of fluoride. Advanced Dental Research. 8, 5-14.

Whitford, G.M. 1996. The metabolism and toxicity of fluoride, Monographs in Oral Science, Base, Karger, New York. 12, 46-58.

Whitford, G.M. 1997. Determinants and mechanisms of enamel fluorosis. Ciba Foundation Symposium 205, 226-241.

WHO (World Health Organization). 1984. Fluorine and Fluorides. Environmental health Criteria 36. World Health Organization, Geneva.

WHO (World Health Organization). 1993. Guidelines for Drinking Water Quality. Volume 1, 2nd edition. World Health Organization, Geneva.

WHO (World Health Organization). 2004. Fluoride in Drinking Water. Background document for development of: WHO Guidelines for Drinking-water Quality, World Health Organization, Geneva.

WHO (World Health Organization). 2011. Guidelines for Drinking Water Quality. Volume 1, 4th edition. World Health Organization, Geneva.

Wong, M.H., Fung, K.F., Carr, H.P. 2003. Aluminum and fluoride content in tea, with emphasis on brick tea, and their health implication. Toxicol. Lett. 137, 111-120.

Yi, J, Cao, J. 2008. Tea and fluorosis. J. Fluorine Chem. 129, pp 76-81.

CHAPTER 4

COMPARING ACTIVATED ALUMINA WITH INDIGENOUS LATERITE AND BAUXITE AS POTENTIAL SORBENTS FOR REMOVING FLUORIDE FROM DRINKING WATER IN GHANA

Craig, Laura, Stillings, Lisa L., Decker, David, L., Thomas, James, M.

Published in: Applied Geochemistry 56 (2015), 50-66

Abstract

Fluoride is considered beneficial to teeth and bones when consumed in low concentrations, but at elevated concentrations it can cause dental and skeletal fluorosis. Most fluoride-related health problems occur in poor, rural communities of the developing world where groundwater fluoride concentrations are high and the primary sources of drinking water are from community hand-pump borehole drilled wells. One solution to drinking high fluoride water is to attach a simple de-fluoridation filter to the hand-pump; and indigenous materials have been recommended as low-cost sorbents for use in these filters. In an effort to develop an effective, inexpensive, and low-maintenance de-fluoridation filter for a high fluoride region in rural northern Ghana, this study conducted batch fluoride adsorption experiments and potentiometric titrations to investigate the effectiveness of indigenous laterite and bauxite as sorbents for fluoride removal. It also determined the physical and chemical properties of each sorbent. Their properties and the experimental results, including fluoride adsorption capacity, were then compared to those of activated alumina, which has been identified as a good sorbent for removing fluoride from drinking water. The results indicate that, of the three sorbents, bauxite has the highest fluoride adsorption capacity per unit area, but is limited by a low specific surface area. When considering fluoride adsorption per unit weight, activated alumina has the highest fluoride adsorption capacity because of its high specific surface area. Activated alumina also adsorbs fluoride well in a wider pH range than bauxite, and particularly laterite. The differences in adsorption capacity are largely due to surface area, pore size, and mineralogy of the sorbent.

1. Introduction

Naturally occurring fluoride in drinking water is largely considered the main contributor of dietary fluoride intake, and populations living in hot climates with high water consumption are potentially at increased risk of exposure (Murray, 1986). Though it is widely agreed that fluoride is considered beneficial to teeth and bones – like many essential nutrients – it is healthful in small amounts but damaging at high concentrations (Fawell et al., 2006). In temperate climates, a concentration of 1 mg L^{-1} fluoride in drinking water has been associated with decreased dental caries (Fawell et al., 2006), but higher concentrations in or near developing tooth enamel can result in dental fluorosis in children and adolescents (Whitford, 1997). Dental fluorosis is an irreversible condition that causes discoloration of the teeth, erosion of enamel, and pitting (Whitford, 1997). Dental fluorosis has been documented in Ghana (Apambire et al., 1997; Apambire, 2000), as well as other parts of the world, including the United States, Latin America, East Africa, and Asia (Fawell et al., 2006). Concentrations above 1.5 mg L^{-1} are associated with dental fluorosis, concentrations at 3 mg L^{-1} or higher are associated with skeletal fluorosis, and concentrations above 10 mg L^{-1} are associated with crippling skeletal fluorosis (WHO, 1984; WHO, 2008). Skeletal fluorosis, which affects all ages, has also been documented in several countries, but is most pronounced in parts of Asia and East Africa (Fawell et al., 2006). Skeletal fluorosis can result in osteosclerosis, ligamentous and tendinous calcification, and bone deformity (Fawell et al., 2006).

As a means of protecting human health, the World Health Organization (WHO) developed guidelines recommending a daily fluoride intake of 1.5 mg L^{-1} or less. But, controlling excess fluoride in drinking water is difficult in poor rural communities where

water sources are dispersed and communal, and where advanced de-fluoridation techniques are unavailable (Fawell et al., 2006). Under these conditions, if another source of drinking water exists, then the recommendation usually is to close the contaminated source (e.g. hand-pump well) and find another water source. In cases where a safe alternative supply of drinking water is not available, which is frequently the situation in northern Ghana (CWSA-CIDA, 2005), a simple cost-effective de-fluoridation system coupled with a maintenance program is needed. In communities with limited resources, the most promising de-fluoridation methods are adsorption, co-precipitation, or contact precipitation (Fawell et al., 2006). Adsorption media include laterite, bauxite, bone charcoal, and activated alumina; co-precipitation techniques, such as the Nalgonda technique developed in India, utilize aluminum sulfate and lime to remove fluoride; and calcium and phosphate compounds are common filter media for contact precipitation (Fawell et al., 2006). Reverse osmosis (Simmons, 1993; Sehn, 2008) and electrodialysis (Adhikary et al., 1989) are also options, but cost and maintenance are substantially higher (Ayoob et al., 2008).

When considering the various methods for de-fluoridation of drinking water, adsorption is widely used and is a more attractive method for fluoride removal when considering cost, simplicity of design, and operation (Mohapatra et al., 2009; Miretzky and Cirelli, 2011). Specifically, adsorption using indigenous materials has been suggested in order to keep costs down (Zevenbergen et al., 1996; Mjengera and Mkongo, 2003; Sarkar et al., 2006; Sarkar et al., 2007; Ayamsegna et al., 2008; Bhatnagar et al., 2011). Laterite, which is abundant in northern Ghana, has been recommended as a low-cost natural sorbent for fluoride removal from drinking water (Sarkar et al., 2006; Sarkar et

al., 2007; Cumberbatch et al., 2008). Alternately, laterite's most aluminum rich ore, bauxite, has also been recommended as a sorbent for removing fluoride (Ayamsegna et al., 2008; Sujana and Anand, 2011). Bauxite is indigenous to Ghana as well, but is found in the more distant Western Region. Based on the above recommendations, the adsorption capacity of Ghanaian laterite and bauxite was tested for potential use in small treatment systems in the rural north. They also were compared to activated alumina – a synthetic material that must be purchased, but one that has proven effective as a sorbent for fluoride removal (Hao and Huang, 1986; Farrah et al., 1987; Fletcher et al., 2006). Cost, preparation, and overall effectiveness were then considered when evaluating each sorbent for use in a rural Ghanaian community with drinking water fluoride concentrations up to 4.6 mg L^{-1} – with Bongo granite identified as the naturally occurring source of groundwater fluoride in the region (Apambire et al., 1997; Apambire, 2000).

2. Materials and methods

2.1. Sorbent preparation

The three sorbents being tested were: Ghana bauxite, which was provided by an aluminum mining company in the country's Western Region; Namoo laterite, which was collected in the study area of the Upper East Region of Ghana; and activated alumina, which was provided by World Vision Ghana with no manufacturing information given. The sorbents were cleaned and sieved well to maintain the purity of the sample and to isolate particle sizes. The activated alumina, with a manufactured grain size range of 0.5 to 1.0 mm, was sieved to remove powder. Bauxite and laterite each were ground and sieved to two desired grain size ranges of 0.5 to 1.0 mm, and 63 to 125 μm. The three sorbents were rinsed well with deionized water until the water ran clear, in order to

remove fine powder. An acid-base wash was then applied to increase sample purity and reproducibility of the titrations and batch adsorption experiments (Huang, 1981). Each sorbent was soaked in 0.01 N NaOH, stirred for 30 minutes, and centrifuged for 30 minutes at 26,890 g relative centrifugal force (RCF) using a Sorvall® RC-5B centrifuge. It was rinsed again with deionized water by pouring off the supernate until the electrical conductivity was less than 5 µS cm^{-1}. The sorbent was soaked again for 30 minutes with 0.01 N HCl, centrifuged, and rinsed as described for the 0.01 N NaOH. Once clean, the sorbent was left to dry and then sieved again to remove final traces of powder with grain size smaller than 0.5 mm for 0.5 to 1.0 mm samples, and smaller than 63 µm for 63 to 125 µm samples.

2.2. Sorbent physical-chemical properties

The specific surface area, and pore surface area and volume of the activated alumina, laterite, and bauxite at grain size 0.5 to 1.0 mm were determined using a Micromeritics® TriStar 3000 static pressure surface area analyzer with $N_{2(g)}$ as the sorbate. The 10-point Brunauer, Emmett, Teller (BET) method was used to determine specific surface area (Brunauer, et al., 1938; Lowell and Shields, 1991). The Barrett, Joyner, Halenda (BJH) adsorption method was used to determine pore area and volume for pores in the range of 1.7 to 300 nm (Barrett et al., 1951; Lowell and Shields, 1991). Using the $N_{2(g)}$ adsorption and desorption isotherm data for calculating the BET surface area and BJH pore area and volume, microporosity (< 2 nm) was also determined by creating *t*-plots (Gregg and Sing, 1982; Hay et al., 2011). The *t*-plot was created by plotting the calculated statistical film thickness (*t*) on the x-axis vs. the volume of liquid

nitrogen adsorbed to the surface on the y-axis (liquid nitrogen density of 0.808 g ml^{-1} at 77 K). The statistical film thickness was calculated from the Harkins-Jura equation:

$$t\ [\text{Å}] = \sqrt{\frac{13.99}{0.034 - \log(\frac{p}{p^o})}} \quad (1)$$

Evidence of micropores and corresponding pore volumes were determined by the linear portions of the *t*-plot and the y-intercept (see Gregg and Sing, 1982; Leofanti et al., 1998; Hay et al., 2011). The statistical thickness (*t*) was presented in nanometers (nm), where 1 nm = 10 angstroms (Å); and p/p^o is the relative pressure used in creating the $N_{2(g)}$ sorption isotherms.

The mineral content of each sorbent was determined using x-ray diffraction (XRD). Each sample was prepared by grinding it initially by hand in a pestle and mortar until it passed through a sieve with openings of 500 µm. The sample was then ground to a powder in a McCrone mill for 8 minutes in 10 ml of methanol. Subsequently, it was air dried, gently re-crushed in a pestle and mortar to break up aggregates formed during drying, and side-loaded into specially-designed sample holders. The samples were then analyzed on a Bruker D8 Advance XRD equipped with a Sol-X (solid state) detector. The resulting XRD scans were viewed and interpreted using the Bruker XRD data evaluation software called EVA®. A background correction was performed on each scan before interpretation. Minerals were identified by matching to reference mineral patterns stored in the ICDD (International Centre for Diffraction Data).

The percent distribution of major oxides in Namoo laterite was determined using a Varian Vista®-PRO for analysis via inductively coupled plasma-atomic emission spectroscopy (ICP-OES). Before analysis, each sample was digested by placing 100 g of

sample into a polypropylene bottle mixed with 0.5 ml of solution of one part HNO_3 and three parts HCl. An additional 3 ml of concentrated HF was then added for a total solution volume of 3.5 ml. The mixture was capped and heated at about 100 ^oC in an oven for one hour and left to cool. The solution was transferred to a 100 ml borosilicate volumetric flask, filled to a total volume of 100 ml with deionized water, and then transferred back to the polypropylene bottle. The dissolved rock in solution was then ready to be analyzed for the oxides Al_2O_3, Fe_2O_3, and SiO_2 using ICP-OES.

The percent distribution of major oxides was determined in activated alumina and Ghana bauxite using x-ray fluorescence (XRF) using a Bruker S8 Tiger WD-XRF. Elements were measured as oxides in semi-quantitative mode using a helium atmosphere. Standard glass discs were analyzed at the start of each analytical work day to assess precision and accuracy of the semi-quantitative calibration curve. After analysis, qualitative XRF spectra were screened to assess accuracy of the peak search algorithm. Quantitative results were calculated based on measured net intensities using the EVAL2® software package. The relationship between net intensities and concentrations was determined using the built-in semi-quantitative calibration curve. Elemental concentrations were calculated and normalized to 100%. Oxygen concentration was calculated by stoichiometry. Uncertainties were determined by replicate analysis of individual samples.

The surface of each sorbent was observed using scanning electron microscopy (SEM) with a Hitachi S-4700 II Scanning Electron Microscope. The sample particles were mounted on the aluminum stubs, and coated with platinum in an Emitech K-575X sputter coater in order to make particles electronically conductive. The images were taken

with a Hitachi cold field emission scanning electron microscope model S-4700-II equipped with the Oxford Energy Dispersive Spectroscope detector for chemical composition analysis.

2.3. Acid-base titrations

The method for acid-base titrations was modified from Huang and Stumm (1973), Huang (1981), and Hao and Huang (1986). One gram of sorbent with grain size 0.5 to 1.0 mm was placed in a Nalgene® polypropylene copolymer centrifuge tube and filled to 40 ml with deionized water. The slurry was soaked for two weeks to fully hydrate the sorbent. Before titration, the liquid was poured off and the sorbent rinsed with deionized water until the electrical conductivity of the rinsate was less than 5 $\mu S\ cm^{-1}$. The sorbent was placed in a 250 ml polypropylene beaker with a small, known volume of deionized water; the ionic strength was adjusted to either 0.1 M or 0.01 M with 1 M NaCl, and the beaker was then filled to a total volume of 150 ml with deionized water for a sorbent-to-solution ratio of 6.67 $g\ L^{-1}$. The beaker was covered leaving ports to permit access for a gel-filled Ag/AgCl pH probe attached to an Orion® 4-Star meter, a tube to bubble $N_{2(g)}$ into the suspension to exclude $CO_{2(g)}$, and for adding titrant. The beaker was placed on a magnetic stir plate, and stirred and bubbled with $N_{2(g)}$ until the pH stabilized, taking two to four hours. Upon stabilization, small increments of 0.1 N certified NaOH (stored in a glove box under $N_{2(g)}$ pressure) or 0.1 N certified HCl was added to the slurry. The pH of each increment was recorded when there was no change in pH (reading to 0.01 pH units) for one to three minutes. This usually took five to ten minutes depending upon the sorbent. If the pH did not stabilize after 10 minutes – which occurred with several

readings for activated alumina and a few for laterite – the pH was recorded and the titration continued.

To check whether sorbent was lost in the rinsing, batch adsorption, or titration, the used sorbent was dried and weighed. Bauxite, laterite, and activated alumina lost 0 to 3% of the initial weight from the titrations and batch adsorption experiments, with an average loss of approximately 1.2%. The surface area of the used sorbents was not determined, but the grain size range was measured again for eleven samples (seven activated alumina and two each laterite and bauxite) to note any decrease. Of the used sorbent, an average of 3.8% (0.038 g of 1 g initial mass) measured under 0.5 mm with a range of 0 to 9% of the grain measuring under 0.5 mm. There was no notable pattern with any of the sorbents regarding grain size loss, but some total mass loss occurred more often with the activated alumina than with the other two sorbents.

2.4. Determining pH dependent surface charge

The millimoles of protons adsorbed to or desorbed from the surface of the three hydrated sorbents were determined by potentiometric titration as described in section 2.3. The surface charge (in mols L^{-1}) of each sorbent was then calculated using the following equations (Huang and Stumm, 1973; Hao and Huang, 1986):

$$H^+ \text{ adsorbed [mols } L^{-1}] = \frac{\text{g sorbent } L^{-1} * \{[(0.1 \text{ N HCl}) * (\text{L titrant added})] - [[H^+] * (\text{L total})]\}}{\text{g sorbent}} \quad (2)$$

$$H^+ \text{ desorbed [mols } L^{-1}] = \frac{\text{g sorbent } L^{-1} * \{[(0.1 \text{ N NaOH}) * (\text{L titrant added})] - [[OH^-] * (\text{L total})]\}}{\text{g sorbent}} \quad (3)$$

The resultant titration curves of pH vs. mmols of surface charge per liter of solution were used to determine intrinsic acidity constants (K_a^{int}) by matching modeled titration curves with the experimentally determined titration curves. The model curves

were created using the generalized two-layer surface complexation model (Dzombak and Morel, 1990) in the PHREEQC program (Parkhurst and Appelo, 1999), which will be discussed in section 2.6.

2.5. Estimating the value for surface site density

In order to calculate acidity constants for surface complexation modeling, the surface site density must be determined for each sorbent. Surface complexation models depend on the assumption that sorbing ions occupy specific sites on the sorbent surface (Sahai and Sverjensky, 1997). Although it is generally understood that surfaces are heterogeneous and energetically distinct, a single site and energetically identical assumption is made for most models (Sahai and Sverjensky, 1997). Even so, accurately determining the number of active surface sites is difficult, in part because the estimated number of surface sites for the same sorbent often varies depending upon the method used (Kosmulski, 2001). Because of the uncertainty regarding the best approach for estimating surface site density, as well as the wide variation in surface site density values presented in the literature for the minerals of interest here, a single representative N_s value was used for all calculations in this study. This was done to be consistent and minimize bias, and because the true value for the number of exchangeable surface sites may be difficult to determine. To identify the optimum N_s value for all three sorbents, surface site density values between 2 and 8 sites nm^{-2} were used in the PHREEQC program and adjusted along with the intrinsic acidity constants, for a best overall fit. The range of 2 to 8 sites nm^{-2} was chosen because this range is most commonly used in surface complexation modeling (e.g. Sigg and Stumm (1980); Dzombak and Morel (1990); Yang et al. (2007); Karamalidis and Dzombak (2010)). In addition, Davis and

Kent (1990) recommended 2.31 sites nm^{-2} for all modeling, which is consistent with Dzombak and Morel (1990).

2.6. Geochemical modeling of acid-base titration data using the generalized two-layer surface complexation model with PHREEQC program

The generalized two-layer model (Dzombak and Morel, 1990) is a surface complexation model in the PHREEQC program (Parkhurst and Appelo, 1999), and was used to describe the adsorption reactions occurring on each sorbent. Surface complexation models, such as the generalized two-layer model, have an advantage over conditional distribution coefficients because they describe surface reactions with quasi thermodynamic constants which are independent of changes in solution concentrations (Hayes, 1987). A key component of the generalized two-layer model is the diffuse layer model proposed by Stumm et al. (1970) and Huang and Stumm (1973) where the oxide-water interface comprises a surface layer for specifically sorbed ions and a diffuse layer of counter-ions in solution. The surface charge is determined by proton adsorption and desorption (equations (2) and (3)), as well as the surface coordination reactions of other ions (Dzombak and Morel, 1990). A diffuse layer of counter-ions in solution adjacent to the charged surface is assumed, with the relationship between surface charge and surface potential fixed by the electric double layer theory. Surface charge of the sorbent is also limited by the number of surface sites and, as a result, the near-surface ion densities are constrained to reasonable values. In addition, adjustments are made for conditions with high surface potential (low ionic strength) to calculate surface charge. Equations used to calculate the surface charge density and intrinsic equilibrium constants, as well as the theory behind the generalized two-layer surface complexation model, can be found in

Dzombak and Morel (1990). Detailed descriptions of surface complexation theory can also be found in Davis and Kent (1990), Hayes et al. (1991), Stumm (1992), and Appelo and Postma (2005).

The generalized two-layer model in PHREEQC was used to determine the intrinsic acidity constants K_a^{int} for proton adsorption onto a hydrated surface as described by the following reactions:

$$S - OH_2^+ \leftrightarrow S - OH + H^+ \quad (4)$$

$$S - OH \leftrightarrow S - O^- + H^+ \quad (5)$$

This was achieved by matching experimental titration curves (section 2.3 and 2.4) and modeled curves. The simulated acid-base titrations used the PHREEQC database. The program's diffuse layer option could be used or ignored, as the same results were achieved with or without it in these simulations. The default option (no diffuse layer) accounted for the surface charge by creating an equal and opposite charge in solution (Parkhurst and Appelo, 1999). The mass action expressions for proton adsorption and desorption (using reactions (4) and (5)) and the corresponding $logK_a^{int}$ were input parameters. Other input parameters were: specific surface area, sorbent-to-solution ratio (6.67 g of sorbent L^{-1}), a single N_s value (as N_t = mols charge L^{-1}), and an inert electrolyte (NaCl) background solution at I = 0.01 and 0.1 M. Several N_s values ranging from 2 to 8 sites nm^{-2} were tested for best fit to experimental data before narrowing to a single N_s value. To identify the optimum N_s value for all sorbents, both the N_s and the $logK_a^{int}$ values were manipulated to fit with an experimentally determined titration curve. Once the optimum N_s value was determined, based on overall best fit for all sorbents, the $logK_a^{int}$ value was then treated as the only adjustable parameter for a best

fit to experimental titration data. A single $logK_{a1}^{int}$ and $logK_{a2}^{int}$ was determined for each sorbent to represent an average intrinsic acidity constant for all minerals comprising each sorbent. The pH of zero net proton charge (pH_{PZNPC}) was estimated by adding pK_{a1}^{int} and pK_{a2}^{int} and dividing by 2.

2.7. Fluoride batch adsorption experiments

The method for conducting fluoride batch adsorption experiments was modified from Hao and Huang (1986). For ease of comparison, the fluoride concentrations in the following sections will be presented in millimoles (mmol) rather than milligrams (mg), with both units presented where possible. To set up the batch adsorption experiments at varied pH, 0.2 g of sorbent at a grain size 0.5 to 1.0 mm (unless noted otherwise) was added to a Nalgene® polypropylene copolymer centrifuge tube; 1 M NaCl was added to achieve the desired ionic strength; 52.64 mmol L^{-1} (1000 mg L^{-1}) NaF fluoride standard was added to attain a final fluoride concentration of 0.53 mmol L^{-1} (10 mg L^{-1}); the desired pH was obtained using 0.1 N HCl or 0.1 N NaOH; and deionized water was added to bring the total volume of the reactor to 30 ml for a sorbent-to-solution ratio of 6.67 g L^{-1}. Batches of twelve to sixteen slurry-filled centrifuge tubes were rocked back and forth for 24 hours using a Labquake®. After rotation, the tubes were centrifuged for 30 minutes at 26,890 g RCF. Ten ml of the supernate was removed for pH analysis using an Accumet® Research AR 20 pH meter and probe, and for fluoride analysis using an Orion 4-Star meter and fluoride ion selective electrode, with TISAB III added to the supernate just before fluoride analysis (Hao and Huang, 1986; APHA, 1998). Each probe was calibrated before use. Calibration checks were conducted on the fluoride probe every 8 to 10 samples in order to maintain an error under 5%.

The method for the fluoride loading batch adsorption experiments was similar to that described above, but with the pH kept constant and the fluoride concentration varied. Also, the sorbent was first rotated 24 hours in Nalgene® polypropylene copolymer centrifuge tubes in a NaCl solution of ionic strength 0.01 M. After 24 hours the pH was measured and adjusted to approximately 6.9 to 7.0, which is within the pH range of high fluoride groundwater in the study area. Once the initial pH was stable, fluoride was added to each centrifuge tube in concentrations ranging from 0.026 to 1.58 mmol L^{-1} (0.5 to 30 mg L^{-1}) for the bauxite and laterite, and 0.026 to 3.16 mmol L^{-1} (0.5 to 60 mg L^{-1}) for the activate alumina. The slurries were rotated another 24 hours before reading the fluoride concentrations and pH. This approach was used because fluoride adsorption will increase pH slightly due to ion exchange with hydroxide (OH^-).

2.8. Geochemical modeling of fluoride adsorption data using the generalized two-layer surface complexation model with PHREEQC program

The generalized two-layer model was used to identify the fluoride adsorption reactions onto each of the three sorbents using the same input parameters described in section 2.6. The model curves were matched with experimental fluoride adsorption curves for both fluoride adsorption vs. pH and fluoride loading (pH_o ~6.9) and ionic strength of 0.01 M NaCl. The constants for the following fluoride adsorption reactions (Karamalidis and Dzombak, 2010) were adjustable input parameters:

$$S - OH + F^- + H^+ \leftrightarrow S - F + H_2O \quad (6)$$

$$S - OH + F^- \leftrightarrow S - OHF^- \quad (7)$$

$$S - OH + 2F^- + H^+ \leftrightarrow S - F_2^- + H_2O \quad (8)$$

To identify the appropriate fluoride adsorption reactions and corresponding equilibrium constants, each of the above reactions was initially added as an input parameter, and the

corresponding equilibrium constant treated as an adjustable parameter. Only the fluoride adsorption reactions that improved the model fit to experimental data were used. The same set of adsorption reactions and corresponding equilibrium constants was used for the fluoride adsorption vs. pH curves and for fluoride loading at constant pH.

2.9. Calculating the Freundlich and Langmuir isotherms and distribution coefficients

A common empirically based method for analyzing sorption is through the use of partition coefficients and isotherms (Honeyman and Leckie, 1986). Because these parameters and relationships are dependent upon the chemical composition of the aqueous solutions, many scientists consider them unsatisfactory (Kent et al., 1986; Honeyman and Santschi, 1988; Davis et al., 1990). However, because they are both widely used and simple, the Freundlich and Langmuir isotherms were calculated from the experimental data collected as described in section *2.7* to estimate the macroscopic distribution of fluoride in bulk solution and that adsorbed to each of the three sorbents at grain size 0.5 to 1.0 mm, with equilibrium conditions assumed. The Freundlich equation is:

$$s_i = K_F \, c_i^n \tag{9}$$

where, *s* is the sorbed concentration (mmol F^- sorbed g^{-1} sorbent); *i* is F^-; c is the solute concentration (mmol F^- L^{-1}); and K_F and *n* are adjustable coefficients. The Freundlich distribution coefficient (K_F) has the units of mmol F^- sorbed per g sorbent while the value for *n*, which measures the degree of non-linearity, is usually less than one (Stumm and Morgan, 1996). The Freundlich coefficients were calculated using the experimental data and the logarithm of equation (9):

$$\log s_i = \log K_F + n \log c_i \tag{10}$$

The above linearized form was then plotted with the log of the adsorbed concentration (s_i) on the y-axis and the log of the solution concentration (c_i) on the x-axis. The slope is *n* and the y-intercept is $logK_F$.

The Freundlich equation is a simple way to plot data empirically. Surface heterogeneity is incorporated into the equation, and it describes adsorption by assuming an unlimited number of adsorption sites (Stumm, 1992; Appelo and Postma, 2005). In contrast, the Langmuir equation assumes a finite number of adsorption sites which is considered more realistic. Also, the surface sites are treated as homogenous with no lateral interactions among the binding sites. The Langmuir equation can be derived from the law of mass action and has a more theoretical background than the Freundlich equation (Stumm, 1992; Appelo and Postma, 2005). The equation has the following form:

$$s_i = s_{max} \frac{K_L c_i}{1+K_L c_i} \quad (11)$$

where *s*, *i*, and *c* are identical to those components described above for the Freundlich equation, with s_{max} the maximum mmol F^- adsorbed per g of sorbent, and K_L is the Langmuir coefficient (L per mmol F^- dissolved). The Langmuir coefficient was calculated using Solver in Microsoft Excel®. The assumed reaction for fluoride adsorption described by the above Freundlich and Langmuir isotherms is:

$$S - OH + F^- \leftrightarrow S - F + OH^- \quad (12)$$

In reaction (12), S is the sorbent and fluoride (F^-) adsorbs via ion exchange with the hydroxide (OH^-).

2.10. Comparing the fluoride adsorption capacity at identical number of surface sites (4.3 mmol L^{-1}) under varied solution conditions

The fluoride adsorption capacity of bauxite, laterite, and activated alumina at grain size 0.5 to 1.0 mm was compared under conditions with equal mmols of surface sites per liter and three solution conditions. One solution was groundwater collected in the study area with a fluoride concentration of 0.21 mmol L^{-1} (4.0 mg L^{-1}), and pH of 7.8 (the pH at time of collection was 7.5 so the solution had aged, with some precipitation likely). The other two solutions were mixed in the laboratory with an ionic strength of 0.01 M NaCl and initial fluoride concentration of 0.27 mmol L^{-1} (5.17 mg L^{-1}). One lab mixed solution had an initial pH of 6.9, and the other was lowered to 4.5 for bauxite and laterite, and 5.5 for activated alumina. The lower pH was set to maximize fluoride adsorption. The sorbent-to-solution ratio for bauxite was 105 g L^{-1}, for laterite it was 26 g L^{-1}, and for activated alumina it was 2 g L^{-1}. The resultant number of sorption sites for all sorbents was 4.3 mmol L^{-1} (at surface site density 4.5 sites nm^{-2}). The experimental set up was similar to that used in section 2.7 for fluoride batch adsorption experiments, but with the above sorbent-to-solution ratios. Also, after 24 hours rotation, these samples were filtered with 0.4 µm filter paper rather than centrifuged as described in section 2.7. The pH and fluoride concentrations were measured as described in section 2.7.

2.11. Determining metals dissolution at low pH, high pH, and fluoride induced

To determine whether notable dissolution had occurred, batch experiments were conducted on each sorbent at pH 4.0 to 4.4 and at pH 9.8, with each solution analyzed for dissolved metals. The three sorbents were also evaluated for possible fluoride induced dissolution of aluminum, and bauxite and laterite for dissolved iron as well, at neutral pH

and initial fluoride concentration of 0.26 and 0.53 mmol L^{-1} (5 and 10 mg L^{-1} respectively). The experimental set up was similar to the batch experiments described in section 2.7. The solution was 0.01 M NaCl, and the sorbent-to-solution ratio was 6.67 g L^{-1} for the solutions containing fluoride and 30 g L^{-1} for the solutions with no fluoride. The solutions were rotated for about 24 hours, then filtered with 0.1 or 0.4 µm filter paper, acidified, and analyzed via inductively coupled plasma mass spectrometry (ICP-MS) for dissolved aluminum (all sorbents), dissolved iron (bauxite and laterite), and dissolved silica (laterite) using EPA Method 200.7. The detection limit for dissolved aluminum was 1.67 (10^{-3}) mmols L^{-1} (0.045 mg L^{-1}), for iron 1.79 (10^{-4}) mmols L^{-1} (0.010 mg L^{-1}), and silica 1.66 (10^{-3}) mmols L^{-1} (0.1 mg L^{-1}). The dissolved metal concentrations of samples with a sorbent-to-solution ratio of 30 g L^{-1} were re-calculated and presented with a sorbent-to-solution ratio of 6.67 g L^{-1}.

3. Results

3.1. Physical and chemical characteristics

3.1.1. Physical characteristics: BET surface area, BJH pore area and volume, t-plot analysis of microporosity, and SEM analysis of surfaces

The BET method was used to determine surface area, and the BJH method was used to determine pore area and volume for pores in the range of 1.7 to 300 nm (Table 4.1), both of which were calculated via $N_{2(g)}$ gas adsorption and desorption isotherms for each sorbent. The BET determined surface area can be unreliable for determining surface area, especially if there is extensive microporosity (<2 nm). Although Sing (1989) noted that the BET method for determining surface area can be fairly accurate if the sorption isotherm is type IV, the monolayer capacity can be identified, and if there is no notable

microporosity. For the three sorbents, the $N_{2(g)}$ sorption isotherms were type IV with a type H3 hysteresis loop (Fig. 4.1a, c, e) (see Sing, 1989; Leofanti et al., 1998; Hay et al., 2011)), and the monolayer capacity was identified. In addition, the BET *c* parameter (Davis and Kent, 1990) was 86 for activated alumina, 278 for bauxite, and 366 for laterite which is generally considered indicative of mesopore (2 to 50 nm) dominated sorbents. Gregg and Sing (1982) consider *c* values between 50 and 150 a valid range indicating no microporosity, but Davis and Kent (1990) found that sorbents with values as high as 475 may also show no microporosity. Similar to the BET method for determining surface area, the BJH method for determining pore area, size, and volume is widely used; but Gregg and Sing (1982) consider it an unreliable method for determining pore size distribution from type IV isotherms with an H3 hysteresis loop. Although Leofanti et al. (1998) noted that, if the sorbent is dominated by mesopores, the BJH method can determine mesopore size distribution and volume fairly well.

Table 4.1. The BET specific surface area, BJH cumulative pore area and volume using adsorption curve only (pores size between 1.7 and 300 nm diameter). The grain size was 0.5 to 1.0 mm for all sorbents.

Sorbent	Surface Area ($m^2\ g^{-1}$)	Pore Area ($m^2\ g^{-1}$)	Pore Volume ($cm^3\ g^{-1}$)
Act. alumina	288.9	281.4	0.35
Gh. bauxite	5.5	5.2	0.01
N. laterite	21.9	18.1	0.02

In Table 4.1 the BET specific surface area and BJH cumulative pore area and volume (pores between 1.7 and 300 nm diameters) are presented. Because of the uncertainty of the BJH pore area values, it is assumed that the results presented in Table 4.1 indicate that surface area and pore area are essentially the same. The surface and pore area as well as the pore volume of the activated alumina are substantially higher than

either bauxite or laterite. At grain size 0.5 to 1.0 mm, the surface area of activated alumina is over fifty times higher than bauxite, and thirteen times higher than laterite.

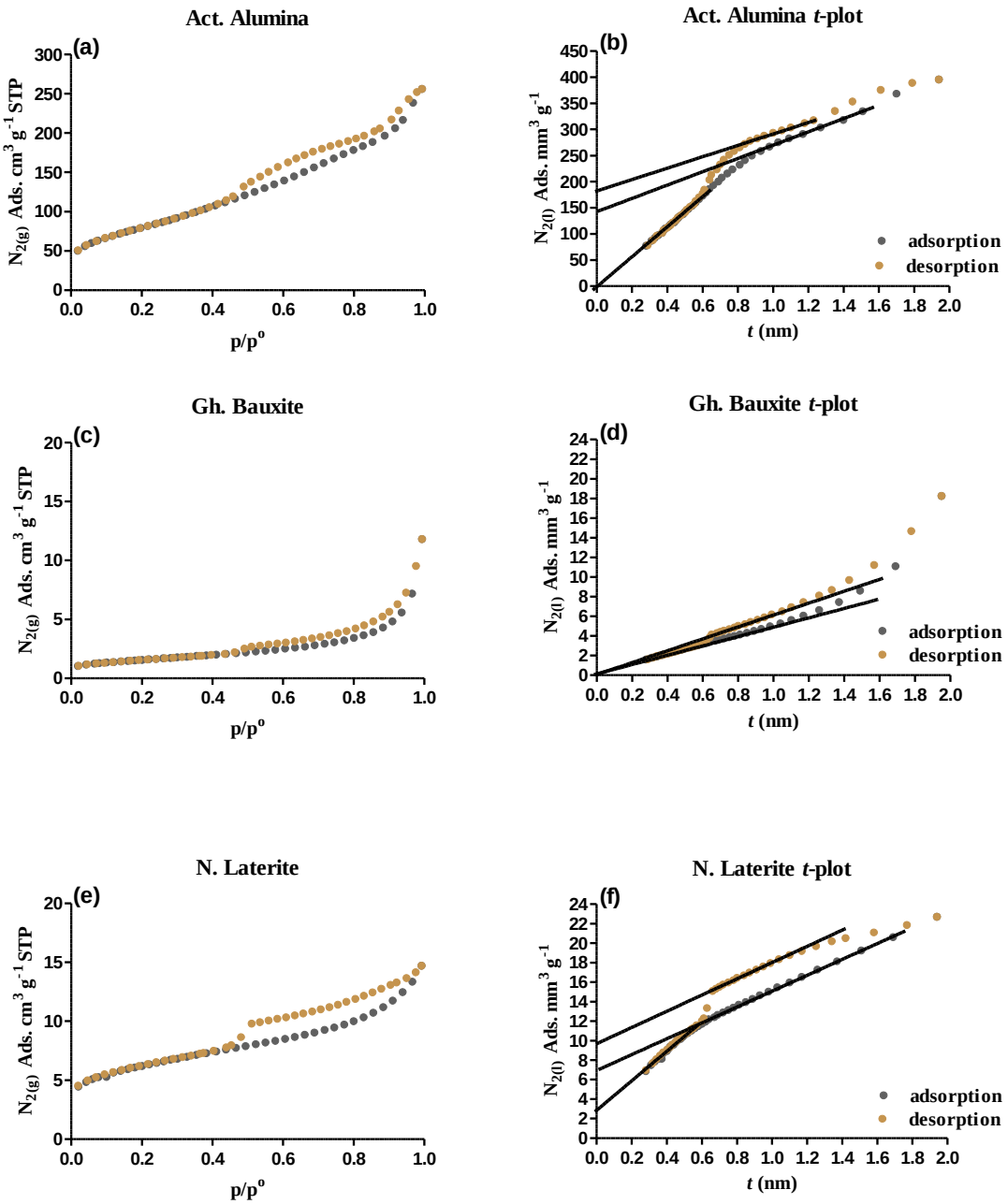

Fig. 4.1. $N_{2(g)}$ adsorption and desorption isotherms for (a) activated alumina, (c) Ghana bauxite, and (e) Namoo laterite; and *t*-plots of $N_{2(l)}$ adsorption and desorption isotherms for (b) activated alumina, (d) Ghana bauxite, and (f) Namoo laterite. The grain size was 0.5 to 1.0 mm for all sorbents.

In addition to the above methods for determining surface area and porosity, the *t*-plot method was applied since it is effective at determining whether micropores are present. Sorption isotherms and corresponding *t*-plots are presented in Fig. 4.1. Table 4.2. The first linear portion of the *t*-plot indicates whether micropores are present by a non-zero intercept, which also measures the micropore volume. The surface area using the *t*-plot was also determined from the slope of the lowest linear portion of the curve (Davis and Kent, 1990). The Bauxite has no micropores, as indicated by a straight line going through zero and the sharp upward deviation of the adsorption and desorption curves from the straight line at increased *t* values (Fig. 4.1d), which is indicative of mesopores (Storck et al., 1998). Laterite has micropores as indicated by a non-zero intercept for the lowest *t* values from 0.3 to 0.5 nm and y-intercept at 2.2 $mm^3\ g^{-1}$ micropore volume (de Boer et al., 1966; Davis and Kent, 1990; Storck et al., 1998; Hay et al., 2011). Laterite has another linear portion at t = 0.7 to 1.7 nm and y-intercept at 7.2 $mm^3\ g^{-1}$ pore volume (Fig. 4.1f). The laterite desorption curve is linear portion between 0.7 and 1.2 nm film thickness, with a y-intercept of 9.9 $mm^3\ g^{-1}$ pore volume. The *t*-plot for activated alumina has a straight line with a zero intercept for the lowest *t* values, which also suggests an absence of micropores and a second line with a y-intercept at 148 $mm^3\ g^{-1}$ pore volume, and film thickness t = 1.0 to 1.5 nm. The desorption curve the linear portion of the desorption curve is between t = 1.0 and 1.2 nm with a y-intercept of 186 $mm^3\ g^{-1}$ pore volume (Fig. 4.1b). The shape of the *t*-plot for laterite (and possibly activated alumina) indicates the presence of both micropores and mesopores, while the shape of the *t*-plot for bauxite indicates the presence of mesopores only (Storck et al., 1998). The BET surface area (Table 4.1) and *t*-plot calculated surface area (Table 4.2) are the same for bauxite,

while for activated alumina the values vary by a little under 4%, and for laterite by nearly 26%.

Table 4.2. The BET *c* value, *t*-plot calculated surface area, film thickness (*t*), and corresponding pore volume. Adsorption = (ads) and desorption = (des) curves from *t*-plots in Fig. 4.1. The grain size was 0.5 to 1.0 mm for all sorbents.

Sorbent	BET *c*	Surface Area (m^2 g^{-1})	Film thickness (nm)	Micropore Volume (cm^3 g^{-1})
Act. alumina (ads)	86	279.1[a]	1.0-1.5	(0.148)[c]
Act. alumina (des)	86	279.1[a]	1.0-1.2	(0.186)[c]
Gh. bauxite (ads)	278	5.5[a]	NA	0.0
Gh. bauxite (ads)	278	5.5[a]	NA	0.0
N. laterite (ads)	366	16.9[b]	0.3-0.5; 0.7-1.7	0.0022 (0.0072)[c]
N. laterite (des)	366	16.9[b]	0.7-1.2	(0.0099)[c]

[a]Zero y-intercept for regression line - lowest linear portion of *t*-plot.
[b]Positive y-intercept (2.2 mm^3 g^{-1} for regression line - lowest linear portion of *t*-plot.
[c]The volumes in parentheses likely also include the low end of mesopores (2-50 nm). Activated alumina may not have micropores.

Finally, in order to view the surface of each sorbent at the microscopic level, SEM images were taken of sorbent samples that were first soaked in deionized water for two weeks. The images of Namoo laterite, Ghana bauxite, and activated alumina are presented in Fig. 4.2. The most notable difference in the three images is with Ghana bauxite, which has a more open and smooth surface structure than laterite or activated alumina.

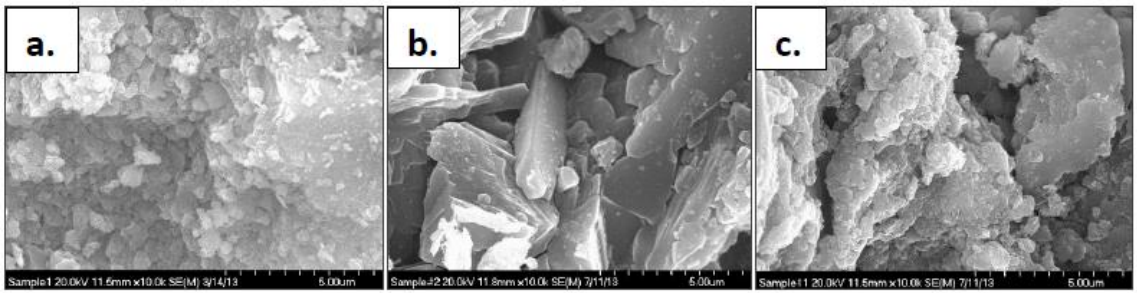

Fig. 4.2. Scanning electron microscopy (SEM) analysis of the three sorbents after soaking for two weeks in de-ionized water for (a) activated alumina, (b) Ghana bauxite, and (c) Namoo laterite. All images are presented at the 5.0 μm scale, located at the lower right side of each image.

Table 4.3. The major oxide compositions of the three sorbents. Activated alumina and Ghana bauxite were analyzed using XRF; and Namoo laterite was analyzed using ICP-OES. Al_2O_3, Fe_2O_3, and SiO_2 were the only oxides determined using ICP-OES.

Sorbent	%Al_2O_3	%Fe_2O_3	%SiO_2	Sum %Oxides
Act. alumina	99.4	0.0	0.0	99.4
Gh. bauxite[a]	70.9	23.6	2.2	99.3
N. laterite	13.5	36.8	45.7	96.0

[a]The other oxide identified in bauxite using XRF was TiO_2 at 2.6%.

Table 4.4. Mineral composition of the three sorbents determined by XRD, with the mineral formulas in brackets.

Sorbent	Silica	Aluminum Oxide	Feldspar	Clay	Iron Oxide	Iron Oxide
Act. alumina[a]		boehmite [γ-AlOOH]				
Gh. bauxite[b]		gibbsite [$Al(OH)_3$]		Kaolinite [$Al_2Si_2O_5(OH)_4$]	hematite [α-Fe_2O_3]	
N. laterite[b,c]	quartz [α-SiO_2]		microcline [$KAlSi_3O_8$]	Kaolinite [$Al_2Si_2O_5(OH)_4$]	hematite [α-Fe_2O_3]	goethite [α-FeOOH]

[a]Activate alumina is more than 50% Al_2O_3 determined from semi-quantitative XRD analysis; [b]kaolinite contains silica and aluminum oxide; [c]microcline contains silica and aluminum oxide.

3.1.2. Geochemical characteristics: XRD and XRF analysis

The oxide distribution of the three sorbents is presented in Table 4.3; and Table 4.4 presents the major minerals comprising each sorbent. Bauxite is primarily Al_2O_3 at 70.9% (identified as mostly gibbsite according to XRD analysis). Bauxite also contains Fe_2O_3 (as hematite) at 23.6%, and 2.2% SiO_2 (in kaolinite; Tables 4.3 and 4.4). Nearly half of Namoo laterite is SiO_2 (quartz, microcline, kaolinite), followed by Fe_2O_3 at 36.8% (as hematite and goethite), and 13.5% Al_2O_3 (within the microcline and kaolinite structures). Activated alumina is essentially pure Al_2O_3 at 99.4% and was identified via XRD as γ-Al_2O_3 and boehmite (γ-AlOOH). Boehmite is a precursor to activated alumina during the temperature driven dehydroxylation process (Wefers and Misra, 1987; Karamalidis and Dzombak, 2010). So the presence of boehmite may be due to incomplete

dehydroxylation to form activated alumina during manufacturing; or it could be from aging and the result of the attachment of water vapor in the air during storage.

3.2. Determining metals dissolution at low pH, high pH, and fluoride induced

The results of aluminum, iron, and silica dissolution at low and high pH are presented in Table 4.1S. Some dissolution was observed at pH 4.0 to 4.4 and at pH 9.8 for all sorbents. At low pH the solubility was not notable for any of the sorbents (all under 1.5 (10^{-3}) mmol L^{-1}). Dissolution of aluminum was one to two orders of magnitude higher at pH 9.8 than at pH 4.0 to 4.4 for all sorbents. Iron dissolution from laterite was also an order of magnitude higher at pH 9.8 than at pH 4.4, with some silica dissolution from laterite occurring at high pH (dissolution not measured at low pH). Activated alumina showed the greatest dissolution at 7.5 (10^{-2}) mmol L^{-1}, which occurred at pH 9.8.

Dissolution of aluminum oxides, such as bayerite and boehmite, can also occur as a result of fluoride adsorption at high fluoride concentrations (Nordin et al., 1999). Because the intake of dissolved aluminum is a possible health risk, the WHO (2008) recommends a limit of 3.7 (10^{-3}) mmol L^{-1} (0.1 mg L^{-1}). Therefore, as a protective measure, dissolved aluminum (and iron) was measured for samples after rotating 24 hours in fluoridated water. The results of dissolution of aluminum and iron due to fluoride adsorption (pH ~7) are presented in Table 4.2S. The dissolution of aluminum from activated alumina is below the detection limit. The dissolution of iron in bauxite and laterite is also below the detection limit. However, there is some dissolution of aluminum from bauxite at initial fluoride concentration of 0.26 mmol L^{-1} (5 mg L^{-1}), and from laterite at initial fluoride concentration of 0.53 mmol L^{-1} (10 mg L^{-1}). For both sorbents dissolved alumina is at the lowest end of the U.S. Environmental Protection Agency's

recommended secondary drinking water standard for aluminum of 1.85 (10^{-3}) to 7.41 (10^{-3}) mmol L^{-1} (0.05 to 0.2 mg L^{-1}) (USEPA, 2014)), and well under the WHO recommended limit of 3.7 (10^{-3}) mmol L^{-1} (0.1 mg L^{-1}) for small water treatment facilities (WHO, 2008).

3.3. Determining the optimum surface site density values by modeling titration data

Table 4.3S lists several surface site density (N_s) values, as determined from previous studies, for the minerals present in activated alumina, Ghana bauxite, or Namoo laterite (Table 4.4). The method used to determine N_s is also listed for each value. For this work, one complication in choosing a representative N_s value is that bauxite and laterite contain several minerals (Table 4.4, 4.3S), and even the activated alumina contains boehmite. After running several simulations for each sorbent using the generalized two-layer model in the PHREEQC program, the value of 4.5 sites nm^{-2} was chosen for all of the modeling, due to the best overall fit for the three sorbents.

3.4. Determining pH dependent surface charge

The H^+ adsorbed to or desorbed from each sorbent vs. pH is presented in Fig. 4.3. The titration curves for activated alumina are not as smooth as those for laterite and bauxite. This is probably because the titrations with activated alumina were continued even when the pH did not stabilize, in order to maintain a 5-10 minute pH stabilization time for each increment of titrant added. The activated alumina titration curves show an expected increase in proton uptake and release with ionic strength (Fig. 4.3a, b). The laterite titration curves also show the expected increase in proton uptake and release with ionic strength (Fig. 4.3e, f). In contrast, the bauxite titration curves show almost no difference with a change in ionic strength (Fig. 4.3c, d).

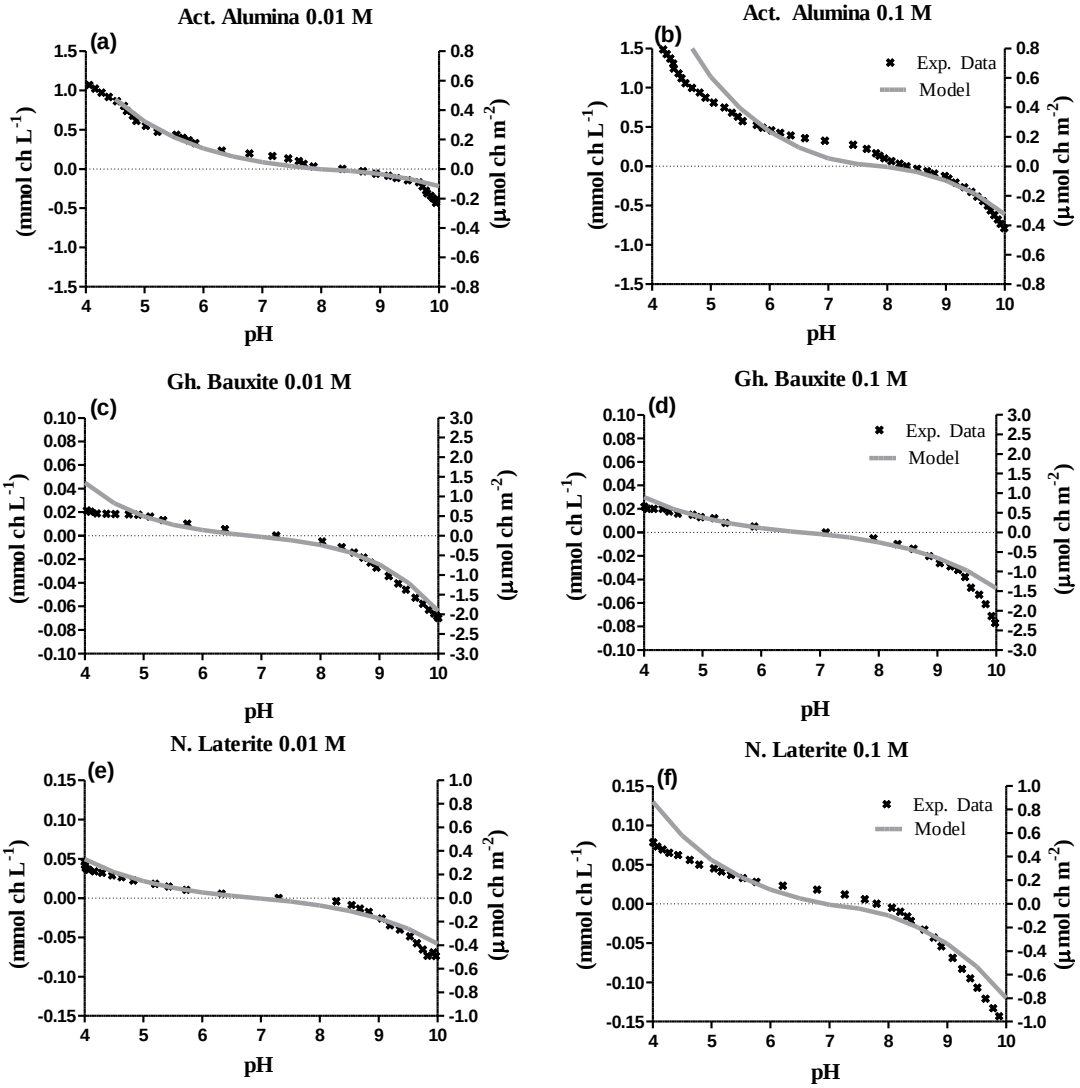

Fig. 4.3. H^+ surface charge (protonated/deprotonated) vs. pH calculated with the generalized two-layer model, and from experimental titration data for (a) activated alumina, I = 0.01 M, (b) activated alumina, I = 0.1 M, (c) Ghana bauxite, I = 0.01 M, (d), Ghana bauxite, I = 0.1 M, (e) Namoo laterite, I = 0.01 M, and (f) Namoo laterite, I = 0.1 M. The left y-axis presents mmol ch. L^{-1} and the right y-axis presents µmol ch. m^{-2}. The total surface site density for all calculations was set at 4.5 sites nm^{-2}, and the acidity constants were adjusted for a best fit with experimental data. The grain size was 0.5 to 1.0 mm, and the sorbent-to-solution ratio was 6.67 g L^{-1} for all experimental titrations.

In conducting the titrations, the starting pH for each acid and base titration varied somewhat – particularly with the poly-mineralic sorbents bauxite and laterite. Therefore, when plotting the curves described above, the average initial pH value for the coupled acid and base titration was used. The starting pH varied the least for activated alumina

since it is a mono-mineralic sorbent. For example, the range for 11 titrations was 8.24 to 8.44 with an average value of 8.37. While for Ghana bauxite the starting pH ranged from 6.69 to 7.72 with an average value of 7.18 (n = 6). The initial pH values for Namoo laterite varied the most, which was probably due to its more complex mineralogy. The range was 6.48 to 8.41 with an average of 7.64 (n = 6). The starting pH range of the titrations presented in Fig. 4.3e and 4.3f was between 6.83 and 7.80, however.

Table 4.5. Modeling of titration data with experimental data to estimate the intrinsic acidity constants (pK_{a1}^{int} and pK_{a2}^{int}) using the generalized two-layer model. The total surface site density was fixed at 4.5 sites nm^{-2}, and the intrinsic acidity constants were adjusted for a best fit curve with experimental titration data. The pH_{PZNPC} was calculated by adding intrinsic acidity constants and dividing by two.

Sorbent:	**Activated**	**Alumina**	**Ghana**	**Bauxite**	**Namoo**	**Laterite**
I (M):	**0.01**	**0.1**	**0.01**	**0.1**	**0.01**	**0.1**
$\boldsymbol{pK_{a1}^{int}}$	5.1	5.0	6.4	4.4	4.2	4.5
$\boldsymbol{pK_{a2}^{int}}$	11.1	10.7	7.4	9.0	9.6	9.6
$\mathbf{pH_{PZNPC}}$	8.1	7.9	6.9	6.7	6.9	7.1

3.5. Modeling surface charge and calculating intrinsic acidity constants and pH_{PZNPC} using the generalized two-layer model with PHREEQC program

The intrinsic acidity constants were determined using the generalized two-layer model by making $logK_a^{int}$ adjustable parameters for a best fit with experimental data. The surface site density was set at 4.5 sites nm^{-2} for all sorbents. Fig. 4.3 presents the model and experimental curves for mmols H^+ adsorbed or desorbed L^{-1} (left y-axis) and µmols m^{-2} sorbent (right y-axis) vs. pH. The best fit pK_a^{int} values as well as the pH_{PZNPC} are presented in Table 4.5. The model curves fit the experimental curves well to moderately well (Fig. 4.3).

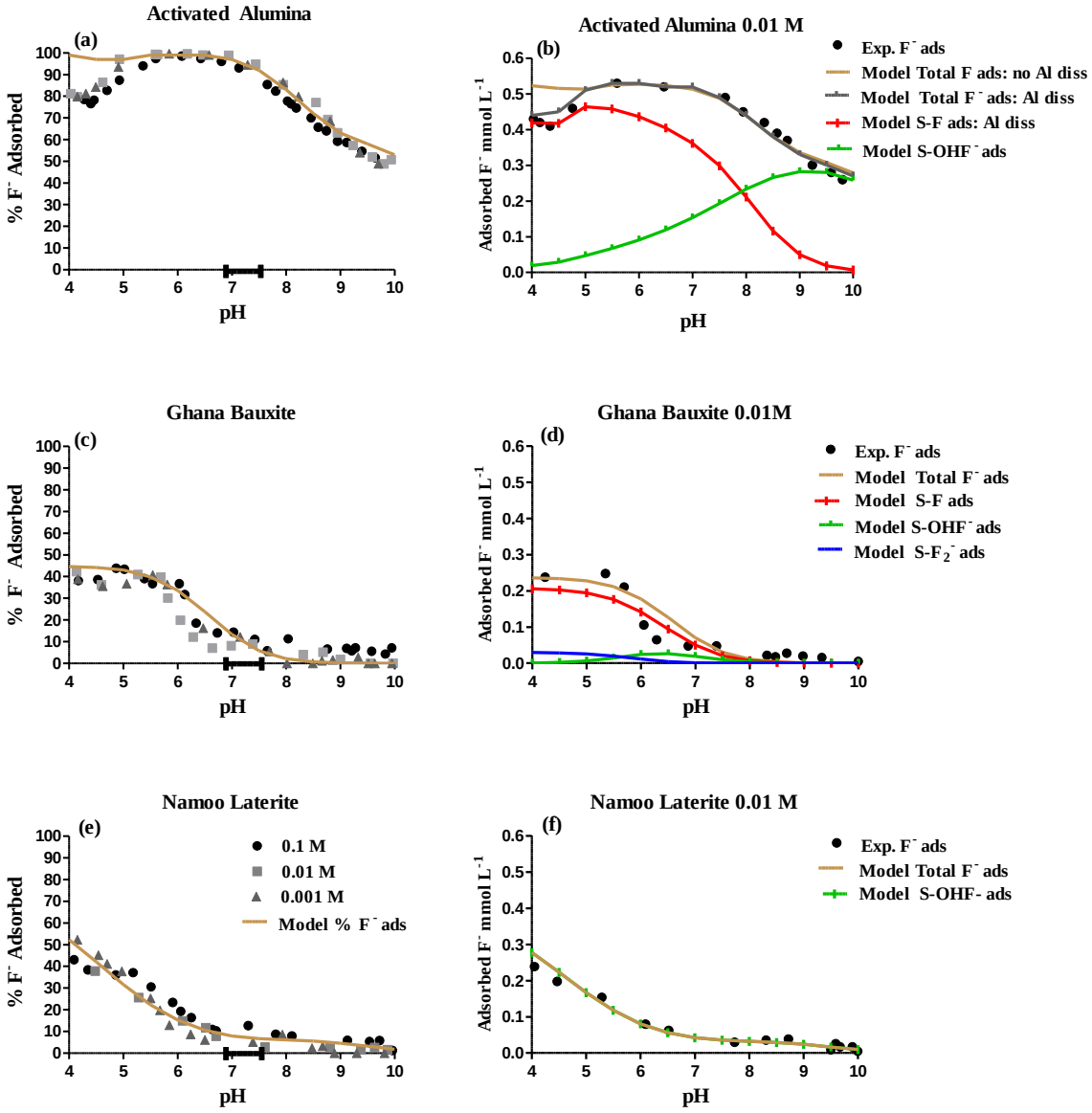

Fig. 4.4. Experimentally determined percent fluoride (F^-) adsorption vs. pH at I = 0.1, 0.01, and 0.001 M NaCl for (a) activated alumina, (c) Ghana bauxite, and (e) Namoo laterite; and adsorbed mmols F^- L^{-1} vs. pH at I = 0.01 M for (b) activated alumina (including model simulation with aluminum dissolution), (d) Ghana bauxite, and (f) Namoo laterite. The black and grey symbols represent experimental data; and colored lines represent the modeled results. The brown curve in each figure represents overall fluoride adsorption vs. pH at I = 0.01 M, and the other colored curves in (b), (d), and (f) describe the specific fluoride adsorption reactions – all using the generalized two-layer model. The pH range of fluoride-rich groundwater is presented by the bar in each figure on the left. The initial fluoride concentration was 0.53 mmol L^{-1} (10 mg L^{-1}); the grain size was 0.5 to 1.0 mm; and the sorbent-to-solution ratio was 6.67 g L^{-1}.

3.6. Fluoride adsorption capacity

3.6.1. Fluoride adsorption vs. pH at I = 0.1, 0.01, and 0.001 M

The fluoride adsorption capacity as a function of pH for Namoo laterite, Ghana bauxite, and activated alumina was determined at three ionic strengths to determine whether changes in ionic strength influence fluoride adsorption (Fig. 4.4a, c, e). The percent fluoride adsorbed was calculated as the difference between the initial fluoride concentration 0.53 mmol L^{-1} (10 mg L^{-1}) and the final concentration remaining in solution, divided by the initial fluoride concentration, and then multiplied by 100. With each set of batch adsorption experiments, the pH was varied between 4 and 10 in order to identify the optimum pH range for fluoride adsorption of the three sorbents.

In the pH range of 6.5 to 7.5, Ghana bauxite adsorbs 10% to 8.9% of fluoride; and Namoo laterite, in the same pH range, adsorbs 10% to 5.5% of fluoride (Fig. 4.4). Ghana bauxite shows its highest fluoride adsorption at pH from 5.5 to pH 4 (approximately 40 to 45% sorption), while Namoo laterite does not adsorb 40% or more fluoride until the pH is approximately 4.5 or lower. In comparison, the activated alumina adsorbs 99% of fluoride at pH between 5.5 and 6.5 (with initial pH about 0.5 lower, since fluoride adsorption increases pH slightly), and maintains a fluoride adsorption of 92-95% at pH 7.5 (Fig. 4.4).

There is no notable difference in fluoride adsorption capacity with change in ionic strength for any of the sorbents, which indicates that ionic strength does not influence the fluoride adsorption capacity (Fig. 4.4). This behavior suggests a strong chemical interaction rather than a weaker electrostatic attraction (Stumm, 1992). These bonding differences are described by the Gibbs total free energy of adsorption:

$$\Delta G_{des} = \Delta G_{chem} + \Delta G_{coul} \quad (13)$$

The ΔG_{des} term is the energy of desorption; the coulombic term, ΔG_{coul}, describes the electrical work required to move ions from a charged surface; and ΔG_{Chem} is the intrinsic chemical energy between ions and surface atoms. That fluoride does not respond to differences in ionic strength for any of the sorbents suggests the electrostatic effect (ΔG_{coul}), which depends on surface charge (Appelo and Postma, 2005), has much less influence than the intrinsic chemical energy (ΔG_{chem}) on fluoride adsorption (Stumm, 1992; Appelo and Postma, 2005).

3.6.2. Fluoride loading at I = 0.01 M and pH_o 6.9

The amount of fluoride adsorbed to activated alumina, Namoo laterite, and Ghana bauxite after 24 hours is presented in Fig. 4.5 in mmol F^- L^{-1} (left y-axis) and µmol F^- m^{-2} sorbent (right y-axis). The results presented in Fig. 4.5 indicate that, at 6.67 g sorbent L^{-1} and neutral pH, activated alumina has dramatically higher adsorption per liter than bauxite and laterite (Fig. 4.5a, b, c left y-axis).

However, bauxite adsorbs much more fluoride per unit area than activated alumina which is slightly better than laterite (Fig. 4.5a, b, c right y-axis). For all of the sorbents, at very high sorbate concentrations surface precipitation may be occurring along with adsorption (Dzombak and Morel, 1990; Stumm, 1992; Sparks, 1995). If surface precipitation has occurred, which is not known, it would contribute to the apparent increase in fluoride adsorption with loading and compromise the accuracy of the described curves.

Table 4.6. Equilibrium constants for fluoride adsorption reactions using the generalized two-layer model. The corresponding fluoride adsorption reactions are: $logK_1$ = reaction (6), $logK_2$ = reaction (7), and, log K_3 = reaction (8). X = no equilibrium constant. The total surface site density was fixed at 4.5 sites nm^{-2}, and the equilibrium constants were adjusted for a best fit curve with experimental fluoride adsorption data.

Sorbent	**LogK_1**	**LogK_2**	**LogK_3**
Act. alumina	10.3	2.9	X
Gh. bauxite	10.0	2.8	12.0
N. laterite	X	3.0	X

3.7. Modeling fluoride adsorption using the generalized two-layer model with PHREEQC program

3.7.1. Modeled fluoride adsorption vs. pH at I = 0.01 M

The modeled curves for overall fluoride adsorption vs. pH at I = 0.01 M compare well with experimental data for the three sorbents (Fig. 4.4a, c, e). Except that the modeled activated alumina curve of F^- adsorption vs. pH only fits experimental data at low pH if the simulation includes dissolved aluminum (0.9 mmol L^{-1}) in solution and the LLNL (Lawrence Livermore National Laboratory) database is used instead of the PHREEQC database (Fig. 4.4b) - although the adsorption reactions and corresponding equilibrium constants for activated alumina are not affected by the presence or absence of dissolved alumina. The equilibrium constants for each fluoride adsorption reaction of the three sorbents are presented in Table 4.6. In Fig. 4.4b, d, f the fluoride adsorption reactions occurring are also modeled. Below pH 8 (approximate pH_{PZNPC}), activated alumina adsorbs fluoride primarily via ion exchange (S-F in Fig. 4.4b and reaction (6)), and above pH 8 adsorbs fluoride primarily via adsorption onto the surface hydroxyls (S-OHF^- in Fig. 4.4b, and reaction (7)). Fluoride adsorption onto bauxite requires reactions (6), (7), and (8) for an optimum fit with experimental data (Fig. 4.4d). However, fluoride adsorption via ion exchange (S-F in Fig. 4.4d, and reaction (6)) dominates. According to the best fit model curves, fluoride adsorption onto laterite differs from activated alumina

and bauxite in that there is no ion exchange occurring (Fig. 4.4f). Instead fluoride adsorbs onto surface hydroxyls exclusively (S-OHF$^-$ and reaction (7)).

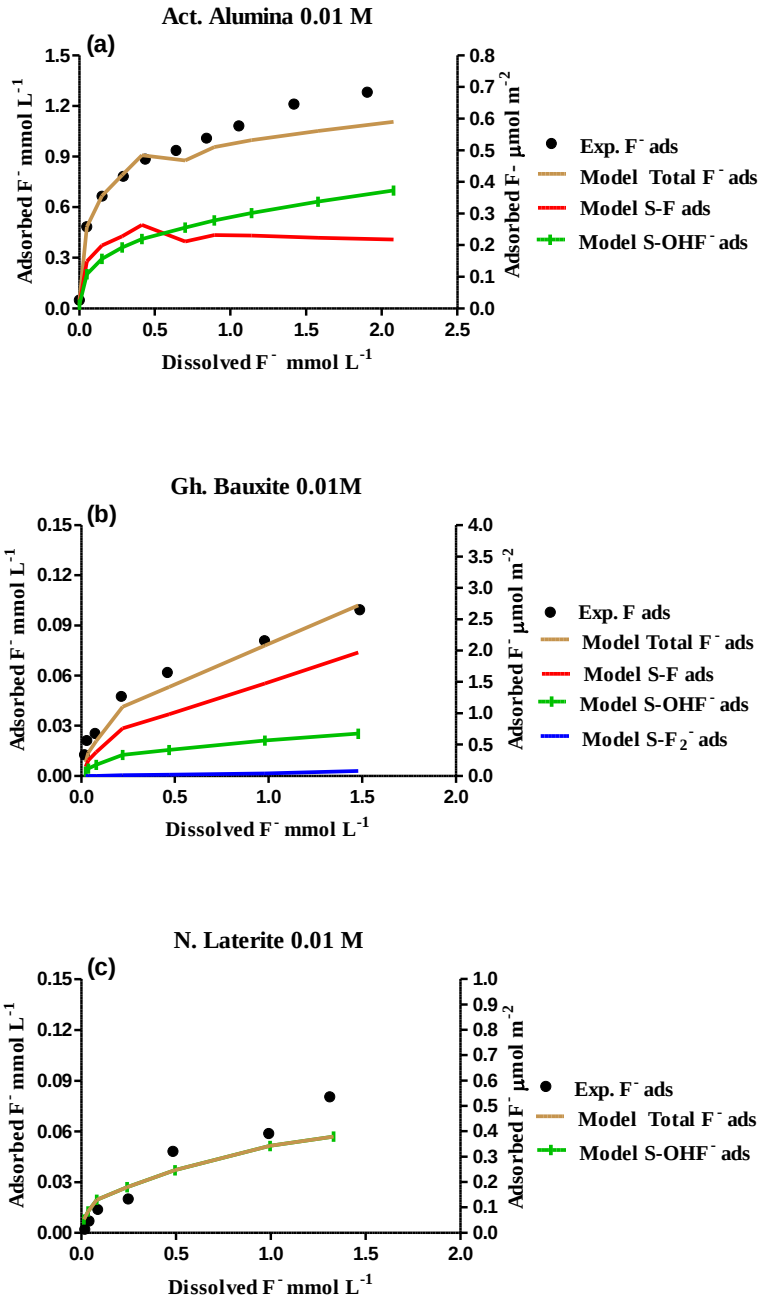

Fig. 4.5. The distribution of fluoride (F$^-$) adsorbed and fluoride concentration remaining in solution for (a) activated alumina, (b) Ghana bauxite, and (c) Namoo laterite The black circles represent experimental data and the colored curves describe the specific fluoride adsorption reactions using the generalized two-layer model. The left y-axis presents adsorbed mmol F$^-$ L^{-1} and the right y-axis presents adsorbed µmol F$^-$ m^{-2}. The ionic strength was 0.01 M NaCl; the grain size was 0.5 to 1.0 mm; and the sorbent-to-solution ratio was 6.67 g L^{-1}.

3.7.2. Modeled fluoride loading at pH_o 6.9 and I = 0.01 M

In addition to modeling fluoride adsorption at initial fluoride concentration of 0.53 mmol L^{-1} (10 mg L^{-1}) vs. pH in the previous section, adsorption was modeled to fit experimental data at initial pH of approximately 6.9, I = 0.01 M, and varied fluoride concentrations (Fig. 4.5). The fluoride adsorption reactions and equilibrium constants used to model fluoride adsorption vs. pH in the previous section were also used to model the fluoride loading in this section (Table 4.6). Fluoride adsorption onto activated alumina (Fig. 4.5a) is dominated by ion exchange (S-F in Fig. 4.5a and reaction (6)) at low fluoride concentrations, and becomes dominated by fluoride adsorption onto the surface hydroxyl (S-OHF^- in Fig. 4.5a and reaction (7)) at elevated fluoride concentrations. Also, at increased fluoride concentrations the modeled adsorption curve shows less adsorption than the experimental curve. Fluoride adsorption onto bauxite occurs primarily via ion exchange (S-F in Fig. 4.5b and reaction (6)) at all concentrations. The modeled curve fits the experimental curve fairly well at all fluoride concentrations, though slightly lower than the experimental curve at low fluoride concentrations. Laterite adsorbs fluoride exclusively via fluoride adsorption onto surface hydroxyls (S-OHF^- Fig. 4.5c and reaction (7)). Similar to activated alumina, at elevated fluoride concentrations the modeled curve shows lower fluoride adsorption than the experimental curve.

3.8. Freundlich and Langmuir isotherms and coefficients

The coefficients for the Freundlich (K_F) and Langmuir (K_L) isotherms using experimental fluoride loading data for Namoo laterite, Ghana bauxite, and activated alumina are presented in Table 4.7. Activated alumina has the highest K_F and K_L coefficients, with its estimated K_F value an order of magnitude higher than the K_F values

for either laterite or bauxite. Experimentally, the laterite and bauxite showed similarly low adsorption at initial fluoride concentration of 0.53 mmol L^{-1} (10 mg L^{-1}) and pH near neutral (Fig. 4.4), with bauxite generally a few percent higher (Section 3.6.1). When modeled to estimate the adsorption coefficients, the K_F and K_L values are higher for bauxite than for laterite (Table 4.7).

Table 4.7. Coefficients of Freundlich and Langmuir adsorption isotherms for Namoo laterite, Ghana bauxite, and activated alumina calculated from data presented in Fig. 5 (using adsorbed mmol F^- g^{-1} sorbent instead of adsorbed mmol F^- L^{-1}). The initial pH was approximately 6.9; the ionic strength was 0.01 M NaCl; the grain size was 0.5 to 1.0 mm; and the sorbent-to-solution ratio was 6.67 g L^{-1}.

Sorbent	Freundlich (K_F) (mmol F adsorbed per g sorbent)		Langmuir (K_L) (L per mmol F dissolved)
Act. alumina	0.177	[n = 0.43; r^2 = 0.95]	7.3 [max mmol F ads g^{-1} = 0.187]
Gh. bauxite	0.013	[n = 0.43; r^2 = 0.99]	4.9 [max mmol F ads g^{-1} = 0.015]
N. laterite	0.010	[n = 0.71; r^2 = 0.98]	2.9 [max mmol F ads g^{-1} = 0.012]

3.9. Comparing fluoride adsorption at 4.3 mmol L^{-1} surface sites

The fluoride adsorption capacity of activate alumina, bauxite, and laterite at equal millimoles of surface sites per liter was evaluated for three high-fluoride solutions with the results presented in Table 4.8. For all three solutions, activated alumina has the greatest fluoride adsorption capacity per gram, followed by laterite. But bauxite has the greatest fluoride adsorption capacity per unit area, followed by activated alumina. As expected for all sorbents, adsorption improves at pH 4.5 for laterite and bauxite, and 5.5 for activated alumina. Fluoride adsorption using the groundwater collected in the study area is lower than adsorption using the laboratory mixed solutions, but the higher groundwater pH (7.8, aged sample – original pH 7.5) will inhibit fluoride adsorption. Major ions were not determined for this sample, but the general assumption is that competing ions, if present, will affect each sorbent similarly with regard to fluoride adsorption.

Table 4.8. Comparing adsorption capacity of the three sorbents at equal millimoles of sorption sites per liter (4.3 mmol sites L^{-1}) and varied fluoridated solutions. At grain size 0.5 to 1.0 mm and 4.5 sites nm^{-2} for all sorbents. GW = groundwater collected in study area; 0.01 M = NaCl solution mixed in the lab.

Sorbent	Solution	pH_o	F_o (mg L^{-1})	F_o (mmol L^{-1})	mmol F sorb g^{-1} sorbent	mmol F sorb m^{-2} sorbent
Act. alumina	GW	7.8	4.00	0.21	57.10 (10^{-3})	1.98 (10^{-4})
Gh. bauxite	GW	7.8	4.00	0.21	1.20 (10^{-3})	2.18 (10^{-4})
N. laterite	GW	7.8	4.00	0.21	1.86 (10^{-3})	0.85 (10^{-4})
Act. alumina	0.01 M	6.9	5.17	0.27	78.20 (10^{-3})	2.71 (10^{-4})
Gh. bauxite	0.01 M	6.9	5.17	0.27	2.05 (10^{-3})	3.72 (10^{-4})
N. laterite	0.01 M	6.9	5.17	0.27	2.35 (10^{-3})	1.07 (10^{-4})
Act. alumina	0.01 M	5.5	5.17	0.27	81.30 (10^{-3})	2.81 (10^{-4})
Gh. bauxite	0.01 M	4.5	5.17	0.27	2.09 (10^{-3})	3.79 (10^{-4})
N. laterite	0.01 M	4.5	5.17	0.27	2.98 (10^{-3})	1.36 (10^{-4})

3.10. Fluoride adsorption onto Namoo laterite and Ghana bauxite at two grain sizes: 63 to 125 µm and 0.5 to 1.0 mm

Fluoride adsorption of Namoo laterite and Ghana bauxite was compared at two grain sizes, at an ionic strength of 0.01 M NaCl and pH range from 4 and 10. The percent fluoride adsorbed was calculated as described in section 3.6.1. The Namoo laterite and Ghana bauxite were ground and sieved to grain sizes 63 to 125 µm and 0.5 to 1.0 mm to see if the adsorption capacity would increase significantly with decreased grain size and increased surface area. For both the laterite and the bauxite, fluoride adsorption capacity increased to about 20% at pH 7, and at low pH it increased to 55-60% (Fig. 4.6).

Fluoride adsorption was also modeled at grain size 63 to 125 µm and compared to the modeled curves at grain size 0.5 to 1.0 mm, using the same method and parameters as described to model fluoride adsorption vs. pH for grain size 0.5 to 1.0 mm (section 2.8). The input parameter that differed in modeling fluoride adsorption at grain size 63 to 125 µm was the 5-point BET specific surface area (method in section 2.2), which was measured at 10.6 m^2 g^{-1} for bauxite and 27.1 m^2 g^{-1} for laterite, rather than the surface areas presented in Table 4.1. In the modeled curves at grain size 63 to 125 µm, bauxite

dramatically overestimated adsorption at pH below 6.5, while laterite showed only a slight increase in fluoride adsorption. The BET surface area for bauxite nearly doubled at grain size 63 to 125 μm, from 5.5 to 10.6 m^2 g^{-1}. In contrast, the BET surface area of laterite increased by a little under 25% from 21.9 to 27.1 m^2 g^{-1}.

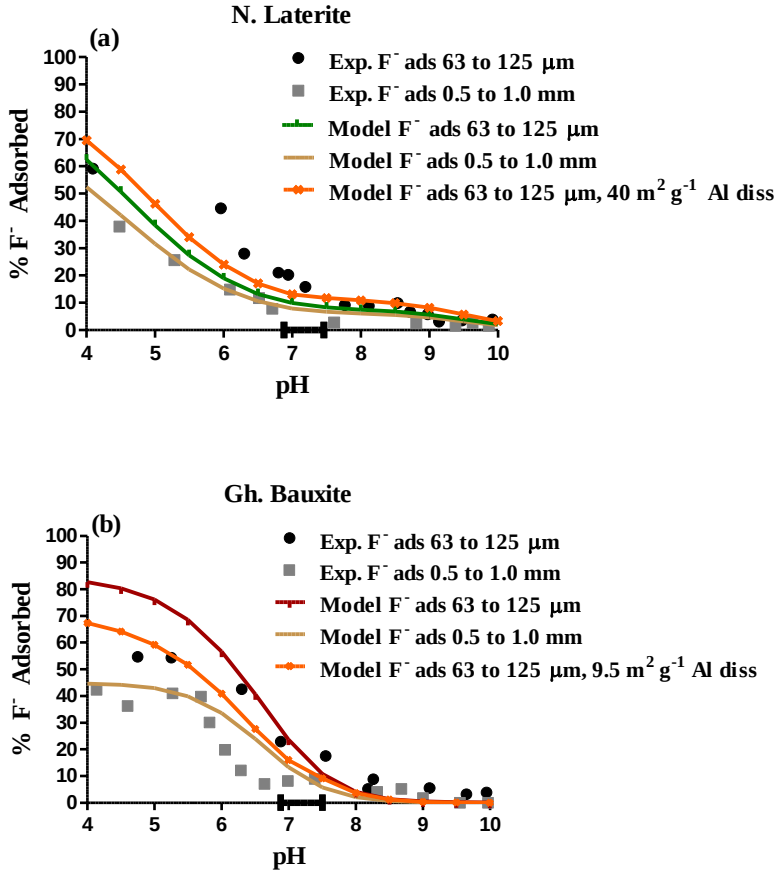

Fig. 4.6. Percent fluoride (F^-) adsorption vs. pH of (a) Namoo laterite at two grain sizes, (b) Ghana bauxite at two grain sizes. The black and grey symbols represent experimental data; and the colored lines represent the modeled results using the generalized two-layer model. The pH range of fluoride-rich groundwater is presented by the bar in each figure. The ionic strength was 0.01 M NaCl; the initial fluoride concentration was 0.53 mmol L^{-1} (10 mg L^{-1}); and the sorbent-to-solution ratio was 6.67 g L^{-1}.

The discrepancy between experimental data and the model curves is not clear. One reason for the poor model fits to experimental data may be a result of inaccurate BET surface areas, in particular for laterite (see section 3.1.1). Also, metals dissolution (if occurring) at low pH and increased fluoride adsorption may contribute to a poor fit

between experimental data and model curves in the low pH range for one or both sorbents. A better model fit for bauxite was attained using a lower surface area of 9.5 m^2 g^{-1} and 0.07 mmol L^{-1} dissolved aluminum (Fig. 4.6b). A similar modeled curve could also be attained for bauxite by leaving the BET surface area at 10.6 m^2 g^{-1} and increasing aluminum dissolution a bit more. The modeled fit for laterite was less responsive, but improved slightly using a much higher surface area of 40 m^2 g^{-1} and 0.035 mmol L^{-1} dissolved aluminum (Fig. 4.6a).

4. Discussion

4.1. Experimental results of fluoride adsorption at grain size 0.5-1.0 mm

Previous adsorption studies conducted on soils indicate that, although iron oxides are good sorbents, aluminum and its hydrolysis species adsorb fluoride more strongly than iron species (Lindsay, 1979). Activated alumina - which is pure aluminum oxide and has very high surface area - is a particularly good sorbent for fluoride (Hao and Huang, 1986; Farrah et al., 1987; Fletcher et al., 2006), as shown in Fig. 4.4. Fluoride adsorption onto activated alumina as presented in this study is consistent with similar adsorption studies conducted using activated alumina (Hao and Huang, 1986 and references therein). Bauxite is also 71% aluminum oxide (mostly as gibbsite) and 24% iron oxide (mostly as hematite). When comparing activated alumina with bauxite at the same sorbent-to-solution ratio in mmols F^- adsorbed L^{-1}, activated alumina adsorbs substantially more fluoride than bauxite (Fig. 4.5 left y-axis). But when comparing them at the same sorbent-to-solution ratio in µmols F^- adsorbed m^{-2} sorbent surface area, bauxite adsorbs much more fluoride than activated alumina (Fig. 4.5 right y-axis). Similarly, when comparing the fluoride adsorption capacity of bauxite and activated alumina, both at 4.3

mmols surface sites L^{-1} (Table 4.8), activate alumina is the better sorbent per unit weight, but bauxite is the better sorbent per unit area. The surface area of bauxite at 5.5 m^2 g^{-1} is so much lower than activated alumina at 288.9 m^2 g^{-1} that it cannot compare when measured per unit mass. To achieve equal mmols of sites L^{-1} in Table 4.8, for example, 52.5 g of bauxite was needed for 1 g activated alumina. The reasons why bauxite has much higher fluoride adsorption capacity per unit area may be because it has more open pore structure (no micropores) and likely has less restricted access to internal surface sites than activated alumina and laterite. It may also be bauxite's mineralogy which results in more types of fluoride adsorption reactions, while still being heavily dominated by ligand exchange (Fig. 4.4d, 4.5b and reaction (6)).

Namoo laterite is 45.7% silica, mostly as quartz which is a very poor sorbent for fluoride (Fan et al., 2003), as well as kaolinite, and feldspar – also poor sorbents for fluoride (Coetzee et al., 2003). The abundance of quartz means that at least one third of the laterite surface cannot adsorb fluoride well at neutral pH. In addition, the aluminum oxide identified within the Namoo laterite is a minor component found within the assessory minerals feldspar and kaolinite (Table 4.4). As a result, hematite and goethite are likely the dominant fluoride sorbents in laterite. The XRD results of the Namoo laterite indicate that goethite is more abundant than hematite. Although the surface area of laterite, at 21.9 m^2 g^{-1}, is about four times higher than the surface area of bauxite, its fluoride adsorption capacity does not reflect this advantage, which is due in part to the mineralogy. The only comparison where laterite is a better sorbent for fluoride than bauxite is with both sorbents at 4.3 mmol sites L^{-1} in mmols F^- adsorbed g^{-1} (Table 4.8). Also, at the same sorbent-to-solution ratio, at neutral pH, and initial fluoride

concentration of 0.53 mmol L^{-1} (10 mg L^{-1}) or higher, laterite adsorbs fluoride almost as well as bauxite (Fig. 4.4d, f, and 4.5b, c left y-axis). But bauxite becomes saturated with adsorbed fluoride more quickly than laterite due to the low surface area, for at lower initial fluoride concentrations bauxite is a slightly better sorbent than laterite (Fig. 4.5b, c left y-axis first three points). Laterite is a much poorer sorbent than bauxite, when comparing adsorption capacity per unit area (at pH 6.9 and 6.67 g L^{-1}) and is just slightly weaker than activated alumina at high F^- loading (Fig. 4.5 right y-axis). Possibly activated alumina needs more time to come to equilibrium than bauxite and laterite. This would be particularly true if much of its surface area is deep within small pores and pores with small pore necks that rely on diffusion which is very slow.

4.2. Generalized two-layer model describing fluoride adsorption reactions

The generalized two-layer surface complexation model (Dzombak and Morel, 1990) was used to determine the fluoride adsorption reactions occurring on the surface of each sorbent. Ligand exchange between the F^- ion in solution and OH^- at the surface (reaction (6)) dominated for activated alumina below pH 8 (Fig. 4.4b) and at lower fluoride loading (Fig. 4.5a), and for bauxite under all conditions (Fig. 4.4d, 4.5b). However, F^- adsorption onto the surface OH^- (reaction (7)), which creates a net negative surface charge, dominated for adsorption onto activated alumina at pH above 8 (Fig. 4.4b) and at elevated fluoride loading (Fig. 4.5a); and it was also the only surface adsorption reaction onto laterite (Fig. 4.4f, Fig. 4.5c). Because a net negative charge is created on the surface, this is likely a weaker adsorption reaction than the ion exchange reaction. In addition, it seems to become a more dominant reaction when the number of surface hydroxyls begins to decrease notably, such as above pH_{PZNPC} for activated

alumina (Table 4.5 and Table 4.4S) which also creates a net negative surface charge, and with increased loading (activated alumina, Fig. 4.5a). The abundance of silica in laterite also means there will be fewer surface hydroxyls (S-OH) and adsorbed protons ($S\text{-}OH_2^+$) at pH below neutral, due to a low pH_{PZC} for quartz, kaolinite, and feldspars (Table 4.4S).

The experimental curves for fluoride loading onto activated alumina and laterite show higher adsorption than the calculated curves using the generalized two-layer surface complexation model (Fig. 4.5a, c). This discrepancy between the experimental data and modeled curves may be due to surface precipitation, which was not incorporated into the modeled curves. Surface precipitation can occur at high anion concentrations, and is hard to distinguish from adsorption (Sposito, 1984, 1986) so this is a reasonable explanation. If surface precipitation is the explanation, and if the models are accurate, one question is why bauxite does not have the same discrepancy between the modeled and experimental curves (Fig. 4.5b) - particularly since the ratio between fluoride in solution and the number of surface sites is so high as a result of low specific surface area compared to laterite, and especially activated alumina.

4.3. Freundlich and Langmuir isotherms describing macroscopic fluoride adsorption

The results from the Freundlich and Langmuir isotherms indicate that at near neutral pH bauxite is a better fluoride sorbent than laterite, and activated alumina is better than both (Table 4.7). Bauxite should adsorb fluoride better than laterite, due to the high percent Al_2O_3 and Fe_2O_3, but, as stated earlier, its lower surface area reduces its adsorption capacity. Because the equation for determining K_F assumes an unlimited number of adsorption sites, the Freundlich isotherm may not be ideal here, where the number of sorption sites is limited due to very low surface area (bauxite) and where the

initial dissolved fluoride concentrations of the experimental data were as high as 1.58 to 3.16 mmol L^{-1} (30 to 60 mg L^{-1}). However, the Langmuir equation assumes a finite number of sorption sites as represented by s_{max}. It also assumes no lateral interaction between sites – one that should be valid here since chemical bonding dominates and electrostatic interactions appear to be minimal (see section 3.6.1). Therefore, between the two, the Langmuir isotherm should be the more appropriate simple macroscopic model to estimate the distribution between fluoride in solution and that adsorbed after 24 hours contact time (assumed as near equilibrium conditions). However, a good fit of experimental data to Langmuir, or other isotherms, does not mean that adsorption alone is occurring (Stumm, 1992). Anion adsorption isotherms have Langmuirian characteristics with one dominant type of binding site (Dzombak and Morel, 1990); and, as stated in the previous section, at high anion concentrations surface precipitation may be occurring (Sposito, 1984, 1986). Therefore, the macroscopic distribution coefficients presented here, like the fluoride loading data, may not accurately represent fluoride adsorption onto any or all of the three sorbents at high concentrations if precipitation is contributing.

4.4. Physical and chemical properties that control fluoride adsorption capacity

4.4.1. Physical properties: surface area, surface structure, and porosity

To maximize adsorption capacity for any sorbent, a very high surface area can be an advantage since it increases the number of surface adsorption sites per unit area. Activated alumina has a specific surface area that is substantially higher than that of laterite, and especially bauxite. However, the surface area of most catalysts (e.g. porous solids) is primarily in the pore space (Leofanti et al., 1998). Similarly, large grained materials such as gravel also tend to have significant intragranular porosity and surface

area, resulting in an increased dependence on diffusive transport and slow exchange times (Tokunga et al., 2003). This indicates that surface area in itself may not determine adsorption capacity of a sorbent if much of the reactive surface is in micropores, or pores with small pore necks which can hinder solute transport processes.

The $N_{2(g)}$ adsorption and desorption isotherms can provide useful information about the pore size and structure. For a clearer quantitative understanding of micropore size distribution, analysis of isotherm data was conducted using a *t*-plot. The results presented in Fig. 4.1d indicate that bauxite is mesoporous, with no microporosity. This assessment is strengthened by the fact that the BET and *t*-plot calculated specific surface areas for bauxite are identical (Table 4.1, 4.2), since the BET method works best on mesoporous materials (Gregg and Sing, 1982). However laterite appears to contain both micropores and mesopores due to the shape of the curve in Fig. 1f and the results in Table 4.2. The results for activated alumina regarding the presence of micropores are less clear. The lower curve (Fig. 1b) indicates no microporosity but, unlike bauxite (Fig. 1d), activated alumina has a second linear portion with a positive y-intercept and a curve shape suggesting the presence of micropores as well as mesopores (Storck et al., 1998). While the *t*-plot calculated surface area for activated alumina is less than 4% lower than the BET calculated surface area, the discrepancy between the two methods for laterite is around 26%. This, along with the other *t*-plot results (Fig. 4.1f, Table 4.2) indicate that laterite clearly contains micropores (including <0.6 nm). Because activated alumina has higher overall surface area, it may also have a greater total volume of mesopores with small pore necks (and possibly micropores) than laterite (Table 4.2). Similar to this work, Hay et al. (2011) found that their sorbents had type IV isotherms and H3 hysteresis loops,

as well as BET *c* values in the range valid for using the BET equation (Davis and Kent, 1990), suggesting an absence of microporosity. However in analyzing micropore size distribution using the *t*-plot method, Hay et al. (2011) also identified micropores in all four of the samples. Sing (1989) noted that some isotherms which appear to be type IV may be a combination of type I (microporous) and type IV. This could explain the apparent inconsistency in the above examples. It also demonstrates the wide variation in surface area and pore structure between many sorbents.

Other useful information about pore structure and microporosity can be determined by observing trends in the $N_{2(g)}$ adsorption and desorption isotherms. For example, the hysteresis loop for all three sorbents closed at p/p^o of about 0.45 (Fig. 4.1), which corresponds to a Kelvin radius for capillary condensation (Hay et al., 2011), and to a pore width of about 2.4 nm for parallel sheets and 3.6 nm for cylindrical pores (Gregg and Sing, 1982). Also the $N_{2(g)}$ isotherms – in particular the bauxite – show a sharp increase as p/p^o approaches unity (Fig. 4.1a, c, e), which suggests capillary condensation in slit shaped pores in-between flat or plate-like surfaces, and is commonly seen in clay aggregate mineral groups (Sing, 1989; Leofanti et al., 1998). The shape of the desorption isotherm indicates that many of the pores are controlled by pore necks that are narrower than the above Kelvin radius for the two shapes (Hay et al., 2011). This is particularly pronounced with the hysteresis pattern in the desorption curve for laterite (Fig. 4.1e, f), as compared to bauxite which displays the least hysteresis (Fig. 4.1c, d).

Variation in the surface of the sorbent, such as fractures, the shape of pores, or whether they are open ended will influence adsorption rate and capacity. Fractures and clay coatings on fractured grains may contain a significant amount of the reactive surface,

even though they may be a small fraction of the total porosity, and can strongly affect transport of sorbing ions (Hay et al., 2011). In addition, because the exchange between bulk solution and the intragranular region is controlled by diffusion, reactions can be slow (Hay et al., 2011 and references therein). This indicates that pore structure, size, and shape can notably impact total adsorption as well as adsorption rates. It also suggests that the effectiveness of a sorbent for removing fluoride may depend on more than just the total surface area. Variation in the shape and size of the pore space may explain some of the differences in fluoride adsorption capacity observed for the three sorbents presented in this work.

4.4.2. Chemical properties: mineralogy, surface charge, and pH_{PZNPC}

The influence of mineralogy on fluoride adsorption capacity was already discussed in section 4.1. Not all oxides are ideal sorbents for anions due in large part to surface charge and the pH at which the sorbent surface has no net charge (pH_{PZC}). Above the pH of zero surface charge, protons are being removed from the sorbent surface, which decreases the number of surface hydroxyls needed for fluoride adsorption or ion exchange, and also creates a net negative surface charge. As mentioned earlier, quartz is a poor sorbent for fluoride adsorption (Fan et al., 2003) due to the fact that surface protons begin to desorb from the surface at pH well below neutral.

In addition to attaining surface charge via proton adsorption to or desorption from the sorbent surface, some minerals have permanent charge which has not been determined in this study. While activated alumina does not have permanent charge, many clays do. This is a result of isomorphic cation substitution, which usually creates a negative charge (e.g. Al^{3+} for Si^{4+}). Although kaolinite, which has five types of functional

groups, has very low permanent charge (Sposito, 1984) and only the aluminols are available to complex anions (Davis and Kent, 1990). In addition, some minerals, such as goethite, have several types of hydroxyl groups with varying reactivity (Davis and Kent, 1990). What this indicates is that several parameters beyond those identified in this study (e.g. pH dependent surface charge, surface and pore area) may affect the adsorption capacity of laterite and bauxite.

Bauxite and laterite have pH_{PZNPC} (and possibly pH_{PZC}) in the range of the pH of local groundwater (6.8 to 7.5). But activated alumina has a much higher pH_{PZNPC} of about 8.0, which results in a greater number of surface hydroxyls for fluoride adsorption at neutral pH. In laterite, the goethite and hematite are likely the strongest sorbents for fluoride (pH of zero charge around neutral, Table 4.4S), while the quartz, feldspar, and kaolinite (with pH of zero charge between 2 and 4.3, Table 4.4S) probably only adsorb fluoride at low pH. In contrast, bauxite is mostly gibbsite and hematite, with a small amount of kaolinite (Table 4.4). It is, in part, the dominance of aluminum and iron oxide that give bauxite the high fluoride adsorption capacity per unit area; and unlike laterite which adsorbs best at pH of 4, the fluoride adsorption capacity of bauxite increases dramatically from pH 7 to pH 6 (Fig. 4.4).

4.5. Dissolution of metals at low pH, high pH, and fluoride induced

The titrations were to a minimum pH of 4 and maximum pH of 10, with minimal dissolution expected in this pH range for the three sorbents. The main oxides present in the three sorbents are aluminum oxide, iron oxide, and silica (mostly as quartz). Yang et al. (2007) documented limited dissolution of aluminum hydroxides in the pH range of 4 to 10. Karamalidis and Dzombak (2010) also noted that gibbsite dissolution was minimal

and could be ignored in the pH range of 4 to 10. The solubility of iron oxide tends to be low in this pH range as well (Hem, 1960; Snoeyink and Jenkins, 1980; Stumm and Morgan, 1996), as does quartz (Stumm and Morgan, 1996). Because the above findings may not apply to the sorbents being evaluated in this study, dissolution at high and low pH was investigated.

The dissolution results of this study show that aluminum dissolution in activated alumina at pH 9.8 was just high enough to be considered as having an impact on experimental results. However, overall, aluminum dissolution in this study was comparable to results from Yang et al. (2007) in the pH range of 4 to 10, where dissolution was considered limited enough to ignore. There was also no noticeable change in the models when dissolved aluminum was added to the simulations at the concentrations presented in Table 4.1S. The dissolution of iron from bauxite and laterite, and silica from laterite were also low enough to ignore for titration experiments, and did not influence the results of the models.

Notable dissolution of aluminum may occur in solutions that are both high fluoride and low pH, or at very high fluoride loading and neutral pH, since both and can cause dissolution of aluminum oxides (Nordin et al., 1999). Although not investigated in this study, the combined effect of high concentrations of protons and fluoride on aluminum dissolution would be useful to determine. This is particularly important if low pH is being considered as a method for improving fluoride adsorption capacity. It also may influence the results of geochemical models, if the dissolved concentration is high enough. As an example, when modeling fluoride adsorption vs. pH for activated alumina, if 0.9 mmol L^{-1} of dissolved aluminum was included in solution, the fluoride complexed

with dissolved aluminum at low pH, and the model curve matched the experimental curve perfectly (Fig. 4.4b). Similarly, including aluminum dissolution to the modeled fluoride adsorption vs. pH for bauxite and laterite at grain size 63 to 125 μm, the model fits to experimental data improved (Fig. 4.6). Further work on aluminum dissolution resulting from high fluoride adsorption and low pH is recommended, both to improve fluoride adsorption models with aluminum oxides as the sorbent, and to better understand potential exposure to aluminum.

4.6. Comparing fluoride adsorption capacity of Ghana bauxite and Namoo laterite with results from previous studies on laterite and bauxite as sorbents for fluoride

Table 4.9 presents results from previous studies of fluoride adsorption onto bauxite and laterite for comparison. None of the samples had been heat or chemically treated prior to analysis. The attempt was to try to loosely compare fluoride adsorption experiments conducted under similar conditions, such as pH, initial fluoride concentration, solution, grain size, and sorbent-to-solution ratio. Many of the studies did not provide the specific surface area data so this parameter was not included in the comparison. Also the initial preparation of each sorbent varied (e.g. acid/base wash, rinsing, drying, sieving) so an assumption was made that initial preparation of samples had an equal effect on their adsorption capacity. The contact time for each experiment varied as well and was not always clear, so an assumption was made that results were at approximate equilibrium. The initial fluoride concentration for most of the studies listed was 0.53 mmol L^{-1} (10 mg L^{-1}). Otherwise the other parameters varied between studies.

In evaluating the fluoride adsorption results presented in Table 4.9, it is important to consider the following influences on the final result presented while comparing the

values. In general, fluoride adsorption will improve at initial pH below 7. Where only the final pH is given, or the average between initial and final pH, the starting pH will be slightly lower than presented in Table 4.9, assuming ion exchange between fluoride and the surface hydroxyl. Fluoride adsorption also usually improves with decreased grain size. In addition, the amount of fluoride adsorbed per gram will improve with a lower sorbent-to-solution ratio. The initial fluoride concentration also influences the amount adsorbed per gram, with lower adsorption at lower initial fluoride concentration. The type of solution also may affect adsorption, depending upon the presence of competing ions, but here the previous parameters listed will probably have the strongest impact on adsorbed mmol $F^- g^{-1}$.

The laterite collected from South Africa, Ghana, and India adsorbed from 0.39 (10^{-2}) to 1.06 (10^{-2}) mmol $F^- g^{-1}$ at initial fluoride concentration 0.53 to 0.55 mmol $F^- L^{-1}$. The bauxite collected from the same three countries adsorbed from 0.95 (10^{-2}) to 9.78 (10^{-2}) mmol $F^- g^{-1}$ at initial fluoride concentrations of 0.51 to 0.55 mmol $F^- L^{-1}$. The variation depended upon the sample itself (e.g. Ghana laterite collected from three areas), the pH of solution, the grain size, and the sorbent-to-solution ratio. However, bauxite was consistently better at adsorbing fluoride than laterite. The conditions of the lowest adsorbing laterite were: initial pH of 8 in Ghana groundwater, grain size 2 mm, and sorbent-to-solution ratio 20 g L^{-1}. The conditions of the two highest adsorbing laterite samples were: (1) final pH 6, grain size <0.280 mm, sorbent-to-solution ratio 20 g L^{-1}; and (2) average pH 7.5, grain size 0.5 mm, sorbent-to-solution ratio not provided. The two lowest adsorbing bauxite samples were: (1) initial pH of 8 in Ghana groundwater, grain size 2 mm, and sorbent-to-solution ratio 20 g L^{-1}; (2) final pH of 7.2 in 0.01 M

NaCl solution (with NaF), grain size 0.5 to 1.0 mm, and sorbent-to-solution ratio of 6.67 g L^{-1}. The conditions of the highest adsorbing bauxite were: average pH of 7.0 in NaF solution, at grain size <0.100 mm, and sorbent-to-solution ratio of 2 g L^{-1}.

Table 4.9. Table of results of fluoride adsorption capacity of bauxite and laterite at pH close to neutral, using samples that were not heat or chemically treated. The results in the last three rows from this study are for comparison, and include activated alumina data. The pH presented is initial, final, or average of initial and final. S1 = NaF laboratory solution, S2 = 0.01 M NaCl with NaF added, GW = Ghana groundwater. ND = no data provided.

Sorbent	$pH_{o,f, or avg}$	F_o (mmol L^{-1})	Grain Size (mm)	Sorbent (g L^{-1})	F Sorbed (mmol g^{-1})	Ref
S. Afr. bauxite	pH_f = 6.0	0.53 S1	<0.180	20	1.3-2.1 (10^{-2})	a
S. Afr. laterite	pH_f = 6.0	0.53 S1	<0.180	20	1.06 (10^{-2})	a
Gh. bauxite	pH_o = 8.0	0.55 GW	~2	20	0.95 (10^{-2})	b
Gh. laterite 1	pH_o = 8.0	0.55 GW	~2	20	0.69 (10^{-2})	b
Gh. laterite 2	pH_o = 8.0	0.55 GW	~2	20	0.39 (10^{-2})	b
India laterite	pH_{avg} = 7.5	0.53 S1	0.5	ND	1.06 (10^{-2})	c
India bauxite	pH_{avg} = 7.0	0.53 S1	<0.100	2	9.78 (10^{-2})	d
Gh. bauxite	pH_f = 7.2	0.51 S2	0.5-1.0	6.67	0.95 (10^{-2})	e
N. laterite	pH_f = 7.4	0.53 S2	0.5-1.0	6.67	0.74 (10^{-2})	e
Gh. bauxite	pH_f = 5.3	0.53 S2	0.063-0.125	6.67	4.34 (10^{-2})	e
N. laterite	pH_f = 4.1	0.53 S2	0.063-0.125	6.67	4.71 (10^{-2})	e
Act. alumina	pH_f = 7.7	0.53 S2	0.5-1.0	6.67	7.25 (10^{-2})	e

[a]Coetzee et al. (2003); [b]Ayamsegna et al. (2008); [c]Sarkar et al. (2006); [d]Sujana and Anand (2011); [e]This work.

5. Conclusions

One of the goals of this study was to characterize potential sorbents to better understand fluoride adsorption and to identify why one sorbent works better than another. In order to keep costs down, two indigenous sorbents were evaluated for use in de-fluoridation filters, and then compared to activated alumina. By using either Ghana bauxite or Namoo laterite as the sorbent in small-scale de-fluoridation filters in northern Ghana, the primary cost involved would be transportation - and in the case of laterite there would be no transportation cost since it is abundant in northern Ghana. Activated alumina, however, would need to be purchased from abroad (usually India or China) and

imported; and the cost per unit weight can be significant unless it is acquired in very large quantities.

The simplest ways to improve adsorption capacity are to (1) decrease the grain size which usually increases the specific surface area, (2) lower the pH to increase the number of surface hydroxyls available for fluoride to exchange with or adsorb to (but not so low as to cause dissolution) (see Fig. 4.6, Table 4.9 bottom rows), and (3) increase the sorbent-to-solution ratio, which increases the total surface area available for adsorption per liter of treated water. However, the manual labor required to produce large quantities of laterite and bauxite – and at a grain size of sand or finer – as well as the high volume of fluoride-free water (e.g. rainwater) needed to clean the sorbent so that the filtered water would not be red or chalky tasting also makes these potential sorbents less viable.

Several studies evaluating the fluoride adsorption capacity of laterite and bauxite have investigated ways to treat the rock in order to improve its adsorption capacity by using processes that must be done in the laboratory and with technically trained staff. One treatment that improved adsorption capacity was to first heat the rock, with the optimum temperature for maximum adsorption at about 500 to 600 ^{o}C (Coetzee et al., 2003; Ayamsegna et al., 2008). In another example, a chemical process conducted on laterite by Maiti et al. (2011) involved soaking the rock with concentrated acid to dissolve it, and then re-precipitating it with strong base. The result was a sorbent with increased surface area and higher sorption capacity.

Also there are other synthetic sorbents to consider that may be both low in cost and effective in small-scale de-fluoridation filters. One is iron oxide (Streat et al., 2008a and 2008b), and the other is hydroxyapatite (Verwilghen et al., 2006; MacDonald et al.,

2011). These synthetic forms have much higher surface area than the natural minerals and they can be manufactured at the laboratory scale in Ghana. The effectiveness and feasibility of these laboratory prepared sorbents could be evaluated and considered for use in small-scale fluoride adsorption filters in rural Ghana and other areas with similar water quality issues.

Acknowledgements

This research was generously funded by the University of Nevada, Reno, the Desert Research Institute, Reno, and a U.S. Environmental Protection Agency Science to Achieve Results Graduate Research Fellowship. Additional funding was provided by a Geological Society of America Graduate Research Grant. We would like to acknowledge World Vision Ghana for its contribution to this work. We also thank Doug Kent of the U.S. Geological Survey for reviewing the manuscript and improving it dramatically by providing insightful comments, as well as an anonymous reviewer, and the executive editor.

Chapter 4: Supplementary data

Table 4.1S. Concentration of dissolved aluminum, iron, and silica from the three sorbents at low and high pH, in solution of 0.01 M NaCl ionic strength, and sorbent-to-solution ratio of 6.67 g L^{-1}. X = not analyzed.

Sorbent	pH	Al (mmol L^{-1})	Fe (mmol L^{-1})	SiO_2 (mmol L^{-1})
Act. Alumina	4.2	1.3 (10^{-3})	X	X
Act. Alumina	9.8	7.5 (10^{-2})	X	X
Gh. Bauxite	4.0	3.6 (10^{-4})	<3.6 (10^{-5})	X
Gh. Bauxite	9.8	1.2 (10^{-2})	8.7 (10^{-5})	X
N. Laterite	4.4	3.9 (10^{-4})	8.6 (10^{-5})	X
N. Laterite	9.8	3.7 (10^{-3})	5.9 (10^{-4})	4.8 (10^{-3})

Table 4.2S. Possible fluoride induced dissolution of aluminum or iron for the three sorbents at initial pH of approximately 7, in solution of 0.01 M NaCl ionic strength, and sorbent-to-solution ratio of 6.67 g L^{-1}. X = not analyzed

Sorbent	F_o (mg L^{-1})	F_o (mmol L^{-1})	Al (mmol L^{-1})	Fe (mmol L^{-1})	SiO_2 (mmol L^{-1})
Act. Alumina	5.0	0.26	<1.67 (10^{-3})	X	X
Act. Alumina	10.0	0.53	<1.67 (10^{-3})	X	X
Gh. Bauxite	5.0	0.26	1.78 (10^{-3})	<1.79 (10^{-4})	X
Gh. Bauxite	10.0	0.53	<1.67 (10^{-3})	<1.79 (10^{-4})	X
N. Laterite	5.0	0.26	<1.67 (10^{-3})	<1.79 (10^{-4})	X
N. Laterite	10.0	0.53	1.89 (10^{-3})	<1.79 (10^{-4})	X

Table 4.3S. Literature values for total surface sites (N_s) of several sorbents, including the method used for determining the number of surface sites.

Sorbent	Formula	Ns (sites nm^{-2})	Method
Goethite[a]	α-FeOOH	2.6-4.0	Acid-base titration
Goethite[b]	α-FeOOH	4.0	Acid-base titration
Goethite[a]	α-FeOOH	5.2-7.3	F-/ligand exchange
Goethite[b]	α-FeOOH	6.0-7.0	F-/ligand exchange
Hematite[c]	α-Fe_2O_3	2.3	Crystal chemistry
Act. Alumina[d]	γ-Al_2O_3	8.0	Infrared
Act. Alumina[e]	γ-Al_2O_3	5.1	FITEQL model
Boehmite[f]	γ-AlOOH	0.88	Acid-base titration
Boehmite[f]	γ-AlOOH	2.2	F-/ligand exchange
Boehmite[g]	γ-AlOOH	1.7	Acid-base titration
Gibbsite[h]	$Al(OH)_3$	8.8	Crystal chemistry
Gibbsite[e]	$Al(OH)_3$	2.8	FITEQL model
Kaolinite[i]	$Al_2Si_2O_5(OH)_4$	2.2-2.7	FITEQL model
Quartz (natural)[j]	α-SiO_2	4.5	Tritium exchange

[a]Davis and Kent (1990); [b]Sigg and Stumm (1980); [c]Pivovarov (1997); [d]Peri (1966) ; [e]Yang et al. (2007); [f]Nordin et al. (1999); [g]Laiti and Ohman (1996); [h]Rosenqvist et al. (2002); [i]Brady et al. (1996); [j]Riese (1982)

Table 4.4S. The pH of zero surface charge for various common minerals and synthetic solids. PZC is pH of total net surface charge, and PZNPC or PPZC are the PZC established by surface binding of H^+ and OH^- only.

Solid	Formula	PZC	PZNPC	PPZC
Quartz[a]	α-SiO_2	2.0-4.0		
Kaolinite[b]	$Al_2Si_2O_5(OH)_4$	3.9-4.3		
Hematite[c]	α-Fe_2O_3			8.4
Hematite[d]	α-Fe_2O_3	5.9, 7.1,7.3		
Goethite[e]	α-FeOOH		8.0	
Goethite[d]	α-FeOOH	7.2, 7.6		
Gibbsite[f]	$Al(OH)_3$			7.8
Gibbsite[g]	$Al(OH)_3$			9.8
Act. Alumina[h]	γ-Al_2O_3	8.1		
Act. Alumina[i]	γ-Al_2O_3	8.5		
Act. Alumina[j]	α -Al_2O_3	9.1		
Boehmite[k]	γ-AlOOH	9.1		
Boehmite[l]	γ-AlOOH	8.5		
Feldspars[m,n]	i.e., $KAlSi_3O_8$		2.0 – 2.4	

[a]Kosmulski et al. (2002); [b]Brady et al. (1996); [c]Breeusma (1973); [d]Borggaard (1983); [e]Bar-Yosef et al. (1975); [f]Kaiser and Guggenberger (2003); [g]Manning and Goldberg (1996); [h]Sprycha (1989); [i]Huang and Stumm (1973); [j]Yopps and Fuerstenau (1964); [k]Wood et al. (1990); [l]Laiti and Ohman (1996); [m]Parks (1967); [n]Stillings et al. (1995).

References

Adhikary, S.K., Tipnis, U.K., Harkare, K.P., Govindan, K.P., 1989. Defluoridation during desalination of brackish water by electrodialysis. Desalination 71, 301-312.

APHA (American Public Health Association), 1998. Standard Methods for the Examination of Wastewater. American Public Health Association, American Water Works Association, Water Environment Federation publication. APHA, 20th ed, Washington DC.

Apambire, W.B., 2000. Geochemical Modeling and Geomedical Implications of Fluoriferous Groundwaters in the Upper East Region of Ghana. Ph.D. dissertation, University of Nevada-Reno.

Apambire, W.B., Boyle, D.R., Michel, F.A., 1997. Geochemistry, genesis, and health implications of fluoriferous groundwaters in the upper regions of Ghana. Environmental Geology 33, 13-23.

Appelo, C.A.J, Postma, D., 2005. Geochemistry, groundwater, and pollution. CRC Press, second ed., Boca Raton.

Ayamsegna, J.A., Apambire, W.B., Bakobie, N., Minyila, S.A., 2008. Removal of fluoride from rural drinking water sources using geomaterials from Ghana. Access to Sanitation and Safe Water: Global Partnerships and Local Actions 33rd Int. Conf., Accra, Ghana.

Ayoob, S., Gupta, V.T., Bhat, V.T., 2008. A conceptual overview on sustainable technologies for defluoridation of drinking water and removal mechanisms. Crit. Rev. Environ. Sci. Technol. 38, 401-470.

Barrett, E.P., Joyner, L. G., Halenda P.P., 1951. The determination of pore volume and area distributions in porous substances. I. Computations from nitrogen isotherms. J. Am. Chem. Soc. 73, 373-380.

Bar-Yosef, B., Posner, A.M., Quirk, J.P., 1975. Zinc adsorption and diffusion in goethite pastes. J. Soil Sci. 26, 1-21.

Bhatnagar, A., Kumar, E., Sillanpää, M., 2011. Fluoride removal from water by adsorption – A review. Chem. Eng. J. 171, 811-840.

Borggaard, O.K., 1983. Effect of surface area and mineralogy of iron oxides on their surface charge and anion adsorption properties. Clays Clay Min. 31, 230-232.

Brady, P.V., Cygan, R.T., Nagy, K.L., 1996. Molecular controls on kaolinite surface charge. J. Colloid Interface Sci. 183, 356-384.

Breeusma, A., 1973. Adsorption of ions on hematite (α-Fe_2O_3). Ph.D. dissertation, Agricultural University, Wageningen, The Netherlands.

Brunauer, S., Emmett, P.H., Teller, E., 1938. Adsorption of gases in multimolecular layers. J. Am. Chem. Soc. 60, 309-319.

Coetzee, P.P., Coetzee, L.L., Puka, R., Mubenda, S., 2003. Characterization of selected South African clays for defluoridation of natural waters. Water SA 29, 331-338.

CWSA-CIDA (Community Water and Sanitation Agency and Canadian International Development Agency), 2005. Briefing Paper for District Assemblies on Fluoride in NORWASP Districts. Field Paper #28.

Cumberbatch, T., Atipoka, F., Ayamgah, G., Batir, B., Berger, D., Freed, L., Momada, F., Nyarku, M., Pervez, N., Ponce, B., Rana, S., Venugopal, V., Volk, L., 2008. The Development of an Indigenous Filter. EPA P3 Award: A National Student Competition for Sustainability Focusing on People, Prosperity, and Planet (2007). Cooper Union for the Advancement of Science and Art, New York.

Davis, J.A., Kent, D.B., 1990. Surface complexation modeling in aqueous geochemistry. In; Hochella Jr. M.F., White A.F. (Eds.), Mineral-water interface chemistry. Reviews in mineralogy vol. 23. Mineral Soc. Am.: Washington DC, pp. 177-260.

Davis, J.A., Kent, D.B., Rea, B.A., Maest, A.S., Garabedian, S.P., 1990. Influence of redox environment and aqueous speciation on metal transport in groundwater: preliminary results of tracer injection studies. In: H. Allen, D. Brown, and E.M. Perdue (Eds.), Metals in Groundwater, Lewis Publishers, Chelsea, MI.

de Boer, J.H., Lippens, B.C., Linsen, B.G., Broekhoff, J.C.P., van den Heuval, A., Osinga, T.J. 1966. The t-curve of multimolecular N_2 adsorption. J. Colloid Interface Sci. 21, 405-415.

Dzombak, D.A., Morel, F.M.M., 1990. Surface Complexation Modeling: Hydrous Ferric Oxide. John Wiley & Sons Inc., New York.

Fan, X., Parker, D.J., Smith, M.D., 2003. Adsorption kinetics of fluoride on low cost materials. Water Res. 37, 4929-4937.

Farrah, H., Slavek, J., Pickering, W.F., 1987. Fluoride interactions with hydrous aluminum oxides and alumina, Aust. J. Soil Res., 55-69.

Fawell, J., Bailey, K., Chilton, J., Dahi, E., Fewtrell, L., Magara, Y., 2006. Fluoride in Drinking-water. WHO Drinking-water Quality Series, World Health Organization, Geneva.

Fletcher, H.R., Smith, D.W., Pivonka, P., 2006. Modeling the sorption of fluoride onto alumina. J. Environ. Eng. 132, 229-246.

Gregg, S.J., Sing, K.S., 1982. Adsorption, Surface Area, and Porosity. Academic Press, London.

Hao, O.J., Huang, C.P., 1986. Adsorption characteristics of fluoride onto hydrous alumina. J. Environ. Eng. 112, 1054-1069.

Hay, M.B., Stoliker, D.L., Davis, J.A., Zachara, J.M., 2011. Characterization of the intragranular water regime within subsurface sediments: Pore volume, surface area, and mass transfer limitations. Water Resour. Res. 47, 1-19.

Hayes, K. F., 1987. Equilibrium, Spectroscopic, and Kinetic Study of Ion Adsorption at the Oxide/Aqueous Interface. Ph.D. dissertation, Stanford University.

Hayes, K. F., Redden, G., Ela, W., Leckie, J.O., 1991. Surface complexation, models: an evaluation of model parameter estimation using FITEQL and oxide mineral titration data. J. Colloid Interface Sci. 142, 448-469.

Hem, J.D., 1960. Some chemical relationships among sulfur species and dissolved ferrous iron. U.S. Geological Service Water Supply Paper. Washington DC.

Honeyman, B.D., Leckie, J.O., 1986. Macroscopic partitioning coefficients for metal ion adsorption: Proton stoichiometry at variable pH and adsorption density. In: Geochemical Processes at Mineral Surfaces, J.A. Davis and K.F. Hayes, ACS Symp. Ser. 323, Am. Chem. Soc., Washington DC, pp. 162-190.

Honeyman, B.D., Santschi, P.H., 1988. Metals in aquatic systems. Environ. Sci. Tech. 22, 862-871.

Huang, C.P., 1981. The surface acidity of hydrous solids. In: Anderson, M.A., Rubin, A.J. (Eds.), Adsorption of Inorganics at Solid-liquid Interfaces. Ann Arbor Science, Michigan, pp. 183-207.

Huang, C.P., Stumm, W., 1973. Specific adsorption of cations on hydrous γ-Al_2O_3. J. Colloid Interface Sci. 43, 409-420.

Kaiser, K., Guggenberger, G., 2003. Mineral surfaces and soil organic matter. Eur. J. Soil Sci. 54, 219-236.

Karamalidis, A.K., Dzombak, D.A., 2010. Surface Complexation Modeling: Gibbsite. John Wiley & Sons Inc., New York.

Kent, D.B., Tripathi, V.S., Ball, N.B., Leckie, J.O., 1986. Surface-complexation modeling of radionuclide adsorption in sub-surface environments. Stanford Civil Engineering Tech. Rept. 294, Stanford CA; also NUREG Rept. CR-4897, SAND 86-7175. 1988.

Kosmulski, M., 2001. Chemical Properties of Material Surfaces. Marcel Dekker Inc., New York.

Kosmulski, M., Mączka, E., Janusz, W., Rosenholm, J.B., 2002. Different zetameters produce different results. J. Colloid Interface Sci. 250, 99-103.

Laiti, E., Ohman, L.O., 1996. Acid/base properties of phenylphosphonic acid complexation at the boehmite water interface. J. Colloid Interface Sci. 183, 441-452.

Leofanti, G., Padovan, M., Tozzola, G., Venturelli, B., 1998. Surface area and pore texture of catalysts. Catal. Today 41, 207-219.

Lindsay, W.L., 1979. Chemical Equilibria in Soils. John Wiley & Sons Inc., New York.

Lowell, S., Shields, J.E., 1991. Powder Surface Area and Porosity. Chapman and Hall Ltd., New York.

MacDonald, L.H., Pathak, G., Singer, B., Jaffé, P.R., 2011. An integrated approach to address endemic fluorosis in Jharkhand, India. J. Water Res. Prot. 3, 457-472.

Maiti, A., Basu, J.K., De, S., 2011. Chemical treated laterite as promising fluoride adsorbent for aqueous system and kinetic modeling. Desalination 265, 28-36.

Manning, B.A., Goldberg, S., 1996. Modeling competitive adsorption of arsenate with phosphate and molybdate on oxide minerals. Soil Sci. Soc. Am. J. 60, 121-131.

Miretzky, P., Cirelli, A.F., 2011. Fluoride removal from water by chitosan derivatives and composites. A review, J. Fluorine Chem. 132, 231-240.

Mjengera, H., Mkongo, G., 2003. Appropriate defluoridation technology for use in fluoridic areas in Tanzania. Phys. Chem. Earth 28, 1097-1104.

Mohapatra, M., Anand, S., Mishra, D.E., Giles, D.E., Singh, P., 2009. Review of fluoride removal from drinking water. J. Environ. Manag. 91, 67-77.

Murray, J.J. (Ed.), 1986. Appropriate Use of Fluorides for Human Health. World Health Organization, Geneva.

Nordin, J.P., Sullivan, D.J., Phillips, B.L., Casey, W.H., 1999. Mechanisms for fluoride-promoted dissolution of bayerite [β-$Al(OH)_3$(s)] and boehmite [ϒ-AlOOH]: ^{19}F-NMR spectroscopy and aqueous surface chemistry. Geochim. Cosmochim. Acta 63, 3513-3524.

Parkhurst, D.L., Appelo, C.A.J., 1999. User's guide to PHREEQC (version 2) – A computer program for speciation, batch-reaction, one-dimensional transport, and inverse geochemical calculations. U.S. Geological Survey, Denver CO.

Parks G. A., 1967. Aqueous surface chemistry of oxides and complex oxide minerals. Equilibrium Concepts in Natural Water Systems. Amer. Chem. Soc. Adv. Chem. Ser. 67, 121- 160.

Peri, J.B., 1966. Infrared study of adsorption of carbon dioxide, hydrogen chloride and other molecules on acid sites on "dry" silica-alumina and ϒ-alumina. J. Phys. Chem. 70, 3168.

Pivovarov, S., 1997. Surface structure and site density of the oxide-solution interface. J. Colloid Interface Sci. 196, 321-323.

Riese, A.C., 1982. Adsorption of radium and thorium onto quartz and kaolinite: a comparison of solution/surface equilibria models. Ph.D. dissertation, Colorado School of Mines.

Rosenqvist, J., Persson, P., Sjöberg, S., 2002. Protonation and charging of nanosized gibbsite (α-$Al(OH)_3$ particles in aqueous suspension. Langmuir 18, 4598-4604.

Sahai, N., Sverjensky, D.A., 1997. Evaluation of internally consistent parameters for the triple layer model by the systematic analysis of oxide surface titration data. Geochim. Cosmo. Acta. 61, 2801-2826.

Sarkar, M., Banarjee, A., Pramanick, P.P., Sarkar, A.R., 2006. Use of laterite for the removal of fluoride from contaminated drinking water. J. Colloid Interface Sci. 302, 432-441.

Sarkar, M., Banarjee, A., Pramanick, P.P., Sarkar, A.R., 2007. Design and operation of fixed laterite column for the removal of fluoride from water. Chem. Eng. J. 131, 329-335.

Sehn, P., 2008. Fluoride removal with extra low energy reverse osmosis membranes: three years of large scale field experience in Finland. Desalination 223, 73-84.

Sigg, L., Stumm, W., 1980. The interactions of anions and weak acids with the hydrous goethite (α-FEOOH) surface. Colloids and Surfaces 2, 101-117.

Simmons, R., 1993. Trace element removal from ash dam waters by nanofiltration and diffusion dialysis. Desalination 89, 325-341.

Sing, K.S.W., 1989. The use of gas adsorption for the characterization of porous solids. Colloids and Surfaces 38, 113-124.

Snoeyink, V.L., Jenkins, D., 1980. Water Chemistry. John Wiley & Sons Inc., New York.

Sparks, D.L., 1995. Environmental Soil Chemistry. Academic Press Inc., California.

Sposito, G., 1984. The Surface Chemistry of Soils. Oxford University Press, New York.

Sposito, G., 1986. On Distinguishing Adsorption from Surface Precipitation. In: Geochemical Processes at Mineral Surfaces, Davis, J.A., Hayes, K.F. (Eds.), ACS Symposium Series 323. Amer. Chem. Soc.: Washington DC, pp. 217-228.

Sprycha, R., 1989. Electric double layer at alumina/electrolyte interface. I. Surface charge and zeta potential. J. Colloid Interface Sci. 127, 12-25.

Stillings, L.L., Brantley, S.L., Machesky, M.L., 1995. Proton adsorption at an adularia feldspar surface. Geochim. Cosmo. Acta 59, 1473-1482.

Storck, S., Bretinger, H., Maier, W.F., 1998. Characterization of micro- and mesoporous solids by physisorption methods and pore-size analysis. App. Catal. 174, 137-146.

Streat, M., Hellgardt, K.L., Newton, N.L.R., 2008a. Hydrous ferric oxide as an adsorbent in water treatment Part 1. Preparation and physical characterization. Process. Safety Environ. Prot. 86, 1-9.

Streat, M., Hellgardt, K.L., Newton, N.L.R., 2008b. Hydrous ferric oxide as an adsorbent in water treatment Part 3. Batch and mini-column adsorption of arsenic, phosphorous, fluorine, and cadmium ions. Process. Safety Environ. Prot. 86, 21-30.

Stumm, W., 1992. Chemistry of the Solid-water Interface. John Wiley & Sons Inc., New York.

Stumm, W., Huang, C.P., Jenkins, S.R., 1970. Specific chemical interactions affecting the stability of dispersed systems. Croat. Chem. Acta 42, 223-244.

Stumm, W., Morgan, J.J., 1996. Aquatic Chemistry. John Wiley & Sons Inc., third ed., New York.

Sujana, M.G., Anand, S., 2011. Fluoride removal studies from contaminated groundwater by using bauxite. Desalination 267, 222-227.

Tokunga, T.K., Olson, K.R., Wan, J., 2003. Moisture characteristics of Hanford gravels: bulk, grain-surface, and intragranular components. Vadose Zone J. 2, 322-329.

USEPA (United States Environmental Protection Agency), 2014. Secondary Drinking Water Regulations: Guidance for Nuisance Chemicals. Website accessed Nov. 22, 2014: http://water.epa.gov/drink/contaminants/secondarystandards.cfm.

Verwilghen, C., Rio, S., Nzihou, A., Gauthier, D., Flamant, G., Sharrock, P.J., 2006. Preparation of high specific surface area hydroxyapatite for environmental applications. J. Mater. Sci. 42, 6062-6066.

Wefers, K., Misra, C., 1987. Oxides and hydroxides of aluminum. Technical Paper No. 19, Alcoa Laboratories, Pennsylvania.

Whitford, G.M., 1997. Determinants and mechanisms of enamel fluorosis. Ciba Foundation Symposium 205, 226-241.

Wood, R., Fornasiero, D., Ralston, J., 1990. Electrochemistry of the boehmite-water interface. Colloids Surf. 5, 389-403

WHO (World Health Organization), 1984. Fluorine and Fluorides. Environmental health Criteria 36. World Health Organization, Geneva.

WHO (World Health Organization), 2008. Guidelines for Drinking Water Quality. Volume 1, 3rd edition. World Health Organization, Geneva.

Yang, X., Sun, Z., Wang, D., Forsling, W., 2007. Surface acid-base properties and hydration/dehydration mechanisms of aluminum (hydr)oxides. J. Colloid Interface Sci. 308, 395-404.

Yopps, J.A., Fuerstenau, D.W., 1964. The zero point of charge of alpha Al_2O_3. J. Colloid Sci. 19, 61-71.

Zevenbergen, C., van Reeuwijk, L.P., Frapporti, G., Louws, R.J., Schuiling, R.D., 1996. A simple method for defluoridation of drinking water at village level by adsorption on Ando soil in Kenya. Sci. Total Environ. 188, 225-232.

CHAPTER 5

ASSESSING CHANGES IN THE PHYSICAL-CHEMICAL PROPERTIES AND FLUORIDE ADSORPTION CAPACITY OF ACTIVATED ALUMINA UNDER VARIED CONDITIONS

Craig, Laura, Stillings, Lisa L., Decker, David, L.

Abstract

Adsorption is a simple method for removing fluoride from water and activated alumina is a good choice, but to be cost-effective it must work well long-term. This study investigates whether physical-chemical properties, surface charge, and fluoride adsorption capacity of activated alumina change with hydration period, and whether fluoride (F^-) adsorption capacity and rate change with grain size. The results show that the mineralogy of activated alumina is affected by the hydration period resulting in a transformation to boehmite and then bayerite with hydration. But hydration period does not impact surface acidity in the pH range used in this study (minimum pH 4.5 ~0.14 C m^{-2}) or adsorption capacity (at pH_o 6.9 ~0.62 µmol F^- m^{-2}). There is also no notable difference in fluoride adsorption capacity between the grain size ranges of 0.5-1.0 mm and 0.125-0.250 mm, nor does specific surface area change significantly with hydration or grain size. However adsorption rate increases dramatically at the finer grain sizes. At an initial F^- concentration of 0.53 mmol L^{-1}, the finer grain sizes adsorb 90% after 1 hour while the larger grain sizes require 24 h; and the pseudo-second-order adsorption rate constant is an order of magnitude higher for the finer grained sorbent at 0.19 g per mg F^- per min vs. 0.025 g per mg F^- per min for the larger grained sorbent at time up to 24 h. The higher rate suggests better access to intragranular pore space at a smaller grain size.

1. Introduction

Adsorption is a low-cost and simple method for removing excess fluoride from drinking water (Mohapatra et al., 2009; Miretzky and Cirelli, 2011), which is particularly important in poor regions of the world where advanced water treatment facilities are not an option. Activated alumina, which is synthesized at the industrial scale, is well established as an effective adsorbent for fluoride removal from water (Hao and Huang, 1986; Farrah et al., 1987; Fletcher et al., 2006); and is more effective than untreated natural sorbents, such as bauxite and laterite, because it has a very high surface area as well as high fluoride adsorption at the pH range of most groundwater (Craig et al., 2015). Unfortunately, activated alumina can also be a costly choice for use in fluoride adsorption filters in rural areas of the developing world where fluorosis is endemic, such as the study area of northern Ghana. Given that activated alumina must be purchased (and in Ghana also imported), it would almost certainly need to be used for extended time in order to be considered practical and cost-effective. Therefore understanding activated alumina's surface characteristics and its long-term effectiveness as a sorbent for fluoride removal are needed in order to determine whether it is an economically feasible sorbent for use in poor, rural areas.

Studies on activated alumina adsorption generally utilize fast titrations with the sorbent first hydrated in deionized water up to two weeks (Huang, 1981; Hao and Huang, 1986; Craig et al., 2015), and do not consider possible changes in adsorption capacity and surface reactivity with varied hydration period and or with slower titrations. However changes in surface reactivity with hydration period were observed at high and low pH by Lefèvre et al. (2002) who documented a decrease in surface reactivity (and acidity) of

activated alumina with increased hydration periods and a progressive transformation to the more stable mineral, bayerite. Lefèvre et al. (2002) also speculated that a decrease in surface reactivity may adversely affect adsorption capacity which is important for practical applications of activated alumina. In addition, Rosenqvist et al. (2002) found that the fast acid-base titrations (2-8 minutes) typically used to determine surface acidity under-estimate the surface charge of gibbsite and other oxides because the readings were taken before reaching equilibrium. Craig et al. (2015) also observed that the pH of activated alumina frequently did not stabilize well during fast titrations, and assumed the resultant surface acidity was under-estimated.

The intent of this study is to further investigate the above findings by (1) documenting differences in surface acidity of activated alumina using a slow titration vs. a fast titration, (2) varying hydration periods from 24 hours to 16 weeks to observe whether this results in a change in surface acidity, physical-chemical structure of activated alumina, and or fluoride loading capacity (sorbent hydrated up to 30 weeks), and (3) evaluating the impact that grain size has on fluoride adsorption capacity and rate. The results will be used to determine fluoride adsorption capacity under varied conditions and the adsorption kinetics of activated alumina. The information can also be used in the design of small-scale de-fluoridation filters in northern Ghana and other areas with similar water quality issues.

2. Materials and methods

2.1. Sorbent preparation

Activated alumina, with a manufactured grain size range of 0.5-1.0 mm, was sieved to remove fine powder with most of the experimental work conducted using this

grain size range. To compare changes in adsorption with changes in grain size, some of the activated alumina was also ground by hand with a pestle and mortar and sieved to a grain size range of 0.125-0.250 mm; and another small portion of the activated alumina was ground to a grain size range of 0.063-0.125 mm but only to determine the specific surface area. The activated alumina was rinsed well with deionized water to remove fine powder, followed by an acid-base wash to increase sample purity and reproducibility of the titrations and batch adsorption experiments (Huang, 1981). It was first soaked in 0.01 N NaOH, stirred for 30 minutes, centrifuged for 30 minutes at 26,890 g relative centrifugal force (RCF) using a Sorvall® RC-5B centrifuge, and rinsed again with deionized water by pouring off the supernate until the electrical conductivity was less than 5 μS cm^{-1}. The activated alumina was soaked once more for 30 minutes with 0.01 N HCl, centrifuged, and rinsed as described for the 0.01 N NaOH. Once clean, it was left to dry and sieved again to remove final traces of powder with grain size under 0.5 mm for 0.5-1.0 mm samples, under 0.125 mm for the 0.125-0.250 mm samples, and under 0.063 mm for the 0.063-0.124 mm samples. The clean, dry, sieved 0.5-1.0 mm sorbent was stored in a plastic container for six months or more before using. The portion that was ground to 0.125-0.250 mm, sieved, cleaned and dried was stored in a plastic container for one month before using.

2.2. Sorbent physical-chemical properties

The specific surface area, pore surface area, volume, and average pore diameter of dry samples were determined using a Micromeritics® TriStar 3000 static pressure surface area analyzer with $N_{2(g)}$ as the sorbate. The 10-point Brunauer, Emmett, Teller (BET) method was used to determine specific surface area (Brunauer, et al., 1938; Lowell and

Shields, 1991), and the Barrett, Joyner, Halenda (BJH) adsorption method was used to determine pore area, volume, and diameter for pore sizes between 1.7-300 nm (Barrett et al., 1951; Lowell and Shields, 1991). Samples were also evaluated for evidence of micropores (< 2 nm) by creating *t*-plots from the adsorption and desorption data used to calculate the BET surface areas and BJH pore area and volume (Gregg and Sing, 1982; Hay et al., 2011). The *t*-plot was created by plotting the statistical film thickness (*t*) on the x-axis vs. the volume of liquid nitrogen adsorbed to the surface (liquid nitrogen density of 0.808 g ml^{-1} at 77 K) on the y-axis. The statistical film thickness was calculated from the Harkins-Jura equation:

$$t\ [\text{Å}] = \sqrt{\frac{13.99}{0.034 - \log(\frac{p}{p^o})}} \quad (1)$$

Evidence of micropores and corresponding pore volumes were determined by the linear portions of the *t*-plot and the corresponding y-intercept (see Gregg and Sing, 1982; Leofanti et al., 1998; Hay et al., 2011). The statistical thickness (*t*) was presented in nanometers (nm), where 1 nm = 10 angstroms (Å); and p/p^o is the relative pressure used to create the $N_{2(g)}$ sorption isotherms.

The mineral content of each sorbent was determined using x-ray diffraction (XRD). Samples were prepared by taking ~5 g of the bulk sample, grinding by hand to a grain size <500 µm, then to a powder in a McCrone mill for 8 minutes in 10 ml of methanol. They were air dried overnight, re-crushed to break up aggregates formed during drying, and side-loaded into sample holders. Grinding the samples to a fine homogenous powder, followed by side-loading, helps to minimize preferred orientation of certain crystal phases within the samples which increases the accuracy of the semi-

quantitative analysis. The samples were run on a Bruker D8 Advance XRD equipped with a Vantec PSD detector; and the XRD scans were interpreted using the software called EVA®. The minerals were identified by matching reference mineral patterns stored in the ICDD (International Centre for Diffraction Data) database to the observed peaks. The method used for semi-quantitative analysis is based on the method of Chung (1975), which assumes that the minerals are identified correctly and that there are no unidentified phases in the sample.

The surfaces of activated alumina samples were observed using scanning electron microscopy (SEM) with a Hitachi S-4700 II Scanning Electron Microscope. Dry samples were placed in the Emitech K-575X sputter coater and coated with platinum to make particles electronically conductive before being inserted in the microscope chamber for imaging. The images were taken with a Hitachi cold field emission scanning electron microscope model S-4700-II equipped with the Oxford Energy Dispersive Spectroscope detector for chemical composition analysis.

2.3. Acid-base titrations

The method for acid-base titrations is modified from Craig et al. (2015 and references therein). One gram of activated alumina at grain size 0.5-1.0 mm was soaked in deionized water for 24 hours up to 16 weeks to fully hydrate the sorbent, and to identify changes in surface acidity with varied hydration period. Before titration, the liquid of the soaked sorbent was poured off. The activated alumina was rinsed well and placed in a 250 ml polypropylene beaker with a small, known volume of deionized water; the ionic strength was adjusted to 0.01 M with 1 M NaCl, and the beaker was then filled to a total volume of 150 ml with deionized water for a sorbent-to-solution ratio of 6.67 g

L^{-1}. The covered beaker was placed on a magnetic stir plate, with a gel-filled Ag/AgCl pH probe attached to an Orion® 4-Star meter inserted in the solution, and stirred and bubbled with $N_{2(g)}$. For the fast titrations, the solution was stirred until the pH stabilized, taking two to four hours, before adding acid or base. The titrant was added in a small increment every 5-10 minutes, at which point the pH was recorded and another increment of titrant was added. This pattern was continued to a pH of 4 for the acid titrations and to a pH of 10 for the base titrations (see Craig et al., 2015). In conducting the slow titrations, the slurry (set up as above) was left to stir overnight before taking the first pH reading. Then small increments of 0.1 N certified NaOH or 0.1 N certified HCl were added approximately every thirty minutes to one hour until the end of the day where the slurry was left to stir overnight, with the pH recorded the next morning. The pH meter was calibrated each morning as well. This process continued for two weeks with the acid titrations, and for one week with the base titration. Only one base titration at two week hydration was conducted due to the time involved to conduct slow titrations, and because the range below the pH of zero proton charge is of primary interest for fluoride adsorption. In order prevent working in pH ranges that tend to increase aluminum dissolution, the slow titrations were completed to a minimum pH of approximately 4.5 and maximum pH of approximately 9.8.

To check whether significant sorbent was lost in the rinsing or from titration, used sorbent from six of the titrations was dried and weighed. Total mass loss was 0-2% for three fast titrations (one 2 week and two 16 week hydrations) and three slow titrations (24 hour, 2 week, and 12 week hydration). The used sorbents were also sieved again to determine the fractional decrease in grain size. Of the six samples, 0-7% with an average

of 2.2% of the used sorbent measured under 0.5 mm showed the greatest percent decrease from the fast titrations. Aluminum dissolution at high and low pH was not investigated for the slow titrations conducted in this study. However, Craig et al. (2015) documented minimal aluminum dissolution from activated alumina at pH 4.5 and 9.8 after 24 hours in a 0.01 M NaCl solution, with greater dissolution at the high pH (dissolved aluminum 7.5 (10^{-2}) mmol L^{-1}). Yang et al. (2007) and Rosenqvist et al. (2002) also observed minimal dissolution of aluminum oxides between pH 4.5 and 9.8.

2.4. Calculating pH dependent surface charge density

The surface charge density (σ) is defined as the equivalents of H^+ attached to or removed from the sorbent per m^2 of sorbent, multiplied by Faraday's constant. It is determined by using the titration data presented in the previous section and the following equations (Huang and Stumm, 1973; Hao and Huang, 1986):

$$\sigma^{+}[\mathrm{C\ m^{-2}}] = \frac{\mathrm{F}*\{[(0.1\ \mathrm{N\ HCl})*(\mathrm{L\ titrant\ added})]-\left[[\mathrm{H^{+}}]*(\mathrm{L\ total})\right]\}}{(\mathrm{A}*(\mathrm{g\ sorbent}))} \quad (2)$$

$$\sigma^{-}[\mathrm{C\ m^{-2}}] = \frac{\mathrm{F}*\{[(0.1\ \mathrm{N\ NaOH})*(\mathrm{L\ titrant\ added})]-[[\mathrm{OH^{-}}]*(\mathrm{L\ total})]\}}{(\mathrm{A}*(\mathrm{g\ sorbent}))} \quad (3)$$

where C is coulombs, F is Faraday's constant (96,490 C mol^{-1}); A is specific surface area of the sorbent (m^2 g^{-1}); and 0.1 N HCl and 0.1 N NaOH are the titrant concentrations.

The titration curves of pH vs. coulombs of surface charge per meter squared were used to determine intrinsic acidity constants (K_a^{int}) by matching modeled titration curves with the experimentally determined titration curves. The model curves were created using the generalized two-layer surface complexation model (Dzombak and Morel, 1990) in the PHREEQC program (Parkhurst and Appelo, 1999).

2.5. Geochemical modeling of acid-base titration data using the generalized two-layer model with PHREEQC program

The generalized two-layer model (Dzombak and Morel, 1990) is a surface complexation model available in PHREEQC (Parkhurst and Appelo, 1999) and was used to describe the adsorption reactions. Dzombak and Morel (1990) provide a detailed description of the generalized two-layer surface complexation model, which was used to determine the intrinsic acidity constants K_a^{int} for proton adsorption onto a hydrated surface as described by the following reactions:

$$S - OH_2^+ \leftrightarrow S - OH + H^+ \quad (4)$$

$$S - OH \leftrightarrow S - O^- + H^+ \quad (5)$$

This was achieved by visually matching modeled curves to the experimental titration curves. The simulated acid-base titrations used the PHREEQC database, and the diffuse layer option was not used since the same results were achieved with or without it. The default option (no diffuse layer) adjusted for the surface charge by creating an equal and opposite charge in solution (Parkhurst and Appelo, 1999). The mass action expressions for proton adsorption and desorption (using reactions (4) and (5)) and the corresponding $logK_a^{int}$ were the only adjustable input parameters. Fixed input parameters were the specific surface area, 6.67 g of sorbent L^{-1}, a single N_s value of 4.5 sites nm^{-2} (as N_t = 1.44 (10^{-2}) mols charge L^{-1}), and an inert electrolyte (NaCl) background solution at I = 0.01 M. The $logK_a^{int}$ value was adjusted for a best fit to experimental titration data. The pH of zero net proton charge (pH_{PZNPC}) was estimated by adding pK_{a1}^{int} and pK_{a2}^{int} and dividing by 2.

2.6. Fluoride loading experiments

The method for conducting fluoride loading experiments is described in Craig et al. (2015). Prior to conducting the fluoride loading batch adsorption experiments with varied hydration periods, the sorbent of grain size range 0.5-1.0 mm was first hydrated in deionized water either 24 hours, 2 weeks, 12 weeks, 16 weeks, or 30 weeks. For the fluoride loading experiment at a finer grain size range, the sorbent of grain size range 0.125-0.250 mm was first hydrated two weeks. The pre-soaked sorbent plus a small known volume of deionized water was placed in a Nalgene® polypropylene copolymer centrifuge tube. Deionized water and 1 M NaCl were added to an ionic strength 0.01 M and the slurry was mixed by rocking the tubes back and forth using a Labquake®. After mixing 24 hours, the pH was adjusted to approximately 6.9-7.0 with 0.1 N HCl. Once the initial pH was stable, fluoride was added to each centrifuge tube in concentrations ranging from and 0.026-3.16 mmol L^{-1} (0.5-60 mg L^{-1}) with a total of 10-13 slurry-filled tubes. The slurries were mixed another 24 hours, after which the tubes were centrifuged for 30 minutes at 26,890 g RCF. Ten ml of the supernate was removed for pH analysis using an Accumet® Research AR 20 pH meter and probe, and for fluoride analysis using an Orion 4-Star meter and fluoride ion selective electrode, with TISAB III added to the supernate just before fluoride analysis (Hao and Huang, 1986; APHA, 1998). Each probe was calibrated before use, with calibration checks conducted on the fluoride probe every 8-10 samples in order to maintain an error under 5%. Possible fluoride induced dissolution of aluminum was evaluated at initial fluoride concentrations from 0.026-0.79 mmol L^{-1} (0.5-15 mg L^{-1}) by taking 10 ml of the post-adsorption supernate, filtering it with 0. 1 µm filters, acidifying, and then analyzing it via inductively coupled plasma

mass spectrometry (ICP-MS) using EPA Method 200.7. The detection limit for dissolved aluminum was 1.67 (10^{-3}) mmols L^{-1} (0.045 mg L^{-1}).

2.7. Geochemical modeling of fluoride adsorption data using the generalized two-layer model with PHREEQC program

The generalized two-layer model (Dzombak and Morel, 1990) was used to identify the fluoride adsorption reactions onto each of the three sorbents using the same input parameters described in section 2.5. The model curves were matched with experimental fluoride adsorption curves for both fluoride adsorption vs. pH, and fluoride loading at pH_o ~6.9 and ionic strength of 0.01 M NaCl. The data for the experimental fluoride adsorption curves are from Craig et al. (2015). The equilibrium constants for following fluoride adsorption reactions (from Karamalidis and Dzombak, 2010) were adjustable input parameters:

$$S - OH + F^- + H^+ \leftrightarrow S - F + H_2O \quad (6)$$

$$S - OH + F^- \leftrightarrow S - OHF^- \quad (7)$$

$$S - OH + 2F^- + H^+ \leftrightarrow S - F_2^- + H_2O \quad (8)$$

To identify the appropriate fluoride adsorption reactions and corresponding equilibrium constants, each of the above reactions was initially added as an input parameter, with the corresponding equilibrium constant treated as an adjustable parameter.

2.8. Adsorption of fluoride vs. time at grain sizes 0.125-0.250 mm and 0.5-1.0 mm

The adsorption rate of fluoride onto activated alumina was monitored at two grain size ranges to observe the degree to which grain size controls the adsorption rate. The method for the kinetic fluoride adsorption experiments is similar to the fluoride loading experiments described in section 2.6 with the following modifications: the activated

alumina was hydrated 2 weeks; the initial fluoride concentration was set at 0.53 mmol L^{-1} (10 mg L^{-1}); each centrifuge tube was mixed by rotating a different length of time, ranging from 5 minutes to 48 hours; and the solution was filtered with a 0.45 µm filter before fluoride analyses instead of being separated from the sorbent via centrifuge. The following pseudo-second-order rate equation was used to calculate the fluoride adsorption rate at two grain size ranges (Kim et al., 2004 and references therein):

$$\frac{t}{q} = \frac{1}{q_e^2\ k_2} + \frac{1}{q_e}\ t \qquad (9)$$

The pseudo-second-order model constants can be determined experimentally (Ho, 2006), where t is time, q is mg fluoride adsorbed per gram sorbent at time t, q_e is fluoride adsorbed at equilibrium and k_2 is the second order rate constant (g sorbent per mg of fluoride adsorbed per minute). The rate constant k_2 and q_e are determined by plotting $\frac{t}{q}$ on the y-axis vs. t on the x-axis, creating a straight line (equation (9)) with a slope of $\frac{1}{q_e}$ and y-intercept of $\frac{1}{q_e^2\ k_2}$. Equation (9) is derived by integrating and rearranging the following kinetic rate equation:

$$\frac{dq}{dt} = k_2(q_e - q)^2 \qquad (10)$$

For the derivation and discussion of equation (9) see Azizian (2004), Ho (2006), and Liu and Shen (2008).

3. Results

3.1. Physical and chemical characteristics of activated alumina

Table 5.1 presents the BET surface area and BJH pore area, volume, and diameter of activated alumina at three grain sizes, and various hydration periods (0, 2 weeks, and

16 weeks). There is generally no notable change in the surface area, pore area, volume, or diameter with varied hydration period or between three grain sizes (expected accuracy of BET surface area +/-10% under favorable conditions (Gregg and Sing, 1982)).

Table 5.1. Grain size, BET specific surface area, and BJH pore area, volume, and diameter using $N_{2(g)}$ adsorption. The cumulative surface area and volume presented below include pores with diameters between 1.7 nm and 300 nm. Samples *a* and *b* are different samples at the same grain size range and no prior hydration, but only sample *b* was analyzed for BJH pore area and volume.

Weeks Hydrated (Grain Size, mm)	Surface Area ($m^2\ g^{-1}$)	Pore Area ($m^2\ g^{-1}$)	Pore Vol. ($cm^3\ g^{-1}$)	Pore Diam. Avg. (nm)
0 (0.5-1.0)*a*	292.1	no data	no data	no data
0 (0.5-1.0)*b*	297.9	320.7[a]	0.39	4.87
2 (0.5-1.0)	288.9	281.4	0.35	4.97
16 (0.5-1.0)	294.8	286.1	0.35	4.93
0 (0.063-0.125)	288.4	no data	no data	no data
0 (0.125-0.250)	285.2	no data	no data	no data
2 (0.125-0.250)	290.2	284.5	0.35	4.95

[a]Pore area is not expected to be higher than surface area, but this may due to technical error or uncertainty of the method itself.

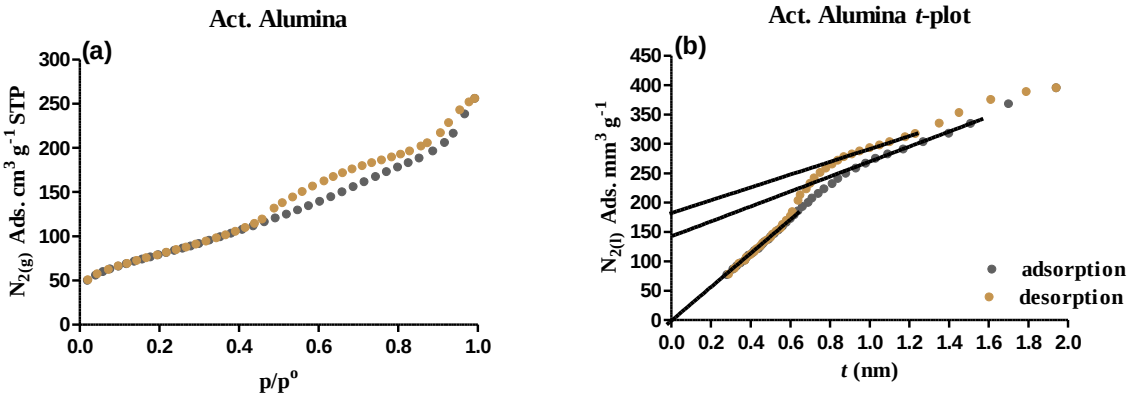

Fig. 5.1. Activated alumina 2 week hydration and grain size 0.5 to 1.0 mm: (a) $N_{2(g)}$ adsorption and desorption isotherms for activated alumina and (b) *t*-plots of $N_{2(l)}$ adsorption and desorption isotherms. The sorption data and *t*-plots presented here are representative of those used to determine results presented in Table 5.2.

Fig. 5.1 is an example of the sorption data and *t*-plot of activated alumina after two weeks hydration. The other sorption and *t*-plots used to calculated the results in Table 5.1 and 5.2 are nearly identical to Fig. 5.1 and are not shown. The first linear portion of the *t*-plot at the lowest *t* values passed through zero, which suggests an absence of micropores (de Bore et al., 1966). Also the specific surface area determined by the

slope of this line (Table 5.2) is less than 5% lower than the BET determined surface area (Table 5.1, 5.2). But even with these strong indicators of mesoporous activated alumina samples, Table 5.2 also shows that the samples may also have larger micropores as well as mesopores due to the shape of the *t*-plot (Stork et al., 1998) and a second linear portion of the curve (t = 0.9-1.5 nm) (Fig. 5.1b). If micropores are present, then the BET determined surface area is also less accurate (Davis and Kent, 1990).

Table 5.2. The BET *c* value, *t*-plot calculated surface area, film thickness (*t*), and corresponding pore volume. Adsorption = (ads) and desorption = (des) curves from *t*-plots.

Week Hydrated (Grain Size, mm)	BET *c*	Surface Area ($m^2\ g^{-1}$)	Film Thickness (nm)	Pore Vol.[a] ($cm^3\ g^{-1}$)
0 (0.5-1.0)b (ads)	79	288.3	1.1-1.4	0.158
0 (0.5-1.0)b (des)	79	288.3	0.9-1.2	0.194
2 (0.5-1.0) (ads)	86	279.1	1.0-1.5	0.148
2 (0.5-1.0) (ads)	86	279.1	1.0-1.2	0.186
16 (0.5-1.0) (ads)	80	285.0	1.0-1.4	0.160
16 (0.5-1.0) (des)	80	285.0	1.0-1.2	0.190
2 (0.125-0.250) (ads)	78	280.3	1.0-1.4	0.154
2 (0.125-0.250) (des)	78	280.3	1.0-1.2	0.179

[a]Pore volumes may include larger micropores, along with small mesopores.

Table 5.3. Semi-quantitative XRD analysis of the transformation of activated alumina with hydration. The percentages are approximations only and take into account crystalline material and not amorphous material, but the overall mineral transformation patterns are important.

Weeks Hydrated	% Act. Alum. (γ-Al_2O_3)	% Boehmite (γ-AlOOH)	% Bayerite (β-$Al(OH)_3$)
2	55	45	0
16	35	30	35
30	25	20	55

The semi-quantitative XRD analyses presented in Table 5.3 show that the percent of activated alumina decreases with increased hydration period (2 weeks, 16 weeks, and 30 weeks) as it begins to transform to boehmite (γ-AlOOH), and then bayerite (β-$Al(OH)_3$). Similarly, the SEM images presented in Fig. 5.2 show that the activated alumina develops a larger crystal structure with increased hydration period. The SEM analyses also indicate an increase in weight percent of oxygen and a decrease in the

weight percent of aluminum with increased hydration period, which suggests that the mineralogy of the hydrated activated alumina is transforming.

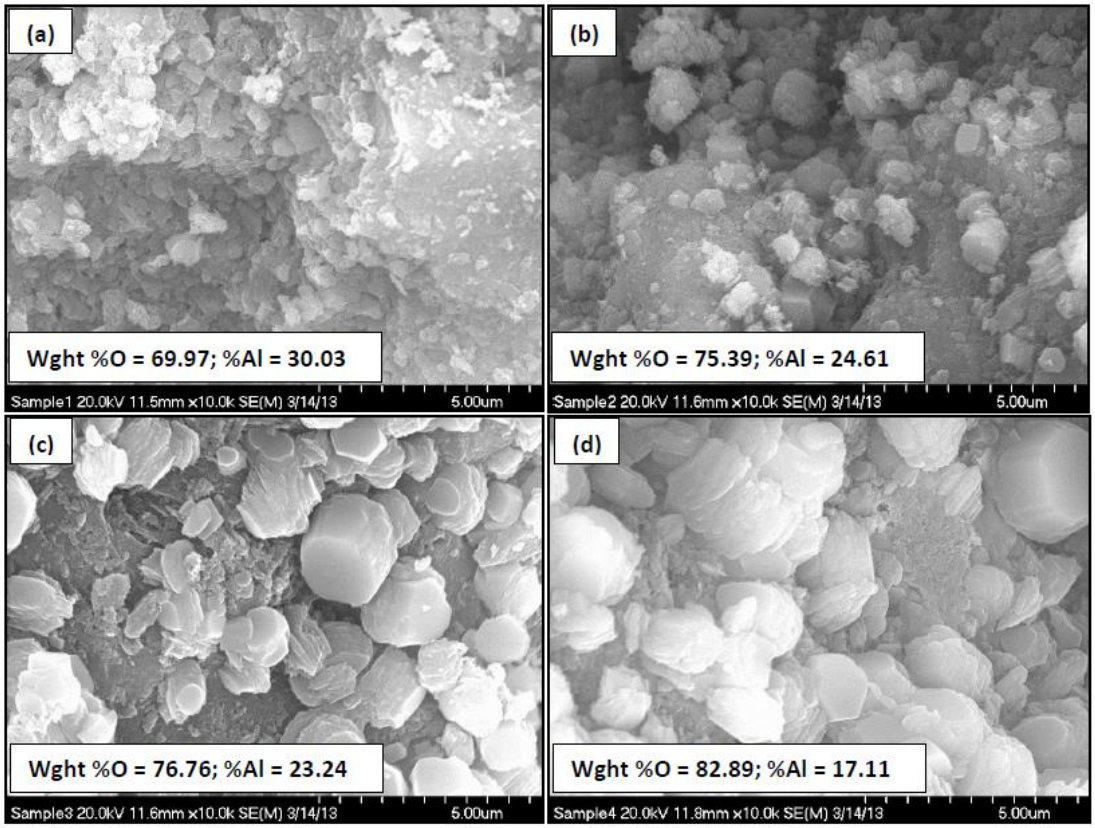

Fig. 5.2. SEM images and weight percent of both oxygen and aluminum of activated alumina samples first hydrated in deionized water for (a) 2 weeks, (b) 4 weeks, (c) 8 weeks, and (d) 16 weeks.

3.2. Surface charge of activated alumina with varied hydration period determined by fast and slow titration

The results of acid-base titrations conducted by Craig et al. (2015) showed a pH drift during the 5-10 minute stabilization time between titrant additions, indicating that equilibrium between solid and solution was not achieved for the grain size 0.5-1.0 mm used in the study. In order to consistently take pH readings within the time generally recommended for these titrations - for example from 2 minutes (Huang, 1981; Huang and Stumm, 1973) to under 20 minutes (Parks and de Bruyn, 1962) - the pH was sometimes recorded before it had stabilized (Craig et al., 2015). In the current study both fast and

slow titrations were conducted to observe whether the titration curves would differ. Both fast and slow titrations with varied hydration (from 24 hours to 16 weeks) were conducted to determine whether the surface charge also changed due to hydration period. In conducting the slow titration the pH was left to stabilize overnight before taking a reading, and the titration and surface charge results were drastically different from those for the fast titration (Fig. 5.3).

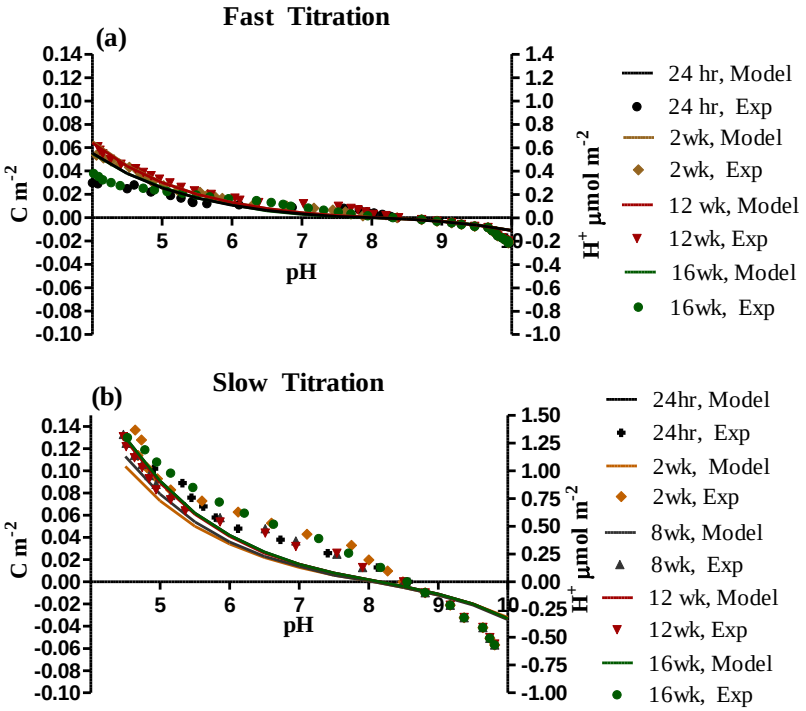

Fig. 5.3. Surface charge vs. pH curves using the generalized two-layer model in for a best fit match with experimental data at varied hydration of activated alumina in C m^{-2} (left y-axis) and µmol H^+ m^{-2} (right y-axis), (a) fast titration: 24 h, 2 wk, 12 wk, 16 wk hydration, and (b) slow titration: 24 h, 2 wk, 8 wk, 12 wk, 16 wk prior hydration. The base hydration was for two weeks only. The grain size was 0.5 to 1.0 mm, I = 0.01 M, and the sorbent-to-solution ratio 6.67 g L^{-1} for all titrations. The total surface site density for all calculations was set at 4.5 sites nm^{-2}, with the acidity constants of the model adjusted for a best fit with experimental data.

The 2 week hydration period fast titration data presented in Fig. 5.3a are from Craig et al. (2015), with the other data from this study. The surface charge calculated using the slow titration data is up to three times higher than that calculated from the fast

titration data (Fig. 5.3b). The curves for the slow titration are also relatively consistent regardless of the length of hydration period, with any slight variation in the titration curve not correlated to hydration period. The fast titration curves (Fig. 5.3a) are slightly less consistent below pH 5, but also do not seem correlated to the length of hydration period. Differences among the fast titration curves are probably because the pH values at each titrant step were recorded before equilibrium was obtained.

Table 5.4. Equilibrium constants for fluoride adsorption reactions intrinsic acidity constants using the generalized two-layer model. The corresponding fluoride adsorption reactions are: $\log K_1$ = reaction (6), $\log K_2$ = reaction (7), and, $\log K_3$ = reaction (8); X = no equilibrium constant; pK_{a1}^{int} and pK_{a2}^{int} are the intrinsic acidity constants corresponding to reactions (4) and (5) respectively. The total surface site density was fixed at 4.5 sites nm^{-2}, and the equilibrium constants were adjusted for a best fit curve with experimental fluoride adsorption data. The pH_{PZNPC} is determined by adding the intrinsic acidity constants and dividing by two.

Titration	$\log K_1$	$\log K_2$	$\log K_3$	pK_{a1}^{int}	pK_{a2}^{int}	pH_{PZNPC}
Fast[a]	10.3	2.9	X	5.1	11.1	8.1
Slow	10.0	2.9	13.9	6.4	9.7	8.1

[a]All values from Craig et al. (2015).

3.3 Modeling surface charge and calculating intrinsic acidity constants using the generalized two-layer model in PHREEQC

The intrinsic acidity constants for the slow titrations were estimated with the generalized two-layer model. Using the input parameters presented in section 2.5, the K_a^{int} value was attained by manipulating it for a best fit between the model curve and the experimental curve (Fig. 5.3b). The modeled results in Fig. 5.3a, which were used to determine the intrinsic acidity constants via fast titrations, are from Craig et al. (2015). The intrinsic acidity constants are presented in Table 5.4, and they differ notably between the fast and slow titrations. Simulations that included dissolved aluminum in solution (1.9 mmol L^{-1}) did not affect the modeled titration curves, and a lower specific surface area (e.g. due to dissolution) resulted in a poorer fit with experimental data. The pK_{a1}^{int} ranged from 6.4-6.7, and the single pK_{a2}^{int} was 9.7 for the five slow titrations in Fig. 5.3b. The

intrinsic acidity constants that created the best model fit for titration data were 7.2 and 8.9 for pK_{a1}^{int} and pK_{a2}^{int} respectively, but it was not possible to get a good model fit for both the adsorption vs. pH and fluoride loading using these values as input parameters (see section 3.4). As a result they were adjusted slightly to 6.4 and 9.7 for pK_{a1}^{int} and pK_{a2}^{int} respectively. Using the second set of pK_a^{int} values and increasing the surface area dramatically and or increasing the surface sites also improved the model fit to experimental data.

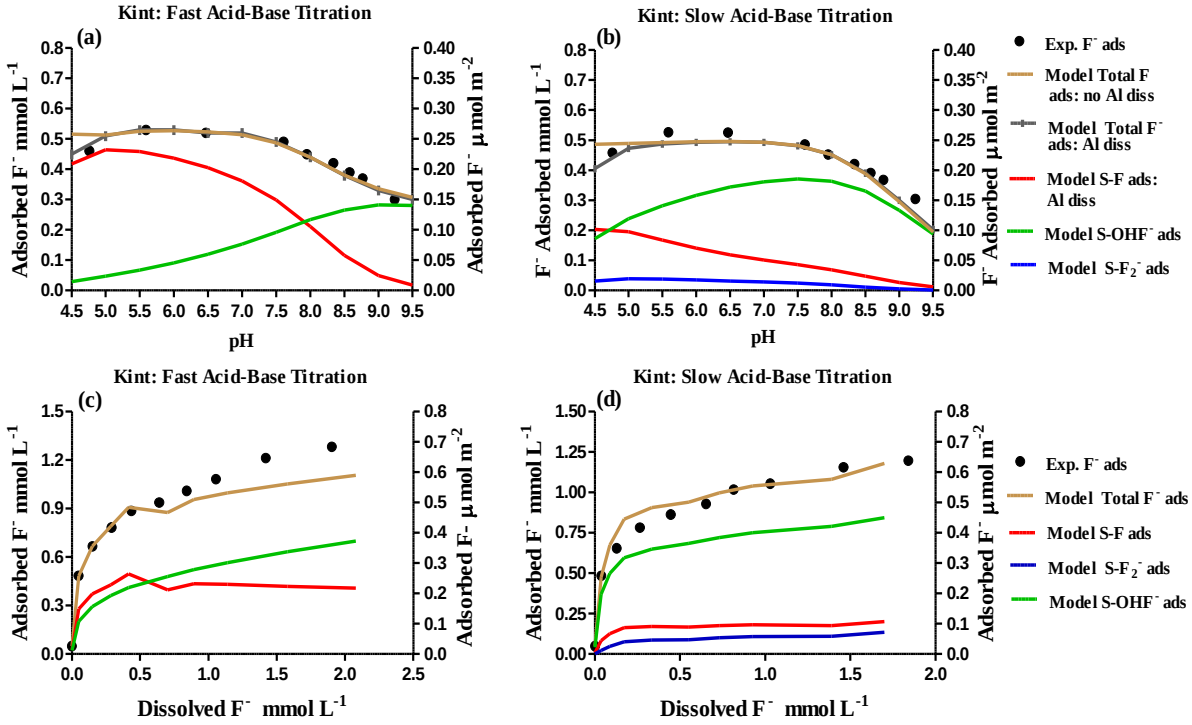

Fig. 5.4. Experimentally determined fluoride (F^-) adsorption vs. pH and best fit modeled curves using the generalized two-layer model with (a) intrinsic acidity constants from fast titration (Fig. 5.3a) and (b) the intrinsic acidity constants from slow titration (Fig. 5.3b). The equilibrium distribution of F^- adsorbed vs. remaining in solution and best fit modeled curves using (c) intrinsic acidity constants from fast titration (Fig. 5.3a) and (d) the intrinsic acidity constants from slow titration (Fig. 5.3b). The results are presented in mmol L^{-1}(left y-axis) and µmol m^{-2} (right y-axis). The experimental data are from Craig et al. (2015). The ionic strength was 0.01 M NaCl, the grain size was 0.5 to 1.0 mm, and the sorbent-to-solution ratio was 6.67 g L^{-1}.

3.4. Modeling fluoride adsorption using the generalized two-layer model in PHREEQC

The fluoride adsorption constants were also estimated with the generalized two-layer model by matching a best fit between the model curve and the experimental curve, as shown in Fig. 5.4. The intrinsic acidity constants for the slow titration (Table 5.4) were input parameters, along with those listed in sections 2.5 and 2.7. The modeled fluoride results in Fig. 5.4a, c which used the fast titration determined intrinsic acidity constants as input parameters, are from Craig et al. (2015). To better constrain the input parameters and to test them under varied solution conditions, both the fluoride vs. pH and fluoride loading at constant pH were modeled. Similar to the results in Craig et al. (2015), at pH below 5 the model curves only fit experimental curves if dissolved alumina was included in solution. The same input parameters were used for both sets of curves (e.g. both fast titration Fig. 5.4a, c; and both slow titration Fig. 5.4b, d), and the fluoride adsorption equilibrium constants (for reactions (6)-(8)) had to fit both sets of experimental curves. A good model fit for both the fluoride adsorption vs. pH and fluoride loading could not be attained using the best fit set of slow titration pK_a^{int} values presented in the previous section. However by increasing pK_{a2}^{int}, the modeled fluoride adsorption increased at high pH which improved the fit to experimental data; and by decreasing pK_{a1}^{int} the modeled fluoride loading decreased which also improved the fit to experimental data.

The equilibrium constants for fluoride adsorption as described by reactions (6)-(8) are presented in Table 5.4. Using different sets of intrinsic acidity constants as input parameters for determining the fluoride adsorption curves presented in Fig. 5.4 affects the adsorption constants (Table 5.4). The fast titration (Fig. 5.4a and c) uses the intrinsic acidity constants determined in Craig et al. (2015), and the slow titration (Fig. 5.4b and d)

uses the intrinsic acidity constants determined in this study. The $\log K_2$ values are the same for both sets of fluoride adsorption models, and the $\log K_1$ values differ just slightly (10.3 for the fast titration, and 10.0 for the slow titration). However, to get the best model fit for the slow titration, reaction (8) also had to be included which was not needed for the fast titrations. Also, for the slow titrations fluoride adsorption onto the surface hydroxyl (reaction (7) (S_OHF^-)) is the dominant adsorption mechanism, while for the fast titrations, ion exchange (reaction (6) (S_F)) dominates at pH below 8, and at low fluoride loading. Only at elevated pH and at high fluoride loading does fluoride adsorption onto the surface hydroxyl begin to dominate (reaction (7) (S_OHF^-)).

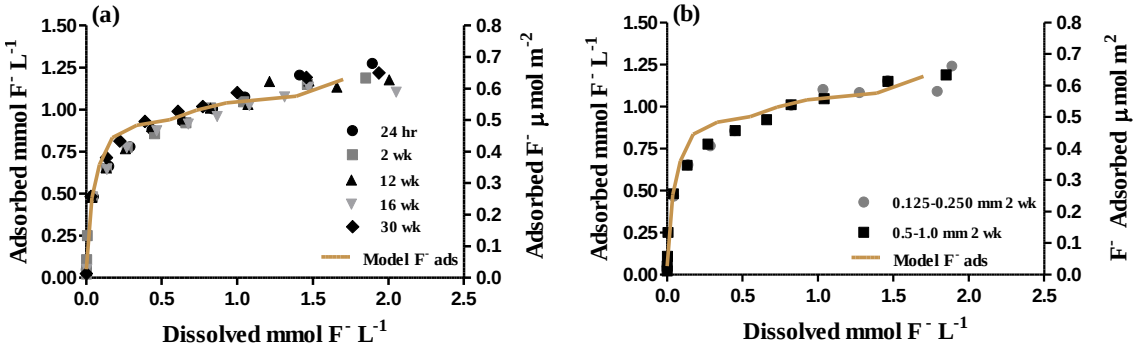

Fig. 5.5. The equilibrium distribution of fluoride (F^-) adsorbed to activated alumina vs. the fluoride concentration remaining in solution in mmol L^{-1} (left y-axis) and µmol m^{-2} (right y-axis) at (a) varied hydration period, and (b) two grain size ranges and two week hydration period. The brown modeled curve is included in (a) and (b). The ionic strength was 0.01 M NaCl, the grain size was 0.5 to 1.0 mm, and the sorbent-to-solution ratio was 6.67 g L^{-1}.

3.5. Fluoride loading onto activated alumina with varied hydration period, and at two grain size ranges

Another and more important concern than hydration-induced changes in surface charge is a potential hydration-induced change in fluoride adsorption capacity. The curves presented in Fig. 5.5a show no notable difference in fluoride adsorption capacity onto activated alumina whether the surface was hydrated for 24 hours or 30 weeks. These data are consistent with the slow titration and surface charge data presented in Fig. 5.3b,

which show little variation in surface charge for different hydration periods. Additionally, when comparing the fluoride adsorption capacity of activated alumina hydrated two weeks at grain sizes 0.125-0.250 mm and 0.5-1.0 mm, the adsorption curves are the same (Fig. 5.55b). Similarly the specific surface area of seven samples at three grain size ranges is 285.2-297.9 $m^2 g^{-1}$ with an average value of 291.1 $m^2 g^{-1}$, median value of 290.2 $m^2 g^{-1}$ and no trend related to grain size (Table 5.1).

Finally, when considering activated alumina as a sorbent for use in de-fluoridation filters, another public health concern is exposure to dissolved alumina (WHO, 2008). Therefore, because of potential risk of exposure to aluminum in the treated drinking water, used supernate from fluoride loading experiments with initial fluoride concentrations up to 0.79 mmol L^{-1} (15 mg L^{-1}) was analyzed for dissolved aluminum. All results were below the detection limit of 1.67 (10^{-3}) mmols L^{-1} (0.045 mg L^{-1}).

3.6. Adsorption of fluoride vs. time at grain sizes 0.125-0.250 mm and 0.5-1.0 mm

The overall adsorption of fluoride onto activated alumina does not change notably between the two grain size ranges (Fig. 5.5b), but adsorption is much faster when the grain size range is decreased from 0.5-1.0 mm to 0.125-0.250 mm (Fig. 5.6). Even though the specific surface area, pore area, and pore sizes are nearly the same between the two grain size ranges (Table 5.1, 5.2), diffusion within the pore spaces appears to be easier and faster at the finer grain size range, resulting in a much faster adsorption. After five minutes and at the larger grain size only about 15% of the fluoride is removed from solution, while at the finer grain size nearly 60% of fluoride is removed in five minutes (Fig. 5.6b). Similarly, 90% of fluoride is removed from solution after 40 minutes at the finer grain size, where at the larger grain size it takes 24 hours to remove up to 90%.

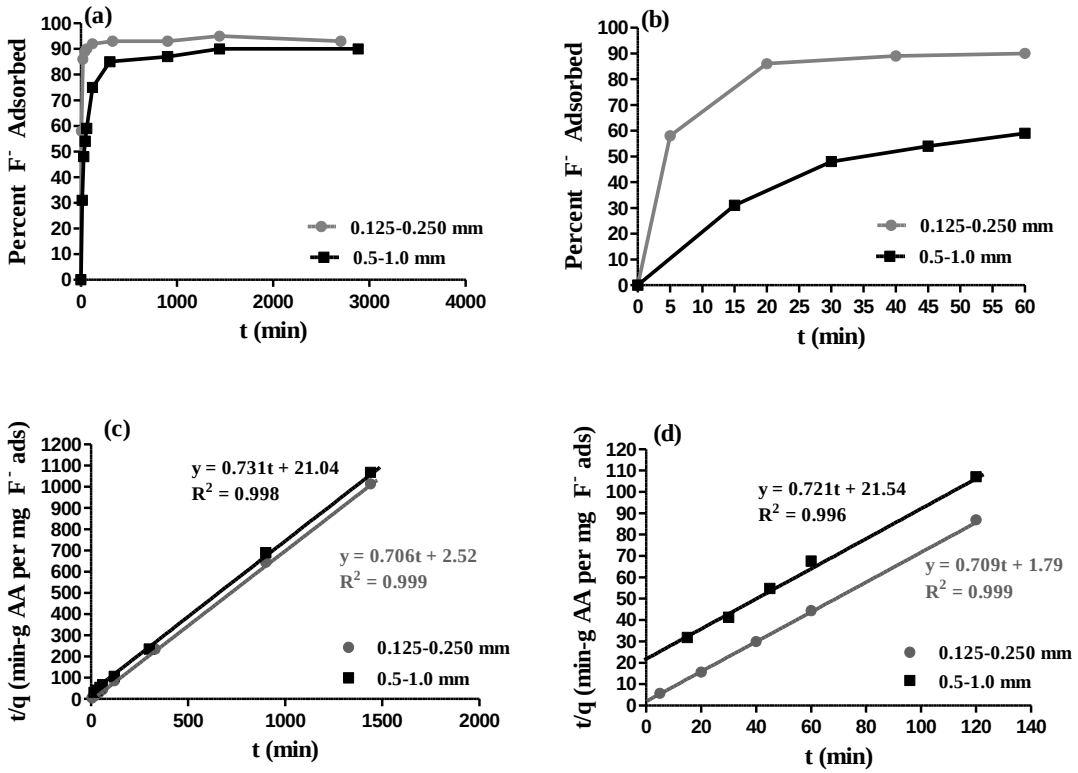

Fig. 5.6. The percent fluoride (F^-) adsorbed vs. time to activated alumina with 2 week hydration, and at two grain size ranges for time in (a) ~48 hours (as minutes), and (b) 60 minutes; and linear regression curves to determine the pseudo-second-order rate constant (k_1) from the y-intercept in (c) 24 hours (1440 min), and (d) 2 hours (120 min). The ionic strength was 0.01 M NaCl, and sorbent-to-solution ratio was 6.67 g L^{-1}.

Table 5.5. The pseudo-second-order rate constants (k_2) determined from the y-intercept of the curves, and equilibrium adsorption (q_e) determined from the slope for two grain sizes, from linear regression curves in Fig. 6b (24 h curve) and c (2 h curve).

Grain Size (mm)	k_2 2 h (g per mg F^- min)	q_e 2 h (mg F^- per g)	k_2 24 h (g per mg F^- min)	q_e 24 h (mg F^- per g)
0.125-0.250	0.28	1.41	0.19	1.42
0.5-1.0	0.024	1.38	0.025	1.37

Using the experimental data described above, the fluoride adsorption rate was also calculated at two grain size ranges. The pseudo-second-order rate constants for the 0.125-0.250 mm activated alumina is an order of magnitude higher than the 0.5-1.0 mm grain size, and the equilibrium concentration (q_e) is also slightly higher with the finer grain activated alumina, as determined from the y-intercept and slope respectively of the 2 and 24 hour linear regression curves (Fig. 5.6c, d and Table 5.5).

4. Discussion

4.1. Changes in physical-chemical characteristics, pH dependent surface charge, and fluoride adsorption capacity with varied hydration period

The mineralogy of activated alumina begins to transform to boehmite and then bayerite when it is hydrated in deionized water for 2, 4, 8 and 16 weeks (Table 5.3). Lefèvre et al. (2002) also observed that the activated alumina transformed to bayerite with increased hydration period. However in this current study the surface area (Table 5.1), did not change notably or with a distinct pattern as a result of hydration period. The surface charge of activated alumina also does not change notably when the activated alumina is hydrated in deionized water a short period of time or a long period of time (Fig. 5.3). The slight variation in proton adsorption observed for the fast titrations at pH below 5 is not clear, but it may be due to slight variations in small pore sizes (and diffusion) of the different sorbent samples, if they contain large micropores (1-2 nm) and or small mesopores. Fluoride adsorption onto activated alumina also does not change with hydration period (Fig. 5.5), which is consistent with the above findings on surface reactivity vs. prior hydration.

The results from this current work differ from those presented in Lefèvre et al. (2002), which found that the surface charge of activated alumina continually decreased when hydrated one day up to 6 months. However, the titration curves presented in Lefèvre et al. (2002) only include results between pH 3.7-3.0 which apparently is where the curves began to vary, with the loss of reactive surface attributed to the increased proportion of a mostly non-reactive phase of bayerite. The results from this study do not show a reduction in surface reactivity, although the acid titrations were only conducted to

a minimum pH 4.5 and maximum of 9.5 to minimize aluminum dissolution. It is possible that, had the titrations been conducted to pH 3.0 (with an adjustment for aluminum dissolution), a similar trend would have occurred. Even so, a decrease in surface reactivity, if occurring, may not matter at the pH range of interest for fluoride adsorption filters, which is near neutral. This is because, at neutral pH only a portion of the charged and hydrated surface is fully protonated resulting in a limited number of surface sites for fluoride adsorption or ion exchange. Therefore, whether some of the surface sites become unreactive at extreme pH values may be irrelevant at near neutral pH.

4.2. Comparing generalized two-layer models using fast and slow titration data

4.2.1. Modeling fast and slow acid-base titrations

The intrinsic acidity constants determined via fast vs. flow titration differ notably (Table 5.4) because the experimental curves also differ notably (Fig. 5.3). The experimental curves underestimate surface charge because the large grain sorbent used in Craig et al. (2015) and in this study needed more than 10 minutes to stabilize. Rosenqvist et al. (2002) also found that titrations using gibbsite generally needed 8-14 hours to equilibrate between each acid or base titration, and these were for sorbent samples with a very fine grain size (nanoscale). From the results of thoroughly characterized gibbsite samples, Rosenqvist et al. (2002) concluded that both singly and doubly coordinated hydroxyl groups on basal planes are involved in surface protonation, with doubly coordinated hydroxyl groups requiring longer reaction times. In this work, the large grain size seems to be a factor, which is likely linked to diffusion processes into the pore area, but may also be linked to number of and access to singly and doubly coordinated hydroxyl groups. The latter depends on whether the reactivity of the activated alumina

surface is similar to that of gibbsite. Eng et al. (2000) evaluated the surface structure of α-Al_2O_3 (0001) and the modeled results indicate that the hydrated surface of the alumina is similar to gibbsite and bayerite basal planes. There are likely similarities between the surface properties of the previously described aluminum oxides and the activated alumina used in this study – particularly because, in this work, the surface begins to transform to boehmite and then bayerite.

The results in Fig. 5.6 confirm that time to equilibrium is slow for the grain size 0.5-1.0 mm. As a result the intrinsic acidity constants determined by modeling a best fit to experimental data are not accurate. However, in modeling fluoride adsorption, which will be discussed in the next section, getting a good fit to both the adsorption vs. pH and the fluoride loading at constant pH using the same set of equilibrium constants for reactions (6)-(8), the intrinsic acidity constants (which were input parameters) determined via slow titration needed to be adjusted slightly. As discussed in sections 3.3 and 3.4, the intrinsic acidity constants that created the best model fit for titration data were 7.2 and 8.9 for pK_{a1}^{int} and pK_{a2}^{int} respectively, but it was not possible to get a good model fit for both the adsorption vs. pH and fluoride loading using these values as input parameters, so they were adjusted to 6.5 and 9.7 for pK_{a1}^{int} and pK_{a2}^{int} respectively which improve modeled fluoride adsorption at high pH in Fig. 5.4b by increasing adsorption, and improve modeled fluoride loading in Fig. 5.4d by lowering adsorption. It was also noted in section 3.3 that increasing the surface area and or the number of surface sites improve the model fit to the slow titration experimental curves (but was not true of the fluoride adsorption curves). The required adjustments may indicate that the titration curves from the slow titrations have overestimated proton adsorption and removal slightly, or the slow

titrations themselves resulted in increased surface acidity, or even that some of the protonated sites are not easily exchangeable with fluoride.

The surface charge determined via slow titration is more consistent with the range of surface charge determined from previous studies for gibbsite and other oxides, with the low range of surface charges apparently due to faster titrations (e.g. Rosenqvist et al. 2002 and references therein). The surface charge of a semi-crystalline γ-alumina (Al_2O_3) in Yang et al. (2007), which was produced by heat treating the gibbsite sample at 550 ^oC for 1.5 hours, was closer to that determined via fast titration in Craig et al. (2015), but the gibbsite itself was closer to the range of the slow titrations conducted in this work. The reaction times for titrations were not provided in Yang et al. (2007).

4.2.2. Modeling fluoride adsorption using intrinsic acidity constants derived from fast and slow titrations

Fig. 5.4 presents fluoride adsorption vs. pH and fluoride loading at constant pH. In determining the fluoride adsorption equilibrium constants for reactions (6)-(8), the only input parameters that varied were the intrinsic acidity constants (see Table 5.4). The result is notably different curves for the fluoride adsorption reactions. Using slow titration data, fluoride reaction (7) (S_OHF^-) dominates heavily under all conditions except at pH 4.5. Also the fluoride loading curve matches the experimental curve at high fluoride loading. It was suggested in Craig at al. (2015) that the poor fit in Fig. 5.4c may be due to surface precipitation, but it should also be noted that the best overall fit In Fig. 5.4d required overestimating fluoride adsorption at low fluoride loading. The flattening of the fluoride adsorption curve with loading in this study (Fig. 5.4d) is similar to that in Craig et al. (2015) (Fig. 5.4c). Surface precipitation may still be occurring at high

fluoride loading, but uncertainty in the models themselves may also influence a poor fit to experimental data.

4.3. Comparing fluoride adsorption capacity and time to equilibrium at two grain sizes

The overall fluoride adsorption capacity does not change between the two grain size ranges compared here (Fig. 5.5), nor does the surface area (Table 5.1) or possible micropore range and volume (Table 5.2). But fluoride adsorption occurs much faster at grain sizes 0.125-0.250 mm than at 0.50-1.0 mm (Fig. 5.6) which suggests that, because the bulk of the surface area is in the pore space, the smaller grain sizes allow for easier and possibly shorter access to the intragranular reactive surface area. And the time differences are dramatic - it only takes one hour for the finer grain sorbent to adsorb 90% of the fluoride in solution while the larger grain sorbent takes 24 hours (Fig. 5.6). Similarly, after five minutes of contact time the finer grain adsorbs nearly 60% while the larger grain sorbent adsorbs a little under 15% of fluoride in solution. With regard to adsorption filters, the finest grain size possible should be used for fast adsorption, while still working within design constraints of the filter type.

5. Conclusions

The fluoride adsorption capacity of the activated alumina evaluated in this study does not decrease with increased hydration period (at least in the pH range of interest down to 4.5), but care are must be taken in conducting potentiometric titrations and allow for sufficient equilibration time in order to accurately estimate the pH dependent surface charge. Although total fluoride adsorption capacity does not change notably with the two grain size ranges evaluated in this study, the adsorption is much faster at a finer grain size. Therefore, the grain size used in a de-fluoridation filter should be as fine as

reasonably possible for the filter design. Finally, another practical question that has not been addressed in this work regarding the design of a small-scale filter for use in a poor rural community, is the longevity of activated alumina as a sorbent when used, regenerated, and re-used. Determining the change in adsorption capacity with re-use is also recommended in order estimate the long term effectiveness of activated alumina as a fluoride sorbent. The described information will be useful in determining the cost vs. benefit of small-scale filters with activated alumina as the sorbent.

Acknowledgements

This research was generously supported by the University of Nevada, Reno, the Desert Research Institute, and a U.S. Environmental Protection Agency Science to Achieve Results Graduate Research Fellowship.

References

APHA (American Public Health Association), 1998. Standard Methods for the Examination of Wastewater. American Public Health Association, American Water Works Association, Water Environment Federation publication. APHA, 20th ed, Washington DC.

Azizian, S. 2004. Kinetic models of sorption: a theoretical analysis. J. Colloid Interface Sci. 276, 47-52.

Barrett, E.P., Joyner, L. G., Halenda P.P., 1951. The determination of pore volume and area distributions in porous substances. I. Computations from nitrogen isotherms. J. Am. Chem. Soc. 73, 373-380.

Brunauer, S., Emmett, P.H., Teller, E., 1938. Adsorption of gases in multimolecular layers. J. Am. Chem. Soc. 60, 309-319.

Chung, F. H. 1975. Quantitative interpretation of X-ray diffraction patterns of mixtures. III. Simultaneous determination of a set of reference intensities. J. Applied Crystallography 8, 17-19.

Craig, L, Stillings, L.L., Decker, D.L., Thomas, J.M. 2015. Comparing activated alumina with indigenous laterite and bauxite as potential sorbents for removing fluoride from drinking water in Ghana. Appl. Geochem. 56, 50-66.

Davis, J.A., Kent, D.B., 1990. Surface complexation modeling in aqueous geochemistry. In; Hochella Jr. M.F., White A.F. (Eds.), Mineral-water interface chemistry. Reviews in mineralogy vol. 23. Mineral Soc. Am.: Washington DC, pp. 177-260.

de Boer, J.H., Lippens, B.C., Linsen, B.G., Broekhoff, J.C.P., van den Heuval, A., Osinga, T.J. 1966. The t-curve of multimolecular N_2 adsorption. J. Colloid Interface Sci. 21, 405-415.

Dzombak, D.A., Morel, F.M.M., 1990. Surface Complexation Modeling: Hydrous Ferric Oxide. John Wiley & Sons Inc., New York.

Eng, P.J., Trainor, T.P., Brown Jr., G.E., Waychunas, G.A., Newville, M., Sutton, S.R., Rivers, M.L. 2000. Structure of the hydrated α-Al_2O_3 (0001) Surface. Science 288, 1029-1033.

Farrah, H., Slavek, J., Pickering, W.F., 1987. Fluoride interactions with hydrous aluminum oxides and alumina, Aust. J. Soil Res., 55-69.

Fletcher, H.R., Smith, D.W., Pivonka, P., 2006. Modeling the sorption of fluoride onto alumina. J. Environ. Eng. 132, 229-246.

Gregg, S.J., Sing, K.S., 1982. Adsorption, Surface Area, and Porosity. Academic Press, London.

Hao, O.J., Huang, C.P. 1986. Adsorption characteristics of fluoride onto hydrous alumina. J. Environ. Eng. 112, 1054-1069.

Hay, M.B., Stoliker, D.L., Davis, J.A., Zachara, J.M., 2011. Characterization of the intragranular water regime within subsurface sediments: Pore volume, surface area, and mass transfer limitations. Water Resour. Res. 47, 1-19.

Ho, Y.S. 2006. Review of second-order models for adsorption systems. J. Hazard. Mater. B136, 681-689.

Huang, C.P., 1981. The surface acidity of hydrous solids. In: Anderson, M.A., Rubin, A.J. (Eds), Adsorption of Inorganics at Solid-liquid Interfaces. Ann Arbor Science, Michigan, pp. 183-207.

Huang, C.P., Stumm, W., 1973. Specific adsorption of cations on hydrous γ-Al_2O_3. J. Colloid Interface Sci. 43, 409-420.

Karamalidis, A.K., Dzombak, D.A., 2010. Surface Complexation Modeling: Gibbsite. John Wiley & Sons Inc., New York.

Kim, Y., Kim, C., Choi, I., Rengaraj, S., Yi, J. 2004. Arsenic removal using mesoporous alumina prepared via a templating method. Environ. Sci. Technol. 38, 924-931.

Lefèvre, G., Duc, M., Lepeut, P., Caplain, R., Fédoroff, M., 2002. Hydration of γ-alumina in water and its effects on surface reactivity. Langmuir 18, 7530-7537.

Leofanti, G., Padovan, M., Tozzola, G., Venturelli, B., 1998. Surface area and pore texture of catalysts. Catal. Today 41, 207-219.

Liu, Y., Shen, L. 2008. From Langmuir kinetics to first- and second-order rate equations for adsorption. Langmuir 24, 11625-11630.

Lowell, S., Shields, J.E., 1991. Powder Surface Area and Porosity. Chapman and Hall Ltd., New York.

Miretzky, P., Cirelli, A.F., 2011. Fluoride removal from water by chitosan derivatives and composites. A review, J. Fluorine Chem. 132, 231-240.

Mohapatra, M., Anand, S., Mishra, D.E., Giles, D.E., Singh, P., 2009. Review of fluoride removal from drinking water. J. Environ. Manag. 91, 67-77.

Parkhurst, D.L., Appelo, C.A.J., 1999. User's guide to PHREEQC (version 2) – A computer program for speciation, batch-reaction, one-dimensional transport, and inverse geochemical calculations. U.S. Geological Survey, Denver CO.

Parks, G.A., de Bruyn, P.L. 1962. The zero point of charge of oxides. J. Phys. Chem. 66, 967-973.

Rosenqvist, J., Persson, P., Sjöberg, S., 2002. Protonation and charging of nanosized gibbsite (α-$Al(OH)_3$ particles in aqueous suspension. Langmuir 18, 4598-4604.

Storck, S., Bretinger, H., Maier, W.F., 1998. Characterization of micro- and mesoporous solids by physisorption methods and pore-size analysis. App. Catal. 174, 137-146.

WHO (World Health Organization), 2008. Guidelines for Drinking Water Quality. Volume 1, 3rd edition. World Health Organization, Geneva.

Yang, X., Sun, Z., Wang, D., Forsling, W., 2007. Surface acid-base properties and hydration/dehydration mechanisms of aluminum (hydr)oxides. J. Colloid Interface Sci. 308, 395-404.

CHAPTER 6

Conclusions and Future Work

Summary of research

The intent of this body of research was to address the ongoing public health problem of fluorosis in northern Ghana by taking a systems approach, which included combining laboratory and field work. The first goal of the field research was to collect baseline hydrogeologic and geochemical data in the study area, with a focus on identifying the location of wells and the distribution of variable concentrations of groundwater fluoride. The second goal of the field research was to spend extended periods of time in the community to in order to better understand the living conditions and to establish relationships with community members and government workers. Three sets of house-to-house surveys were conducted to estimate household size, identify seasonal household water sources (and fluoride exposure from drinking water), document the daily diet, and assess the level of understanding of the cause of brown and damaged teeth (dental fluorosis). In addition, daily water intake was determined for selected participants from age five to 70 years. Field data were used to correlate the distribution of dental fluorosis to fluoride concentrations in drinking water; and the water consumption data were used to estimate fluoride intake from water, which was then used to recommend fluoride limits in drinking water for small children to adults. Laboratory experiments were also conducted to investigate the fluoride adsorption capacity of two indigenous sorbents, bauxite and laterite, for use in simple, low-cost, small-scale de-fluoridation filters in fluoridic areas of Ghana. Their adsorption capacity was compared

to that of activated alumina, which is established as a good sorbent fluoride removal from water (Hao and Huang, 1986; Farrah et al., 1987; Fletcher et al., 2006).

Addressing fluorosis in the Upper East Region

The data show that groundwater fluoride concentrations in the study area of Namoo tend to be highest in the vicinity of Bongo granite, which is the source of groundwater fluoride, and decrease steadily with distance from Bongo granite. The survey data indicate that the highest concentrations of dental fluorosis (including the most severe cases) are in households that consume water with average fluoride concentrations ~3 mg L^{-1}. However, there were also cases of dental fluorosis in households that consume water with fluoride well under 1 mg L^{-1}, which is also well below the WHO recommended limit of 1.5 mg L^{-1} (WHO, 2011). Water consumption data show that daily water intake is about double that of more temperate climates, which partly explains this finding. Individual sensitivity, and unidentified sources of fluoride (e.g. in the diet or other water sources) may also contribute to increased number of cases of dental fluorosis in communities with low fluoride drinking water. The recommendation is to provide very low fluoride drinking water (< 1.0 mg F^- L^{-1}) to children under 6-8 years and even lower in the first two years. However because finding alternative sources low fluoride water can be quite costly, the current limit of 1.5 mg F^- L^{-1} is appropriate for older children and adults. The survey results also show that only 24% of households understand the cause of dental fluorosis. Therefore, an active and long-term educational program is needed.

De-fluoridation filters as an option for water treatment

Installing small-scale de-fluoridation filters may be an option for providing low fluoride drinking water to communities with elevated fluoride in their drinking water.

The results indicate that laterite and bauxite would be needed in large quantities to be effective. Decreasing the grain size substantially would improve adsorption capacity, as would lowering the pH (<6 for bauxite and <4.5 for laterite). In contrast, activated alumina adsorbs fluoride well at the pH of the local groundwater and it has much higher surface area so, per unit weight, it is notably better than bauxite and laterite. But it needs to be purchased and imported, which increases the cost. Larger-scale water treatment would be a more cost-effective option, whatever sorbent is used. It would also allow for better quality control and the application of more advanced techniques (e.g. lower pH, using a powder grain size, laboratory synthesized or modified sorbents, high pH rinse and re-use of sorbent). This would also increase costs and, to be sustainable, the users would need to pay a small fee when collecting treated water.

Alternatives to water treatment

In some communities, it may be possible to provide an alternative source of low fluoride drinking water. Rainwater catchment systems are one option, although it is unlikely that a system set up for a single family would provide enough drinking water for the entire year. If maintained properly these systems can provide a very clean source of low fluoride water for part of the year. Rainwater catchment systems have been set up in some schools in parts of northern Ghana, but to date the results have not been successful (Bongo District Assembly personal communication, 2012). It appears that the rainwater catchment systems were neglected. Also, as discussed in Chapter 2, it may be possible to collect low fluoride water from designated hand-pump wells and pipe it to areas that have no alternative source of low fluoride drinking water. The initial costs would be high,

however. Dilution by mixing high fluoride and low fluoride water is another option for increasing the volume of water with fluoride concentrations of 1.5 mg L^{-1} or lower.

Future work

There are tentative plans to install two activated alumina de-fluoridation filters in Namoo under partnership with World Vision (see Fig. 1.3). These filters would be attached to the two hand-pump wells in Namoo with groundwater fluoride concentrations above 4.0 mg L^{-1} (in Nayire and Done). According to researchers at World Vision, the preliminary results from previous trials using the same filters have not been promising. The users found the filters deliver treated water too slowly. They often bypassed the treatment option altogether and collected untreated water directly from the hand-pump well for drinking and washing. Obstacles such as this would clearly need to be addressed. Pretreating larger volumes of water and then storing it in a tank may be more effective, for example. Alternatives to water treatment should be considered. A trial using rainwater catchment systems is recommended. Discussions with the Bongo District Assembly and community members about the above options, as well as piped low fluoride water to high fluoride areas, are also recommended.

Developing an education program in the health clinics and schools is a high priority as well; for if the cause of fluorosis is not well understood, then any treatment options or recommendations of an alternative water supply will be ignored. What may be most important, however, is to address the underlying problem of poverty. If residents continue to have limited access to reliable sources of water and food, and lack money to pay for school, health care, and other household expenses, then fluorosis and other health

issues will never be a priority. The final recommendation for future work is to consider options for providing paid employment in the area, including larger scale farming.

References

Farrah, H., Slavek, J., Pickering, W.F., 1987. Fluoride interactions with hydrous aluminum oxides and alumina, Aust. J. Soil Res., 55-69.

Fletcher, H.R., Smith, D.W., Pivonka, P., 2006. Modeling the sorption of fluoride onto alumina. J. Environ. Eng. 132, 229-246.

Hao, O.J., Huang, C.P., 1986. Adsorption characteristics of fluoride onto hydrous alumina. J. Environ. Eng. 112, 1054-1069.

WHO (World Health Organization). 2011. Guidelines for Drinking Water Quality. Volume 1, 4th edition. World Health Organization, Geneva.

APPENDIX A: Fast titration data & PHREEQC

See Supplementary Data

APPENDIX B: Slow titration data & PHREEQC (activated alumina)

See Supplementary Data

APPENDIX C: Fluoride loading & PHREEQC

See Supplementary Data

APPENDIX D: Fluoride adsorption vs. pH & PHREEQC

See Supplementary Data

APPENDIX E: Fluoride adsorption vs. time (activated alumina)

See Supplementary Data

APPENDIX F: Micropore size distribution/t-plots

See Supplementary Data

APPENDIX G: Groundwater level, well depth, well location

See Supplementary Data

APPENDIX H: Climate (T, RH, solar, precipitation, wind)

See Supplementary Data

APPENDIX I: Water chemistry

See Supplementary Data

APPENDIX J: X-ray diffraction

Bongo granite sample 1

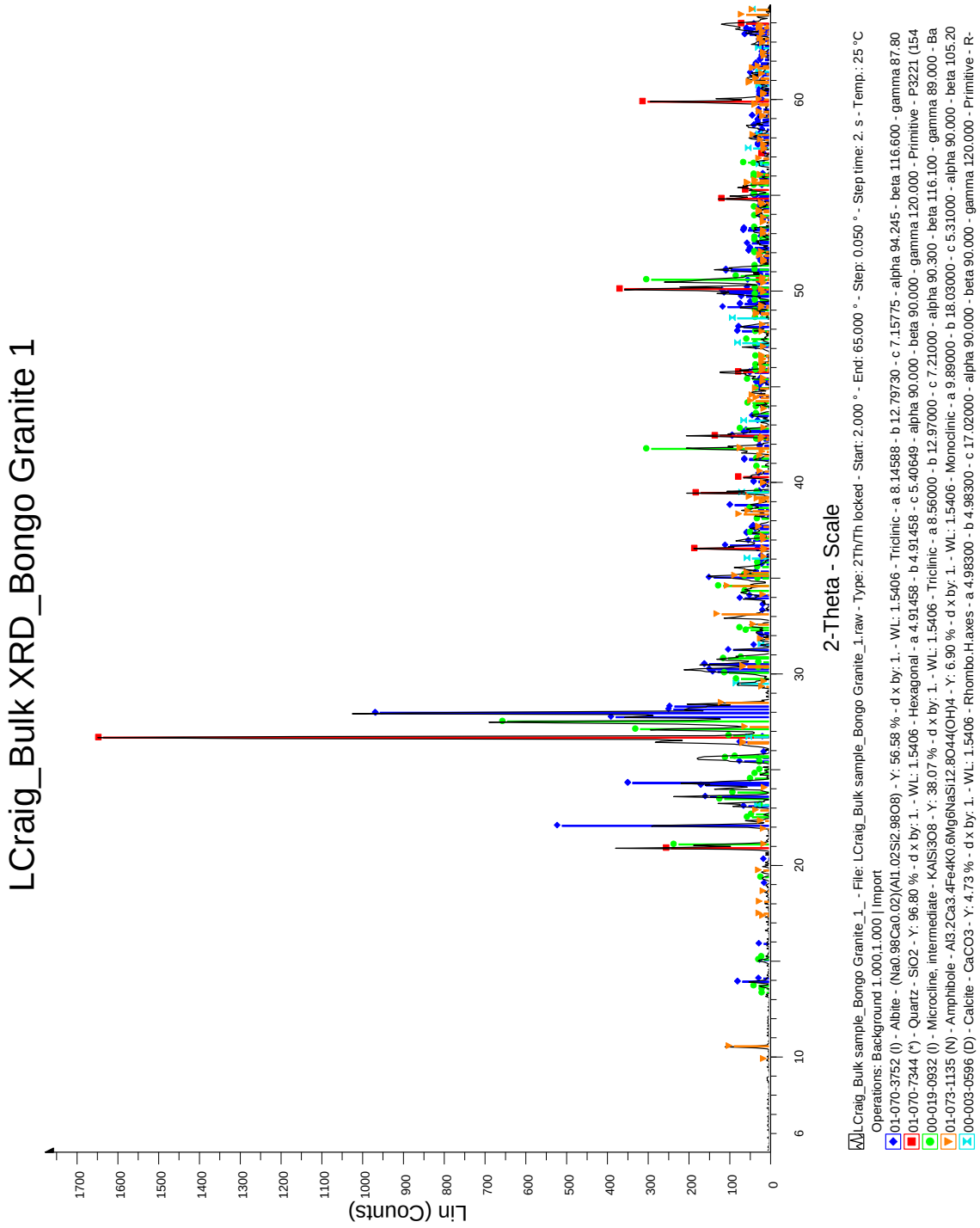

Bongo granite sample 2

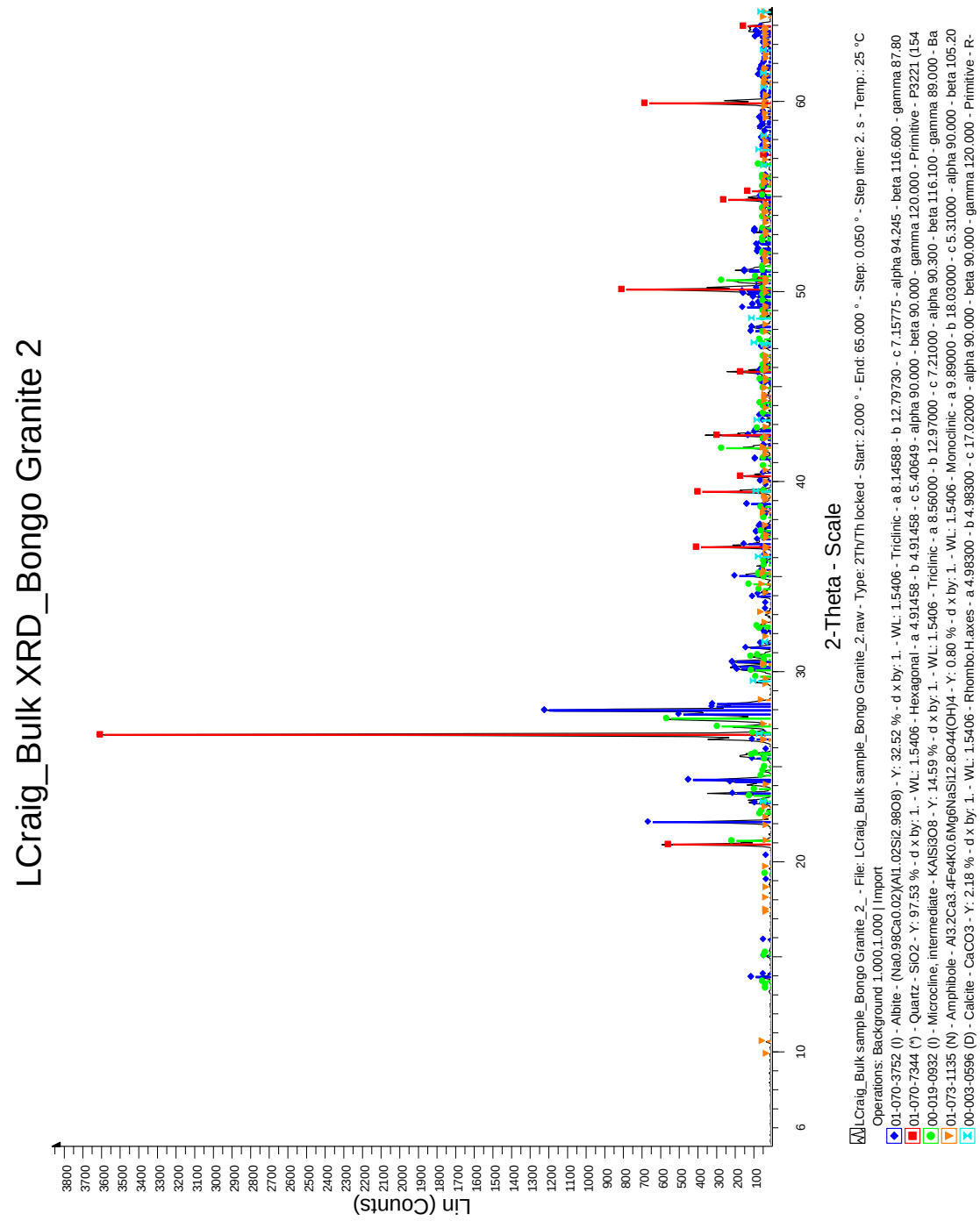

Bongo granite sample 3

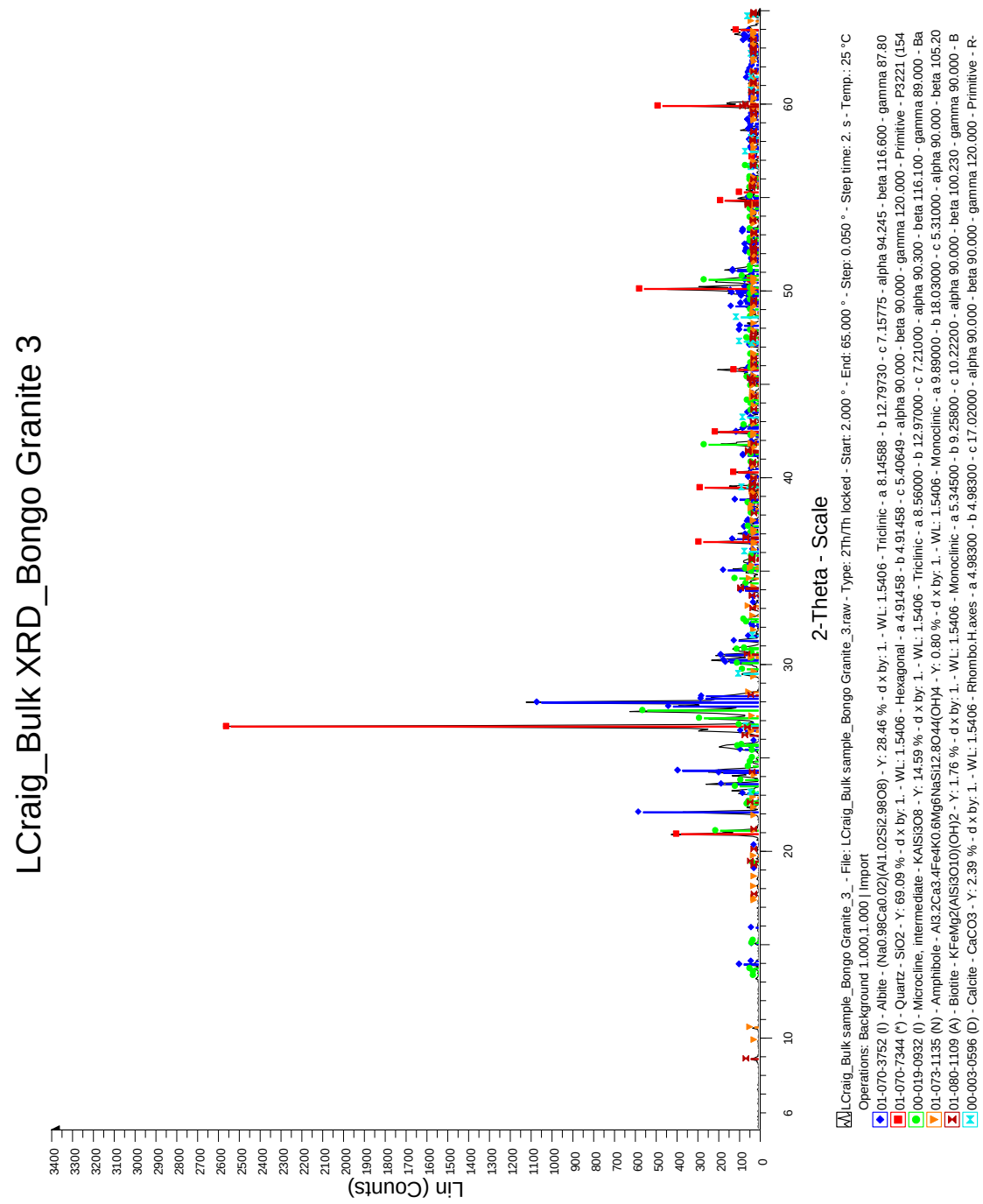

Namoo laterite

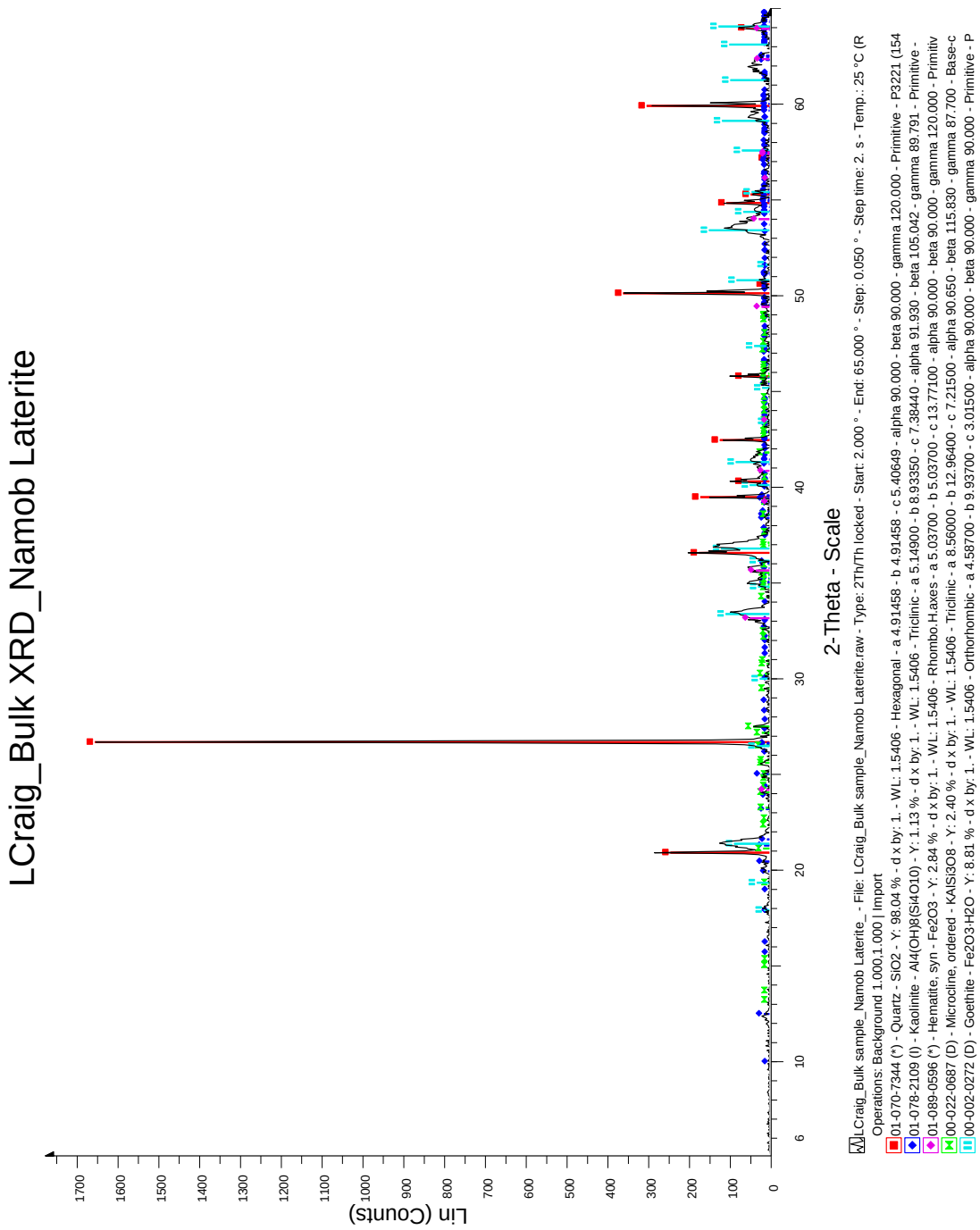

Ghana bauxite

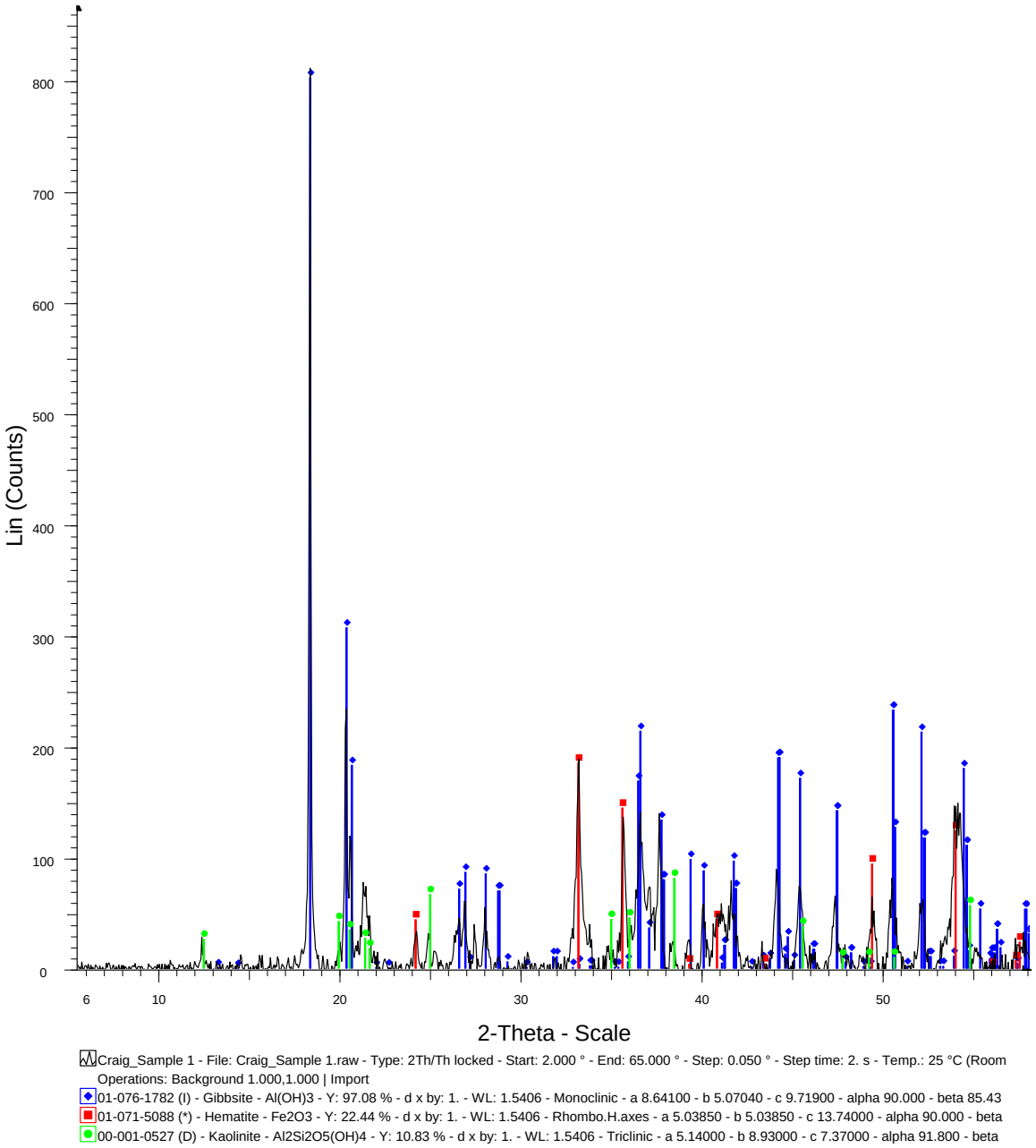

Activated alumina, sample 1 = 2 week hydration

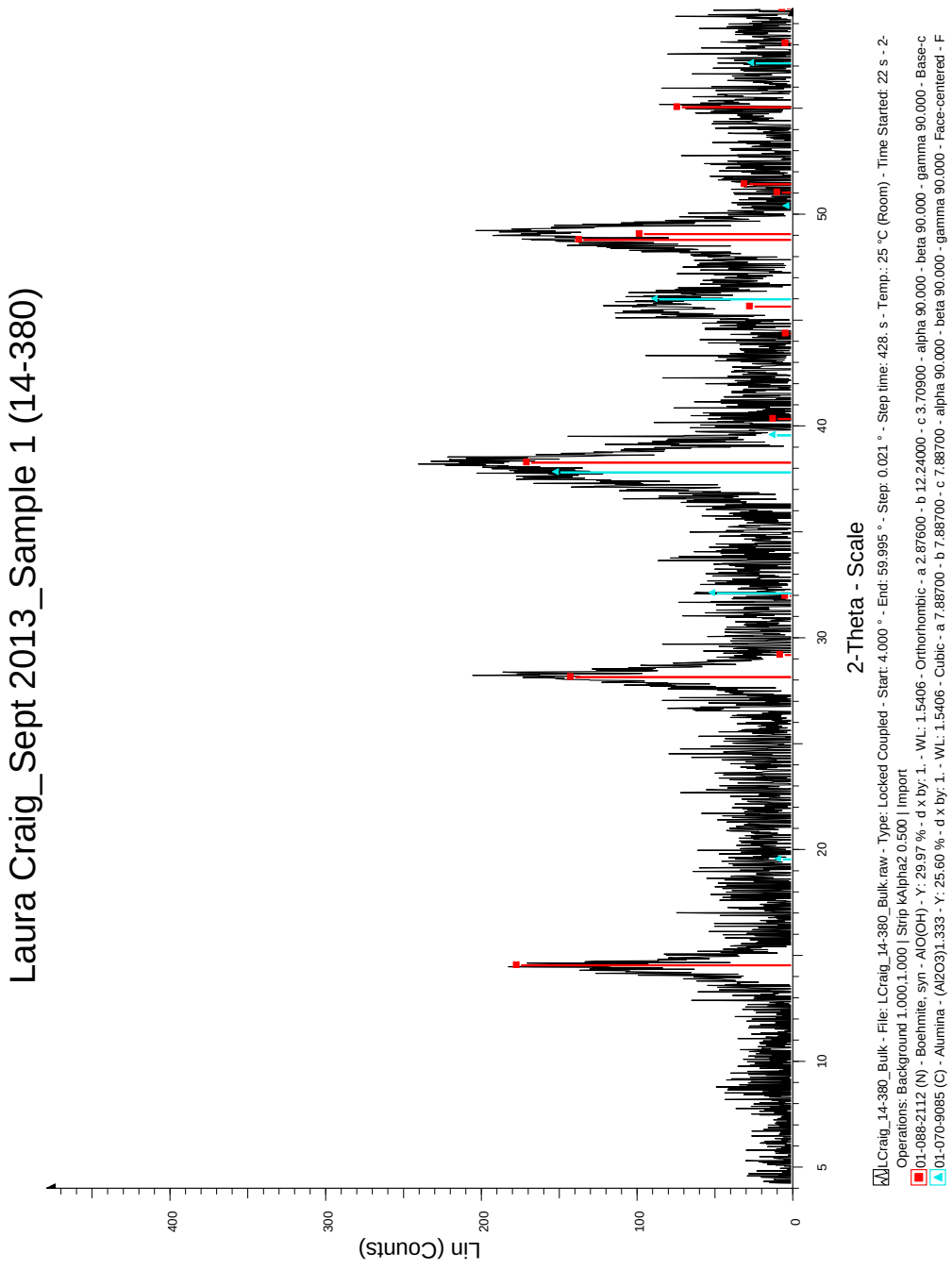

Activated alumina, sample 2 = 16 week hydration

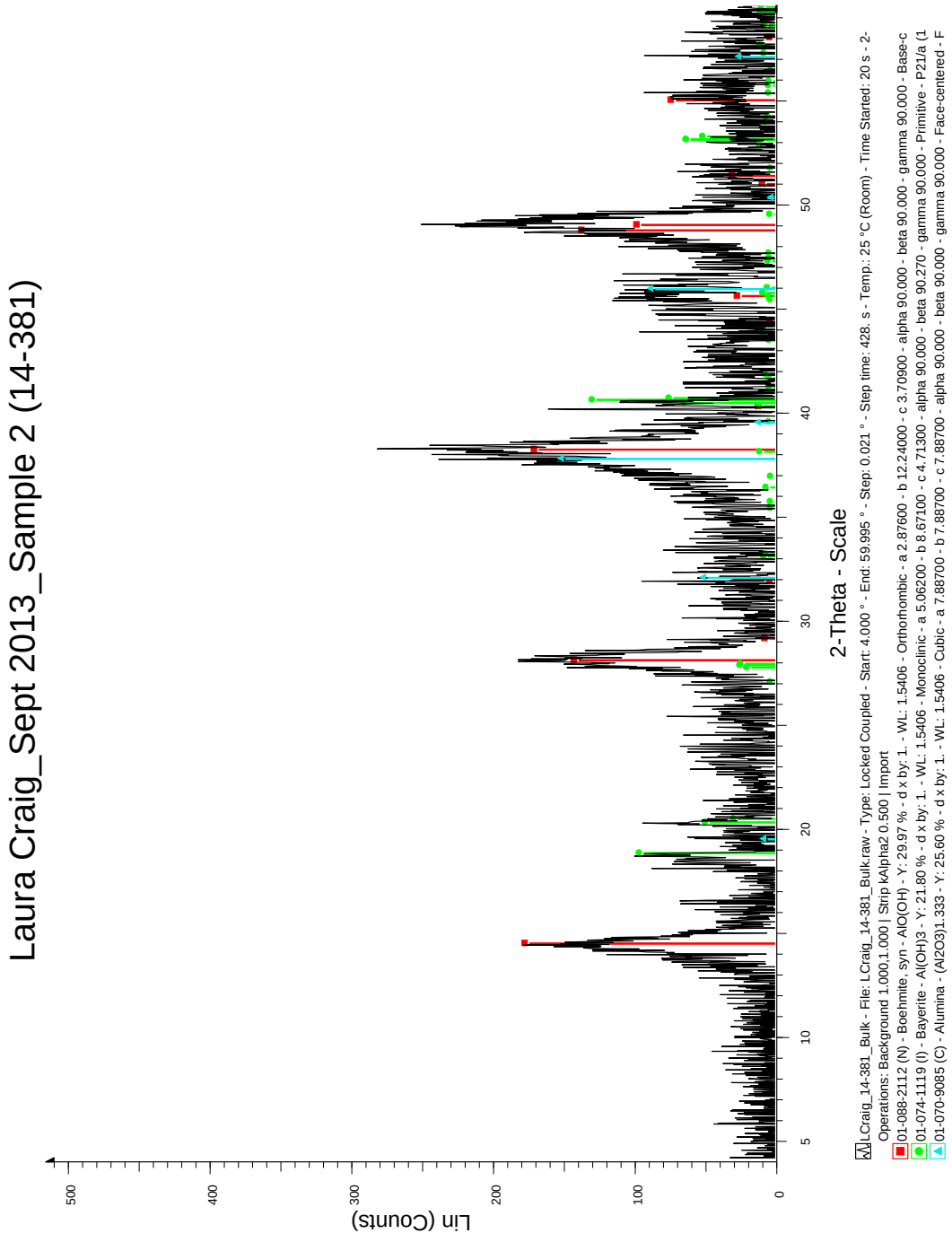

Activated alumina, sample 2 = 30 week hydration

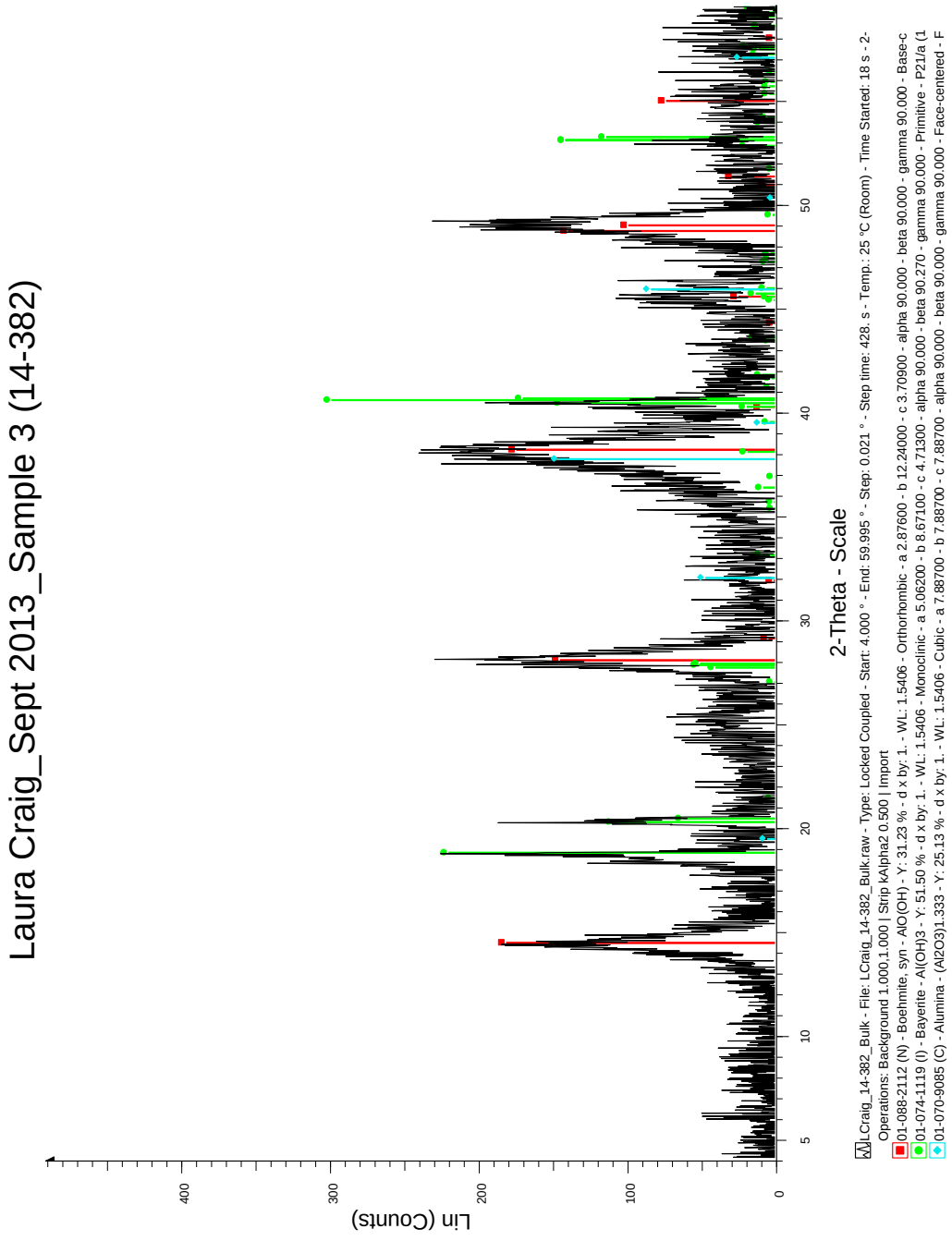

APPENDIX K: X-ray fluorescence

Fig. 1: Bongo granite sample 1, 2, 3

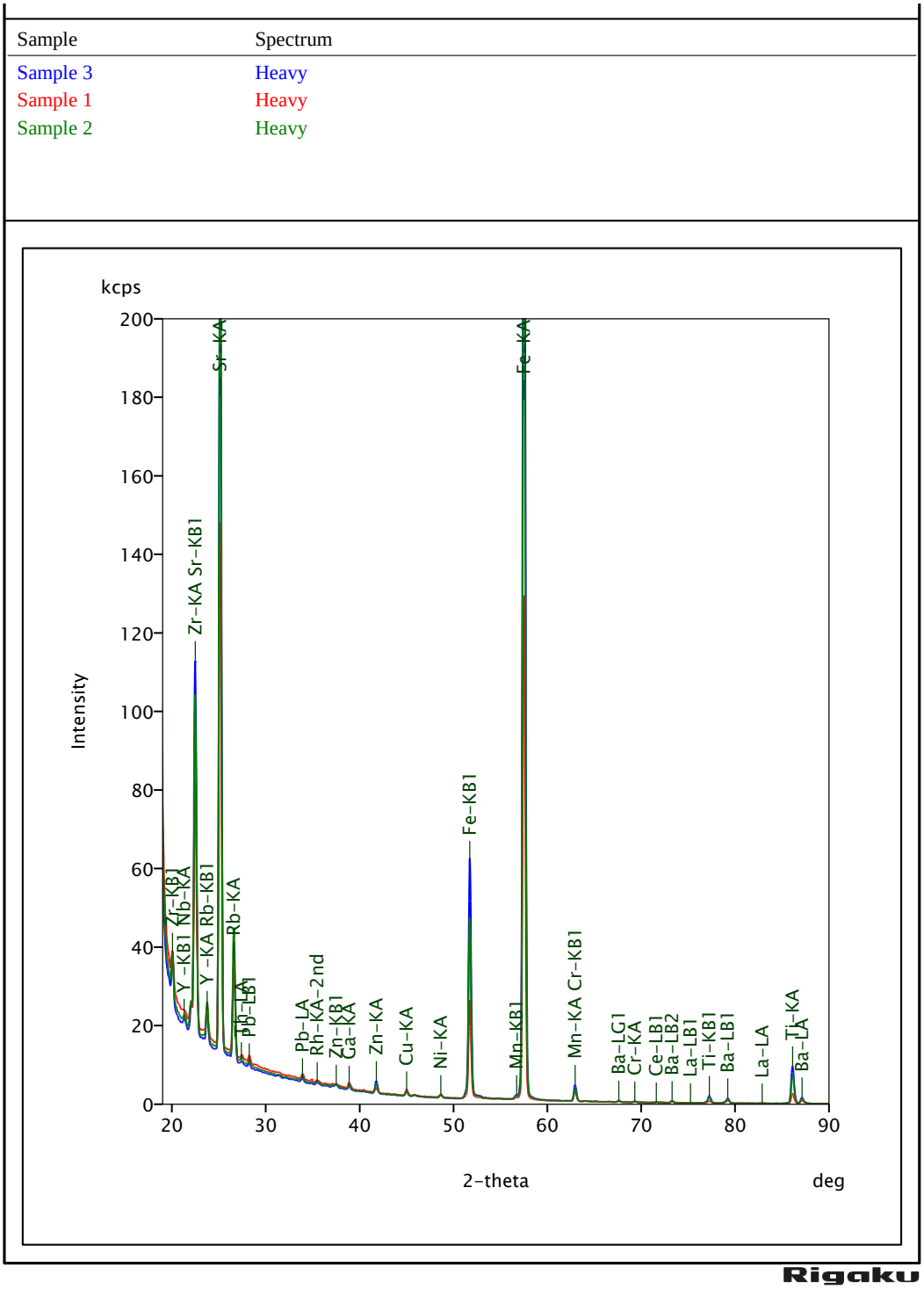

Fig. 2: Bongo granite sample 1, 2, 3

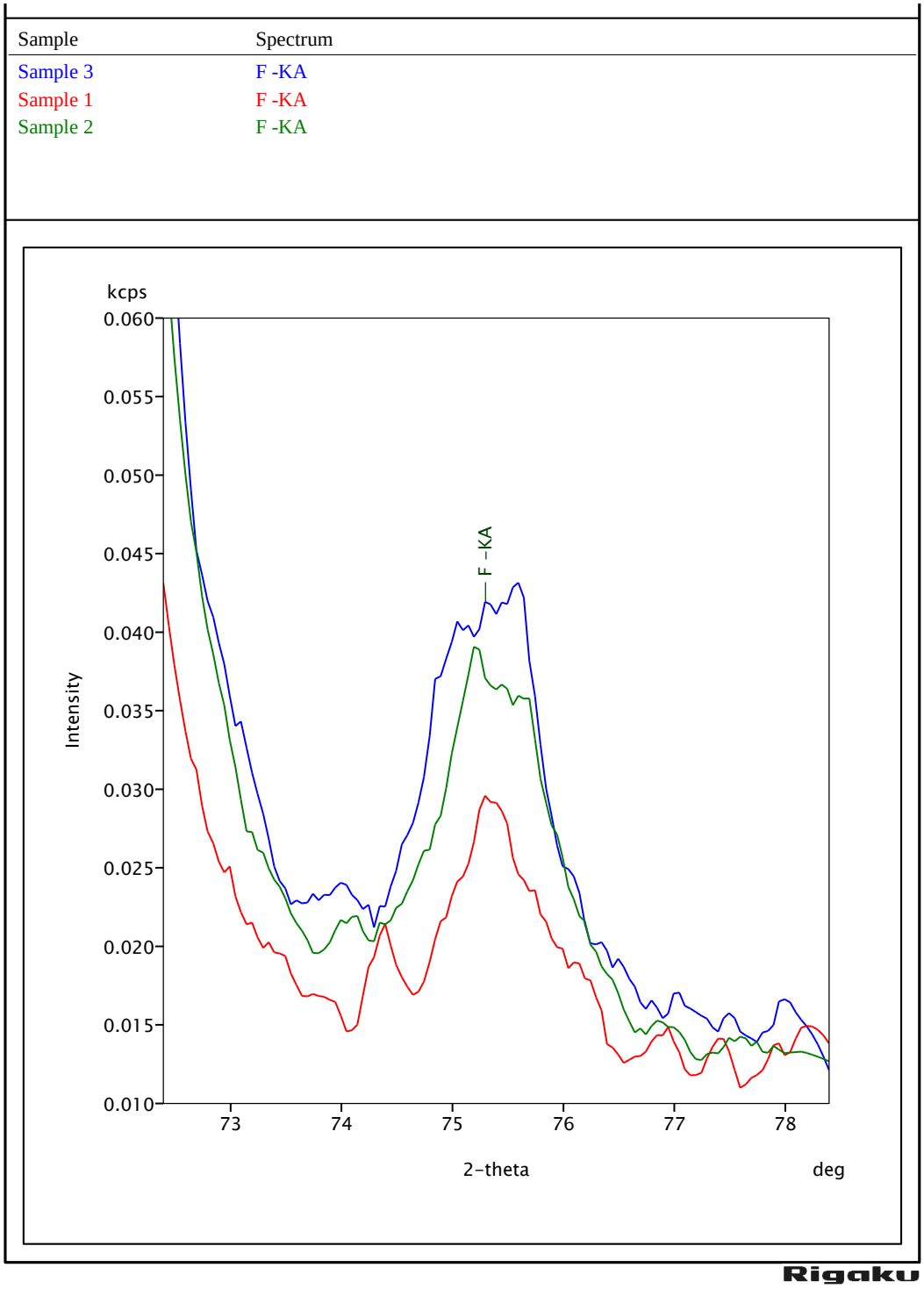

Fig. 3: Bongo granite sample 1, 2, 3

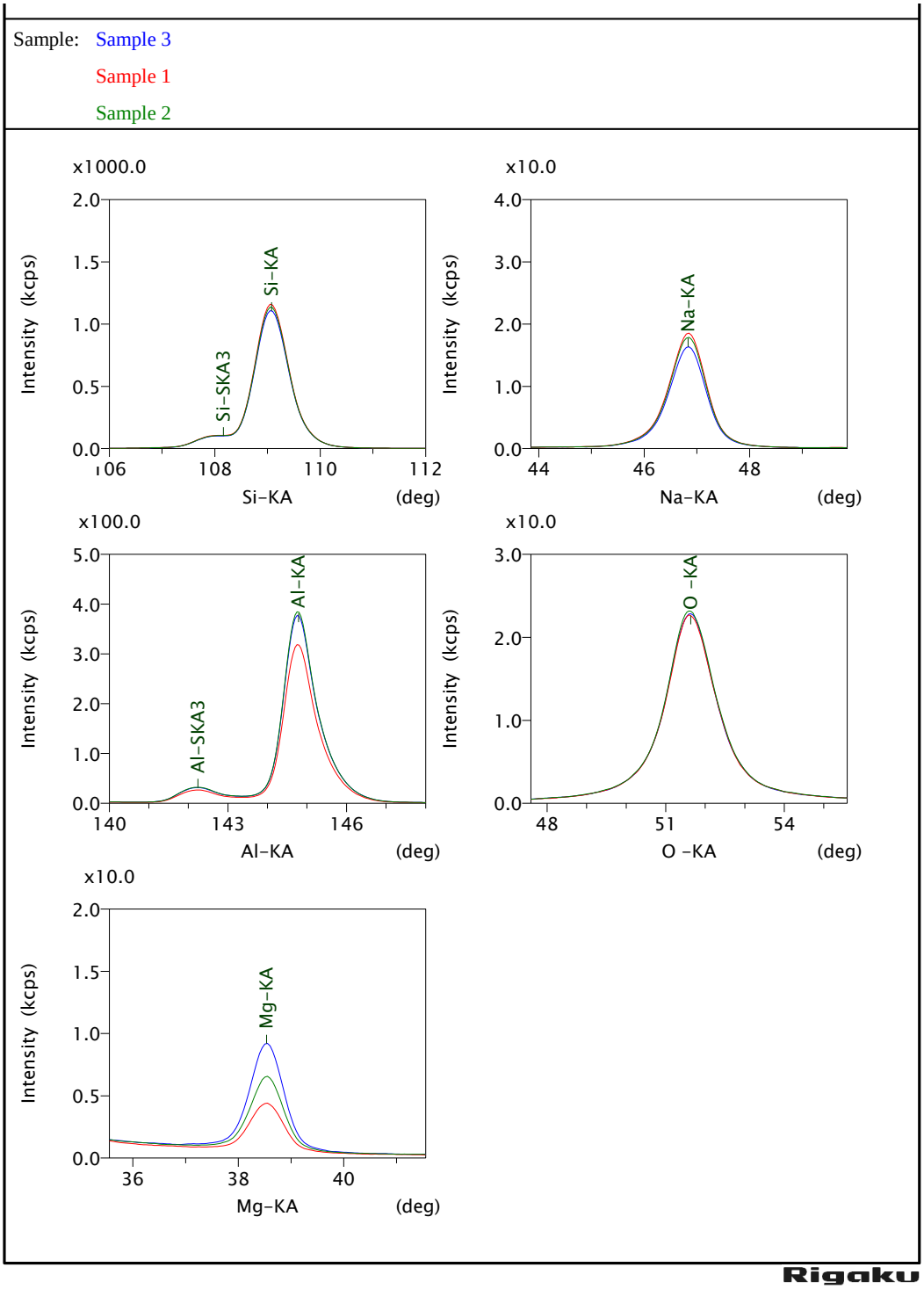

Fig. 4: Bongo granite sample 1, 2, 3

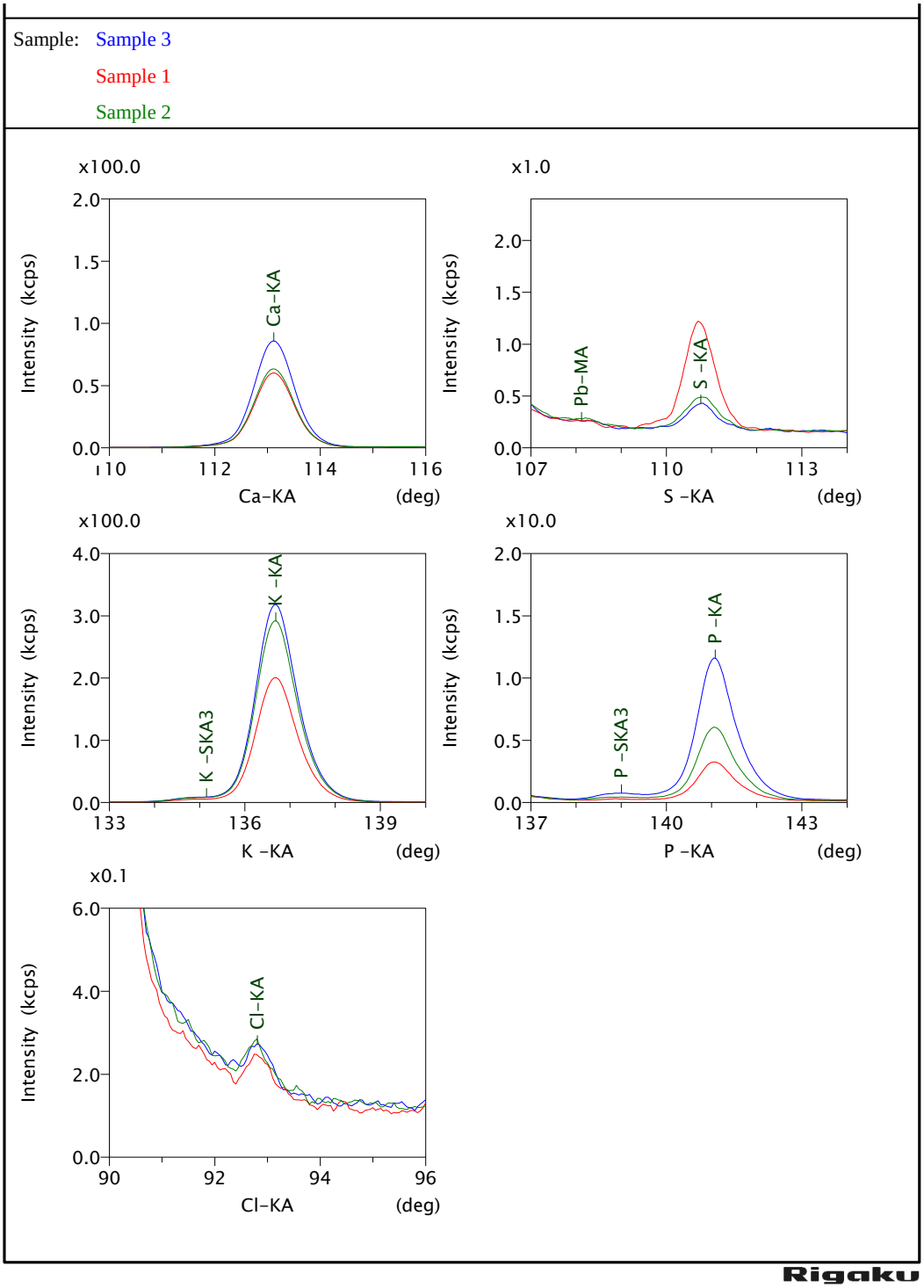

Ghana bauxite

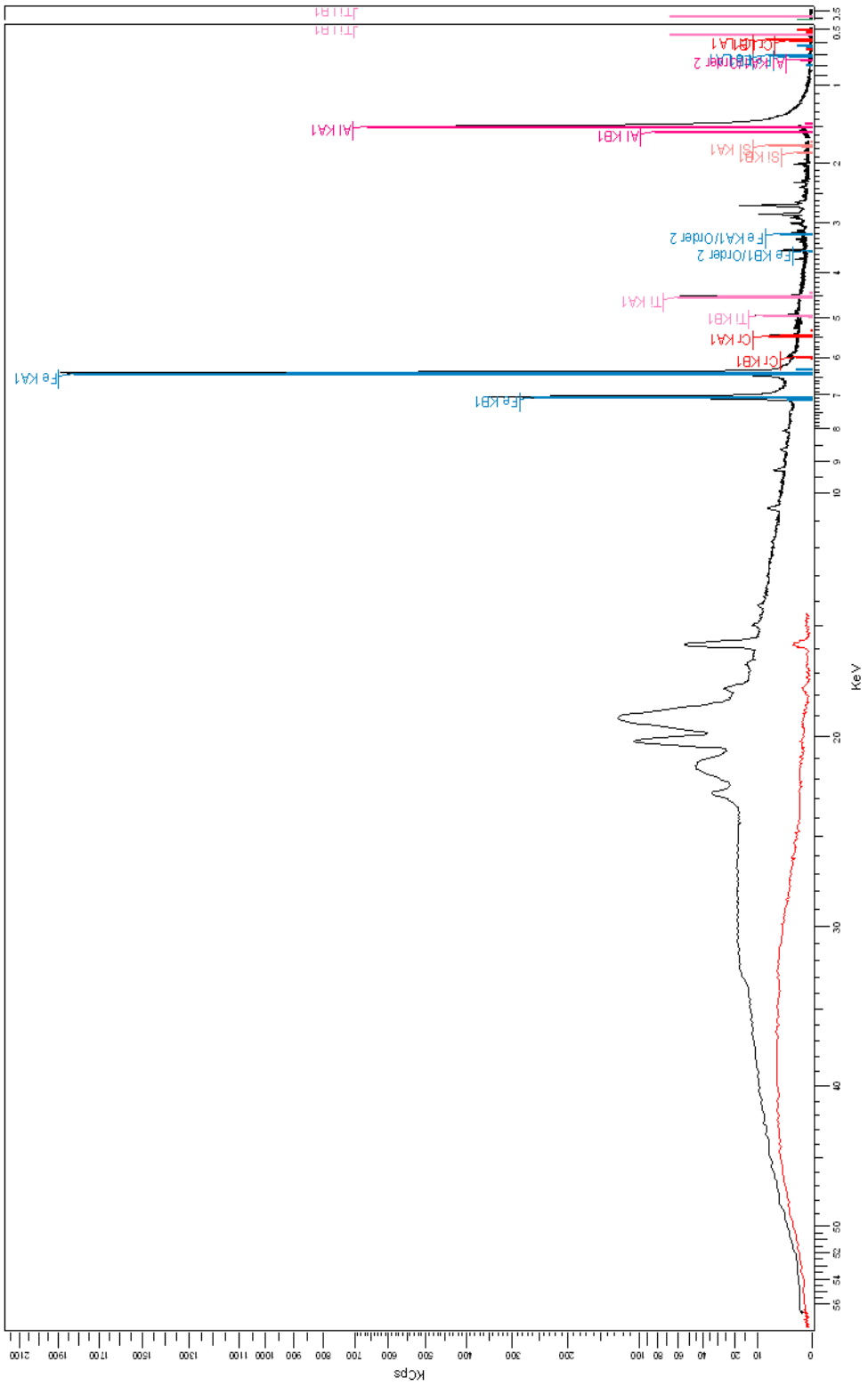

Activated alumina